

Proceedings of the
Third International Workshop on
Multiple Partonic Interactions at the LHC

MPI@LHC 2011

November 21–25, 2011

Hamburg, Germany

Editors: Simon Plätzer and Markus Diehl

Verlag Deutsches Elektronen-Synchrotron

Impressum

Proceedings of the Third International Workshop on Multiple Partonic Interactions at the LHC (MPI@LHC 2011) November 21–25, 2011, Hamburg, Germany

Conference homepage
<http://mpi11.desy.de/>

Slides at
<http://indico.desy.de/conferenceTimeTable.py?confId=4176>

Online proceedings at
<http://mpi11.desy.de/proceedings>

The copyright is governed by the Creative Commons agreement, which allows for free use and distribution of the articles for non-commercial activity, as long as the title, the authors' names and the place of the original are referenced.

Editors:
Simon Plätzer and Markus Diehl
August 2012
DESY-PROC-2012-03
ISBN 978-3-935702-68-3
ISSN 1435-8077

Published by
Verlag Deutsches Elektronen-Synchrotron
Notkestraße 85
22607 Hamburg
Germany

Printed by
Kopierzentrale Deutsches Elektronen-Synchrotron

Committees and Support

International Advisory Board

P. Bartalini (National Taiwan University, Taipei, TW),
C. Buttar (University of Glasgow, Glasgow, UK),
J. Butterworth (University College London, London, UK),
L. Fanò (Istituto Nazionale di Fisica Nucleare, Perugia, IT),
R. Field (University of Florida, Gainesville, US),
I. Hinchliffe (Lawrence Berkeley National Laboratory, Berkeley, US),
H. Jung (Deutsches Elektronen-Synchrotron, Hamburg, DE),
F. Krauss (Institute of Particle Physics Phenomenology, Durham, UK),
S. Lami (Istituto Nazionale di Fisica Nucleare, Pisa, IT),
M. Mangano (European Organization for Nuclear Research, Meyrin, CH),
A. Moraes (University of Glasgow, Glasgow, UK),
A. Morsch (European Organization for Nuclear Research, Meyrin, CH),
G. Pancheri (Istituto Nazionale di Fisica Nucleare, Frascati, IT),
M. Schmelling (Max-Planck-Institut für Kernphysik, Heidelberg, DE),
T. Sjöstrand (Lund University, SE),
Y. Srivastava (Università degli Studi di Perugia, Perugia, IT),
J. Stirling (Institute for Particle Physics Phenomenology, Durham, UK),
M. Strikman (Pennsylvania State University, University Park, US),
D. Treleani (Università degli Studi di Trieste, Trieste, IT)

Programme Committee

M. Diehl, H. Jung, J. Katzy, Z. Nagy

Local Organizing Committee

K. Borras, M. Diehl, H. Jung, J. Katzy, M. Medinnis, K. Mönig, Z. Nagy,
S. Plätzer, T. Schörner-Sadenius, G. Steinbrück, K. Stemmler, G. Weiglein

Support

We gratefully acknowledge a grant from Deutsche Forschungsgemeinschaft (DFG) and would like to thank Deutsches Elektronen-Synchrotron DESY and the University of Hamburg for their support.

Preface

The third international workshop on multiple partonic interactions (MPI) took place at DESY in Hamburg from 21 to 25 November 2011.

MPI are often crucial for interpreting results obtained at the Large Hadron Collider (LHC). The quest for a sound understanding of the dynamics behind MPI – particularly in the era of the LHC – has thus focused the aim of this workshop. It concentrated on phenomenology at previous hadron colliders and early LHC results, as well as theoretical considerations and the modeling of MPI in Monte Carlo event generators.

The workshop fostered close contact between the experimental and theoretical communities. It provided a setting to discuss many of the different aspects of MPI, eventually identifying them as a unifying concept between apparently different lines of research and evaluating their impact on the LHC physics programme.

In a total of 45 plenary talks, two round table discussions and a poster session, the workshop covered experimental results, Monte Carlo development and tuning, phenomenology and dedicated measurements of MPI, progress of theoretical understanding as well as the role of MPI in diffraction and small- x physics. Connections to closely related research within the fields of heavy ion physics and cosmic rays have also been covered.

It is a pleasure to thank Antje Brandes, Michaela Grimm and Katja Stemmler for their tireless support before and during the workshop. We thank Kirsten Sachs and Maren Stein for their help in preparing these proceedings.

Hamburg, August 2012
Simon Plätzer and Markus Diehl

Contents

1	Experimental results	1
	Underlying event, minimum bias and forward energy flow measurements with CMS	3
	Sunil Bansal	
	Minimum bias and underlying event measurements with ATLAS	11
	Michael Leyton	
	J/ψ production as a function of charged particle multiplicity in pp collisions at $\sqrt{s} = 7$ TeV with the ALICE experiment	21
	Sarah Porteboeuf-Houssais	
2	Monte Carlo development and tuning	31
	Obtaining the CMS ridge effect with multiparton interactions	33
	Sara Alderweireldt, Pierre Van Mechelen	
	Inclusive distributions in pp collisions at LHC energies compared with an adjusted DPMJET-III model with chain fusion	41
	Fritz W. Bopp, Johannes Ranft	
	Multiparton interactions in Herwig++	51
	Stefan Gieseke, Christian A. Röhr, Andrzej Słodmok	
	ATLAS MPI tunes with various PDFs	57
	Deepak Kar	
	Tuning of the multiple parton interaction model in Herwig++ using early LHC data	67
	Stefan Gieseke, Christian A. Röhr, Andrzej Słodmok	
	The ATLAS Monte Carlo tuning system	75
	Sebastian Wahrmund	
3	Phenomenology of MPI	79
	<i>MPI@LHC 2011</i>	v

NLO predictions for $Wb\bar{b}$ production via double parton scattering at the LHC	81
Edmond L. Berger	
Correlations in multiparton interactions	89
Tomas Kasemets	
Fluctuations of the nucleon transverse parton densities and inelastic collisions at the LHC	97
Mark Strikman	
Double heavy meson production through double parton scattering	107
Sergey P. Baranov, Alexander M. Snigirev, Nikolai P. Zotov	
4 Measuring MPI	115
Measurement of hard double-partonic interactions in $W \rightarrow l\nu + 2$ jet events using the ATLAS detector at the LHC	117
Eleanor Dobson	
Study of multiple partonic interactions in $D\bar{0}$	127
Georgy Golovanov	
5 Small-x and diffraction	135
Vector mesons and DVCS at HERA	137
Marcella Capua	
Pinning down the self-similar gluon distribution from momentum sum rule	145
Akbari Jahan, Dilip K. Choudhury	
Evolution in multiple interactions: a first step beyond the 'double DGLAP' approximation	151
Jochen Bartels	
Low-x evolution of parton densities	161
Alexey Yu. Illarionov, Anatoly V. Kotikov	
Unintegrated gluon distribution and soft pp collisions at LHC	169
Andrei Grinyuk, Hannes Jung, Gennady Lykasov, Artem Lipatov, Nikolai P. Zotov	
Isolated jet production with multi-Regge kinematics at Tevatron and LHC	177
Bernd Kniehl, Vladimir Saleev, Alexandera Shipilova	
6 Theoretical considerations for the description of MPI	185
A new look at multiple parton collisions	187
Yuri L. Dokshitzer	

Single and double perturbative splitting diagrams in double parton scattering	197
Jonathan R. Gaunt, W. James Stirling	
Multi-gluon correlations in the color glass condensate	205
Tuomas Lappi	
Unitarity and consistency in multiple hard collisions	215
Ted C. Rogers, Mark Strikman	
Energy flow observables in hadronic collisions	221
Francesco Hautmann	
Collinear distributions in double parton scattering	227
Mikhail G. Ryskin, Alexander M. Snigirev	
Theoretical considerations on the double Drell-Yan process as a prototype for multiparton interactions	235
Markus Diehl, Daniel Ostermeier, Andreas Schäfer	
7 Connections to other fields	245
Forward photon spectrum in 7 TeV pp collisions measured by the LHCf experiment	247
Koji Noda	
8 Outlook	255
Overview of experimental results presented at MPI@LHC 2011	257
Arthur Moraes	
Multiple interactions: summarizing remarks (theory)	265
Jochen Bartels	
MPI models in Monte Carlo generators	273
Hannes Jung, Simon Plätzer	

Chapter 1

Experimental results

Underlying event, minimum bias and forward energy flow measurements with CMS

Sunil Bansal for the CMS Collaboration

Department of Physics, Universiteit Antwerpen - Campus Groenenborger,
Groenenborgerlaan 171, 2020 Antwerpen, Belgium

DOI: <http://dx.doi.org/10.3204/DESY-PROC-2012-03/2>

A measurement of the underlying activity in scattering processes using leading track-jet and Drell-Yan events with energy scale over a wide range has been presented. Studies of inclusive and identified hadron production in proton-proton collisions, including charged particle transverse momentum, pseudorapidity and event-by-event multiplicity distributions at $\sqrt{s} = 0.9, 2.36$ and 7 TeV are shown. Results on two-particle angular correlations are also presented. We also present the measurements of the forward energy flow in Minimum Bias events and in events with hard jets produced at central rapidities, as well as in the events having a W/Z boson in the central region. Results are compared to various Monte Carlo models and to perturbative QCD calculations.

1 Introduction

In hadron-hadron scattering the “underlying event” (UE) is defined as any hadronic activity that is additional to what can be attributed to the hadronization of partons involved in the hardest scatter and its initial and final state QCD radiation. The UE activity is thus due to the hadronization of partonic constituents that have undergone multiple parton interactions (MPI), as well as to beam-beam remnants, concentrated along the beam direction. It is important for the precision measurements of Standard Model processes and the search for new physics at high energies.

The majority of proton-proton (pp) collisions at hadron colliders are soft, i.e., without any hard scattering of the proton partonic constituents. It is important to measure inclusive and identified hadron production in proton-proton collisions, including charged particle transverse momentum, pseudorapidity, event-by-event multiplicity distributions and particle correlations. The energy flow measured in the forward region is directly sensitive to the parton radiations and MPIs.

These measurements have been performed at various centre-of-mass energies by the CMS [1] experiment and compared with various MC predictions.

2 Results

The UE measurement is performed in plane *transverse* to the beam direction in the regions having least contamination from hard interactions, even though it cannot in principle be

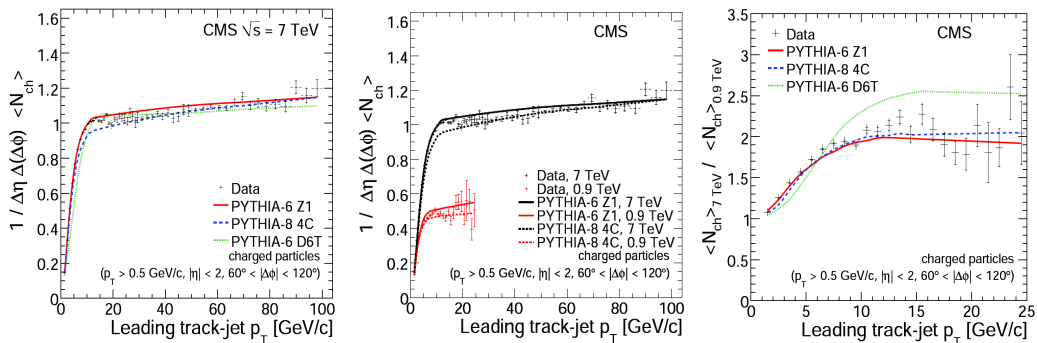


Figure 1: (left) Particle density as function of leading track-jet p_T in *transverse* region for data and prediction of various MCs at $\sqrt{s} = 7$ TeV. (centre) Comparison of particle density for \sqrt{s} of 0.9 TeV and 7 TeV. (right) Ratio of particle density at 0.9 and 7 TeV centre-of-mass energy for data and different MCs predictions.

uniquely separated from initial and final state radiation. Two different approaches have been considered by CMS, analyzing dijet events at $\sqrt{s} = 0.9$ and 7 TeV and di-muon final states in Drell-Yan events at 7 TeV. In the first analysis [2, 3] the direction of the hard scatter is identified with that of the leading track-jet, i.e. the object with largest p_T formed using a jet algorithm applied to reconstructed tracks. The leading track-jet p_T is taken to define the hard scale in the event. In the Drell-Yan analysis [5] the lowest scale is set by the di-muon invariant mass, and UE observables are studied as a function of resultant p_T and invariant mass of the muon pair.

A strong increase of the UE activity, quantified through the particle density (Figure 2) and the energy density (here not shown) of charged particles in the *transverse* region ($60^\circ < \Delta\phi < 120^\circ$), is observed with increasing leading track-jet p_T . At $\sqrt{s} = 7$ TeV this fast rise is followed above ~ 8 GeV/c by a *saturation* region with nearly constant multiplicity and small Σp_T increase. By comparing data taken at $\sqrt{s} = 0.9$ and 7 TeV, a strong growth with increasing centre-of-mass energy of the hadronic activity in the *transverse* region is also observed for the same value of the leading track-jet p_T , as reported in Figure 2 (right). The predictions of several tunes of the PYTHIA program version 6 [15] and of the new version PYTHIA-8 [9] have been compared to the measurements, with a good description of most distributions at $\sqrt{s} = 7$ TeV and of the \sqrt{s} dependence from 0.9 to 7 TeV provided by the Z1 tune [4].

After excluding the muons in DY events, both the *towards* ($\Delta\phi < 60^\circ$) and the *transverse* region are equally sensitive for the UE measurement. The UE activity in the DY events shows flat dependency on invariant mass (60-120 GeV/c²), which confirm the *saturation* hypothesis (illustrated in Figure 2 (right)). The UE activity as a function of $p_T^{\mu\mu}$ (illustrated in Figure 2 (left, centre)) shows very slow increase, both in the *towards* and *transverse* region, in particle density and do not show the fast rise as in case of track-jet analysis because the energy scale for selected DY events is very high and lies in the *saturation* region. The activity in the *transverse* region is higher than the *towards* region, which is due to spill-over contribution of hard-component in *away* region ($\Delta\phi > 120^\circ$).

Inclusive primary charged-hadron multiplicity densities have been measured with three different and complementary techniques [6, 7] as a function of the particle transverse mo-

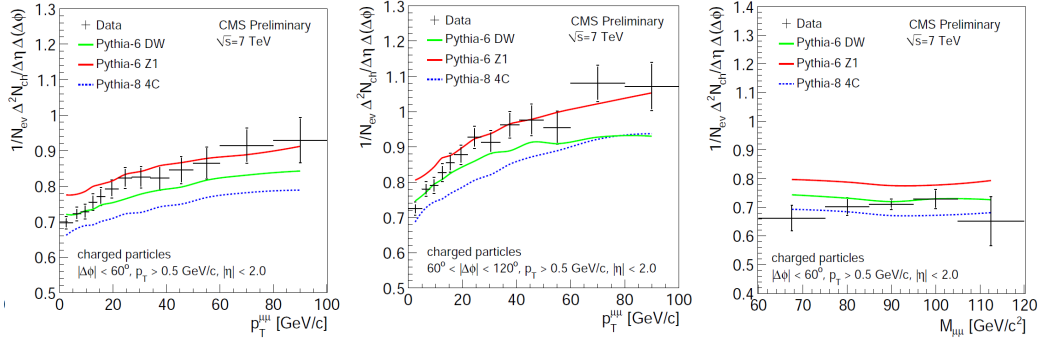


Figure 2: (left) Particle density as function of transverse momentum of muon pair ($p_T^{\mu\mu}$) in the *towards* region for the Drell-Yan events for data and prediction of various MCs at $\sqrt{s} = 7$ TeV. (centre) Corresponding particle density in the *transverse* region. (right) Particle density as a function of invariant mass of muon pair ($M_{\mu\mu}$) in the *towards* region.

mentum p_T and pseudorapidity η , in the pseudorapidity region of $|\eta| < 2.4$ for inelastic non-single-diffractive (NSD) Minimum Bias interactions. The results at 0.9 TeV have been found to be in agreement with previous measurements in pp and p \bar{p} collisions. The new measurements at 2.36 and 7 TeV, higher than most predictions, show a steeper than expected increase of charged-hadron multiplicity density with collision energy, as shown in Figure 3 (left) for central η region.

Minimum Bias measurements of the phase-space-invariant differential yield Ed^3N_{ch}/dp^3 , with N_{ch} the number of primary charged particles, have also been extended in the hundreds GeV/c region by using jet triggers [8]. As shown in Figure 3 (centre), the 7 TeV data are most consistent with PYTHIA-8, which agrees at the 10% level over the full p_T range of the measurement. Additionally, as shown in Figure 3 (right), the consistency of the 0.9 and 7 TeV spectra has been demonstrated with an empirical $x_T = 2p_T/s$ scaling that unifies the differential cross sections from a wide range of collision energies onto a common curve. Furthermore, within the theoretical uncertainties of the next-to-leading-order (NLO) calculations, the residual breaking of x_T scaling above $p_T \approx 8$ GeV/c is consistent between the measured cross sections and the NLO calculations. This result has removed a large uncertainty from an important ingredient of existing and future heavy-ion PbPb measurements, namely the pp reference spectrum corresponding to the energy of the LHC 2010 PbPb run: 2.76 TeV per nucleon. By employing a combination of techniques to interpolate between the CMS results at $\sqrt{s} = 0.9$ and 7 TeV, including information from existing CDF measurements at $\sqrt{s} = 0.63, 1.8,$ and 1.96 TeV [10, 11, 12], a pp reference at $\sqrt{s} = 2.76$ TeV (here not shown) has been constructed over a large range of transverse momentum ($p_T = 1$ -100 GeV/c) with systematic uncertainties of less than 13%.

Production of K_S^0 , Λ , and Ξ^- identified particles has been measured at \sqrt{s} of 0.9 and 7 TeV [13]. From a sample of 10 million strange particles, the p_T distributions (here not shown) were measured out to 10 GeV/c for K_S^0 and Λ , and out to 6 GeV/c for Ξ^- . The Tsallis function fits [14] of the distributions show for all the species a flattening of the exponential decay as the \sqrt{s} increases. The average p_T values are found to increase with particle mass and \sqrt{s} , in agreement with predictions and other experimental results. While the PYTHIA [15] p_T

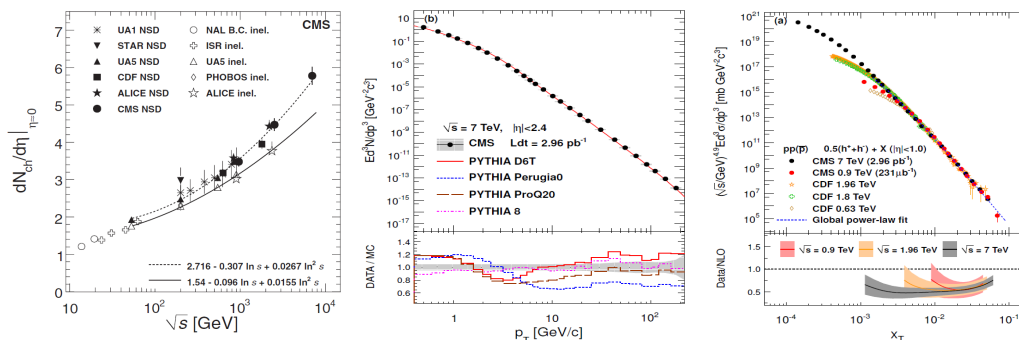


Figure 3: (left) Average value of charged multiplicity density $dN_{ch}/d\eta$ in the central η region as a function of \sqrt{s} in pp and $p\bar{p}$ collisions (the solid and dashed curves are second-order polynomial fits for the inelastic and non-single-diffractive event selections, respectively). (centre) Invariant charged particle differential yield at $\sqrt{s} = 7$ TeV compared with the predictions of four tunes of the PYTHIA MC generator; lower panel: the ratio of the CMS measurement to the four PYTHIA tunes (the grey band corresponds to the statistical and systematic uncertainties added in quadrature). (right) Inclusive charged particle invariant differential cross sections, scaled by $\sqrt{s}^{4.9}$, for $|\eta| < 1.0$ as a function of the scaling parameter x_T (the result is the average of the positive and negative charged particles).

distributions used in the analysis show significant variation based on tune and version, they are all broader than the data distributions. The measurement of the production in function of rapidity y (illustrated in Figure 4 (left) for K_S^0) shows a \sqrt{s} increase in strange particles production approximately consistent with the results for inclusive charged particles. As in the inclusive charged particle case, PYTHIA fails to match this increase, the deficit between PYTHIA and data being significantly larger for the two hyperons at both energies with a factor of three discrepancy for Ξ^- production at $\sqrt{s} = 7$ TeV. An enhancement of double-strange baryons to single-strange baryons, and/or an enhancement of strange baryons to strange mesons, would be an indication of a quark-gluon plasma or other collective effects. However, the production ratios $N(\Lambda)/N(K_S^0)$ and $N(\Xi^-)/N(\Lambda)$ versus p_T (here not shown) and y (reported in Figure 4 (centre) for $N(\Lambda)/N(K_S^0)$) show no change with \sqrt{s} . Thus, the deficiency in PYTHIA is likely originating from parameters regulating the frequency of strange quarks appearing in colour strings.

The charged hadron multiplicity distributions P_n of non-single-diffractive events were measured from an analysis of the Minimum Bias data at the three \sqrt{s} of 0.9, 2.36, and 7 TeV [16]. Charged tracks are reconstructed down to $p_T = 100$ MeV/c with high efficiency and low background contamination. A full correction for detector resolution and acceptance effects and an extrapolation to zero transverse momentum yield measurements of the charged hadron multiplicity distribution for increasing central pseudorapidity ranges from $|\eta| < 0.5$ to $|\eta| < 2.4$, shown in Figure 4 (right). Although some event generators provide an adequate description of Tevatron and LEP data, none is able to describe simultaneously the multiplicity distributions and the p_T spectrum at $\sqrt{s} = 7$ TeV. In general, models predict too few low-momentum particles, indicating that by increasing the amount of multiple-parton interactions (MPI) one effectively introduces too many hard scatters in the event. The change of slope in P_n in the widest central pseudorapidity intervals observed at $\sqrt{s} = 7$ TeV, combined with the strong

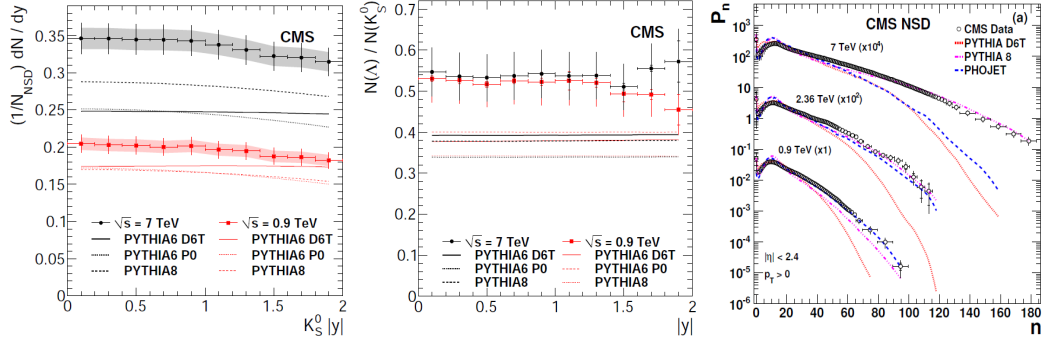


Figure 4: (left) K_S^0 production per non-single-diffractive (NSD) events versus $|\eta|$: the inner vertical error bars, when visible, show the statistical uncertainties, the outer the statistical and point-to-point systematic uncertainties summed in quadrature; the normalization uncertainty is shown as a band; three PYTHIA predictions are overlaid. (centre) The production ratio $N(\Lambda)/N(K_S^0)$ in non-single-diffractive events versus $|\eta|$ at each \sqrt{s} (the inner vertical error bars, when visible, show the statistical uncertainties, the outer the statistical and all systematic uncertainties summed in quadrature), together with three PYTHIA predictions. (right) The charged hadron multiplicity distributions with $|\eta| < 2.4$ for $p_T > 500$ MeV/c at $\sqrt{s} = 0.9, 2.36,$ and 7 TeV, compared to two different PYTHIA models and the PHOJET model; for clarity, results for different $\sqrt{s} = 0.9$ are scaled by powers of 10 as given in the plots.

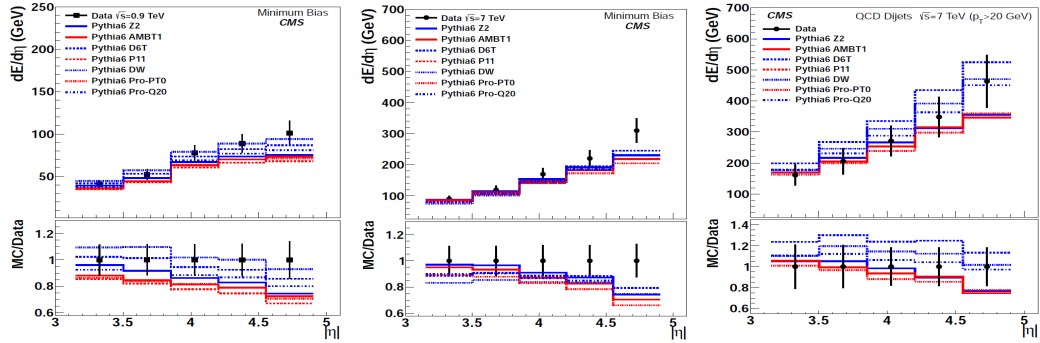


Figure 5: (left) Forward energy flow in Minimum Bias events for centre-of-mass energy of $\sqrt{s} = 0.9$ TeV for data and prediction of various tunes for PYTHIA-6. (centre) Forward energy flow in Minimum Bias events for centre-of-mass energy of $\sqrt{s} = 7$ TeV for data and prediction of various tunes for PYTHIA-6. (right) Energy flow for events with dijet events with transverse momentum $p_T > 20$ GeV/c for centre-of-mass energy of $\sqrt{s} = 7$ TeV for data and prediction of various tunes for PYTHIA-6.

linear increase of the normalized C_q moments (here not shown), indicates a clear violation of KNO scaling [17] with respect to lower energies. Such observation merits further studies.

A measurement of the energy flow in the forward region ($3.15 < |\eta| < 4.9$) was done for $\sqrt{s} = 0.9$ and 7 TeV [18]. The energy flow, corrected for detector effects, is measured both in Minimum Bias events and in events with a hard scale provided by a dijet system at central

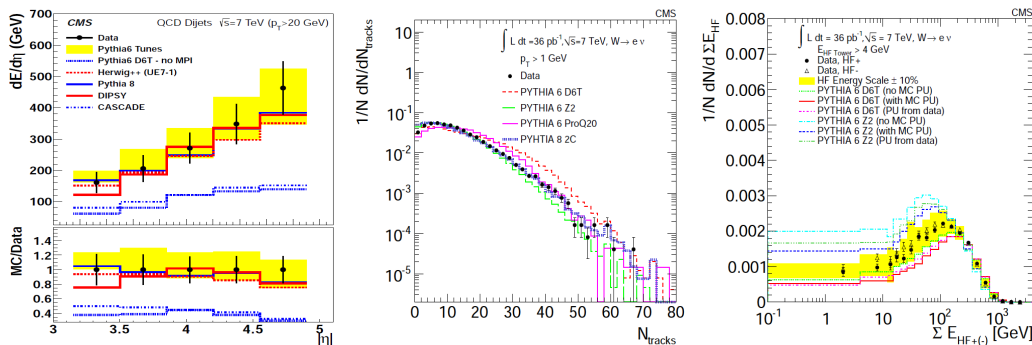


Figure 6: (left) Energy flow for events with dijet events with transverse momentum $p_T > 20$ GeV/c for centre-of-mass energy of $\sqrt{s} = 7$ TeV for data and prediction of various event generators. (centre) Number of tracks in central region of detector and with transverse momentum $p_T > 1$ GeV for events having $W \rightarrow e\nu$ candidates for data and various MCs. (right) Forward energy for events having $W \rightarrow e\nu$ candidates, summing all HF towers with energy larger than 4 GeV, for data and various MCs.

pseudorapidities ($|\eta| < 2.5$) as illustrated in Figure 5. The jets are required to have transverse energy greater than 8 (20) GeV at $\sqrt{s} = 0.9$ (7) TeV. There is significant increase in energy as centre-of-mass energy increases from 0.9 TeV to 7 TeV (shown in Figure 5 (left and centre)) and measurement are different for Minimum Bias and QCD dijet events (clear from Figure 5 (centre and right)). Even if this increase is reproduced by the MCs for Minimum Bias and dijet events, none of the MC simulations can describe all four energy flow measurements. In general the MC generators produce a somewhat too flat energy flow distribution for the Minimum Bias data. Multiple interactions are needed in order to describe the data, since it is found that MC predictions without MPI (PYTHIA-6 run without MPI and CASCADE [20]) significantly undershoot the data. The description given by cosmic ray MC generators (such as EPOS [21], QGSJET [22] and SIBYLL [23]) is found to be excellent as clear from 6 (left). Central charged-particle multiplicities, forward energy flow, and correlations between them have been studied in W and Z events, identified by the vector-boson decays to electrons and muons [19]. None of the studied MC tunes provides simultaneously a satisfactory description of the charged particle multiplicity in the central pseudorapidity region ($|\eta| < 2.5$) and the forward energy flow ($3 < |\eta| < 4.9$) as illustrated in Figure 6 (centre, right). The PYTHIA-6 Z2 and PYTHIA-6 2C tunes give a reasonable description of the central charged-particle multiplicity, but predict too many events with relatively low energy depositions in the forward calorimeters. The PYTHIA-6 D6T tune predicts too many events with high charged-particle multiplicities, too few events with low-energy depositions, and too many events with very large energy depositions in the forward calorimeters. The Pro-Q20 tune provides the best description of the forward energy distribution and a good description of the charged-particle multiplicity, when a track p_T threshold of 0.5 GeV is applied. However, the charged-particle multiplicity with $p_T > 1.0$ GeV is not well described, though the prediction is closer to the data than that for the D6T tune. Strong positive correlations between the energy measured in the two forward calorimeters (i.e. at positive and negative rapidities) and the charged-particle multiplicity are observed in the data and in Monte Carlo models (not shown here). However, the correlations in the various MC tunes are different from those seen in the data.

3 Conclusion

In the present proceeding a measurement of the underlying event in different processes at different centre-of-mass energies, some of Minimum Bias measurements and measurements of forward energy flow in different processes with different centre-of-mass energies conducted by the CMS collaboration at the LHC are briefly summarized. The huge amount of data coming from the first two years of data acquisition has provided important information to better constrain phenomenological models of the soft hadron production and provide insight on understanding MPI. These measurements are crucial for precision measurements of Standard Model processes and for new physics searches.

References

- [1] CMS Collaboration, JINST **3** (2008) S08004.
- [2] CMS Collaboration, Eur. Phys. J. C **70** (2010) 555.
- [3] CMS Collaboration, J. High Energy Phys. **09** (2011) 109.
- [4] R. Field, arXiv:1010.3558 [hep-ph].
- [5] CMS Collaboration, CMS-PAS-QCD-10-040.
- [6] CMS Collaboration, J. High Energy Phys. **02** (2010) 041.
- [7] CMS Collaboration, Phys. Rev. Lett. **105** (2010) 022002.
- [8] CMS Collaboration, CMS-QCD-10-008, CERN-PH-EP-2011-049b [arXiv:1104.3547v1 [hep-ex]], accepted by J. High Energy Phys.
- [9] T. Sjostrand, S. Mrenna and P. Z. Skands, Comput. Phys. Commun. **178** (2008) 852.
- [10] CDF Collaboration, Phys. Rev. D **79** (2009) 112005.
- [11] CDF Collaboration, Phys. Rev. D **82** (2010) 119903.
- [12] CDF Collaboration, Phys. Rev. Lett. **61** (1988) 1819.
- [13] CMS Collaboration, J. High Energy Phys. **05** (2011) 064.
- [14] C. Tsallis, J. Stat. Phys. **52** (1988) 479.
- [15] T. Sjostrand, S. Mrenna and P. Z. Skands, JHEP **05** (2006) 026.
- [16] CMS Collaboration, J. High Energy Phys. **01** (2011) 079.
- [17] Z. Koba, H. B. Nielsen and P. Olesen, Nucl. Phys. B **40** (1972) 317.
- [18] CMS Collaboration, CMS-FWD-10-011.
- [19] CMS Collaboration, arXiv:1110.0181 [hep-ex].
- [20] H. Jung et al., Eur. Phys. J. C **70** (2010) 1237-1249.
- [21] K. Werner, F. M. Liu and T. Pierog, Phys. Rev. C **74** (2006) 044902.
- [22] N. N. Kalmykov, S. S. Ostapchenko and A. I. Pavlov, Bull. Russ. Acad. Sci. Phys. **58** (1994) 1966.
- [23] R. S. Fletcher, T. K. Gaisser, P. Lipari and T. Stanev, Phys. Rev. D **50** (1994) 5710.

Minimum bias and underlying event measurements with ATLAS

Michael Leyton on behalf of the ATLAS Collaboration
CERN, 1211 Genève 23, Switzerland

DOI: <http://dx.doi.org/10.3204/DESY-PROC-2012-03/1>

A summary of some of the recent minimum bias and underlying event measurements by the ATLAS collaboration is given. The results of several analyses using low-luminosity proton-proton collision data from the LHC taken at center-of-mass energies of $\sqrt{s} = 0.9, 2.36$ and 7 TeV are presented. Data are compared to predictions by several different Monte Carlo event generators. The measurements expose limitations of the phenomenological models in properly describing the measured observables in all regions of phase space.

1 Introduction

Properties of minimum bias and the underlying event have previously been studied over a wide range of energies. In particular, results from experiments at CERN and Fermilab have been used to tune the PYTHIA [1] and PHOJET [2] Monte Carlo (MC) event generators. Due to uncertainties in the modeling of the energy dependence of soft inelastic interactions, these generators give widely varying predictions at LHC energies. Recent results from the ATLAS collaboration are presented here and compared to these predictions.

2 LHC and ATLAS

The Large Hadron Collider (LHC) [3] is a proton-proton (pp) collider located at CERN and currently operating at a center-of-mass (CM) energy of $\sqrt{s} = 7$ TeV. It is designed to go up to twice that energy, with an instantaneous luminosity of $\mathcal{L} = 10^{34} \text{cm}^{-2} \text{s}^{-1}$.

ATLAS [4] is a 4π general-purpose detector designed for high-luminosity studies at the LHC. Layers of tracking detectors, calorimeters and muon chambers cover almost the entire solid angle around ATLAS. The Inner Detector (ID) is responsible for tracking charged particles within a pseudorapidity range of $|\eta| < 2.5$.¹ It consists of a multi-layer silicon tracker with both pixels and strips, in addition to a transition radiation straw tracker, all of which are immersed in a solenoidal magnetic field of 2 T.

The calorimeters surround the Inner Detector and are responsible for measuring the energies of charged and neutral particles within a pseudorapidity range of $|\eta| < 4.9$. The calorimeters are

¹The ATLAS reference system is a right-handed coordinate system with its origin at the nominal interaction point at the center of the detector. Cylindrical coordinates (r, ϕ) are used in the plane transverse to the beam axis, ϕ being the azimuthal angle around the beam axis. The pseudorapidity is defined in terms of the polar angle θ with respect to the beam axis as $\eta = -\ln \tan(\theta/2)$. The transverse momentum p_T is defined relative to the beam axis.

specialized for measuring electromagnetic or hadronic particles, the latter of which include jets of particles formed by hadronization of quarks and gluons. They also detect missing transverse energy (\cancel{E}_T) by summing all of the measured energy deposits.

The ATLAS detector has a three-level trigger system. For the measurements presented herein, the first level trigger (L1) relies on the beam pickup timing devices (BPTX) and the minimum bias trigger scintillators (MBTS). The BPTX are composed of electrostatic beam pickups attached to the beam pipe at a distance $z = \pm 175$ m from the center of the ATLAS detector. The MBTS are mounted at each end of the detector in front of the endcap-calorimeter cryostats at $z = \pm 3.56$ m and are segmented into eight sectors in azimuth and two rings in pseudorapidity ($2.09 < |\eta| < 2.82$ and $2.82 < |\eta| < 3.84$).

3 Soft QCD at the LHC

All physics at the LHC essentially comes from the interactions of quarks and gluons. Hard processes are characterized by high transverse momentum (p_T) and are well described by perturbative QCD. Soft interactions, on the other hand, are characterized by low transverse momentum and require non-perturbative phenomenological models. These soft interactions are actually the dominant processes at the LHC. They can include diffraction, Multiple-Partonic Interactions (MPI), soft initial- and final-state radiation (ISR/FSR), as well as beam-beam remnants.

While these are all separate phenomena, the different components are often grouped according to experimental trigger. Minimum bias (MB) interactions, for example, are the processes that are selected with a loose trigger intended to select inelastic collisions with as little bias as possible. The underlying event (UE) is the collection of all the soft processes that accompany a high- p_T interaction of interest. It is typically studied as a function of the highest- p_T particle in the event.

Modeling of these soft interactions is important because they impact all other high- p_T measurements. At higher luminosities, for example, minimum bias interactions are a major background, numbering up to 25 interactions on average per bunch crossing at LHC design luminosity. A proper model of the UE is also important for precise high- p_T measurements since it can affect the \cancel{E}_T resolution, lepton identification and jet resolution. Studying the UE is critical for understanding the evolution of QCD with collision energy, as well as understanding the systematic corrections on many studies such as mass measurements.

While soft QCD is modeled by some MC generators, including PYTHIA, PHOJET and HERWIG/JIMMY [5], it tends to be phenomenological, requiring tuning to data. However, non-perturbative effects, such as soft diffraction, hadronization and low- p_T parton scattering, are difficult to separate experimentally. Also, the description of hard processes by the MC generators must be preserved while tuning the soft processes. The results presented here show that it is difficult to describe both MB and the UE with the same parameters.

4 Data samples and selection

The measurements presented here were made using pp collision data recorded at $\sqrt{s} = 0.9, 2.36$ and 7 TeV during low-luminosity running of the LHC in 2009 and the beginning of 2010. The low instantaneous luminosity ensures that there are relatively few overlapping pp collisions in each bunch crossing (a background known as *pile-up*), important when measuring soft-QCD

observables. Data were collected with stable colliding beams and correspond to an integrated luminosity of $\int \mathcal{L} dt \leq 230 \mu\text{b}^{-1}$.

4.1 Event selection

Events were selected using a single-arm MBTS trigger, formed from BPTX and MBTS L1 trigger signals. The MBTS trigger was configured to require one hit above threshold on either side of the detector ($2.09 < |\eta| < 3.84$). Events were additionally required to have at least one reconstructed primary vertex, while also vetoing events with a second primary vertex with 4 or more tracks. This event selection imposes little bias on the measurements presented here, while reducing the contribution from empty events, beam background and pile-up events to a negligible level.

4.2 Track selection

Tracks were selected by requiring their p_T and η to be within the specified phase space of the measurement. A good track quality was ensured by requiring a minimum number of hits in the silicon detectors, dependent on the p_T of the track. Tracks associated to particles coming from the primary interaction (known as *primary*² particles) were selected by requiring their impact parameters, measured with respect to the reconstructed primary vertex of the event, to be within a specified range.

4.3 Corrections

Data shown here have been fully corrected back to particle level in order to measure the distributions of stable (charged) particles coming from the primary pp interaction. This allows a direct comparison to MC generator predictions. Corrections are applied at both the event and track level.

The event-level corrections correct for missing events due to trigger and vertex requirements. Both trigger and vertex corrections were derived from data, the former by measuring the trigger efficiency of the MBTS with respect to a control trigger using the Inner Detector and the latter by directly measuring the primary vertex reconstruction efficiency using all triggered events.

The track-level corrections correct for detector inefficiencies and resolutions. The tracking efficiency was derived from MC samples taken through the full GEANT [6] detector simulation. The track-level corrections were applied in two dimensions (η , p_T) in order to eliminate most of the model dependence. Corrections for non-primary particles and particles outside of the kinematic range were also applied.

All corrections were derived separately for the different analyses and phase space regions. Measurements were not extrapolated into regions of phase space not seen by the detector (e.g. very low- p_T or far-forward particles). No attempt was made to correct for the contribution coming from diffractive processes; however, phase space regions with a suppressed diffractive component were considered (see Table 1). The event selection at the particle level is always well defined and reproducible, e.g. number of charged particles $n_{\text{ch}} \geq 2$, with $p_T > 100$ MeV and $|\eta| < 2.5$.

²Primary particles are defined as all particles with lifetime longer than 0.3×10^{-10} s originating from the primary interaction or from subsequent decay of particles with shorter lifetime.

5 Minimum bias measurements

‘Minimum bias’ is an experimentally defined term, referring to the selection of inelastic events with the minimum possible requirements necessary to ensure that an inelastic collision occurred. Minimum bias events can include both non-diffractive and diffractive processes, although the precise definition and relative contributions vary among experiments and analyses. Typically, minimum bias events are dominated by soft interactions, with low transverse momentum and low particle multiplicity.

The ATLAS MBTS trigger (see Section 4.1) is almost fully efficient, with a slightly lower efficiency in low- n_{ch} events. In an attempt to disentangle the effects coming from diffractive processes, ATLAS has measured the properties of minimum bias events in various phase space regions [7], as listed in Table 1. The high-multiplicity selections ($n_{\text{ch}} \geq 6, n_{\text{ch}} \geq 20$) were chosen specifically to reduce the contribution of diffractive processes to a negligible level. Kinematic properties that have been measured include the charged-particle multiplicity (n_{ch}), the charged-particle transverse momentum (p_T) and pseudorapidity (η) spectra and the average transverse momentum of charged particles as a function of the charged-particle multiplicity ($\langle p_T \rangle$ vs. n_{ch}).

Table 1: Phase space regions considered by the ATLAS minimum bias analysis [7]. The diffraction-suppressed phase space ($n_{\text{ch}} \geq 6, p_T > 500$ MeV, $|\eta| < 2.5$) was used for the PYTHIA AMBT1 tune [8]. The most inclusive phase space ($n_{\text{ch}} \geq 2, p_T > 100$ MeV, $|\eta| < 2.5$) was used for the PYTHIA AMBT2b tune [9]. The common LHC phase space was chosen by the LHC minimum bias and underlying event working group [10] in order to directly compare measurements across LHC experiments.

	Most inclusive		Diffraction suppressed		High p_T	LHC comparison	
$n_{\text{ch}} \geq$	2	1	20	6	1	1	1
p_T [GeV] >	0.1	0.5	0.1	0.5	2.5	0.5	1.0
$ \eta <$	2.5	2.5	2.5	2.5	2.5	0.8	0.8

Fig. 1 shows the corrected charged-particle multiplicity distributions at $\sqrt{s} = 7$ TeV for the most inclusive phase space region ($n_{\text{ch}} \geq 2, p_T > 100$ MeV, $|\eta| < 2.5$) considered by the analysis. There is an excess in the models relative to the data at low n_{ch} and a deficiency at high n_{ch} , a clear indication that the models have difficulty in describing both the low and high- n_{ch} regions simultaneously. The simulation predicts a significantly harder p_T spectrum for $p_T > 3$ GeV. Again here, the models have difficulty in describing the low- p_T ($p_T < 500$ MeV) and high- p_T ($p_T > 3$ GeV) regions simultaneously. At low values of n_{ch} , none of the models describe the $\langle p_T \rangle$ data very well. For $n_{\text{ch}} > 20$ the models vary widely both in slope and in absolute value.

Fig. 2 shows the corrected charged-particle multiplicity distributions for the diffraction-suppressed phase space region ($n_{\text{ch}} \geq 6, p_T > 500$ MeV, $|\eta| < 2.5$) at $\sqrt{s} = 7$ TeV. A comparison between Figs. 1 and 2 shows that the modeling of diffraction plays an important role here. However, the pseudorapidity density distribution (right plot) shows that diffraction is not the only culprit for the discrepancy between data and MC.

The energy evolution of minimum bias properties has also been studied by measuring the same distributions at two additional center-of-mass energies from early LHC running, $\sqrt{s} = 0.9$

MINIMUM BIAS AND UNDERLYING EVENT MEASUREMENTS WITH ATLAS

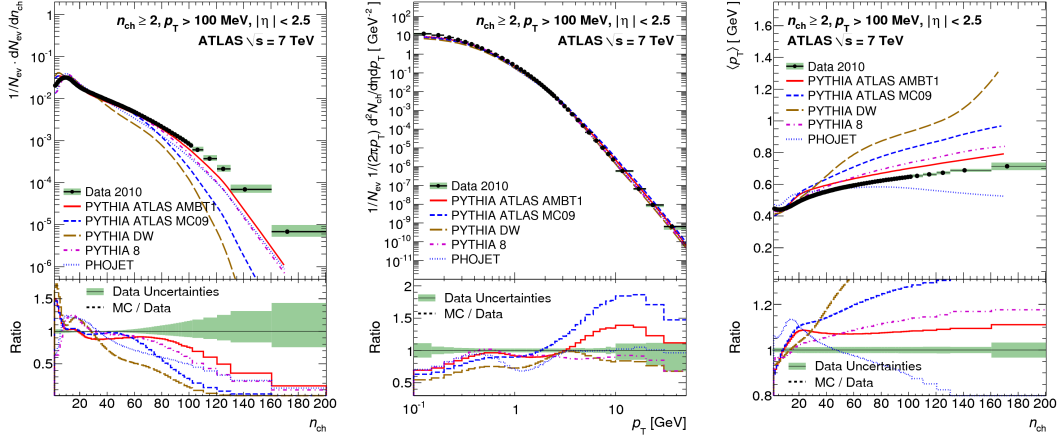


Figure 1: Corrected charged-particle multiplicity distribution (*left*), charged-particle multiplicity as a function of transverse momentum (*middle*) and the average transverse momentum as a function of the number of charged particles in the event (*right*) at $\sqrt{s} = 7$ TeV for the most inclusive phase space region ($n_{ch} \geq 2$, $p_T > 100$ MeV, $|\eta| < 2.5$) considered by the ATLAS minimum bias analysis [7]. The vertical error bars represent the statistical uncertainties, while the shaded areas show statistical and systematic uncertainties added in quadrature. The ratio of MC to data is shown at the bottom of each plot.

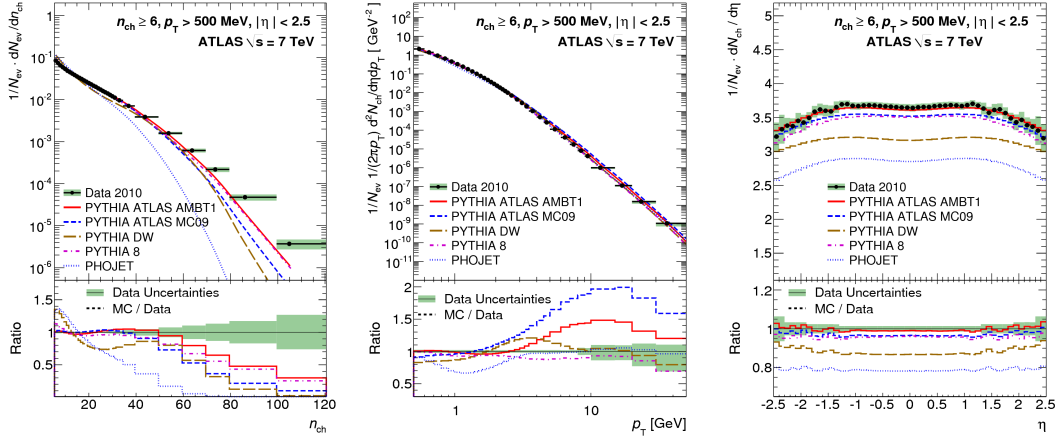


Figure 2: Corrected charged-particle multiplicity distribution (*left*) and charged-particle multiplicities as a function of transverse momentum (*middle*) and pseudorapidity (*right*) at $\sqrt{s} = 7$ TeV for the diffraction-suppressed phase space region ($n_{ch} \geq 6$, $p_T > 500$ MeV, $|\eta| < 2.5$) considered by the ATLAS minimum bias analysis [7]. The vertical error bars represent the statistical uncertainties, while the shaded areas show statistical and systematic uncertainties added in quadrature. The ratio of MC to data is shown at the bottom of each plot.

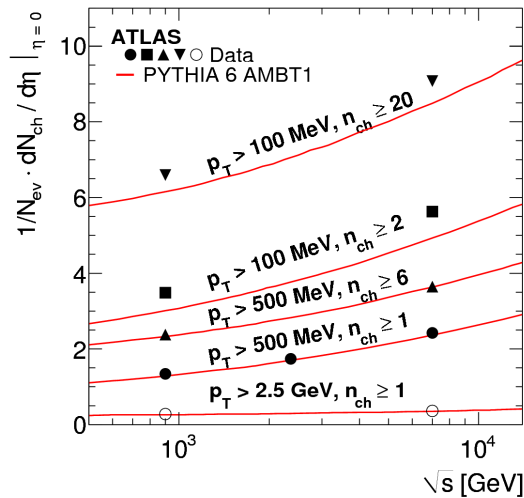


Figure 3: Average charged-particle multiplicity per unit of pseudorapidity in the central region ($\eta = 0$) as a function of the center-of-mass energy \sqrt{s} . All measured phase space regions (see Table 1) and center-of-mass energies ($\sqrt{s} = 0.9, 2.36$ and 7 TeV) from the ATLAS minimum bias analysis [7] are shown and compared to predictions by PYTHIA 6, with the AMBT1 tune [8]. Errors shown on data points are combined statistical and systematic uncertainties.

and 2.36 TeV. Fig. 3 shows a comparison of the pseudorapidity density in the central region ($\eta = 0$) as a function of \sqrt{s} for all phase space regions considered by ATLAS. The data points are compared to the first ATLAS tuning of PYTHIA 6 using ATLAS data, tune AMBT1 [8]. The AMBT1 tune gives a good description of the energy dependence for phase spaces with $p_T > 500$ MeV. However, the AMBT1 tune underestimates the amount of activity in the low- p_T region for both the most inclusive and diffraction-suppressed phase spaces.

6 Underlying event measurements

The underlying event is an irreducible background to all processes at hadron colliders such as the LHC. It consists essentially of all of the soft processes accompanying a hard scatter due to additional interacting partons from the same protons. From an experimental point of view, it is impossible to separate these contributions; however, topological properties of the event can be used to define a set of physics observables that are sensitive to different aspects of the UE.

The UE measurements performed by ATLAS thus far follow the lead of the analysis pioneered at the Tevatron by determining a high- p_T object in each event and then subdividing the azimuthal angle into *toward*, *transverse* and *away* regions, defined according to the azimuthal angular difference $\Delta\phi$ relative to the high- p_T object. The transverse region ($60^\circ < |\Delta\phi| < 120^\circ$) is assumed to be perpendicular to the axis defined by the hard $2 \rightarrow 2$ parton process and is therefore most sensitive to activity coming from the UE. The toward region is defined $|\Delta\phi| < 60^\circ$ and the away region $|\Delta\phi| > 120^\circ$.

ATLAS has measured properties of the UE using two independent methods: a track-based measurement using tracks reconstructed by the Inner Detector and associated to charged primary particles [11] and a cluster-based measurement using energy deposited in the calorimeters and associated to both charged and neutral primary particles [12]. The activity in all three regions with respect to the leading particle (either the highest- p_T track or cluster) has been studied. Observables measured by ATLAS include the particle density, the scalar $\sum p_T$ and the average p_T of particles per event $\langle p_T \rangle$. In both measurements, the highest- p_T particle was required to have transverse momentum $p_T^{lead} > 1$ GeV.

Fig. 4 shows the corrected (charged-)particle multiplicity distributions at $\sqrt{s} = 7$ TeV as a function of the azimuthal angle with respect to the leading track or particle $\Delta\phi$, for both the track- and cluster-based measurements and for various minimum values of p_T^{lead} . The development of a ‘jet-like’ region of higher density in the toward and away regions is observed as the p_T of the leading track or particle increases. The amount of UE activity is underestimated by most generators by about 20%. The particle density also has a different angular distribution than predicted by MC.

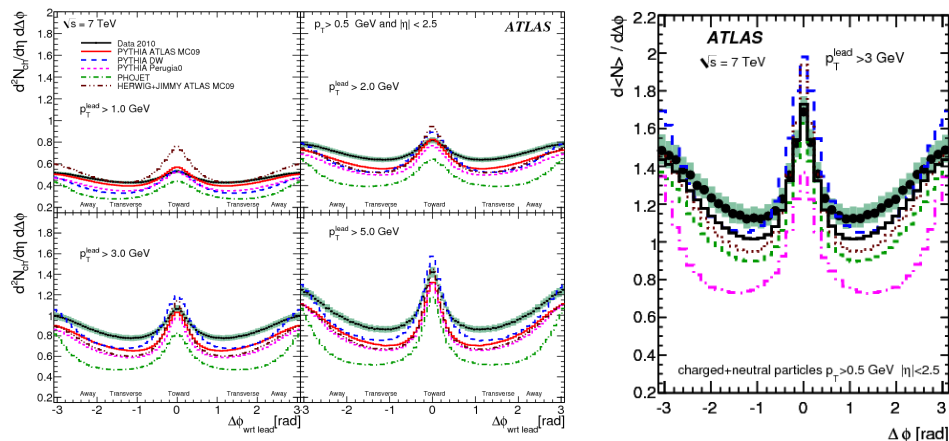


Figure 4: ϕ distribution of (charged)-particle densities ($p_T > 500$ MeV, $|\eta| < 2.5$) at $\sqrt{s} = 7$ TeV with respect to the leading (charged) particle (at $\Delta\phi = 0$), from the track-based (*left*) [11] and cluster-based (*right*) [12] underlying event measurements by ATLAS. The leading (charged) particle has been required to have a minimum p_T^{lead} as indicated on each of the plots and is excluded here. The error bars show the statistical uncertainty while the shaded areas show the combined statistical and systematic uncertainty.

The average number of charged particles in the transverse region doubles when going from $p_T^{lead} > 2$ GeV to > 5 GeV. Comparing the track-based measurement for $p_T^{lead} > 5$ GeV to the charged-particle distributions measured in the inclusive minimum bias spectrum, the activity in the UE is about a factor of two larger than the number of charged particles per unit pseudorapidity [11], a feature known as the ‘pedestal’ effect. This is because the UE selection requires a greater exchange of momentum, thereby reducing the diffractive contribution. Given that there is one hard scatter in the event, it is more probable to have MPI and the UE therefore has more activity than MB.

Fig. 5 (*left*) shows the corrected stable particle scalar $\sum p_T$ density at $\sqrt{s} = 7$ TeV in the transverse region as a function of the p_T of the leading particle (p_T^{lead}) from the cluster-based measurement. The summed particle p_T in the plateau characterizes the mean contribution of the underlying event to jet energies. The higher number density implies a higher p_T density as well. Most of the MC tunes considered show 10-15% lower $\sum p_T$ than the data in the plateau part of the transverse region.

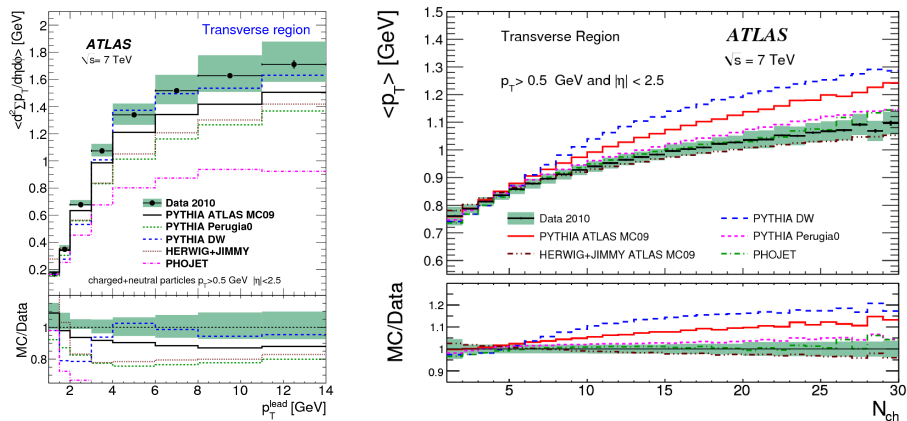


Figure 5: (*left*) Corrected scalar $\sum p_T$ density of stable particles ($p_T > 500$ MeV, $|\eta| < 2.5$) at $\sqrt{s} = 7$ TeV in the transverse region as a function of the p_T of the leading particle (p_T^{lead}) from the cluster-based underlying event measurement by ATLAS [12]. (*right*) Corrected mean p_T of charged particles at $\sqrt{s} = 7$ TeV for $p_T^{lead} > 1$ GeV as a function of the charged-particle multiplicity in the transverse region from the track-based underlying event measurement by ATLAS [11]. For both plots, the error bars show the statistical uncertainty while the shaded areas show the combined statistical and systematic uncertainty.

Fig. 5 (*right*) shows the corrected mean p_T of charged particles (p_T) at $\sqrt{s} = 7$ TeV versus the charged-particle multiplicity n_{ch} in the transverse region from the track-based UE measurement. The correlation between $\langle p_T \rangle$ and n_{ch} in each region is sensitive to the amount of hard versus soft processes contributing to the UE. Although not shown here, the profile in the away region is very similar to that of the transverse region, showing a monotonic increase of $\langle p_T \rangle$ with n_{ch} . The models tend to overestimate $\langle p_T \rangle$ in both the transverse and toward regions.

7 Conclusions

Data from the LHC provide a new energy scale for studying soft QCD. Charged-particle multiplicities have been measured by ATLAS in various regions of phase space, helping to disentangle the contribution coming from diffractive processes. The results of these measurements indicate a deficit of activity in models that were previously tuned to data from the Tevatron. Activity coming from the underlying event has been measured by ATLAS using track-based and cluster-based methods, providing statistically independent results. The activity measured in data is generally above the predictions from current model tunes.

The (charged-)particle distributions presented here expose limitations in the phenomenological models that prevent a simultaneous description of all measured observables in all regions of phase space. This is especially true when including particles with $p_T < 500$ MeV. The AMBT1 tune of PYTHIA 6, for example, highlighted that observables such as the pseudorapidity density are not well described by MC generators, even if they were taken as input to the tuning procedure. While some of these discrepancies can be reduced by further tuning of the MC event generators, it is likely that new formulations of certain components of the models will soon be needed.

Acknowledgments I would like to thank the LHC and ATLAS collaborations for their contributions to these measurements. I also thank the ATLAS speakers committee and the organizing committee of the MPI workshop for the opportunity to present these results. This work was supported in part by the Alexander von Humboldt Foundation.

References

- [1] T. Sjöstrand, S. Mrenna and P. Skands, *JHEP* **05**, 026 (2006).
- [2] R. Engel, *Z. Phys. C* **66**, 203 (1995).
- [3] L. Evans et al., *JINST* **3**, S08001 (2008).
- [4] ATLAS Collaboration, *JINST* **3**, S08003 (2008).
- [5] M. Bahr et al., *Eur. Phys. J. C* **58**, 639 (2002).
- [6] GEANT4 Collaboration, *Nucl. Instrum. Methods* **A506**, 250 (2003).
- [7] ATLAS Collaboration, *New J Phys.* **13**, 053033 (2011).
- [8] ATLAS Collaboration, Tech. Rep. ATLAS-PHYS-PUB-2010-002, CERN, Geneva (2010).
- [9] ATLAS Collaboration, Tech. Rep. ATLAS-PHYS-PUB-2011-008, CERN, Geneva (2011).
- [10] http://lpsc.web.cern.ch/LPCC/index.php?page=mb_ue_wg_docs
- [11] ATLAS Collaboration, *Phys. Rev. D* **83**, 112001 (2011).
- [12] ATLAS Collaboration, *Eur. Phys. J. C* **71**, 1636 (2011).

J/ψ production as a function of charged particle multiplicity in pp collisions at $\sqrt{s} = 7$ TeV with the ALICE experiment

Sarah Porteboeuf-Houssais for the ALICE Collaboration

Laboratoire de Physique Corpusculaire (LPC), Clermont Université, Université Blaise Pascal, CNRS-IN2P3, Clermont-Ferrand, France

DOI: <http://dx.doi.org/10.3204/DESY-PROC-2012-03/5>

We report on the first measurement of J/ψ production as a function of charged particle pseudo-rapidity density $dN_{\text{ch}}/d\eta$ in pp collisions at $\sqrt{s} = 7$ TeV with the ALICE experiment at the LHC. J/ψ mesons are detected down to $p_{\text{T}} = 0$ via their decays into e^+e^- pairs at mid-rapidity ($|y| < 0.9$) and into $\mu^+\mu^-$ pairs at forward rapidity ($2.5 < y < 4$). $dN_{\text{ch}}/d\eta$ is measured within $|\eta| < 1$. We compare results in the two different J/ψ rapidity ranges. Preliminary PYTHIA simulations are also presented.

1 Introduction

The production mechanism of heavy quarkonium states (eg. J/ψ) is very complex and is not fully understood. Various models such as the Color Singlet, nonrelativistic QCD approach (NRQCD) and the Color Evaporation Model aim to explain how a heavy resonance state can be produced in a hard process [1, 2]. This field is very active in theory development. In particular, describing the J/ψ production cross-section and polarization is a challenge for most of the models [3, 4, 5], including also the last LHC data [6, 7, 8, 9]. Furthermore, J/ψ production could be accompanied by a hadronic activity (hadrons produced in a cone around J/ψ) and it was pointed out that new observables are needed to constrain models [10]. In addition, it was proposed in [11, 12, 13] that initial state effects could modify J/ψ production due to gluon density fluctuations and a special transverse structure of the nucleon.

To look at exclusive final states and not only inclusive ones, it is needed to have a full description of hard processes in a complete event. A description of the interplay between the hard and the soft components of the event as well as of color flow and energy conservation is mandatory. In high energy proton-proton collisions, the total event multiplicity can have a substantial contribution from Multi-Parton Interactions (MPI). With MPI, several parton-parton interactions can occur in a single pp collision. MPI are commonly used to describe the soft underlying event but can also contribute on the hard and semi-hard scale, this contribution becoming more and more relevant with increasing energy [14, 15, 16]. The NA27 experiment performed a study that related open charm production and underlying event properties for pp collisions at $\sqrt{s} = 27$ GeV. It was found that the charged particle multiplicity distribution in events with and without charm production differs by 20% [17], indicating already a different behavior in multiplicity distribution.

In addition to MPI, other non-trivial effects could have an impact on multiplicity dependence and hard interactions. The measured charged particle multiplicity in pp collisions at LHC energies reaches values higher than in peripheral Cu-Cu at RHIC at $\sqrt{s_{NN}} = 200$ GeV [18]. With the high energy density reached in pp collisions at LHC energies, some models predict the occurrence of collective behaviour at LHC energies [19, 20], and one could consider the possibility of a modification of J/ψ yield in high multiplicity pp events due to collective phenomena [21].

In this article, we report on the measurement of relative J/ψ production $(dN_{J/\psi}/dy) / \langle dN_{J/\psi}/dy \rangle$ at mid ($|y| < 0.9$) and forward ($2.5 < y < 4$) rapidities as a function of the relative charged particle multiplicity $(dN_{ch}/d\eta) / \langle dN_{ch}/d\eta \rangle$ for pp collisions at $\sqrt{s} = 7$ TeV at LHC measured by the ALICE experiment [22]. We will then discuss a preliminary comparison with PYTHIA 6.4 simulations.

2 J/ψ production as a function of the relative charged particle multiplicity

A detailed description of the ALICE setup can be found in [23]. The J/ψ is detected in the di-electron channel with the central barrel ($|\eta| < 0.9$) and in the di-muon channel with the muon spectrometer ($-4 < \eta < -2.5$ ¹). The description of the part of the ALICE setup used in this analysis can be found in [22].

The results shown here were obtained by analyzing pp collisions at $\sqrt{s} = 7$ TeV collected in 2010. A sample of 3.0×10^8 minimum bias (MB) events and 6.75×10^6 μ -MB triggered events were used for J/ψ measurement in the di-electron and di-muon channels. This corresponds to an integrated luminosity of 4.5 nb^{-1} and 7.7 nb^{-1} respectively for the di-electron and di-muon channels. The MB pp trigger is defined with a signal in one of the two VZERO detectors, plus one readout chip signal in the Silicon Pixel Detector (SPD), in coincidence with proton bunches from both sides of the interaction region. The μ -MB trigger requires, in addition to the MB trigger, the detection of at least one muon with $p_T^{\text{trig}} > 0.5$ GeV/c in the acceptance of the muon arm. More details on the data sets, triggers, running conditions and relative normalization can be found in [22]. Events with an interaction vertex not within $|z_{vtx}| < 10$ cm are rejected. Pile-up events are identified by the presence of a second interaction vertex reconstructed in addition to the main vertex. They are rejected if the distance along the beam axis between the two vertices is larger than 0.8 cm, and if the second vertex has at least three associated tracklets. A tracklet is defined as any combinations of two hits in the SPD layers, one hit in the inner layer and one in the outer.

The charged particle density $dN_{ch}/d\eta$ is estimated using the number of tracklets N_{trk} reconstructed from hits in the SPD. Using simulated events, it was verified that N_{trk} is proportional to $dN_{ch}/d\eta$. Fig. 1 shows the distribution of the relative charged particle density $(dN_{ch}/d\eta) / \langle dN_{ch}/d\eta \rangle$ after correction for SPD inefficiencies. $\langle dN_{ch}/d\eta \rangle$ was measured for inelastic pp collisions with at least one charged particle in $|\eta| < 1$ and is equal to $6.01 \pm 0.01(\text{stat.})_{-0.12}^{+0.20}(\text{syst.})$ [24]. Vertical dashed lines show the limit of the 5 bins in multiplicity used in this analysis.

For J/ψ measurement in the di-electron channel, tracks are selected by requiring transverse momentum $p_T > 1$ GeV/c and a pseudo-rapidity cut of $|\eta| < 0.9$. Particle identification is

¹In the official ALICE reference frame the muon spectrometer is located at negative z positions and thus negative (pseudo-)rapidities. Since pp collisions are symmetric relative to $y = 0$, we have dropped the minus sign when rapidities are quoted.

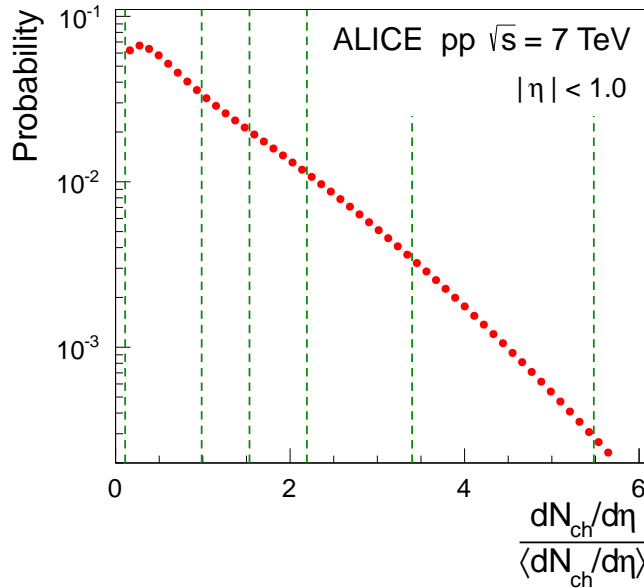


Figure 1: Distribution of the relative charged particle density $(dN_{ch}/d\eta)/\langle dN_{ch}/d\eta \rangle$ at mid-rapidity ($|\eta| < 1.0$) after correction for SPD inefficiencies. Vertical lines indicate the boundaries of multiplicity bins considered in this article.

performed by measuring the specific energy deposit dE/dx in the Time Projection Chamber (TPC) of the central barrel. The invariant mass distributions of e^+e^- pairs are measured in intervals of the charged particle multiplicity as measured via the SPD tracklets. Examples of such mass distributions are shown, for the lowest and highest multiplicity intervals in the two left panels of Fig. 2. The track rotation method (green squares in Fig. 2, left panel) is used to describe the combinatorial background in each multiplicity intervals as well as the like sign distributions (open blue circles in Fig. 2, left panel).

For J/ψ analysis in the di-muon channel, muon candidates are selected by requiring that at least one of the two muon candidates matches a trigger track reconstructed from at least three hits in the trigger chambers of the muon spectrometer. To remove muons produced at small angles that have crossed a significant fraction of the beam shield, a cut is applied on the radial coordinate of the track at the end of the front absorber ($R_{abs} > 17.5$ cm). To reject events very close to the edge of the muon spectrometer acceptance a cut is applied on the rapidity of the pair ($2.5 < y < 4$). To obtain the number of J/ψ in each multiplicity interval, a fit is used on the corresponding di-muon invariant mass distribution in the range $2 < M_{inv} < 5$ GeV/ c^2 . The line shapes of the J/ψ and $\psi(2S)$ are parametrised using a Crystal Ball function, while the underlying continuum is fitted with the sum of two exponential functions. Details on the quality of the fit results can be found in [6]. The two right panels of Fig. 2 show the measured di-muon invariant mass distributions together with the results of the fit procedure for the lowest and highest multiplicity intervals.

Fig. 3 presents the ratio of the J/ψ yield in a given multiplicity interval relative to the

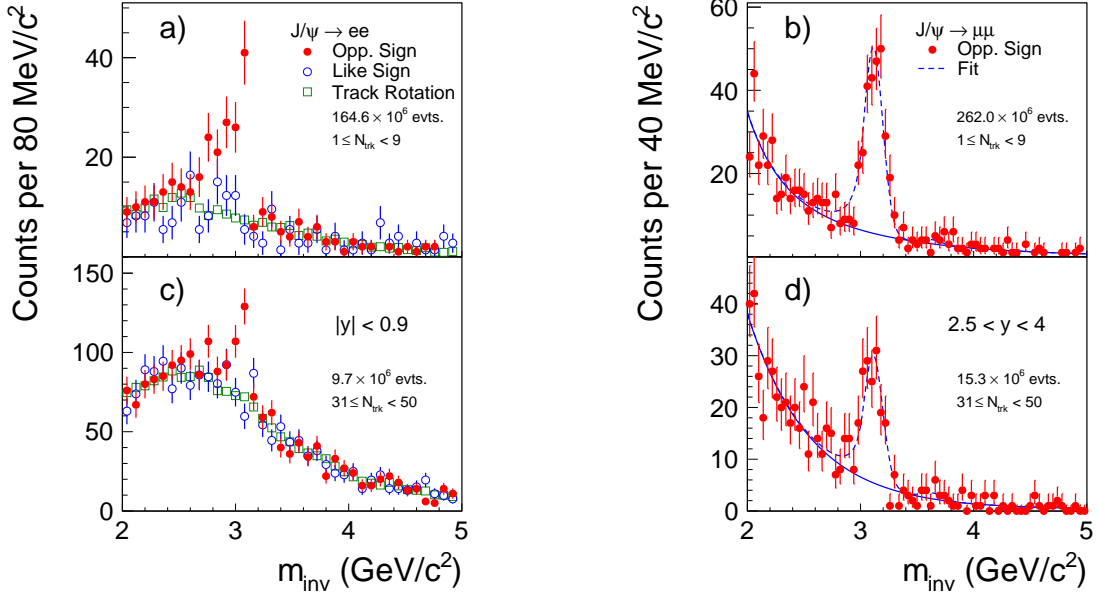


Figure 2: Opposite sign invariant mass spectra of the selected e^+e^- pairs [(a),(c)] and $\mu^+\mu^-$ pairs [(b),(d)] (full symbols) for the lowest [(a),(b)] and highest [(c),(d)] multiplicity bins. The number of events quoted in the figures refers to the corresponding minimum bias events.

minimum bias yield. Corrections regarding geometrical acceptance, reconstruction efficiency and their systematics cancel out in the ratio $(dN_{J/\psi}/dy)/\langle dN_{J/\psi}/dy \rangle$, where $(dN_{J/\psi}/dy)$ denotes the J/ψ yield measured in a given multiplicity bin and $\langle dN_{J/\psi}/dy \rangle$ corresponds to the averaged value for minimum bias reactions. It was checked by Monte Carlo simulations that these corrections do not depend on $dN_{\text{ch}}/d\eta$, in the range under consideration ($dN_{\text{ch}}/d\eta < 32.9$). The number of events used for the normalization of $\langle dN_{J/\psi}/dy \rangle$ is corrected for the fraction of inelastic events not seen by the trigger condition. After applying acceptance and efficiency corrections these values correspond to the values that can be extracted from data published in [6]: $\langle dN_{J/\psi}/dy \rangle = (8.2 \pm 0.8(\text{stat.}) \pm 1.2(\text{syst.})) \times 10^5$ for $J/\psi \rightarrow e^+e^-$ in $|y| < 0.9$, and $\langle dN_{J/\psi}/dy \rangle = (5.8 \pm 0.2(\text{stat.}) \pm 0.6(\text{syst.})) \times 10^5$ for $J/\psi \rightarrow \mu^+\mu^-$ in $2.5 < y < 4$.

For the di-electron analysis, the uncertainty due to background subtraction was obtained as the absolute differences using the like-sign and the track rotation methods. It is found to be between 2% and 12% for the different multiplicity intervals. For the di-muon analysis this is evaluated by varying the functional form of the background description (polynomial instead of exponential). It depends on the signal to background ratio and varies between 3% and 4%. For the muon measurement an additional systematic uncertainty comes from pile-up events and is estimated to be 6% in the first multiplicity interval and 3% in the others. To account for the possible changes of the p_T spectrum with event multiplicity, an additional systematic uncertainty is determined by varying the $\langle p_T \rangle$ of the J/ψ spectrum that is used as input to the determination of the Monte Carlo corrections between 2.6 and 3.2 GeV/c. A systematic uncertainty of 1.5% (3.5%) is found for the di-electron (di-muon) analysis. The total systematic error on $(dN_{J/\psi}/dy)/\langle dN_{J/\psi}/dy \rangle$ is given by the quadratic sum of the different contributions

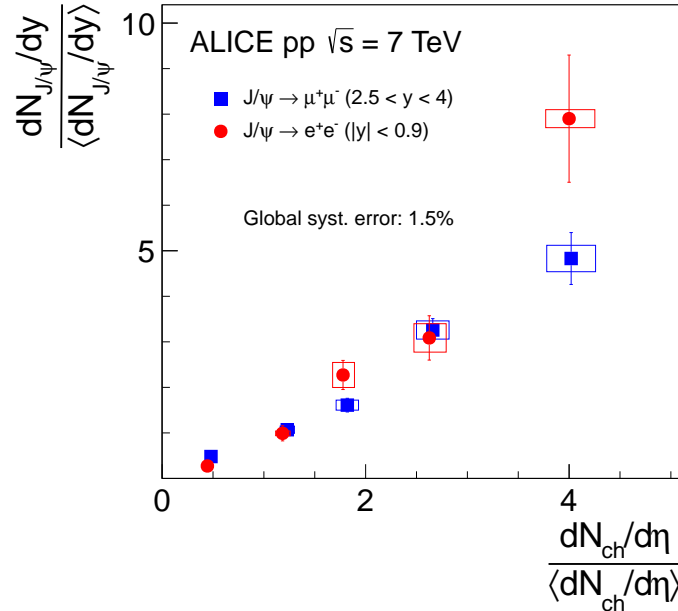


Figure 3: $dN_{J/\psi}/dy$ as a function of the charged particle multiplicity density at mid-rapidity $dN_{ch}/d\eta$. Both values are normalized by the corresponding value for minimum bias pp collisions. Two measurements are shown: in red circles at mid-rapidity ($J/\psi \rightarrow e^+e^-$, $|y| < 0.9$) and in blue squares at forward rapidities ($J/\psi \rightarrow \mu^+\mu^-$, $2.5 < y < 4$). Statistical uncertainties of the J/ψ yields are represented by error bars, while boxes reflect the quadratic sum of the point-to-point systematic uncertainties.

and amounts to 2.5 – 12 % depending on the multiplicity interval for the di-electron result. In the case of the di-muon analysis, it varies between 8% in the first and 6% in the last multiplicity interval. An additional global uncertainty of 1.5% on the normalization of $\langle dN_{J/\psi}/dy \rangle$ is introduced by the correction of the trigger inefficiency for all inelastic collisions. More detailed explanations on the estimation of systematic uncertainty estimated in this analysis can be found in [22].

In Fig. 3 an approximately similar linear increase of the relative J/ψ yield $(dN_{J/\psi}/dy) / \langle dN_{J/\psi}/dy \rangle$ with $(dN_{ch}/d\eta) / \langle dN_{ch}/d\eta \rangle$ is observed in both rapidity ranges. The enhancement relative to minimum bias J/ψ yield is a factor of approximately 5 at $2.5 < y < 4$ (8 at $|y| < 0.9$) for 4 times the minimum bias charged particle multiplicity. A possible explanation for the observed correlation could be that J/ψ is always accompanied by a strong hadronic activity biasing high multiplicity events. Such a mechanism could imply particular spatial distributions and J/ψ -hadron correlations could clarify the situation. Another possible mechanism would be initial density fluctuations accompanied by a specific structure of the nucleon. This mechanism seems to explain a factor 4 to 5 for charged multiplicity in J/ψ events 5 times larger than in minimum bias events [13].

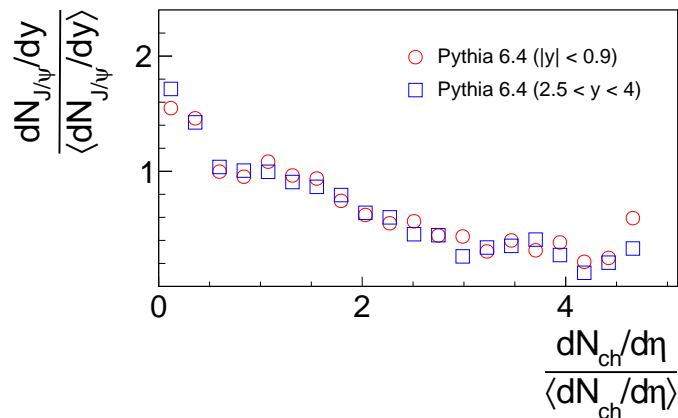


Figure 4: Relative J/ψ yield $(dN_{J/\psi}/dy)/\langle dN_{J/\psi}/dy \rangle$ as a function of the relative charged particle multiplicity density around mid-rapidity $(dN_{ch}/d\eta)/\langle dN_{ch}/d\eta \rangle$ calculated with PYTHIA 6.4.25 in the PERUGIA 2011 tune MSTP(5)=350. Results are shown at forward ($2.5 < y < 4$) and central ($|y| < 0.9$) rapidities for J/ψ produced in hard scatterings via the NRQCD framework (MSEL=63).

3 First PYTHIA 6.4 comparison

To compare our results to the predictions of a model, the model has to be able to reproduce all aspects of an event : the hard, the soft and semi-hard part of the event in a consistent framework. Event generators seem well suited to fulfill such a requirement. The considered event generator should also include heavy quarks (c and b) and heavy resonances such as J/ψ considering the correct masses of heavy quarks, energy conservation and color flow. Few models are left and none of them was built considering this new observable of J/ψ yield versus multiplicity. The first one we can think of is PYTHIA 6.4 [25] which is a pp event generator commonly used at the LHC. This is not the best model addressing quarkonium production, but it is extensively used, tuned and debugged. In this sense, this study is a first attempt of model-comparison for J/ψ yield versus multiplicity.

Detailed explanations on the physics model of PYTHIA 6.4 can be found in [25]. A pp event is composed by a hard $2 \rightarrow 2$ process. The two partons from the incoming protons can evolve through initial state radiation processes (ISR) before the hard subprocess. The two produced partons can also evolve with final state radiation processes (FSR). To produce J/ψ , several models are available, the color singlet (ISUB=86 with gluon fusion) where a J/ψ is produced with a gluon to ensure momentum conservation, and NRQCD (ISUB=421-439) where a pre-resonant state is produced. This pre-resonant state will then decay into a J/ψ emitting a soft gluon. In addition to the first hard interaction, a MPI scenario with varying impact parameter allows other incoming partons to undergo hard and semi-hard interactions. The first one is the hardest one. The following ones are ordered in hardness. In the last model of MPI implemented in PYTHIA 6.4, other interactions also evolve through ISR and FSR. In PYTHIA 6.4, quarkonia production in hard process is only available in the first hard interaction and not in the following ones of the MPI scenario. This was corrected in PYTHIA 8. In addition to

the hard production, J/ ψ can be produced from B decays. This source can be easily turned off, imposing B hadrons to be stable. J/ ψ can also be produced by the fragmentation of a cluster made of a $c\bar{c}$ pair produced by the branching of one or two gluons into $c\bar{c}$ pairs. Those gluons come from ISR and FSR. At the end of the procedure all produced partons are connected with strings that will fragment into hadrons via the LUND string model [25].

In this study the version PYTHIA 6.4.25 is used with Perugia 2011 (P2011) tune, a recent tuning of PYTHIA including the fit of LHC pp data at 7 TeV. It is well suited to describe multiplicity distributions. We consider in this article only MSTP(5)=350 which is the major P2011 tune [26]. B hadrons are forced to be stable. Two different data samples are generated. The first one is minimum bias (MSEL=1) for the denominator of our observable. The second sample used in the denominator contains J/ ψ . It is generated with MSEL=63 : J/ ψ are generated in hard processes with the NRQCD framework implemented in PYTHIA [25]. This second sample also contains J/ ψ produced by cluster fragmentation. The identification of J/ ψ from hard processes and J/ ψ from cluster fragmentation can be done with the flavour code of the mother, allowing the separation of the two contributions. Finally, the same kinematical cuts than in the ALICE experimental data sets are used to identify J/ ψ and charged particles. As in the data analysis the samples are normalised by the number of events and the mean number of charged particles. The obtained results are shown in Fig. 4 for PERUGIA 2011 tune with MSTP(5)=350. Results for J/ ψ produced in hard scattering only are presented for the same rapidity regions as in the data analysis.

Concerning cluster contribution, further studies indicate that this contribution is strongly enhanced by the color reconnection mechanism. Clusters come from gluons originating from ISR and FSR. Therefore, this contribution should scale with multiplicity, because high multiplicity events correspond to events with a high partonic activity (MPI, ISR, FSR) and so an enhanced probability to form a cluster. Nevertheless this contribution in PYTHIA 6.4.25 does not seem to be under control due to the way color reconnection is implemented [26] and warnings concerning the physics model of the cluster implementation can be found in the PYTHIA manual [25]. Thus, this contribution is excluded in results of Fig. 4.

The J/ ψ production from hard processes only, decreases as a function of relative multiplicity, which is in disagreement with the trend observed in the data (Fig. 3). A naïve interpretation would be that if the first hard process is independent from the other aspects of the event (ISR, FSR, MPI, underlying event), the J/ ψ yields should be flat as a function of multiplicity. It is not observed with PYTHIA 6.4.25, and further studies with other models are needed to understand this behaviour. E.g. a study with PYTHIA 8 might provide further insight. In PYTHIA 8, MPI could play a role in J/ ψ production with the possibility of quarkonium production in all the parton-parton interactions of the MPI scenario. Other event generators, such as CASCADE [27], that contains J/ ψ production [28] should be tested as well.

4 Conclusions

In summary, we have presented the first measurement of the J/ ψ yield as a function of the charged particle multiplicity $dN_{\text{ch}}/d\eta$, performed by the ALICE collaboration [22]. J/ ψ mesons are detected at mid-rapidity ($|y| < 0.9$) and forward rapidity ($2.5 < y < 4$), while $dN_{\text{ch}}/d\eta$ is determined at mid-rapidity ($|\eta| < 1$). An approximately linear increase of the J/ ψ yields with the charged particle multiplicity is observed. The increase is similar at forward and mid-rapidity, exhibiting an enhancement relative to minimum bias J/ ψ yield by a factor of about 5

at $2.5 < y < 4$ (8 at $|y| < 0.9$) for ~ 4 times the minimum bias charged particle multiplicity. A first comparison with PYTHIA 6.4 simulations was shown. J/ψ yields originated from the first hard interaction do not follow the same trend as seen in the data. Further studies are needed to explore the physics involved in such a new observable. From the experimental side the study of charged particle multiplicity dependence of Υ , open charm and also other hard observables such as jet and Drell-Yan production could bring more informations. Multiplicity studies for various p_T classes are also of interest. One could also propose an underlying event study replacing the leading jet by a J/ψ and J/ψ -hadrons correlation studies. From the event generators side, new studies are needed with PYTHIA 6.4, considering new tunes and other sets parameter. Other models should also be tested such as PYTHIA 8 and CASCADE.

References

- [1] N. Brambilla *et al.*, "Heavy quarkonium: progress, puzzles, and opportunities", Eur. Phys. J.C71 (2011), p.1534, arXiv:hep-ph/1010.5827
- [2] J. P. Lansberg, "On the mechanisms of heavy-quarkonium hadroproduction", Eur. Phys. J. C61 (2009) p.693, arXiv: hep-ph/0811.4005
- [3] M. Butenschoen and B. A. Kniehl, "Reconciling J/ψ production at HERA, RHIC, Tevatron, and LHC with NRQCD factorization at next-to-leading order," Phys. Rev. Lett. **106** (2011) 022003 arXiv:hep-ph/1009.5662
- [4] M. Butenschoen and B. A. Kniehl, "J/psi polarization at Tevatron and LHC: Nonrelativistic-QCD factorization at the crossroads," arXiv:hep-ph/1201.1872
- [5] J. P. Lansberg, " J/ψ production at $\sqrt{s}=1.96$ and 7 TeV: Color-Singlet Model, NNLO* and polarisation," arXiv:hep-ph/1107.0292
- [6] K. Aamodt *et al.* [ALICE Collaboration], "Rapidity and transverse momentum dependence of inclusive J/ψ production in pp collisions at $\sqrt{s} = 7$ TeV," Phys. Lett. B **704** (2011) 442 arXiv:hep-ex/1105.0380
- [7] G. Aad *et al.* [ATLAS Collaboration], "Measurement of the differential cross-sections of inclusive, prompt and non-prompt J/ψ production in proton-proton collisions at $\sqrt{s} = 7$ TeV," Nucl. Phys. B **850** (2011) 387 arXiv:hep-ex/1104.3038
- [8] V. Khachatryan *et al.* [CMS Collaboration], Eur. Phys. J. C **71** (2011) 1575 arXiv:hep-ex/1011.4193
- [9] R. Aaij *et al.* [LHCb Collaboration], "Measurement of J/ψ production in pp collisions at $\sqrt{s}=7$ TeV," Eur. Phys. J. C **71** (2011) 1645 arXiv:hep-ex/1103.0423
- [10] Z. Conesa del Valle *et al.*, "Three Days Of Quarkonium Production In Proton-Proton And Proton-Nucleus Collisions. Proceedings, Workshop, Quarkonium 2010, Palaiseau, France, July 29-31, 2010," Nucl. Phys. B, Proc. Suppl. 214 (2011) 187 p
- [11] L. Frankfurt *et al.*, "Evidence for color fluctuations in the nucleon in high-energy scattering," Phys. Rev. Lett. **101** (2008) 202003 arXiv:hep-ph/0808.0182
- [12] M. Strikman, "Transverse structure of the nucleon and multiparton interactions," Prog. Theor. Phys. Suppl. **187** (2011) 289
- [13] M. Strikman, "Comments on the observation of high multiplicity events at the LHC," Phys. Rev. D 84 011501(R) 2011, arXiv:hep-ph/1105.2285 and private communication
- [14] H. J. Drescher *et al.*, "Parton based Gribov-Regge theory," Phys. Rept. **350** (2001) 93 arXiv:hep-ph/0007198
- [15] T. Sjostrand and M. van Zijl, "A Multiple Interaction Model for the Event Structure in Hadron Collisions," Phys. Rev. D **36** (1987) 2019
- [16] P. Bartalini *et al.*, arXiv:1003.4220
- [17] M. Aguilar-Benitez *et al.* [LEBC-EHS Collaboration], "COMPARATIVE PROPERTIES OF 400-GeV/c PROTON - PROTON INTERACTIONS WITH AND WITHOUT CHARM PRODUCTION," Z. Phys. C **41** (1988) 191

- [18] B. Alver *et al.* [PHOBOS Collaboration], “Phobos results on charged particle multiplicity and pseudorapidity distributions in Au+Au, Cu+Cu, d+Au, and p+p collisions at ultra-relativistic energies,” *Phys. Rev. C* **83** (2011) 024913 arXiv:nucl-ex/1011.1940
- [19] A. Kisiel, *Phys. Rev. C* **84** (2011) 044913 arXiv:nucl-th/1012.1517
- [20] K. Werner, I. Karpenko and T. Pierog, “Hydrodynamical evolution in heavy ion collisions and p p scatterings at the LHC: Ridges in A A and p p scattering,” *Acta Phys. Polon. Supp.* **4** (2011) 629
- [21] S. Vogel *et al.*, “Heavy Quark Energy Loss in High Multiplicity Proton Proton Collisions at LHC,” *Phys. Rev. Lett.* **107** (2011) 032302 arXiv:hep-ph/1012.0764
- [22] K. Aamodt *et al.* [ALICE collaboration], submitted to PLB, arXiv:hep-ex/1202.2816.
- [23] K. Aamodt *et al.* [ALICE Collaboration], “The Alice Experiment At The Cern LHC,” *JINST* **3** (2008) S08002
- [24] K. Aamodt *et al.* [ALICE Collaboration], “Charged-particle multiplicity measurement in proton-proton collisions at $\sqrt{s} = 7$ TeV with ALICE at LHC,” *Eur. Phys. J. C* **68** (2010) 345 arXiv:hep-ex/1004.3514
- [25] T. Sjostrand, S. Mrenna and P. Z. Skands, *JHEP* **0605** (2006) 026 arXiv:hep-ph/0603175
- [26] P. Z. Skands, “Tuning Monte Carlo Generators: The Perugia Tunes,” *Phys. Rev. D* **82** (2010) 074018 arXiv:hep-ph/1005.3457, and private communication
- [27] H. Jung, “The CCFM Monte Carlo generator CASCADE” *Comput. Phys. Commun.* 143 (2002), 100-111, arXiv:hep-ph/0109102
- [28] H. Jung, S. Baranov, M. Deak, A. Grebenyuk, F. Hautmann, M. Hentschinski, A. Knutsson and M. Kramer *et al.*, “The CCFM Monte Carlo generator CASCADE version 2.2.03,” *Eur. Phys. J. C* **70** (2010) 1237 [arXiv:1008.0152 [hep-ph]].

Chapter 2

Monte Carlo development and tuning

Obtaining the CMS ridge effect with multiparton interactions

Sara Alderweireldt¹, Pierre Van Mechelen¹

¹Universiteit Antwerpen, Groenenborgerlaan 171, 2020 Antwerpen, België

DOI: <http://dx.doi.org/10.3204/DESY-PROC-2012-03/50>

We show that the “ridge” phenomenon in the two-particle angular correlation function, as observed by the CMS experiment, can be reproduced by implementing an impact parameter dependent azimuthal correlation of the scattering planes of individual partonic interactions. Such an approach is motivated by the observation that even for moderate impact parameters a substantial number of partonic interactions may be produced, while at the same time the protons are sufficiently far apart to create a preferential direction in azimuth.

A re-tune of the PYTHIA6 Z2 tune based on underlying event and minimum bias distributions measured at the LHC shows that a better description of data can be obtained with this approach and that some tension existing between underlying event and minimum bias distributions can be removed. We show that, even though the CMS result on the angular correlation function itself is not used in the re-tune, we can predict the appearance of long-range, near-side angular correlations in proton-proton collisions.

1 Introduction

The CMS ridge effect is a two-particle angular correlation effect observed by the Compact Muon Solenoid (CMS) experiment in Large Hadron Collider (LHC) proton-proton collisions at high charged track multiplicities ($N_{ch} > 110$) and in a specific transverse momentum range ($p_T = 1 - 3$ GeV). This effect, together with other visible structures in the $R(\Delta\eta, \Delta\phi)$ correlation distribution, was described in [1].

Two-particle correlation function $R(\Delta\eta, \Delta\phi)$ is defined as:

$$R(\Delta\eta, \Delta\phi) = \left\langle (\langle N \rangle - 1) \left(\frac{S_N(\Delta\eta, \Delta\phi)}{B_N(\Delta\eta, \Delta\phi)} - 1 \right) \right\rangle_{bins} \quad (1)$$

Data is binned according to charged track multiplicity N_{ch} . The signal $S_N(\Delta\eta, \Delta\phi)$ consists of the charged two-particle density, while the background $B_N(\Delta\eta, \Delta\phi)$ is given by the distribution of uncorrelated particle pairs – the product of two single-particle distributions. Finally, the data is averaged, weighted with bin multiplicity, over all bins. The analysis is repeated for four sets of data. On one hand two minimum bias sets (all N_{ch}), one including all particles with transverse momenta above 0.1 GeV and the other including all particles with transverse momenta between 1 and 3 GeV. On the other hand two high-multiplicity sets ($N_{ch} > 110$), again with the same two transverse momentum selections.

Some of the effects reported in [1], including the near-side peak at $(\Delta\eta, \Delta\phi) = (0, 0)$, the away-side ridge at $(\Delta\eta, \Delta\phi) = (\Delta\eta, \pi)$ and the Gaussian ridge at $(\Delta\eta, \Delta\phi) = (0, \Delta\phi)$ can be explained with single two-to-two partonic interactions. The first two are visible in all sets of data, while the third one is most clear in the minimum bias $p_T > 0.1$ GeV case. A fourth effect, the near-side ridge, a long-range azimuthal correlation at $(\Delta\eta, \Delta\phi) = (\Delta\eta, 0)$ only visible in high-multiplicity events at moderate p_T , requires further study. It is for this last effect that we propose a model.

For our study we observe the effect of our modification of the PYTHIA6 [2] Monte Carlo (MC) event generator on select observables and consider changes in a few existing PYTHIA6 parameters to counteract the side-effects of our modification. This latter step can be considered a re-tuning to CMS data. Note that we only use a limited set of CMS data and start from the existing PYTHIA6 tune Z2 [3]. More global tuning including other experiments' data was not within the scope of this study, but may be added later.

2 The azimuthal alignment model

For large enough impact parameter b (figure 1), the multiparton interactions in proton-proton collisions tend to lie in the collision plane of the hardest interaction and the final state particles will have similar azimuthal angle ϕ – this results in near-side effects. Furthermore, an explanation for the ridge effect with multiparton interactions would require enough such interactions to be taking place, which leads to high-multiplicity events. At the same time we require that the multiparton interactions are semi-hard, and thus yield moderate- p_T particles. Finally, we are dealing with incoming partons with very different x_{bj} and as such will have interactions in a broad pseudo-rapidity range η – this gives rise to long-range effects. So far, everything is still consistent with the observations made by CMS.

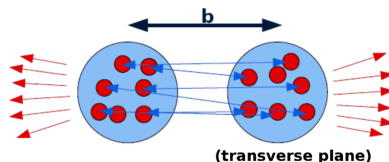


Figure 1: Protons separated by impact parameter b .

What is still a problem, is that high-multiplicity events are generally central collisions which have an impact parameter $b \sim 0$, while the definition of the collision plane of the hardest interaction requires large b . In light of this issue, we study whether a small upward fluctuation in the amount of multiparton interactions, for the case of moderate impact parameter, suffices to explain the CMS ridge effect.

The modification we introduce goes on top of the most recent multiparton interaction model currently in PYTHIA6 [4]. In this existing model, the amount of multiparton interactions, a measure for the activity, is inversely proportional to impact parameter b (VINT(139), rescaled to $b_{avg} = 1$ for the minimum bias case). The azimuthal angle $\hat{\phi}$ (VINT(24)) is chosen randomly. This last point makes that angular correlations – also the long-range, near-side ones – would be missing in events generated with PYTHIA6.

We propose sampling random points (x_i, y_i) in Gaussian proton profiles (figure 2), these protons being separated by impact parameter b , and using trigonometry to calculate the ϕ -offset from the hardest interaction. To allow for some tuning freedom we add a scaling parameter α to the impact parameter b . Ideally, the scaling parameter would be one. This results in:

$$\phi_i = \phi_{hardest} + \arctan\left(\frac{y_2 - y_1}{(x_2 + \alpha \cdot b/b_{avg}) - x_1}\right) \quad (2)$$

We implement the modification for two different modes of the multiparton interaction model of PYTHIA6 which both make use of hadronic overlap according to Gaussian distributions. In those cases, the above ϕ -definition makes sense. In our tuning activity reported in section 3, we focus on the mode which uses double-gaussian matter profiles (MSTP(82) = 4).

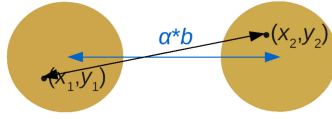


Figure 2: Sampling of random points in Gaussian proton profiles, separated by impact parameter b , and introduction of scaling parameter α to allow some tuning freedom.

The modification has several implications. We study two sets of data: CMS underlying event (UE) data [3], showing the charged multiplicity N_{ch} and transverse momentum sum $\sum p_T$ in the region transverse to a jet or hard interaction (figure 3), and CMS minimum bias (MB) data [5], showing the charged multiplicity N_{ch} integrated over azimuthal angle ϕ . By introducing the modification, we generate interactions with an azimuthal separation from the hardest interaction smaller than would be the case with the previous uniform azimuthal distribution. The interactions get shifted to the toward/away regions and the plateau for $N_{ch}^{transverse}$ drops (figure 4, top). Re-raising this plateau to describe the data requires a re-tune, modifying the p_T -cutoff and by proxy the activity, N_{ch} . The p_T -cutoff in PYTHIA6 is given by:

$$p_T^{min}(E_{CM}) = p_T^0 \cdot \left(\frac{E_{CM}}{E_{REF}}\right)^\gamma = PARP(82) \cdot \left(\frac{E_{CM}}{E_{REF}}\right)^{PARP(90)} \quad (3)$$

In contrast with the clear effect on UE results, we expect little or no sensitivity to the modification for the MB results, which are integrated over azimuth ϕ (figure 4, bottom). Possibly this difference in sensitivity also allows to lift some of the tension which exists between the UE and MB descriptions.

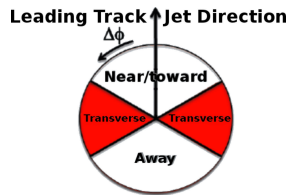


Figure 3: Areas in $\Delta\phi$ with respect to the leading track jet.

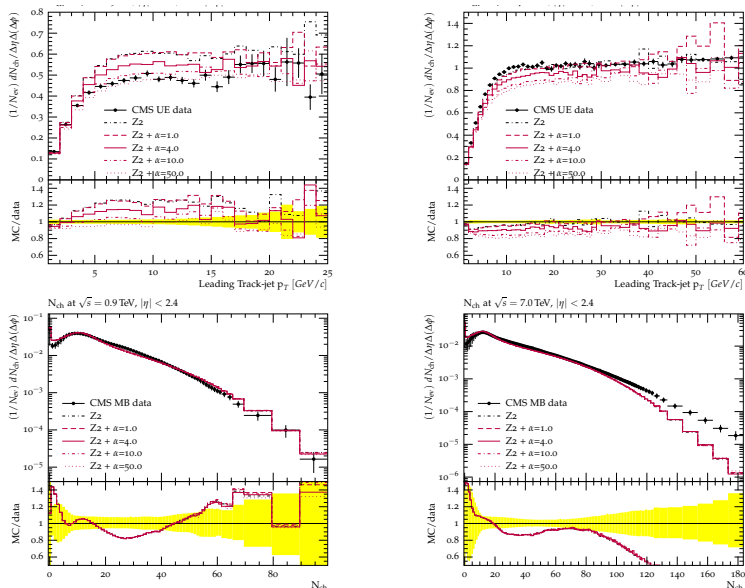


Figure 4: Overview of the sensitivity of N_{ch} observables in CMS UE (top) and MB (bottom) data to changes in scaling parameter α [purple], with Z2 [black] as a reference.

3 Tuning

In this second part we report the results of our small-scale automatized three-parameter re-tuning to the two earlier described CMS data sets. We start off with a review of the sensitivity of the observables to the three parameters and end with two tunes, one simple tune to just four N_{ch} distributions (transverse & total N_{ch} and 0.9 & 7.0 TeV) and one two-step tune to all MB and UE observables in the data sets. The first tune allows us to get a feeling of the parameter space in play, while the second one aims to reach a more solid result fixing the p_T -cutoff based on the MB observables (insensitive to scaling parameter α) and then using the UE observables to fix α . For the actual tuning, we make use of the PROFESSOR package [6], which takes care of automated tuning based on RIVET plots [7] of observables with reference data. For the interpretation of the tune result we make the comparison with existing tune Z2* rather than with tune Z2. Z2* is a PROFESSOR re-tuning of Z2 to CMS UE data, for parameters PARP(82) and PARP(90).

3.1 Sensitivity

The first observation (figure 5) is that PYTHIA6 p_T^0 -reference PARP(82) and energy-scaling parameter PARP(90) affect all activity, both transverse and total activity at both 0.9 and 7.0 TeV. For variations in the p_T^0 -reference (red/blue solid) the effect is the same at both energies, while for variations in the energy-scaling parameter (green/orange dashed) the effect is opposite at the two energies. This is to be expected since 0.9 and 7.0 TeV lie on both sides of reference energy 1.8 TeV used in the p_T -cutoff formula. On the part of α (figure 4), we can see a clear effect in the transverse region (UE dataset) and little to no effect in the ϕ -integrated case (MB dataset).

OBTAINING THE CMS RIDGE EFFECT WITH MULTIPARTON INTERACTIONS

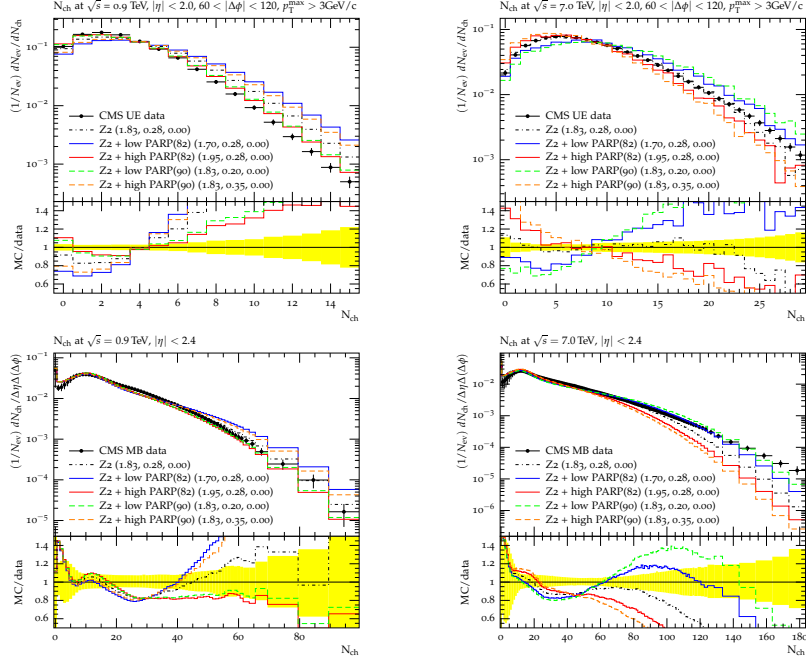


Figure 5: Overview of the sensitivity of N_{ch} observables in CMS UE (top) and MB (bottom) data to changes in PARP(82) [blue, red solid] and PARP(90) [green, orange dashed], with Z2 [black] as a reference. In brackets the values (PARP(82), PARP(90), α) are marked.

3.2 Tune one

This first crude tune, which we call Z2R, is made with the PROFESSOR package to just four observables (two UE and two MB) and confirms what is also more or less visible by eye. We want a moderate α , so as not to destroy the match with data so much that it cannot be restored (either in MB, UE or both), while still having enough power to introduce the intended long-range near-side effect. Next, we need a slight lowering in the p_T -reference (compared to optimal tune Z2*) to re-raise the N_{ch} plateau in the transverse region. The energy-dependence will be of less importance. We find exactly this in our Z2R PROFESSOR tune (table 1), for which we used the cubic interpolation mode. In general we find that, to begin with, the match with data for the four observables to which we tuned, is of the same quality as in the case of Z2*. Furthermore, also for the observables in the dataset which we did not include in the tuning, the match remains acceptable. We show the graphical result of tune Z2R (red solid) in figure 6, with tunes Z2 (black dotted) and Z2* (blue dashed) as reference.

	PARP(82)	PARP(90)	α
Z2	1.83	0.28	0.00
Z2*	1.93	0.23	0.00
Z2R	1.87	0.23	4.15

Table 1: Result of the 1-step 3-parameter tune to 4 observables.

3.3 Tune two

The second tune we consider is made in two-steps, we call it Z2R'. This time using all the observables in the same UE and MB CMS datasets, we again perform an automatized PROFESSOR tune with cubic interpolation. In the first step, the p_T -cutoff (both PARP(82) and PARP(90)) is fixed to the MB data, disregarding any match with UE data. In the second step, α is tuned to the UE data. After the first step, the match with data is good for MB, but less so for UE. After the second step, also the match with UE is restored to an acceptable level, comparable to the Z2* tune. Quantitatively, we again find the tune to be insensitive to PARP(90), while PARP(82) and α settle on values inbetween those of Z2* and Z2R (table 2, figure 6).

	PARP(82)	PARP(90)	α
Z2	1.83	0.28	0.00
Z2*	1.93	0.23	0.00
Z2R	1.87	0.23	4.15
Z2R'	1.90	0.23	2.67

Table 2: Result of the 2-step 3-parameter tune to all UE and MB observables.

3.4 The CMS ridge

Finally we consider correlation function $R(\Delta\eta, \Delta\phi)$, comparing results using tunes Z2R and Z2R' with those from the original paper (figure 7 (top row)). In the middle row, the results for Z2R are shown. It is clear that for high-multiplicity moderate- p_T events (middle, left), the long-range near-side ridge is visible, fully in agreement with the CMS results. In the same row (middle, centre), one can see that also for moderate-multiplicity events a ridge is visible, denoting that perhaps the effect of the modification is too strong. In the bottom row, the same plots are shown for tune Z2R'. Here, the effect is not strong enough at high-multiplicity (bottom, left), as no near-side ridge is visible, while it is still too strong at moderate-multiplicity (bottom, centre), where an unwanted ridge is visible. For high-multiplicity events, including all $p_T > 0.1$ GeV (middle/bottom, right), both tunes show similar effects. There is no near-side ridge and some broadening around $\Delta\eta = 0$ is visible, both in agreement with CMS data, but there is an unexplained additional peak at $(\Delta\eta, \Delta\phi) = (0, \pi)$.

4 Conclusions

We proposed a modification of PYTHIA6, explaining the ridge effect with multiparton interactions. The model introduces a correlation between the azimuth of the event planes of individual multiparton interactions and the event plane of the hardest interaction. This correlation can be naturally explained in a physical picture based on the impact parameter between the protons. The two main implications of this modification are the appearance of the near-side ridge in high-multiplicity moderate- p_T events and a shift in the activity in the transverse region. This latter effect can be counteracted by a re-tune of the p_T -cutoff parameters to underlying event data. In a slightly broader picture, minimum bias data can be included in the re-tuning. Implementing this with the PROFESSOR package, we found tunes Z2R and Z2R'.

OBTAINING THE CMS RIDGE EFFECT WITH MULTIPARTON INTERACTIONS

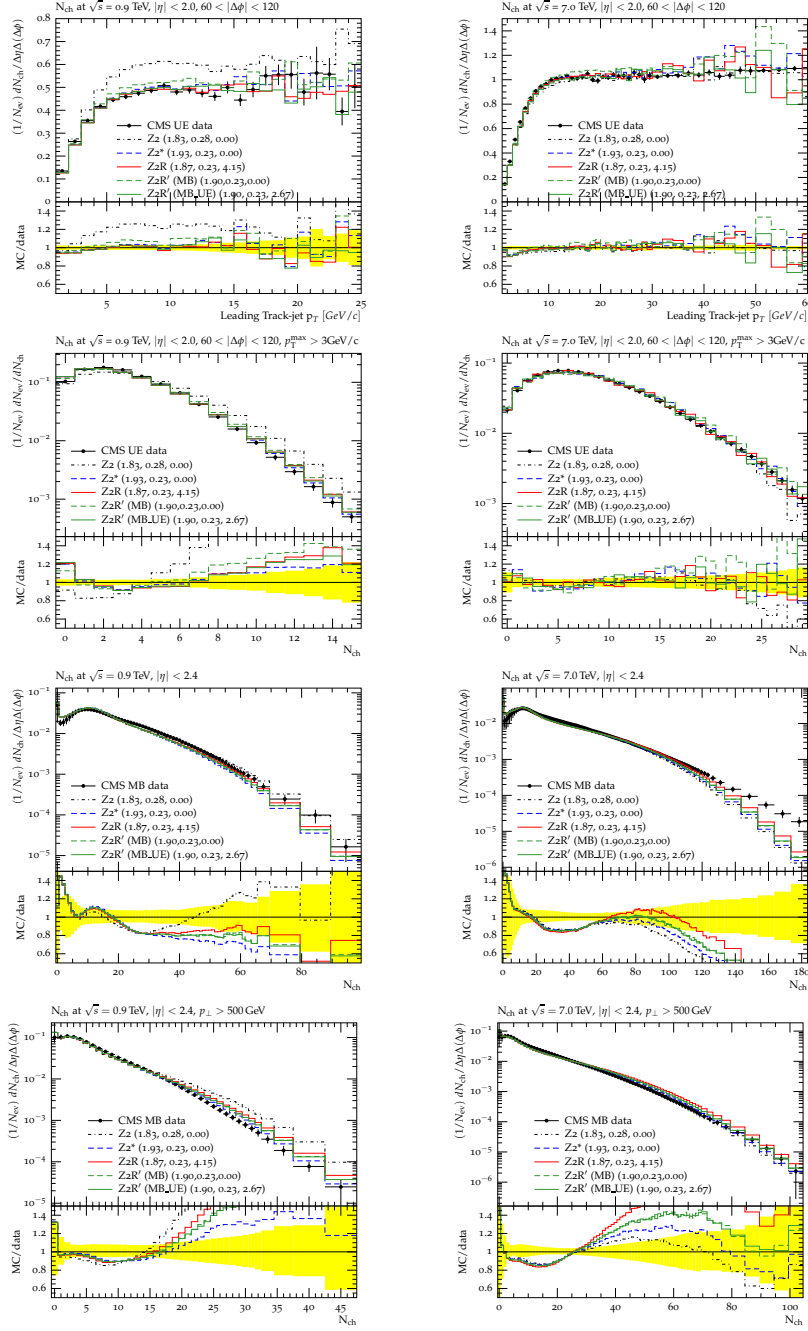


Figure 6: Performance of the **Z2R** [red solid] and the **Z2R'** [green dashed (intermediate), solid (final)] tunes, compared to tunes **Z2** [black dashdotted] and **Z2*** [blue dashed], for select observables in the full UE (rows 1-2) and MB (rows 3-4) data set. The four observables used for tune Z2R are given in rows 1 and 3.

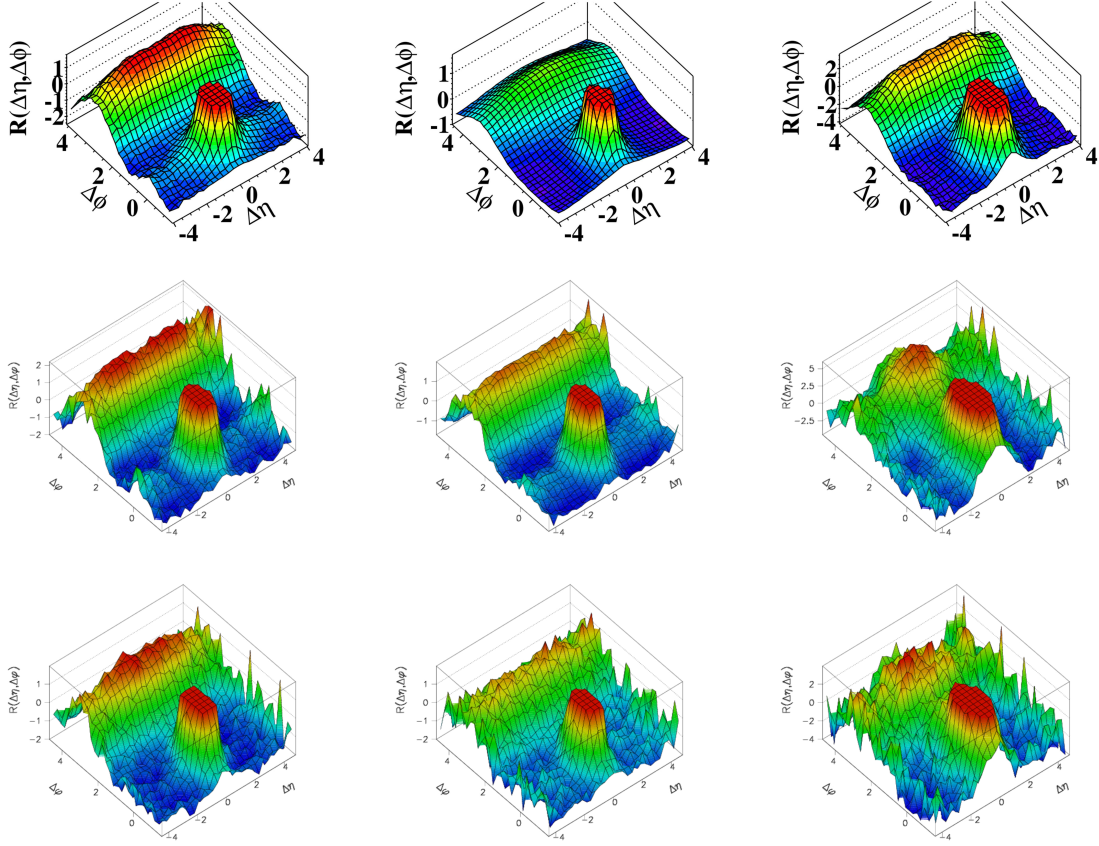


Figure 7: Results for $R(\Delta\eta, \Delta\phi)$: original (top row), Z2R (middle row) and Z2R' (bottom row); (left) high multiplicity, moderate p_T ; (centre) minimum bias, moderate p_T ; (right) high multiplicity, all $p_T > 0.1$ GeV.

References

- [1] CMS Collaboration, “Observation of Long-Range, Near-Side Angular Correlations in Proton-Proton Collisions at the LHC”, JHEP 1009 (2010) 091, arXiv:1009.4122.
- [2] T. Sjöstrand and S. Mrenna and P. Skands, “PYTHIA 6.4: physics and manual”, JHEP 0605 (2006) 026, arXiv:0603175.
- [3] CMS Collaboration, “Measurement of the Underlying Event Activity at the LHC with $\sqrt{s} = 7$ TeV and Comparison with $\sqrt{s} = 0.9$ TeV”, JHEP 1109 (2011) 109, CMS PAS QCD-10-010, arXiv:1107.0330.
- [4] P. Skands and D. Wickes, “Non-perturbative QCD Effects and the Top Mass at the Tevatron”, Eur. Phys. J. C52 (2007) 133, arXiv:0703081.
- [5] CMS Collaboration, “Charged particle multiplicities in pp interactions at $\sqrt{s} = 0.9, 2.36,$ and 7.0 TeV”, JHEP 1101 (2011) 079, CMS-PAS-QCD-10-004, arXiv:1011.5531.
- [6] A. Buckley et. al., “Systematic event generator tuning for the LHC”, Eur. Phys. J. C65 (2010) 331-357, arXiv:0907.2973.
- [7] A. Buckley et. al., “Rivet user manual”, arXiv:1003.0694.

Inclusive distributions in pp collisions at LHC energies compared with an adjusted DPMJET-III model with chain fusion

Fritz W. Bopp, Johannes Ranft

Siegen University, Siegen, Germany

DOI: <http://dx.doi.org/10.3204/DESY-PROC-2012-03/57>

A DPMJET-III model (DPMJET-III-2011) with chain fusion adjusted to include energy-dependent parameters is used to calculate inclusive distributions in p-p collisions at LHC energies. Presented are charged hadron rapidity distributions, transverse momentum distributions, multiplicity distributions as well as multiplicities at mid-rapidity as function of the collision energy. For hadrons with strangeness we present rapidity distributions and transverse momentum distributions. With the considered merely energy-dependent adjustments the obtained agreement with the transversal Λ and Ξ distribution is not satisfactory.

1 Introduction

Monte Carlo codes based on the two-component Dual Parton Model involving soft and hard hadronic collisions producing chains of particles are available since almost 20 years [1]. The present codes are:

PHOJET for h-h and γ -h collisions [2]
DPMJET-III for h-h, h-A and A-A collisions [3]

In distinction to earlier versions DPMJET-III is based on PHOJET for its h-h collisions. In such collision it is therefore - except for a few additions like the fusion discussed below - identical to PHOJET. PHOJET describes the production of strings. For the string decay it calls PYTHIA version 6.412 [4]. For a few special cases we found it necessary to change the PYTHIA fragmentation. These were done in the DPMJET part, leaving the PYTHIA code itself untouched. As we use the full program we will refer below just to DPMJET-III. We now outline its main additions.

Comparing DPMJET-III to RHIC data it was learned that something had to be done to decrease the particle density. As the strings are quite dense in impact parameter space interactions between strings are plausible. The expected percolation was modeled as fusion of close hadronic chains implemented in DPMJET-III [5] in 2004. The obtained reduction was very essential for central collisions of heavy ions, but fusion also changes the particle production in very high energy p-p collisions when the number of contributing chains obtained by a Glauber or eikonal formalism gets sizable.

RHIC and Fermilab data also contain interesting information about particle-antiparticle ratios [6]. For the baryon/antibaryon distribution the string fusion mentioned above can be

significant (i.e. two quark-antiquark strings can fuse to a diquark-antidiquark string yielding baryons and antibaryons).

In the diquark string decay used in PYTHIA one observes a dip in the ratio of the $\Omega/\bar{\Omega}$ spectra not seen in the data. A solution of the problem is to include a small contribution of diquark-diantiquark meson production in the first rank so that Ω can appear in the second rank. The idea is that such tetra-quark mesons are always produced but decay too fast to be identified in mass plots.

The LHC experiments did compare DPMJET-III to particle production at LHC-energies, see [7], [8] and [9]. There were some successful predictions of DPMJET. However, LHC experiments found that around 7 TeV the multiplicity rises faster with energy than predicted by DPMJET-III.

In order to make the program usable for ongoing data analyses at LHC energies we adjusted the program to improve the agreement with available experimental results. We allowed for an energy-dependence of string decay parameters. No differentiation between softer and harder strings was attempted. The new results of this modified version will be reported in section 3 and 4.

2 Modifications of DPMJET-III needed for LHC energies

There are essentially three additional modifications of DPMJET-III implemented in order to get better agreement with LHC data on particle production.

- (1) The first modification is connected to a problem with collision scaling known since 2004 [10]. DPMJET-III uses an eikonal formalism to determine the size of various multiple scattering contributions $P_{n,\{\alpha_i^f\},\{\alpha_i^b\}}$ where n is the number of chains and $\alpha_i^{f/b}$ is the Regge intercept depending on the diquark, valence quark or sea quark nature of the forward/backward parton of i -th chain. Let us consider the forward direction. For each such configuration the attributed energy fractions $\{x_i\}$ to these partons are then chosen with a factorizing structure function of the form:

$$P_{n,\{\alpha_i\}} \int \prod_i^n x_i^{\alpha_i-1} \delta(1 - \sum_j^n x_j)$$

in which the energy available for a scattering process depends on the remainder. There are two kinds of chains in DPMJET: Hard chains produced by hard collisions of partons from the colliding hadrons (typically large p_\perp) and soft chains representing soft hadron production in the collisions. In the factorizing formalism soft processes affect the energy sampled in hard processes. The discussion concerns the DPMJET part. PHOJET avoids the problem.

This turned out to be too simple. Experiments [11] gave evidence for collision scaling in not too central scattering processes¹. Collision scaling means, that exactly as many hard chains are produced as predicted by considering just hard collisions.

To correct for the missing collision scaling an additional parameter was introduced [10] which increases the number of hard collisions in such a way that collision scaling is obtained. We here adjusted these constants to the LHC data.

¹For central heavy ion collision collision scaling is lost as transport effects become important. So far these effects are not implemented.

- (2) LHC experiments [7, 8, 9] found that the produced hadron multiplicity rises with energy somewhat faster than the model. To obtain this faster rise with collision energy one needs to introduce energy-dependent parameters. This is not unreasonable. The time scale of the initial scattering is inversely proportional to the energy. This causes a more localized string and a widening of the p_{\perp} -distribution of the string ends, which was observed as one contribution to the multiplicity dependence of the average transverse momentum $\langle p_{\perp} \rangle_n$. There are of course many different parameters in PYTHIA which can be tuned in an energy-dependent way.

The solution which was adopted for the moment is not to search for a suitable, possible theoretically plausible energy-dependence but just to adjust parameters. The two parameters which determine the multiplicity of fragmenting chains are the Lund parameters PARJ(41) and PARJ(42) for which we use the following values:

$$\begin{array}{r}
 \text{for } E_{cm} \text{ (TeV)} \\
 \text{PARJ(41)} \\
 \text{PARJ(42)}
 \end{array}
 = \left| \begin{array}{c|c|c|c}
 \leq 3.0 & \in [3.0, 7.0] & \in [7.0, 14.0] & \geq 14.0 \\
 0.2 & 0.2 + (E_{cm} - 3)/40 & 0.3 + (E_{cm} - 7)/140 & 0.35 \\
 0.8 & 0.8 - (E_{cm} - 3)/20 & 0.6 - (E_{cm} - 7)/70 & 0.5
 \end{array} \right|$$

We do not continue to change PARJ(41) and PARJ(42) for E_{cm} larger than the maximum LHC energy of 14000 GeV. For the moment (in "DPMJET-III-2011") we replace in the FORTRAN code PARJ(41) and PARJ(42) by the values given in the table above as soon as in the input cards a change of PARJ(41) and PARJ(42) is demanded.

- (3) The third modification is connected to the production of strange hadrons. The production of K_s^0 mesons and of Λ and Ξ^- hyperons in p-p collisions was measured by the CMS Collaboration [19]. The program gave more K_s^0 than measured by CMS, while it obtained less Λ and Ξ^- production than measured by CMS. To increase the agreement with the measurements in this regard more energy-dependent parameters have to be introduced.

Hyperon and strange meson production in DPMJET-III is controlled by the Lund parameters PARJ(1), PARJ(2), PARJ(3), PARJ(5) and PARJ(6). The default of the parameter PARJ(2) was not touched. For the other parameters the following energy-dependent values (in the energy range up to $E_{cm} = 14$ TeV) were implemented:

$$\begin{array}{r}
 \text{for } E_{cm} \text{ (TeV)} \\
 \text{PARJ(1)} \\
 \text{PARJ(3)} \\
 \text{PARJ(5)} \\
 \text{PARJ(6)}
 \end{array}
 = \left| \begin{array}{c|c|c|c|c|c}
 \leq 0.5 & \in [0.5, 0.9] & \in [0.9, 1.0] & \in [1.0, 3.0] & \in [3.0, 7.0] & \geq 7.0 \\
 0.1 & 0.1 + \frac{(E_{cm}-0.5)}{4} & & & 0.2 & \\
 0.4 & 0.4 + \frac{(E_{cm}-0.5)}{0.25} & & & 2.0 & \\
 & & 0.5 & & \left| 0.5 - \frac{(E_{cm}-3.0)}{80} \right| & 0.45 \\
 & & & & 0.5 + \frac{(E_{cm}-1.0)}{10.91} & 1.05
 \end{array} \right|$$

3 Comparison of DPMJET-III-2011 results with LHC data on charged hadron production

We start to discuss the non single diffractive (nsd) and inelastic ($inel$) pseudo-rapidity distribution $dN_{ch}/d\eta_{cm}$ measured by the CMS and ALICE Collaborations.

In figure 1 we present for p-p collisions the non single diffractive data from CMS [12] at 900, 2360 and 7000 GeV and the non single diffractive and inelastic data from ALICE [13]

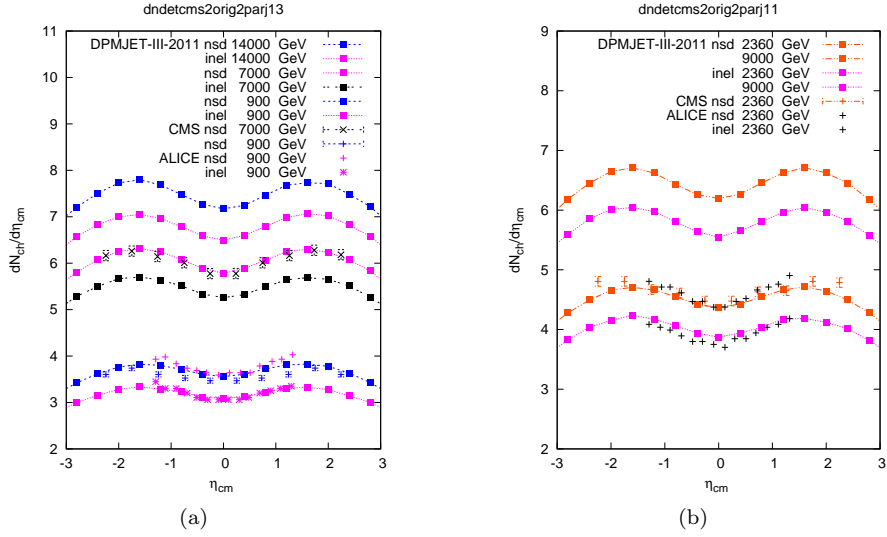


Figure 1: Central η_{cm} distributions of charged particles in (a) $\sqrt{s} = 900, 7000$ and 14000 GeV and (b) $\sqrt{s} = 2360$ and 9000 GeV p-p collisions compared to non single diffractive (*nsd*) and inelastic (*inel*) pseudo-rapidity distributions obtained with DPMJET-III-2011. The experimental data are from the CMS Collaboration [12] for *nsd* collisions and from the ALICE Collaboration [13] for *nsd* and *inel* collisions.

at 900 and 2360 GeV and compare them with the results from DPMJET-III-2011. Excellent agreement is obtained.

Also included are the results at 9000 and 14000 GeV in p-p collisions. At these energies the distributions are expected to be measured at the LHC in the future.

The energy-dependence of the central density $dN/d\eta_{cm}$ at $\eta_{cm} = 0$ is presented in figure 2(a) for p-p collisions of *nsd* and *inel* events. The DPMJET-III-2011 results are compared with data from various energies. In all cases a good agreement is obtained.

In figure 2(b) we compare p_t distributions from the DPMJET-III-2011 in p-p collisions at $\sqrt{s} = 900, 2360$ and 7000 GeV with representative experimental data points from the CMS Collaboration [7]. The agreement between the modified program and the CMS data points is good.

In figures 3 we compare the multiplicity distributions for $|\eta| < 1$ with experimental data from the ALICE Collaboration [13]. Again a reasonable agreement is obtained.

Unfortunately here the situation becomes even more problematic. In figure 4(a) we compare the dn/dy_{cm} distributions of Ξ hyperons in the DPMJET-III-2011 with the measurements of CMS. The modified model predicts Ξ distributions about three times as large as measured by CMS.

We have modified the parameters in such a way, that the Λ hyperons agree with the CMS data. The same parameters should also lead to agreement for the Ξ hyperons. They do not (figure 5). We can only conclude, that so far we do not fully understand the production of Ξ hyperons.

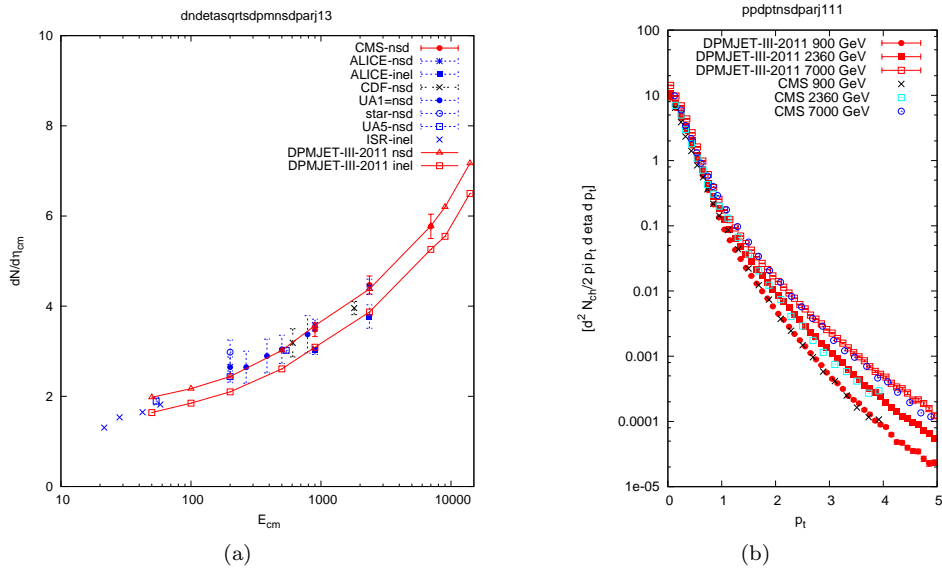


Figure 2: (a) Central η_{cm} values of all charged particles in p - p collisions compared to DPMJET-III-2011 results. The experimental data are from the CMS Collaboration [12] for nsd collisions and from the ALICE Collaboration [13] for nsd and $inel$ collisions. Further data are from UA5 [14], the ISR [15], STAR [16], UA1 [17] and CDF [18]. (b) Transverse momentum distributions in p - p collisions at $\sqrt{s} = 900, 2360$ and 7000 GeV. We compare data from the CMS Collaboration [7] to DPMJET-III-2011 results.

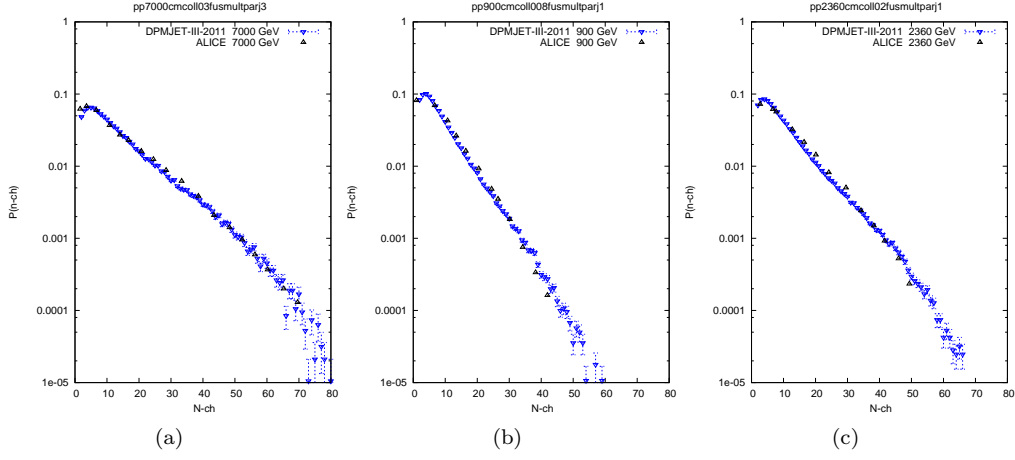


Figure 3: (a) Multiplicity distributions in p–p collisions at $\sqrt{s} = 7000$ GeV. We compare data for $|\eta| < 1$ from the ALICE Collaboration [13] to the DPMJET-III-2011 result. (b) Multiplicity distributions in p–p collisions at $\sqrt{s} = 2360$ GeV. We compare data for $|\eta| < 1$ from the ALICE Collaboration [13] to the DPMJET-III-2011 result. (c) Multiplicity distributions in p–p collisions at $\sqrt{s} = 900$ GeV. We compare data for $|\eta| < 1$ from the ALICE Collaboration [13] to the DPMJET-III-2011 result.

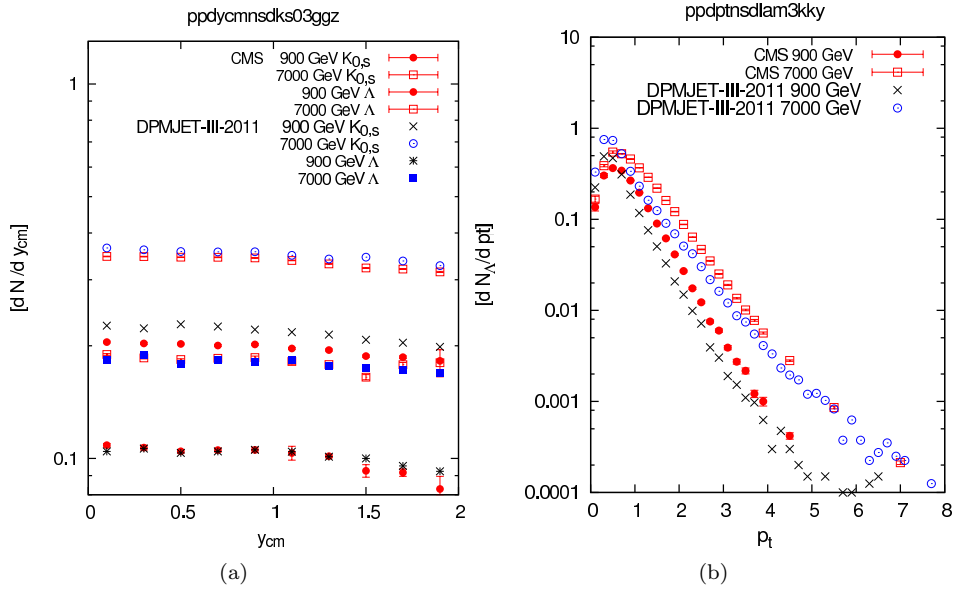


Figure 4: (a) dn/dy_{cm} distributions in p–p collisions of K_s^0 and \bar{K}_s^0 as well as Λ and $\bar{\Lambda}$. We compare LHC data from the CMS Collaboration [19] to the DPMJET-III-2011 result. (b) Transverse momentum distributions of Λ and $\bar{\Lambda}$. We compare experimental data from the CMS Collaboration [19] to the DPMJET-III-2011 result.

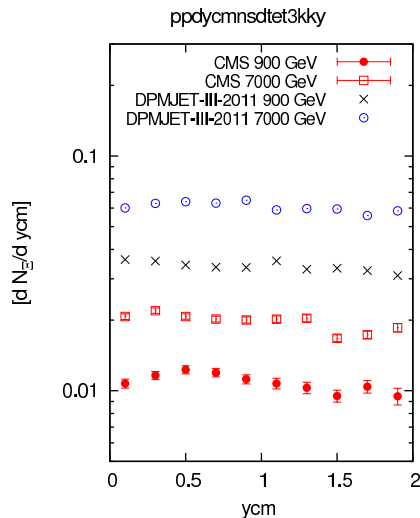


Figure 5: dn/dy_{cm} distributions of Ξ and $\bar{\Xi}$. We compare experimental data from the CMS Collaboration [19] to DPMJET-III-2011 calculations.

4 Comparison of DPMJET–III-2011 results with LHC data on the production of strange hadrons

Strange hadron production in p-p collisions was measured by the CMS Collaboration [19]. It determined the production of K_s^0 mesons and the production of Λ and Ξ^- hyperons.

Similar data on the production of strange hadrons were also given by the ALICE Collaboration [20]. We did not include them so far as they do not affect the consideration discussed below.

In figure 4(a) we compare the production of K_s^0 and Λ hyperons in dependence of the dn/dy_{cm} . With energy-dependent parameters good agreement of the DPMJET-III-2011 and the CMS measurements is obtained.

But the situation is not perfect. CMS also measures transverse momentum distributions. Comparing transverse momentum distributions we find the shape of the distributions to differ. This can be seen in figure 4(b) showing the transverse momentum distributions of Λ hyperons. Above 1 GeV the model is below the data. A similar problem seems to appear in many model calculations [21].

If we would also adjust the parameters in such a way, that the agreement between the transverse momentum distributions is optimal in this region, we would obtain a disagreement in the dn/dy_{cm} distributions.

5 Conclusions

DPMJET-III is a code for hadron production in hadron-hadron, photon-hadron, hadron-nucleus and nucleus-nucleus collisions [2, 3], which is about 10 to 15 years old. The measurements

of hadron production in p-p collisions at LHC energies gave the occasion to check how well DPMJET-III agrees to the data in this higher energy region. We knew already from comparisons at the lower FERMILAB energies, that not all features of DPMJET-III are valid at higher energies, a well known example is the collision scaling [22] in hadron-nucleus and nucleus-nucleus collisions and which is not a property of DPMJET-III.

Comparing DPMJET-III with the LHC data we found further problems of DPMJET-III. The energy-dependence of hadron production measured by the LHC collaborations at 7 TeV differs from the one predicted by the original DPMJET-III. In the present paper we find, that this energy-dependence can be corrected in DPMJET-III by making in DPMJET-III the PYTHIA-parameters energy dependent. We consider the introduction of energy-dependent parameters only as a temporary solution to get agreement of DPMJET-III with the new LHC data.

A more permanent solution will require deeper changes in the program. Of course the parameters entering DPMJET-III, PHOJET and PYTHIA should not be adjusted per hand to determine the energy-dependence of the hadron production models. This energy-dependence should be an intrinsic property of the hadron production models. We conclude that we need a new version of the model which agrees better with the data in the new energy region opened by the LHC.

References

- [1] P. Aurenche, F. W. Bopp, R. Engel, D. Pertermann, J. Ranft, S. Roesler, *Comput. Phys. Commun.* **83** (1994) 107-123. [arXiv:hep-ph/9402351].
- [2] R. Engel, *Z. Phys. C* **66** (1995) 203;
R. Engel and J. Ranft, *Phys. Rev. D* **54** (1996) 4244.
- [3] S. Roesler, R. Engel and J. Ranft, *Proc. of Monte Carlo 2000*, Springer Verlag, Lisboa (2000), p.1033 [arXiv:hep-ph/0012252].
- [4] T. Sjostrand, S. Mrenna, P. Z. Skands, *JHEP* **0605** (2006) 026 [arXiv:hep-ph/0603175].
- [5] J. Ranft, R. Engel and S. Roesler, *Nucl. Phys. B (Proc. Suppl.)* **122** (2003) 392.
- [6] F. W. Bopp, J. Ranft, R. Engel, S. Roesler, *Phys. Rev. C* **77** (2008) 014904 [hep-ph/0505035].
- [7] CMS Collaboration, arXiv:1005.3299 [hep-ex], arXiv:1011.5531 [hep-ex] and arXiv:1012.1605 [hep-ex].
- [8] ALICE Collaboration, arXiv:1004.3514 [hep-ex], arXiv:1007.0719 [hep-ex], arXiv:1010.2448 [hep-ex] and arXiv:1102.2369 [hep-ex].
- [9] ATLAS Collaboration, arXiv:1003.3124 [hep-ex] and arXiv:1010.0843 [hep-ex].
- [10] F. W. Bopp, J. Ranft, R. Engel and S. Roesler, "RHIC data and the multichain Monte Carlo DPMJET-III", arXiv:hep-ph/0403084 based on a poster subm. to the 17th Int. Conf. on Ultra relativistic nucleus-nucleus collisions, Oakland, Calif. USA (2004).
- [11] J. L. Klay, *J. Phys. G* **31** (2005) S451-S464 [arXiv:nucl-ex/0410033].
- [12] CMS Collaboration, *J. High Energy Phys.*, **2010** (2010) 02041.
- [13] ALICE Collaboration, arXiv:1102.2369 [hep-ex].
- [14] UA5 Collaboration, *Z. Phys. C* **33** (1986) 1.
- [15] Aachen-CERN-Heidelberg-Munich Collaboration, *Nucl. Phys. B* **129** (1977) 365.
- [16] STAR Collaboration, *Phys. Rev. C* **79** (2009) 034909.
- [17] UA1 Collaboration, *Nucl. Phys. B* **335** (1990) 261.
- [18] CDF Collaboration, *Phys. Rev. D* **41** (1990) 2330.
- [19] CMS Collaboration, arXiv:1102.4282 [hep-ex] and with corrections as given in <http://hepdata.cedar.ac.uk/view/p8016>.

- [20] K. Aamodt, A. Abrahantes Quintana, D. Adamova, A. M. Adare, M. M. Aggarwal, G. Aglieri Rinella, A. G. Agocs, S. Aguilar Salazar *et al.*, *Eur. Phys. J. C* **71** (2011) 1594 [arXiv:1012.3257 [hep-ex]].
- [21] Hai-Yan Long et al., arXiv:1103.2618 [hep-ph].
- [22] S. S. Adler *et al.* [PHENIX Collaboration], *Phys. Rev. Lett.* **91** (2003) 072303. [arXiv:nucl-ex/0306021].

Multiparton interactions in Herwig++

Stefan Gieseke^{1*}, Christian Röhr¹, Andrzej Siodmok^{1,2}

¹Karlsruhe Institute of Technology (KIT), 76128 Karlsruhe, Germany

²University of Manchester, Manchester, UK

DOI: <http://dx.doi.org/10.3204/DESY-PROC-2012-03/45>

We summarize the implementation of a model for multiple partonic interactions in HERWIG++. Some studies of colour reconnection models are presented and conclusions are drawn regarding the underlying physics.

1 Introduction

Tevatron and early LHC data have shown the importance of Multiple Partonic Interaction (MPI) models in order to give an accurate Monte Carlo simulation of minimum bias events and the underlying event in hard partonic collisions [1, 2, 3, 4, 5, 6, 7, 8, 9, 10, 11, 12, 13]. The major Monte Carlo event generators HERWIG [14], PYTHIA [15, 16] and SHERPA [17] by now all have an MPI model in order to simulate the underlying event. In this contribution, we summarize the MPI model in the event generator HERWIG++.

2 MPI model in Herwig++

The starting point of our model is the observation that the hard inclusive cross section for dijet production,

$$\sigma^{\text{inc}}(s; p_t^{\text{min}}) = \sum_{i,j} \int_{p_t^{\text{min}2}} dp_t^2 f_{i/h_1}(x_1, \mu^2) \otimes \frac{d\hat{\sigma}_{i,j}}{dp_t^2} \otimes f_{j/h_2}(x_2, \mu^2),$$

eventually exceeds the total cross section at hadron colliders. This leads us to the interpretation that in fact the inclusive cross section counts not only single hard events but all hard events that occur in parallel during the very same hadron-hadron collision. With the key assumption of *independent* multiple partonic interactions we may interpret this as

$$\sigma^{\text{inc}} = \bar{n} \sigma_{\text{inel}},$$

with the average number of hard scatters \bar{n} and σ_{inel} the ‘unitarized’ inelastic cross section. With statistically independent scatters (eikonal approximation) we are lead to a Poisson distribution of the number m of additional scatters,

$$P_m(\vec{b}, s) = \frac{\bar{n}(\vec{b}, s)^m}{m!} e^{-\bar{n}(\vec{b}, s)}.$$

*Speaker

Hence, we get σ_{inel} :

$$\sigma_{\text{inel}} = \int d^2\vec{b} \sum_{m=1}^{\infty} P_m(\vec{b}, s) = \int d^2\vec{b} \left(1 - e^{-\bar{n}(\vec{b}, s)}\right) .$$

Comparing with a unitarized scattering amplitude in scattering theory in the eikonal approximation $a(\vec{b}, s) = \frac{1}{2i}(e^{-\chi(\vec{b}, s)} - 1)$ we can identify the eikonal function $\chi(\vec{b}, s)$,

$$\sigma_{\text{inel}} = \int d^2\vec{b} \left(1 - e^{-2\chi(\vec{b}, s)}\right) \quad \Rightarrow \quad \chi(\vec{b}, s) = \frac{1}{2}\bar{n}(\vec{b}, s) .$$

The eikonal function or the average number of scatters is calculated in the parton model as

$$\begin{aligned} \bar{n}(\vec{b}, s) &= L_{\text{partons}}(x_1, x_2, \vec{b}) \otimes \sum_{ij} \int dp_t^2 \frac{d\hat{\sigma}_{ij}}{dp_t^2} \\ &= \sum_{ij} \frac{1}{1 + \delta_{ij}} \int dx_1 dx_2 \int d^2\vec{b}' \int dp_t^2 \frac{d\hat{\sigma}_{ij}}{dp_t^2} D_{i/A}(x_1, p_t^2, |\vec{b}'|) D_{j/B}(x_2, p_t^2, |\vec{b} - \vec{b}'|) . \end{aligned}$$

We assume the momentum \otimes transverse space distributions to factorize,

$$D_{i/A}(x, p_t^2, |\vec{b}|) = f_{i/A}(x, p_t^2) G_A(|\vec{b}|) .$$

Here, $f_{i/A}(x, p_t^2)$ are the ordinary parton distribution functions and the spatial distribution of partons $G_A(|\vec{b}|)$, which is obtained from elastic e^-p scattering, so we get

$$\bar{n}(\vec{b}, s) = \sum_{ij} \frac{1}{1 + \delta_{ij}} \int dx_1 dx_2 \int d^2\vec{b}' \int dp_t^2 \frac{d\hat{\sigma}_{ij}}{dp_t^2} f_{i/A}(x_1, p_t^2) G_A(|\vec{b}'|) f_{j/B}(x_2, p_t^2) G_B(|\vec{b} - \vec{b}'|) .$$

Now we can carry out the \vec{b}' integration, factor off the overlap function $A(\vec{b})$ and identify the inclusive cross section,

$$\bar{n}(\vec{b}, s) = A(\vec{b}) \sigma^{\text{inc}}(s; p_t^{\text{min}}) , \quad A(\vec{b}) = \int d^2\vec{b}' G_A(|\vec{b}'|) G_B(|\vec{b} - \vec{b}'|) .$$

So, finally we arrive at the following expression for the eikonal,

$$\chi(\vec{b}, s) = \frac{1}{2}\bar{n}(\vec{b}, s) = \frac{1}{2}A(\vec{b})\sigma^{\text{inc}}(s; p_t^{\text{min}}) .$$

This model of independent partonic interactions was first implemented in Pythia [18] and similarly in the JIMMY add-on to the old HERWIG program [19]. In all models, first a number of additional hard scatters is computed according to the probability distribution resulting from the Poissonian with \bar{n} as calculated above. The additional hard scatters are simulated as a primary hard scatter. The differences of the available implementations are hidden in the details of the application of the parton shower to the various hard processes and the treatment of the parton distribution functions for the additional scatters and the overlap function. These, as inclusive quantities, are not anymore well-defined when several partons are extracted from the proton and hence the remnant extraction has to be modelled. The underlying event model in SHERPA [17] is quite similar but will be replaced by a new approach soon. The current model

in PYTHIA follows the idea of interleaved partonic interactions and showering and differs quite significantly from the model discussed here [20, 21].

In HERWIG++ this model has been implemented and released as well [22]. The only two parameters of the model are the minimum transverse momentum p_t^{\min} of the additional hard scatters and the parameter μ^2 that characterizes the inverse proton radius in the overlap function $A(\vec{b}; \mu^2)$. At that stage good agreement with available Tevatron data on the underlying event was found.

As a second step, also soft interactions were implemented [23]. The model is based on adding a soft term to the eikonal function. The simplest possibility, using the same overlap function as for hard interactions, was studied but discarded [24]. The current ansatz we use is the same functional form of the overlap function with a second independent parameter μ_{soft}^2 and the soft cross section σ_{soft} . The differential distribution of soft scatters in transverse momentum is based on a Gaussian below p_t^{\min} , which has been introduced above. The parameters of the Gaussian are fixed by demanding a smooth continuation from hard to soft transverse momenta and the soft cross section. The additional parameter μ_{soft}^2 is fixed with the elastic slope parameter that can also be calculated within our model. With this extension of the model a good description of Tevatron underlying event data has been found.

3 Colour reconnection model

First observations of minimum bias events at the LHC [3] have shown that an important model detail is missing: a colour reconnection model. The pseudorapidity distribution of charged particles comes out very much peaked towards the forward regions, opposed to the rapidity plateau found in the data. Hints towards the colour structure were found, as only one model parameter, namely the probability that a soft interaction is colour disrupted from the rest of the hard event or not, has shown some sensitivity to this distribution.

The need for a colour reconnection model is quite clear from the point of view of the colour preconfinement property of QCD which is the basis of the hadronization model in HERWIG. Preconfinement tells us that partons that are close in phase space, particularly in momentum space, will most often also be neighboured in colour space. This property is given in parton shower models as the colour structure evolution during parton shower evolution retains the history of the colour charge. In the multiple interaction model, however, this is not the case. The partons from the additional hard interactions are all extracted from the proton remnants without respecting a possible colour flow of the event as a whole. Hence, it is possible that jets from different hard events in the multiple interaction chain can end up in similar directions in momentum space and therefore should have been created closely in colour space as well. As the multiple interaction model sets up the colour connection between different hard events *ad hoc* we should be able to improve the description of the hadronic final state with colour connections that resemble our QCD picture of preconfinement, which now have to be modelled.

The goal of any colour reconnection model is to ensure that all (or most) colour–anticolour charge pairs end up closely in phase space by some criterion. In our case we define closeness of pairs as having a small invariant mass, or in the HERWIG case, a small cluster mass. We may say that a *colour length*

$$\lambda = \sum_{\text{pairs } ij} m_{ij}^2$$

should be minimized. Here, ij are all $3 \otimes \bar{3}$ pairs that may form a colour neutral cluster in the

hadronization model. In practice it is computationally too expensive to find the true minimum for a full partonic final state at the LHC with $\mathcal{O}(100)$ partons. Furthermore, we may not really want to find the true minimum as the colour line picture we use is only true in the limit of infinite colours and we may very well have fluctuations about the minimum.

Based on this physical picture there are two colour reconnection models implemented in HERWIG++. In the *plain* model, which is similar to the model in Fortran HERWIG, all clusters pairs are iterated in a random order and whenever a swap of colours is preferable, i.e. λ becomes smaller, this is done with a given probability which is the only model parameter. This model has shown to give the desired results and is implemented in HERWIG++.

One of the shortcomings of this model is that it is not so easy to assess how close we come to the true minimum and which clusters are taken into account as only a single random stream of clusters is presented to the model. In order to study its physical significance we have implemented a second model that we would like to discuss here a bit more in detail. Here, we try to minimize the colour length λ with a Metropolis algorithm. This has the advantage that the minimization procedure is quite physical and can be controlled by the parameters of the model which have some kind of thermodynamical counterpart. A similar model was discussed also for PYTHIA [25].

The algorithm is, again, based on random colour rearrangements between randomly chosen clusters, but now in a more controlled way.

- First an initial ‘temperature’ T is chosen which is related to a typical value of $\Delta\lambda = \lambda_{\text{new}} - \lambda_{\text{old}}$.
- Based on this temperature, we try a certain number of random colour rearrangements, proportional to the total number of available clusters.
- For each rearrangement $\Delta\lambda$ is computed. If $\Delta\lambda < 0$ the new configuration is accepted. If $\Delta\lambda > 0$, we only accept the new configuration with probability $\exp(-\Delta\lambda/T)$.
- After a number of attempts the temperature is decreased by a given factor.
- The algorithm terminates if no more rearrangements were made or a maximum number of loops has been passed.

It is known well, that if run with a suitable set of parameters this algorithm will come very close to the true minimum. The key point is that the algorithm also allows for fluctuations in the wrong direction, controlled by the temperature parameter, in order to also look for minima in previously unexplored paths. We could confirm this for a few examples where we also determined the true minimum by brute force. For our application, however, we left the parameter choice open and had them determined by tuning to minimum bias and underlying event data. The good results were also shown at this workshop [26].

The result is quite interesting, as actually quite small initial temperatures and a quick reduction of temperature is preferred by the model. So, effectively the model is making random colour rearrangements in more or less a *single* stream of clusters, chosen randomly. This is exactly what happens in our plain reconnection model. So, physically, the model does not really want to find the true minimum but rather wants to keep some non-optimal colour correlations due to deviations from the large N_c limit or other fluctuations of colour.

In addition we have studied a few properties of the model performance that are relevant for the formation of the hadronic final state. Fig. 1 shows the relative change in colour length for

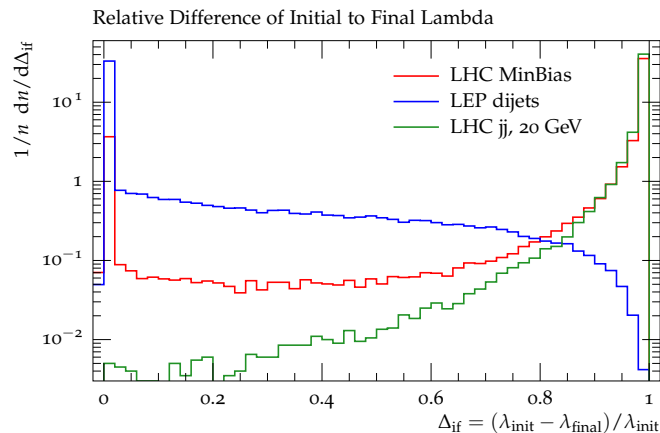


Figure 1: Relative change of colour length in various situations

two types of events at the LHC, namely minimum bias events and dijets ($p_T > 20$ GeV), and LEP events. Clearly the colour length presented to the model at LEP is already close to the minimum as there the simulation of whole hadronic final state is controlled by QCD. At the LHC the situation is the opposite as there the underlying events play a role, and possibly also non-perturbative effects from the hadron remnants.

4 Conclusions

We have summarized the multiple partonic interaction models in HERWIG++ and described the ongoing work on colour reconnections in some detail. The colour reconnection models have found to be vital for the description of LHC data and we have studied the physical significance of our model with a second model for a controlled minimization of the colour length. This study has confirmed our physical picture of an initial lack of colour preconfinement in modelling hadron collider events with MPI.

Acknowledgements We thank the organizers for a very pleasant and fruitful workshop. This work has been supported by the Helmholtz Alliance “Physics at the Terascale”.

References

- [1] T. Affolder et al., “Charged jet evolution and the underlying event in $p\bar{p}$ collisions at 1.8 TeV”, Phys.Rev. D **65** (2002) 092002.
- [2] T. Aaltonen et al., “Studying the Underlying Event in Drell-Yan and High Transverse Momentum Jet Production at the Tevatron”, Phys.Rev. D **82** (2010) 034001. (arXiv:1003.3146).
- [3] G. Aad et al., “Charged-particle multiplicities in pp interactions at $\sqrt{s} = 900$ GeV measured with the ATLAS detector at the LHC”, Phys.Lett. B **688** (2010) 21–42. (arXiv:1003.3124).
- [4] G. Aad et al., “Measurement of underlying event characteristics using charged particles in pp collisions at $\sqrt{s} = 900$ GeV and 7 TeV with the ATLAS detector”, Phys. Rev. D **83** (2011) 112001. (arXiv:1012.0791).
- [5] G. Aad et al., “Charged-particle multiplicities in pp interactions measured with the ATLAS detector at the LHC”, New J.Phys. **13** (2011) 053033. (arXiv:1012.5104).

- [6] G. Aad et al., "Measurements of underlying-event properties using neutral and charged particles in pp collisions at 900 GeV and 7 TeV with the ATLAS detector at the LHC", *Eur.Phys.J. C* **71** (2011) 1636. (arXiv:1103.1816).
- [7] V. Khachatryan et al., "Transverse momentum and pseudorapidity distributions of charged hadrons in pp collisions at $\sqrt{s} = 0.9$ and 2.36 TeV", *JHEP* **1002** (2010) 041. (arXiv:1002.0621).
- [8] V. Khachatryan et al., "Transverse-momentum and pseudorapidity distributions of charged hadrons in pp collisions at $\sqrt{s} = 7$ TeV", *Phys.Rev.Lett.* **105** (2010) 022002. (arXiv:1005.3299).
- [9] V. Khachatryan et al., "First Measurement of Hadronic Event Shapes in pp Collisions at $\sqrt{s}=7$ TeV", *Phys.Lett. B* **699** (2011) 48–67. (arXiv:1102.0068).
- [10] S. Chatrchyan et al., "Measurement of the Underlying Event Activity at the LHC with $\sqrt{s} = 7$ TeV and Comparison with $\sqrt{s} = 0.9$ TeV", *JHEP* **1109** (2011) 109. (arXiv:1107.0330).
- [11] K. Aamodt et al., "Charged-particle multiplicity measurement in proton-proton collisions at $\sqrt{s} = 0.9$ and 2.36 TeV with ALICE at LHC", *Eur.Phys.J. C* **68** (2010) 89–108. (arXiv:1004.3034).
- [12] K. Aamodt et al., "Charged-particle multiplicity measurement in proton-proton collisions at $\sqrt{s} = 7$ TeV with ALICE at LHC", *Eur.Phys.J. C* **68** (2010) 345–354. (arXiv:1004.3514).
- [13] K. Aamodt et al., "Transverse momentum spectra of charged particles in proton-proton collisions at $\sqrt{s} = 900$ GeV with ALICE at the LHC", *Phys.Lett. B* **693** (2010) 53–68. (arXiv:1007.0719).
- [14] M. Bähr et al., "Herwig++ Physics and Manual", *Eur. Phys. J. C* **58** (2008) 639–707. (arXiv:0803.0883).
- [15] T. Sjöstrand, S. Mrenna, P. Skands, "PYTHIA 6.4 Physics and Manual", *JHEP* **05** (2006) 026. (arXiv:hep-ph/0603175).
- [16] T. Sjöstrand, S. Mrenna, P. Skands, "A Brief Introduction to PYTHIA 8.1", *Comput. Phys. Commun.* **178** (2008) 852–867. (arXiv:0710.3820).
- [17] T. Gleisberg et al., "Event generation with SHERPA 1.1", *JHEP* **02** (2009) 007. (arXiv:0811.4622).
- [18] T. Sjostrand, M. van Zijl, "A Multiple Interaction Model for the Event Structure in Hadron Collisions", *Phys.Rev. D* **36** (1987) 2019.
- [19] J. Butterworth, J. R. Forshaw, M. Seymour, "Multiparton interactions in photoproduction at HERA", *Z.Phys. C* **72** (1996) 637–646. (arXiv:hep-ph/9601371).
- [20] T. Sjöstrand, P. Z. Skands, "Multiple interactions and the structure of beam remnants", *JHEP* **03** (2004) 053. (arXiv:hep-ph/0402078).
- [21] T. Sjöstrand, P. Z. Skands, "Transverse-momentum-ordered showers and interleaved multiple interactions", *Eur. Phys. J. C* **39** (2005) 129–154. (arXiv:hep-ph/0408302).
- [22] M. Bähr, S. Gieseke, M. H. Seymour, "Simulation of multiple partonic interactions in Herwig++", *JHEP* **07** (2008) 076. (arXiv:0803.3633).
- [23] M. Bähr, J. M. Butterworth, S. Gieseke, M. H. Seymour, "Soft interactions in Herwig++" arXiv:0905.4671.
- [24] M. Bähr, J. M. Butterworth, M. H. Seymour, "The Underlying Event and the Total Cross Section from Tevatron to the LHC", *JHEP* **01** (2009) 065. (arXiv:0806.2949).
- [25] P. Z. Skands, D. Wicke, "Non-perturbative QCD effects and the top mass at the Tevatron", *Eur.Phys.J. C* **52** (2007) 133–140. (arXiv:hep-ph/0703081).
- [26] A. Siodmok, "Tuning of multiple partonic interactions model in Herwig++ using the early LHC data", these proceedings.

ATLAS MPI tunes with various PDFs

Deepak Kar for the ATLAS Collaboration

CERN, 1211 Genève 23, Switzerland

DOI: <http://dx.doi.org/10.3204/DESY-PROC-2012-03/54>

The latest development in ATLAS MC generator tunings using LHC data will be discussed. PYTHIA 6 generator have been tuned with a variety of PDFs. Pythia 8 tunes have been constructed for six different PDFs, and are primarily aimed at an optimal description of minimum bias, for use in pile-up simulation. Also tunes of Herwig+JIMMY were performed for the final time inside ATLAS. Interesting effects were observed in MPI simulation when using MC-adapted PDFs.

1 Introduction

This article describes the effort within ATLAS to provide Monte Carlo (MC) generator parameter sets – “tunes” – which provide an optimal description of this ATLAS data for use in future LHC physics studies. These tunes have been constructed for the PYTHIA 6 [1], Pythia 8 [2] and HERWIG/JIMMY [3, 4] event generators, making maximal use of the available published data from ATLAS as well as the Tevatron and LEP experiments, for a variety of parton density functions (PDFs).

The effect of PDFs on MC tunes has gained a lot of attention recently. LHC experiments are more and more using NLO parton shower Monte-Carlos for many of the processes, but historically LO PDFs has been used for the LO parton shower Monte Carlo generation. MC-adapted PDFs [5–7] are a relatively new concept which provide PDFs especially designed for LO generators. The idea is to obtain the behavior of a LO PDF – in particular the LO gluon distribution – in the phase space relevant for the soft QCD models, while at the same time modifying the high- x PDFs such that the predictions of the LO MC generator for hard processes closely resemble the full NLO predictions, i.e. using NLO PDFs in NLO MC calculations. ATLAS was the first experiment to use these “mLO” PDFs in MC production campaigns. It has been shown by comparison to Tevatron data [8] that there is no final answer yet as to which PDFs give the best results. PDF effects on MC model predictions are difficult to obtain unless the PDF-dependent model parameters are tuned to the data. This note presents comparisons of full tunes to a variety of MC-adapted, NLO and LO PDFs to LHC data to further check this approach to PDF construction.

The tuning strategy [9–11] employed was to tune only to published ATLAS $\sqrt{s} = 7$ TeV and $\sqrt{s} = 900$ GeV minimum bias (MB) [12] and leading track and cluster underlying event (UE) [13, 14] data, and also to CDF leading jet and Drell-Yan UE [15] and MB [16] data at $\sqrt{s} = 1.96$ TeV. Since it was seen that tuning to LHC and Tevatron data with three different center-of-mass energies is very challenging, more weight was put on ATLAS 7 TeV distributions, and for Pythia 8 CDF data was not included in the tuning. For HERWIG/JIMMY, due to the limitation of the energy extrapolation model, the tuning input came from 7 TeV and ~ 2 TeV

PDF type	PDF set	Used in tuning
Leading order (LO)	CTEQ6L1 [20]	HERWIG/JIMMY, PYTHIA 6, Pythia 8
	MSTW08LO [21]	HERWIG/JIMMY, PYTHIA 6, Pythia 8
Modified leading order (mLO)	MRSTMCa1 (LO**) [6]	HERWIG/JIMMY, PYTHIA 6, Pythia 8
	CT09MC2 [22]	HERWIG/JIMMY, PYTHIA 6
	MRST2007 (LO*) [5]	PYTHIA 6, Pythia 8
Next-to leading order (NLO)	CTEQ6.6 [23]	HERWIG/JIMMY, PYTHIA 6, Pythia 8
	CT10 [24]	HERWIG/JIMMY, PYTHIA 6, Pythia 8
	MSTW08NLO [21]	HERWIG/JIMMY
	HERAPDF1.0 [25]	HERWIG/JIMMY
	HERAdis [26]	HERWIG/JIMMY
	NNPDF2.1 [27]	HERWIG/JIMMY, PYTHIA 6

Table 1: PDF sets used for tuning with corresponding MC generator

data only. The set of HERWIG/JIMMY and PYTHIA 6 tunes were named AMBT2 and AUET2 depending on whether minimum bias or underlying event data was used in the MPI stage of the tuning. The tunes were performed using the stand-alone AGILE event generator interface [17] (except for C++ Pythia 8) to steer parameters and switches and to feed events to the Rivet [18] analysis package. The parameter optimization was done using the Professor [19] tool.

PDFs from different PDF groups such as CTEQ, MSTW and, for the first time, also HERA and NNPDF2.1 were used and shown in Table 1, along with which generator-tunes used which set.

2 Herwig/Jimmy

The HERWIG event generator is a general-purpose shower and hadronisation generator similar to PYTHIA 6 but with an angular-ordered (rather than p_{\perp} -ordered) parton showers, and a cluster-based rather than string-based hadronisation model. Notably, HERWIG itself does not have an MPI model: this feature is added by the JIMMY add-on generator, and this combination in this article is referred to as HERWIG/JIMMY. The MPI parameters are tuned [9].

Since the JIMMY MPI model is by design not valid for multiple scattering where the signal process is itself a soft scatter, minimum bias data cannot be used for tuning of this generator. As the underlying event data from ATLAS and CDF represent a smooth transition from minimum bias to UE-type processes, the softest parts of these observables must also be excluded from fits. In the ATLAS UE data, and that from the CDF 2001 UE study, the events are considered to be closer to minimum bias than hard QCD, and so JIMMY is instructed to generate the softest possible scatters by setting its UE mode to 0, via $JMUE0 = 0$ and setting the lower phase space cut in p_T in hadronic jet production, $PTMIN$, to the value of the MPI cut-off, $PTJIM$. The cut-off for multiple parton interactions modeled with JIMMY is a single parameter, $PTJIM$, without any dependence on \sqrt{s} . In order to make the model fit to data for various collider energies, we apply the following energy dependence of $PTJIM$ which is inspired by the ‘‘pomeron’’ energy evolution of the similar cut-off in the PYTHIA 6 model:

$$PTJIM(\sqrt{s}) = PTJIM_0 \cdot \left(\frac{\sqrt{s}}{1800 \text{ GeV}} \right)^{\text{EXP}}, \quad (1)$$

where the tuning parameter $PTJIM_0$ is the value for $PTJIM(\sqrt{s})$ at the reference energy 1800 GeV. The energy exponent tuning parameter, EXP , was manually set at 0.274 in the MC08 JIMMY tune, and was kept fixed at this value for all PDFs). The final MPI parameter for tuning is the hadronic form factor radius: although JIMMY allows the proton and anti-proton radius to be set separately ($JMRAD(73)$, $JMRAD(93)$), we use the same variable, $PRRAD$, for both.

Equivalently-weighted tunes were performed for a total of ten PDFs. We found that the data distributions can be described to a similar degree for all PDFs. The Figures 1. show these tunes, compared with ATLAS 7 TeV UE data. Left-hand plot shows the comparison of data to the AUET2 tunes for the LO and mLO PDFs, as well as the AUET1 tune for the mLO LO* PDF; the right-hand plot is a comparison of data with all the AUET2 tunes for NLO PDFs.

The JIMMY/HERWIG model does not have as many parameters as in PYTHIA 6, where a ‘‘color reconnection’’ mechanism can be used to level out the differences between the two classes of observable, and so one will always be described better than the other. This is particularly obvious in the observables featuring $\langle p_{\perp} \rangle$. The regions governed by soft physics are not described due to the missing soft physics in JIMMY/HERWIG. It can generally be said that the PDF effect can be ‘‘tuned away’’ with the available parameters, meaning that very similar agreement can be reached for all PDFs studied. However some differences are visible, e.g. the $\langle p_{\perp} \rangle$ vs. N_{ch} observables are a bit better described by the mLO PDFs than by the LO and NLO PDFs.

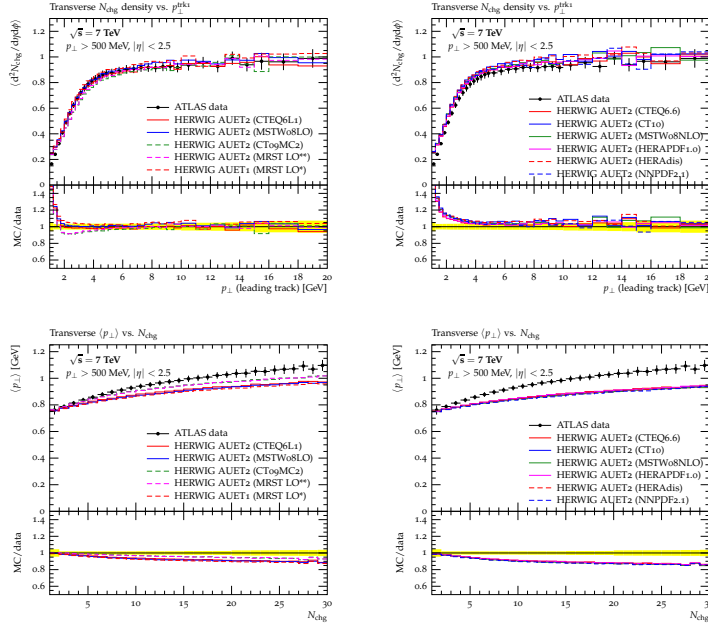


Figure 1: Comparison plots of the new HERWIG/JIMMY AUET2 tunes to 7 TeV ATLAS track-based UE data. Left column: LO and mLO PDFs. Right column: NLO PDFs. The track p_{\perp} cut for all observables is 500 MeV.

3 Pythia 6

The PYTHIA 6 MC generator is used as the main general-purpose event generator in ATLAS, including in connection with the higher-order matrix element generators. It is based, as are all general-purpose showering/hadronisation generators, on (leading-order) partonic matrix elements augmented with QCD radiation resummation via initial- and final-state parton showers, a non-perturbative model for the combination of the resultant partons into physical hadrons, a standard treatment of the decays of these hadrons, and – importantly for this note – a phenomenological modeling of the bulk interactions of the colliding protons via the formalism of multiple partonic interactions (MPI). We will focus on the MPI tuning part in this article, for the details of hadronisation and final state shower setup, and shower tune, one can refer to [10, 11]. We use a five-parameter tuning space and numerically optimize the description of MPI-sensitive data from ATLAS and CDF, with weighted emphasis on the ATLAS observables. We just list briefly the parameters used in this tuning:

- The p_{\perp} cut-off/regularize value used to avoid soft divergences in the model, set for a reference scale of $\sqrt{s} = 1800$ GeV, and the exponent used in its energy evolution to other beam energies are given by `PARP(82)` and `PARP(90)` respectively.
- The hadronic matter distribution is modeled by a double-Gaussian distribution, parameterized by `PARP(83)` and `PARP(84)`: as these parameters are strongly correlated, we fixed `PARP(83)` to its AMBT1 value of 0.356 and only tuned `PARP(84)`.
- The final parameters are `PARP(77)` and `PARP(78)`, which control the probabilities of color reconnection occurring for fast-moving (high- p_{\perp}) and general color strings.

The tunes were constructed with equal fitting weights for several PDFs. As there is neither theoretical nor practical motivation for use of NLO PDFs in description of minimum bias observables, and mLO PDFs were observed in the previous tuning to introduce strong and untuneable deviations from data in minimum bias, we only attempt to describe underlying event (UE) observables here: in other words we extend the PDF coverage of the AUET2B tune series, but not the AMBT2B one. The behaviors of the resulting tunes in ATLAS underlying event observables are shown in Figures 2.

ATLAS MPI TUNES WITH VARIOUS PDFs

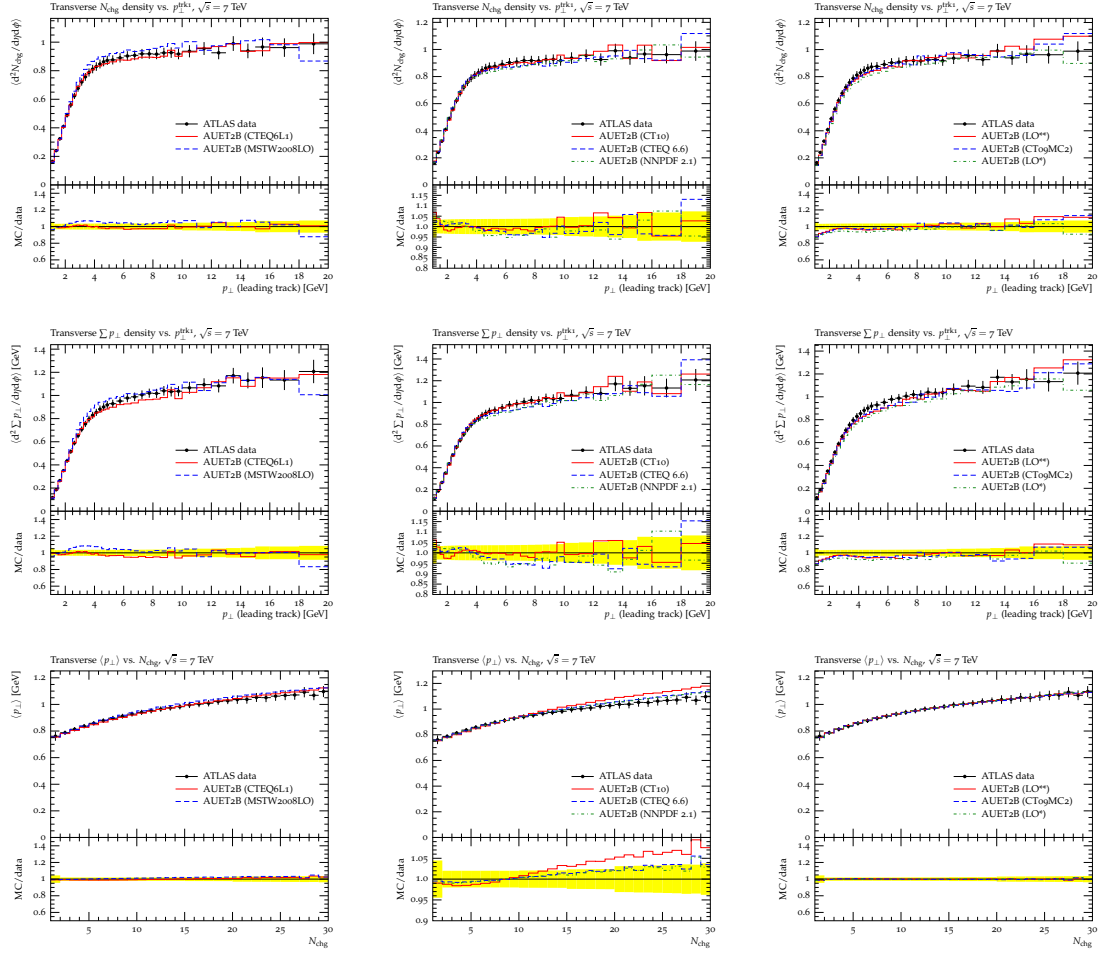


Figure 2: Comparison plots of the new PYTHIA 6 tunes to ATLAS underlying event data at 7 TeV [13, 14]. The tunes corresponding to LO, NLO and mLO PDFs are shown respectively in the left, center and right columns. The yellow shaded areas represent data uncertainty.

4 Pythia 8

The use of the C++ Pythia8 generator is gaining more popularity, partly because this is the version being supported and developed by the authors, and partly because it has better diffractive modeling than PYTHIA 6. Pythia 8 tunes have been performed using a newly introduced feature in version 8.153, where the width of the transverse matter distribution varies depending on the momentum fraction of the interacting partons. The parameters tuned are MultipleInteractions:ecmPow (subsequently referred to as ecmPow), MultipleInteractions:pT0Ref (subsequently referred to as pT0Ref), BeamRemnants:reconnectRange (subsequently referred to as reconnectRange) and MultipleInteractions:a1 (subsequently referred to as a1). The MultipleInteractions:a1 parameter represents the constant in the Gaussian matter distribution width and

the rest are described with the corresponding PYTHIA 6 parameters for easy reference in Table 2. The other parameters are same from tune 4C [28], except that SpaceShower:rapidityOrder is turned off, as there are some indications from multi-jet matching results that the shower gets closer to the matrix-element results when it is switched off.

MPI parameter	Equivalent PYTHIA 6 parameter
MultipleInteractions:pT0Ref	PARP(82)
MultipleInteractions:ecmPow	PARP(90)
BeamRemnants:reconnectRange	PARP(77), PARP(78)
MultipleInteractions:bProfile	MSTP(82)
If MultipleInteractions:bProfile = 2 (double-Gaussian matter dbn.)	
MultipleInteractions:coreFraction	PARP(83)
MultipleInteractions:coreRadius	PARP(84)
If MultipleInteractions:bProfile = 3 (exp/Gaussian overlap dbn.)	
MultipleInteractions:expPow	PARP(83)

Table 2: Pythia 8 MPI parameters

The tuning was done separately for six different PDFs. It was found that with the LO PDFs, a common tune (named A2) for minimum bias and underlying event could be obtained. However, for higher order PDFs, this was not the case, and underlying event (AU2) tunes were performed. Figure 3 shows the new LO MB tunes (and tune 4C and 4Cx [29]), compared with ATLAS minimum bias data at $\sqrt{s} = 7$ TeV. Figure 4 shows the tunes for all PDFs compared with ATLAS underlying event data at $\sqrt{s} = 7$ TeV.

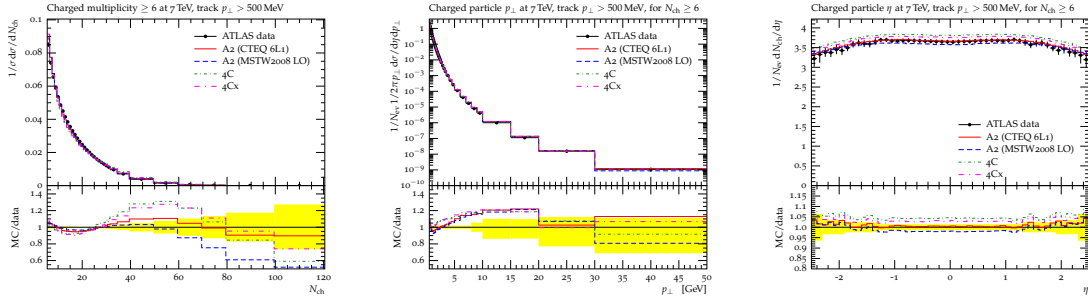


Figure 3: Comparison plots of the new Pythia 8 tunes to ATLAS minimum-bias event data [12] at 7 TeV. The yellow shaded areas represent data uncertainty.

ATLAS MPI TUNES WITH VARIOUS PDFs

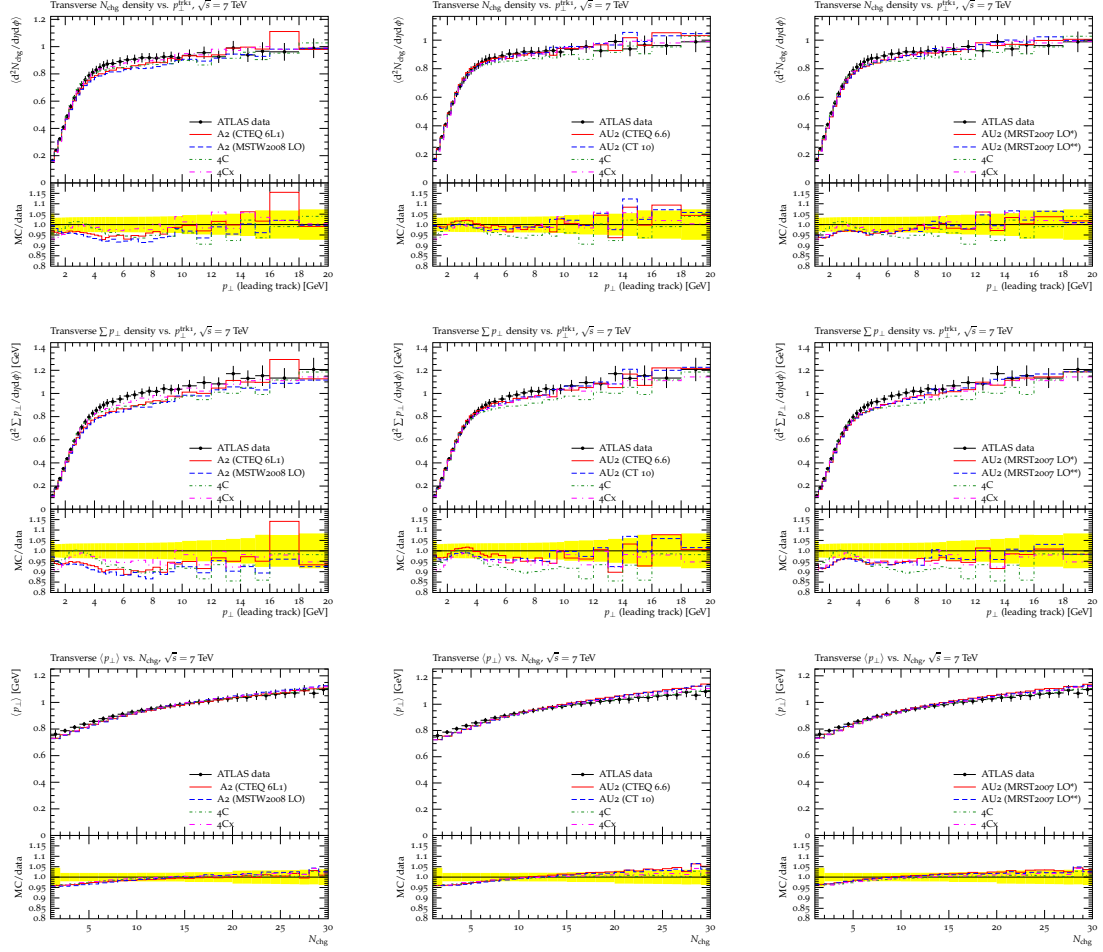


Figure 4: Comparison plots of the new Pythia8 tunes to ATLAS underlying event data at 7 TeV [13, 14]. The tunes corresponding to LO, NLO and mLO PDFs are shown respectively in the left, center and right columns. The yellow shaded areas represent data uncertainty.

5 Effect of PDFs

We observed that for HERWIG/JIMMY tunes the cut-off parameter PTJIM group according to the PDF type with the mLO PDFs yielding the highest values, followed by the LO and the NLO PDFs, seen in Figure 5. Since a high cut-off values means that less activity is required by the parton shower to match the data this result is in agreement with the expectation that the mLO PDFs create more activity from the beginning.

The tunings presented in this note, for both the PYTHIA 6 and Pythia8 generators, have indicated a significant connection between the PDF being used and both the parameter values obtained and some qualitative features of MPI-influenced observables. For PYTHIA 6 results show a strong differentiation between the tunes to LO and mLO PDFs. The LO** PDF arguably

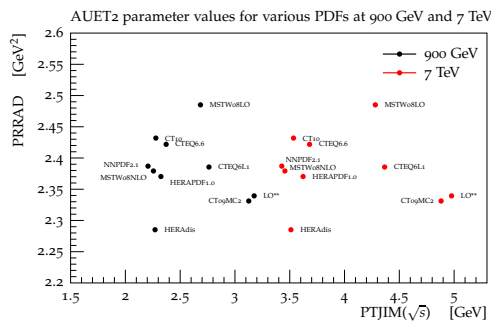


Figure 5: Observed grouping of tuning results of PTJIM by PDF type.

has the worst behavior for minimum bias observables, with a very substantial overshoot in the description of charged multiplicity from $N_{ch} \gtrsim 40$ for a track p_{\perp} cut of 500 MeV. All the mLO PDFs display a factor-of-2 overshoot in the minimum bias p_{\perp} spectra for much of the available range, an observable well described for both LO PDFs. The underlying event observables are also in general described better by the LO PDFs, with the two MRST mLO PDFs (LO* and LO**) undershooting the turn-over region. NLO PDFs seem to prefer lower values of the PARP(82) and PARP(90) MPI parameters that are typically favored by LO and mLO PDFs. Similarly for Pythia 8, we saw that the different PDFs prefer particular values of the tuning parameters. The tunes corresponding to two LO PDFs need very different set of tune values, although they behave very similarly in MB and UE plots. The behavior of tunes corresponding to mLO PDFs (LO* and LO**) are very similar, however they almost reduce back to the single Gaussian matter distribution. This is in fact a common feature for all the tunes, with very low a_1 values. The tunes corresponding to NLO PDFs seem to demand a stronger color reconnection strength than the others, but somewhat lower MPI p_T cut-off and energy exponent. Respectively these parameter shifts mean that NLO PDF tunes have less MPI cross-section screening (i.e. more activity) at Tevatron energies than LO/mLO equivalents, and the increase in screening scale with center-of-mass energy is slower than for lo/mLO PDF tunes.

6 Conclusions

In this article we have presented latest tunes of the HERWIG/JIMMY, PYTHIA 6 and Pythia 8 event generators, with different PDFs. The effect of PDFs on the tunes has been studied, and this represents an ongoing effort to decide which PDF and tune combinations will give the best description of the available data.

References

- [1] T. Sjostrand, S. Mrenna, and P. Skands, "*PYTHIA 6.4 physics and manual*", JHEP **05** (2006) 026 (arXiv:0603175 [hep-ph]).
- [2] T. Sjostrand, S. Mrenna, and P. Skands, "*A brief introduction to Pythia 8.1*", Comput. Phys. Commun. **178** (2008) 852–867 (arXiv:0710.3820 [hep-ph]).
- [3] G. Corcella et al., "*HERWIG 6.5 release note*", arXiv:0210213 [hep-ph].
- [4] J. M. Butterworth, J. R. Forshaw, and M. H. Seymour, "*Multiparton interactions in photoproduction at HERA*", Z. Phys. **C72** (1996) 637–646 (arXiv:9601371 [hep-ph]).

- [5] A. Sherstnev and R. S. Thorne, "Parton distributions for LO generators", Eur. Phys. J. **C55** (2008) 553–575 (arXiv:0711.2473 [hep-ph]).
- [6] A. Sherstnev and R. Thorne, "Different PDF approximations useful for LO Monte Carlo generators", arXiv:0807.2132 [hep-ph].
- [7] H.-L. Lai, J. Huston, S. Mrenna, P. Nadolsky, D. Stump, W.-K. Tung, and C.-P. Yuan, "Parton distributions for event generators", arXiv:0910.4183 [hep-ph].
- [8] T. Kasemets and T. Sjostrand, "A comparison of new MC-adapted parton densities", Eur.Phys.J **C69** (2010) 019 (arXiv:1007.0897 [hep-ph]).
- [9] The ATLAS Collaboration, "New ATLAS event generator tunes to 2010 data", 2011. <https://cdsweb.cern.ch/record/1345343>. ATL-PHYS-PUB-2011-008.
- [10] The ATLAS Collaboration, "ATLAS tunes of PYTHIA 6 and PYTHIA 8 for MC11", 2011. <http://cdsweb.cern.ch/record/1363300>. ATL-PHYS-PUB-2011-009.
- [11] The ATLAS Collaboration, "Further ATLAS tunes of PYTHIA 6 and PYTHIA 8 for MC11", 2011. <http://cdsweb.cern.ch/record/1400677>. ATL-PHYS-PUB-2011-014.
- [12] The ATLAS Collaboration, "Charged-particle multiplicities in pp interactions measured with the ATLAS detector at the LHC", New J. Phys. **13** (2011) 053033 (arXiv:1012.5104 [hep-ex]).
- [13] The ATLAS Collaboration, "Measurement of underlying event characteristics using charged particles in pp collisions at $\sqrt{s} = 900$ GeV and 7 TeV with the ATLAS detector", Phys. Rev. D **83** (2011) 112001 (arXiv:1012.0791 [hep-ex]).
- [14] The ATLAS Collaboration, "Measurements of underlying-event properties using neutral and charged particles in pp collisions at 900 GeV and 7 TeV with the ATLAS detector at the LHC", Eur. Phys. J. **C71** (2011) 1636 (arXiv:1103.1816 [hep-ex]).
- [15] The CDF Collaboration, et al., "Studying the Underlying Event in Drell-Yan and High Transverse Momentum Jet Production at the Tevatron", arXiv:1003.3146 [hep-ex].
- [16] The CDF Collaboration, T. Aaltonen et al., "Measurement of Particle Production and Inclusive Differential Cross Sections in $p\bar{p}$ Collisions at $\sqrt{s} = 1.96$ TeV", Phys. Rev. **D79** (2009) 112005 (arXiv:0904.1098 [hep-ex]).
- [17] A. Buckley, "CEDAR: tools for event generator tuning", PoS **ACAT2007** (2007) 050 (arXiv:0708.2655 [hep-ph]).
- [18] A. Buckley, J. Butterworth, L. Lonnblad, H. Hoeth, J. Monk, et al., "Rivet user manual", arXiv:1003.0694 [hep-ph].
- [19] A. Buckley, H. Hoeth, H. Lacker, H. Schulz, and J. E. von Seggern, "Systematic event generator tuning for the LHC", arXiv:0907.2973 [hep-ph].
- [20] Pumplin, J. and others, "New generation of parton distributions with uncertainties from global QCD analysis", JHEP **07** (2002) 012 (arXiv:0201195 [hep-ph]).
- [21] A. D. Martin, W. J. Stirling, R. S. Thorne, and G. Watt, "Parton distributions for the LHC", Eur. Phys. J. **C63** (2009) 189–285 (arXiv:0901.0002 [hep-ph]).
- [22] H.-L. Lai et al., "Parton Distributions for Event Generators", JHEP **04** (2010) 035 (arXiv:0910.4183 [hep-ph]).
- [23] P. M. Nadolsky et al., "Implications of CTEQ global analysis for collider observables", Phys. Rev. **D78** (2008) 013004 (arXiv:0802.0007 [hep-ph]).
- [24] H.-L. Lai et al., "New parton distributions for collider physics", Phys. Rev. **D82** (2010) 074024 (arXiv:1007.2241 [hep-ph]).
- [25] H1 and ZEUS Collaboration, F. D. Aaron et al., "Combined Measurement and QCD Analysis of the Inclusive ep Scattering Cross Sections at HERA", JHEP **01** (2010) 109 (arXiv:0911.0884 [hep-ex]).
- [26] Aharrouche et al., "Double differential Z, W cross sections and their ratios in the electron channels", Tech. Rep. ATL-COM-PHYS-2010-325, CERN, Geneva, Jun, 2010. <http://cdsweb.cern.ch/record/1269075/>.
- [27] R. D. Ball et al., "Impact of Heavy Quark Masses on Parton Distributions and LHC Phenomenology", arXiv:1101.1300 [hep-ph].
- [28] R. Corke and T. Sjostrand, "Interleaved parton showers and tuning prospects", JHEP **03** (2011) 032 (arXiv:1011.1759 [hep-ph]).
- [29] R. Corke and T. Sjostrand, "Multiparton Interactions with an x-dependent Proton Size", JHEP **05** (2011) 009 (arXiv:1101.5953 [hep-ph]).

Tuning of the multiple parton interaction model in Herwig++ using early LHC data

Stefan Gieseke¹, Christian A. Röhr¹, Andrzej Siódmok^{1,2*}

¹Institut für Theoretische Physik, Karlsruhe Institute of Technology, Karlsruhe, Germany

²School of Physics & Astronomy, University of Manchester, U.K.

DOI: <http://dx.doi.org/10.3204/DESY-PROC-2012-03/48>

In this short note we present tunes of the Multiple Parton Interactions model in Herwig++ using the early LHC data. Measurements of the charged particle multiplicities and of the momentum flow in the underlying event in inelastic pp collisions are used to constrain the parameters of the model. The tunes aim to consistently describe both the new LHC measurements and pre-LHC data from the Tevatron and LEP.

1 Introduction

In recent years the LHC has collected data at an impressive rate which presents the opportunity to study physics not only at the new high-energy frontier but also with a higher precision. This means that QCD effects, both perturbative and non-perturbative can be studied in more detail. In particular, the first physics results from the LHC experiments were measurements of Minimum-Bias (MB) [1, 2] and Underlying Event (UE) characteristics [3] which are crucial to constrain and tune the parameters of multiple parton scattering models widely used in General Purpose Monte Carlo Generators [4–7]. In this short note we present tunes of the Multiple Parton Interactions (MPI) model in Herwig++ using these early LHC data sets.

2 Tuning of the model to the first LHC data

Before the LHC data was available, the two main parameters of the MPI model in Herwig++ [8–10], the inverse proton radius μ^2 and the minimum transverse momentum p_{\perp}^{\min} , were tuned by calculating the total χ^2 using the Tevatron UE data [11, 12]. From this, we found a region in the two-dimensional parameter plane spanned by p_{\perp}^{\min} and μ^2 , where we obtain a similarly good overall χ^2 (deep blue area in Fig. 1(a)) and for which we get a truly satisfactory description of the data. As an example see Fig. 1(b).

Despite providing a very good description of the CDF UE data, it turned out that this model was too simple to describe the Minimum Bias ATLAS data collected at 900 GeV [1]. In particular, the model's results for the charged-particle multiplicity as a function of pseudorapidity and the average transverse momentum as a function of the particle multiplicity, $\langle p_{\perp} \rangle (N_{\text{ch}})$ presented in Fig. 2, were highly unsatisfactory. The different colour lines in Fig. 2 represent

*Speaker

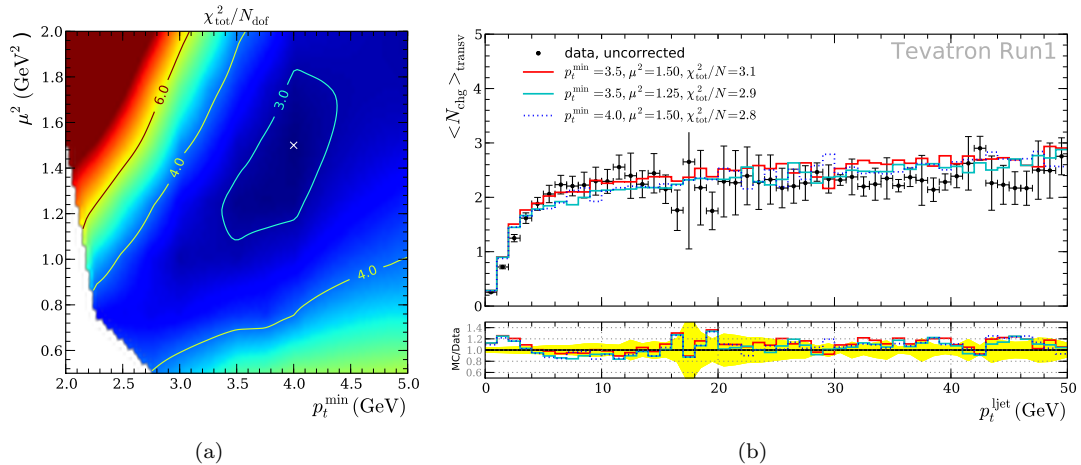


Figure 1: Tuning the MPI model to pre-LHC data, plots taken from [10]. The left-hand plot shows contour plots for the χ^2 per degree of freedom for the fit to the CDF underlying event data. The cross indicates the location of Herwig++ preferred tune. In the right-side plot we see the multiplicity in the transverse region measured by CDF. The histograms show Herwig++ for three different MPI parameter sets.

different settings of the MPI model which give a satisfactory description of the Tevatron data for two different PDF sets: CTEQ6.1 [13] and MRST LO** [14]. As presented in more detail in [15–17], even a dedicated tuning of the MPI model parameters did not improve this description, which suggests that an important model detail is missing.

This triggered new developments of the MPI model to include non-perturbative colour reconnections (CR). They are described in more detail in a separate contribution to this workshop [18]. Currently two different colour reconnection implementations are available in Herwig++: a rather simple and plain model (pCR) and a statistical model (sCR). In this contribution we focus on the plain model, but at the end we also show some comparisons with the statistical model. Both CR models can be regarded as an extension of the cluster model [19], which is used for hadronization in Herwig++. Therefore, in principle both models require a re-tuning of the hadronization model, which is a difficult and time consuming process. The difficulty is due to the fact that the large number of hadronization parameters in Herwig++ have to be tuned to a wide range of experimental data, primarily from LEP. However, because the colour structure of the LEP final states is well-defined by the perturbative parton shower evolution, by construction of the CR model we do not expect that it will change this structure significantly. This was confirmed by comparison of Herwig++ results with and without CR against LEP data. For the case of the pCR model, an example is shown in Fig. 3. The full set of plots showing that the LEP data description in Herwig++ with and without CR is of the same quality can be found on the Herwig++ web page [20]. These results allowed us to factorize the tuning procedure and to keep using the well-tested default Herwig++ tune for parton shower and hadronization parameters, and tune only parameters of the CR and MPI models. In the case of the MPI model with plain CR, there are only two parameters steering the colour structure of the multiple interactions, p_{disrupt} and p_{reco} , which we included in the tuning procedure along with p_{\perp}^{min} and μ^2 . The Professor package was applied to produce a four-

TUNING OF THE MULTIPLE PARTON INTERACTION MODEL IN HERWIG++ . . .

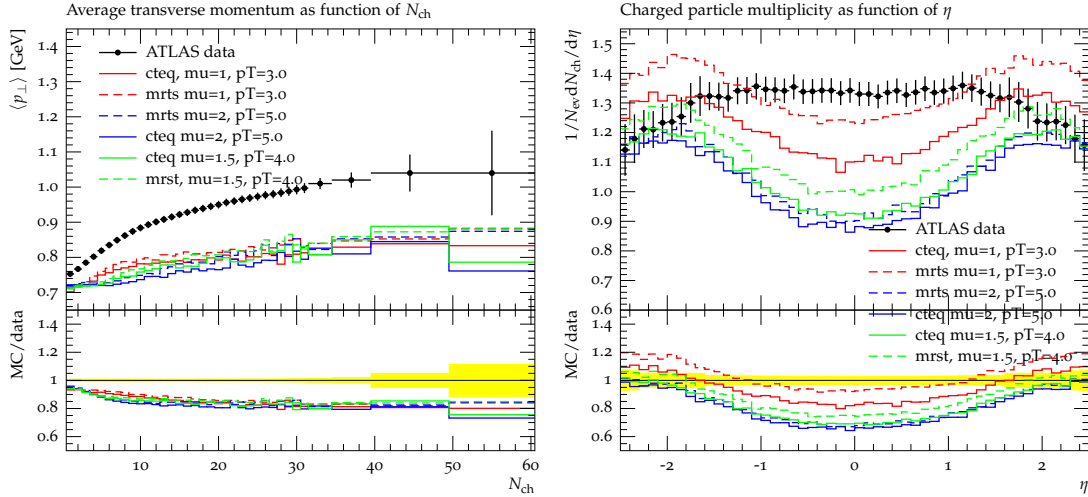


Figure 2: Comparison of Herwig++ 2.4.2 (without CR) to ATLAS minimum-bias distributions at $\sqrt{s} = 0.9$ TeV with $N_{ch} \geq 2$, $p_{\perp} > 500$ MeV and $|\eta| < 2.5$. The different colour lines represent different settings of the MPI model which give a satisfactory description of the Tevatron data for two different PDF sets CTEQ6.1 and MRST LO**.

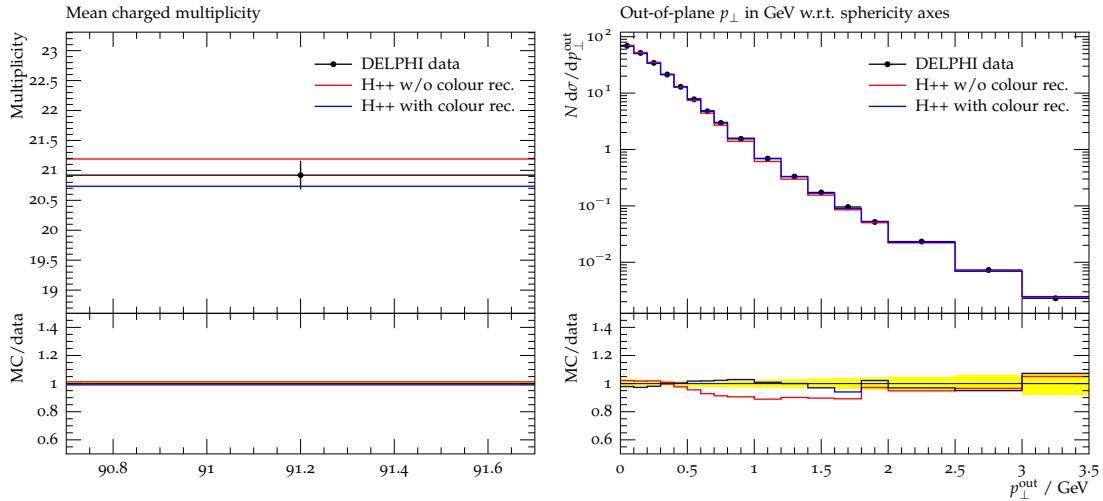


Figure 3: An example of comparison of Herwig++ with pCR (blue line) and without pCR (red line) to the measurements from DELPHI detector at LEP.

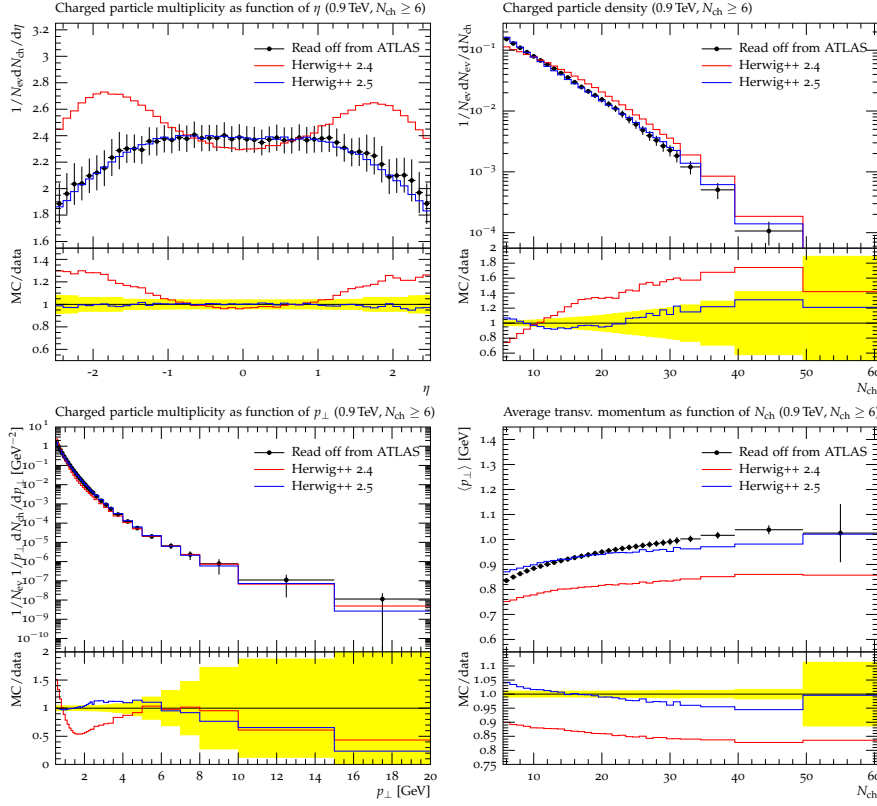


Figure 4: Comparison of Herwig++ 2.4.2 without CR model and Herwig++ 2.5 with pCR model to ATLAS minimum-bias distributions at $\sqrt{s} = 0.9$ TeV with $N_{\text{ch}} \geq 6$, $p_{\perp} > 500$ MeV and $|\eta| < 2.5$. The ATLAS data was taken from plots published in Ref. [2].

dimensional tuning of parameters by a combination of response parametrization and numerical fit optimization as described in [21]. The Rivet package [22] was used to analyse the generated events and compare results against the experimental data. Initially we wanted to determine whether the new model would be able to improve the description of the MB data, therefore we started by tuning to ATLAS MB data. Because currently there is no model for soft diffractive physics in Herwig++ we use diffraction-reduced ATLAS MB analysis with an additional cut on the number of charged particles: $N_{\text{ch}} \geq 6$. All four available MB observables were used without additional weightings to any observable. The results of this tune are shown by the blue lines in Fig. 4. In the top-left of this figure we can see that colour reconnection helps to achieve a better description of $\langle p_T \rangle(N_{\text{ch}})$. The other three distributions are now well described giving the impression that the CR was the missing piece of the MPI model in Herwig++. The next very important question was whether the new model would be able to describe the UE data collected by ATLAS [3] at 7 TeV. As before we used the Professor tool to tune the parameters of the model. This time we used two observables for the tune, the mean number of stable charged particles per unit of η - ϕ , $\langle d^2 N_{\text{ch}} / d\eta d\phi \rangle$, and the mean scalar p_{\perp} sum of stable particles per

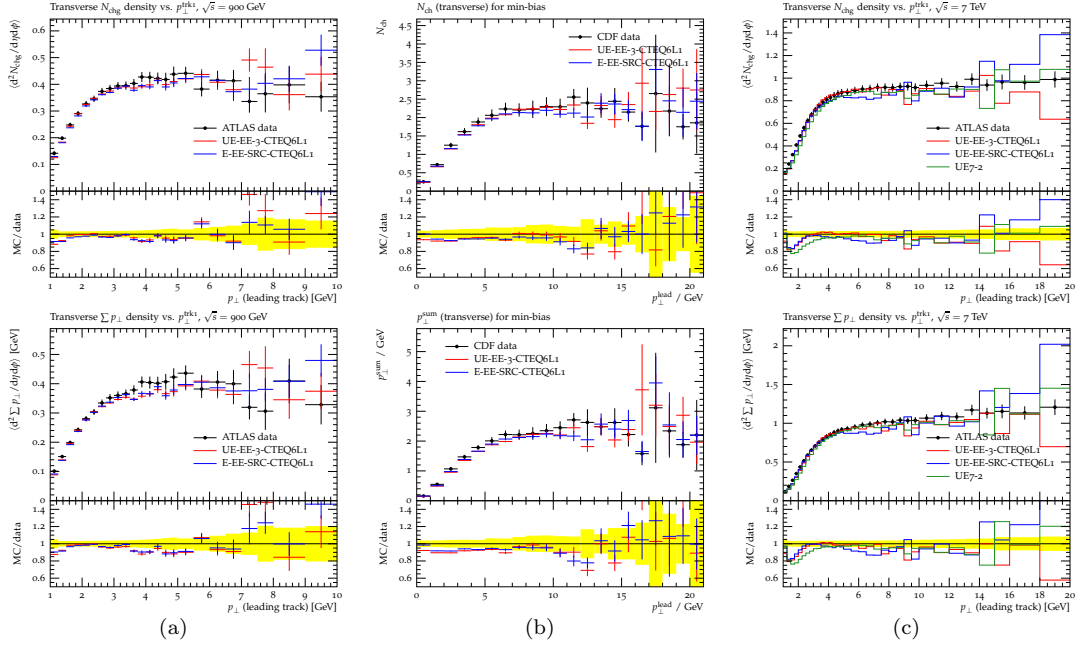


Figure 5: ATLAS data at 900 GeV (1st column), CDF data at 1800 GeV (2nd column) and ATLAS data at 7 TeV (3rd column), showing the density and $\sum p_{\perp}$ of the charged particles in the transverse area as a function of p_{\perp}^{lead} . The data is compared with UE-EE-3, UE-7 and UE-EE-sCR tunes.

unit of η - ϕ , $\langle d^2 \sum p_{\perp} / d\eta d\phi \rangle$, both as a function of p_{\perp}^{lead} in the kinematic range $p_{\perp} > 500$ MeV and $|\eta| < 2.5$. The resulting tune, named UE7-2, gives very satisfactory results for not only the tuned observables but also all other observables provided by ATLAS in Ref. [3]. In Fig 5(c) we present two selected examples: $\langle d^2 N_{\text{ch}} / d\eta d\phi \rangle$ and $\langle d^2 \sum p_{\perp} / d\eta d\phi \rangle$ as a function of p_{\perp}^{lead} for the lower p_{\perp} cut ($p_{\perp} > 500$ MeV) in the transverse region (which is the most sensitive region with respect to multiple interactions) compared to the Herwig++ UE7-2 results (green line). The full comparison with all ATLAS UE and MB data sets is available on the Herwig++ tune page [20]. We repeated the tuning process for the UE data collected by ATLAS at 900 GeV and CDF at 1800 GeV and obtained as good results as for 7 TeV. It is worth mentioning that the ATLAS UE observables with the lower p_{\perp} cut, were not available during the preparation of the UE7-2 tune but are also very well described by the tune, see [20]. These results can therefore be treated as a prediction of the model. At this stage different UE tunes were mandatory for different hadronic centre-of-mass energies \sqrt{s} . In the next section we address the question of whether an energy-independent UE tune can be obtained using the present model.

3 Centre-of-mass energy dependence of UE tunes

To study the energy dependence of the parameters properly, we need to define a set of observables measured at different collider energies, for which description is sensitive to the MPI model parameters. The experimental data should be measured at all energies in similar phase-

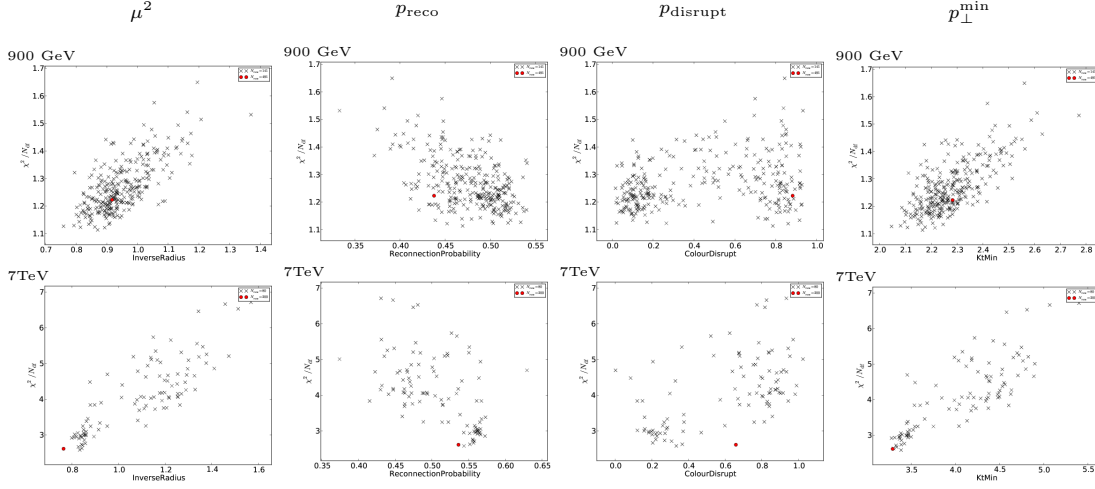
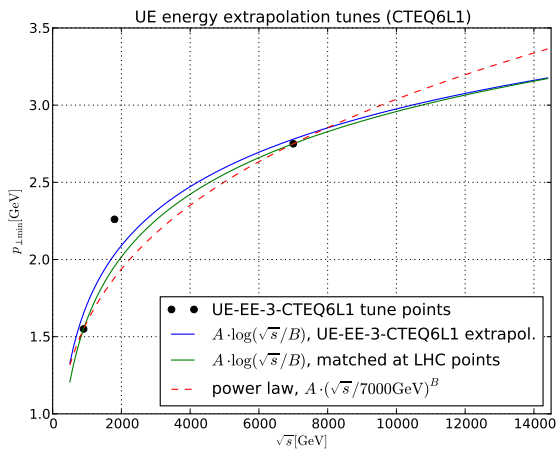


Figure 6: The spread of UE-EE tuning results for the μ^2 , p_{reco} , $p_{disrupt}$ and p_{\perp}^{\min} tunes, using cubic generator response parameterizations with all generator runs (red circles) and with subsets of generator runs (black crosses). The first row shows results for tunes to the data at 900 GeV and the second at 7 TeV.

space regions and under not too different trigger conditions. These conditions were met by two UE observables, $\langle d^2 N_{ch}/d\eta d\phi \rangle$ and $\langle d^2 \sum p_{\perp}/d\eta d\phi \rangle$ measured as a function of p_{\perp}^{lead} (with $p_{\perp}^{\text{lead}} < 20$ GeV) by ATLAS at 900 GeV and 7000 GeV (with $p_{\perp} > 500$ MeV) and CDF at 1800 GeV, therefore we used them for this task. For each hadronic centre-of-mass energy we performed independent four-dimensional tunings.

Fig. 6 shows the spread of the tuning results for each parameter against Professor’s heuristic χ^2 . In the first row we present results for 900 GeV and in the second row for 7000 GeV. Each point is from a separate tune, made using various combinations of generator runs at points in the parameter space. We see that the parameters are not well constrained and are sensitive to the input MC runs. This is due to what we have already seen at the beginning of section 2 during the tuning of the MPI model without CR to the Tevatron data, namely the strong and constant correlation between p_{\perp}^{\min} and μ^2 (represented by a dark blue area of Fig. 1(a)). This reflects the fact that a smaller hadron radius will always balance against a larger p_{\perp} cutoff as far as the underlying-event activity is concerned. When we fix one of these two parameters, the rest of the parameters are much less sensitive to the input MC runs. The most important information we can see on these figures is that the experimental data for the two different energies (900 GeV and 7 TeV) can not be described by the same set of model parameters. More precisely, the experimental data prefers different p_{\perp}^{\min} values for different hadronic centre-of-mass energies \sqrt{s} , while the rest of the parameters can remain independent of the energy. This observation led us to the creation of energy-extrapolated UE tunes, named UE-EE-3, in which all parameters are fixed except p_{\perp}^{\min} , which varies with energy. The parameter values for the UE-EE-3 tune for two different PDF sets, CTEQ6L1 and MRST LO**, are given in Table 1. As before we only present a selection of example observables for the UE-EE-3 tunes using the CTEQ6L1 PDF set. In Fig. 5 we show $\langle d^2 N_{ch}/d\eta d\phi \rangle$ and $\langle d^2 \sum p_{\perp}/d\eta d\phi \rangle$ as a function of p_{\perp}^{lead} for lower p_{\perp} cut ($p_{\perp} > 500$ MeV). We can see that the quality of the data description


 Figure 7: Example p_{\perp}^{\min} energy extrapolation for UE-EE-3 CTEQ6L1 tune.

For PDF \sqrt{s} [GeV]	CTEQ6L1 p_{\perp}^{\min} [GeV]	MRST LO** p_{\perp}^{\min} [GeV]
900	1.55	1.86
1800	2.26	2.55
2760	2.33	2.62
7000	2.75	3.06
8000	2.85	3.21
14000	3.16	3.53

For PDF	CTEQ6L1	MRST LO**
μ^2	1.35	1.11
p_{reco}	0.61	0.54
p_{CD}	0.75	0.80

Table 1: Parameters values from UE-EE-3 tunes for two different PDF sets.

by the UE7-2 tune and the energy-dependent tunes is on the same level. Because we do not know of any convincing physics argument how p_{\perp}^{\min} should depend on the energy, in order to provide predictions for different energies we fit a function of the form $A \cdot \log(\sqrt{s}/B)$, where A and B are free fit parameters, to the three p_{\perp}^{\min} values obtained in the UE-EE-3 tuning. Some examples of possible fits are shown in Fig. 7. Based on this, we provide p_{\perp}^{\min} values (see Table 1) for three different energies (2760, 8000 and 14000 GeV), for which in the future the LHC should provide experimental data, which then in turn can be confronted with the model predictions. Finally, although we do not present the details of how we obtained the tunes for the sCR model, we compare its results to the pCR for the observables included in Fig. 5. The results for both CR models give very similar results. The sCR model, however, allows for a much deeper understanding of the mechanism of colour reconnections, as is described in the already mentioned separate contribution to this workshop [18].

4 Conclusions and outlook

We have shown that by tuning the MPI model with CR, we can obtain a proper description of non-diffractive MB ATLAS observables. We present for the very first time the energy-extrapolated tune UE-EE-3, which is an important step towards the understanding of the energy dependence of the model. News concerning Herwig++ tunes are available on the tune wiki page [20].

Acknowledgements We thank the organizers for a very pleasant and fruitful workshop. This work has been supported by the Helmholtz Alliance "Physics at the Terascale". We wish to acknowledge Adam Weber for his critical reading of this proceedings.

References

- [1] G. Aad *et al.* [ATLAS Collaboration], Phys. Lett. B **688** (2010) 21 (arXiv:1003.3124 [hep-ex]).
- [2] G. Aad *et al.* [ATLAS Collaboration], New J. Phys. **13** (2011) 053033 (arXiv:1012.5104 [hep-ex]).
- [3] G. Aad *et al.* [Atlas Collaboration], Phys. Rev. D **83** (2011) 112001 (arXiv:1012.0791 [hep-ex]).
- [4] M. Bahr *et al.*, Eur. Phys. J. C **58** (2008) 639 (arXiv:0803.0883 [hep-ph]).
- [5] T. Sjostrand, S. Mrenna and P. Z. Skands, JHEP **0605** (2006) 026 (arXiv:hep-ph/0603175).
- [6] T. Sjostrand, S. Mrenna and P. Z. Skands, Comput. Phys. Commun. **178** (2008) 852 (arXiv:0710.3820 [hep-ph]).
- [7] T. Gleisberg, S. Hoeche, F. Krauss, M. Schonherr, S. Schumann, F. Siegert and J. Winter, JHEP **0902** (2009) 007 (arXiv:0811.4622 [hep-ph]).
- [8] M. Bahr, S. Gieseke and M. H. Seymour, JHEP **0807** (2008) 076 (arXiv:0803.3633 [hep-ph]).
- [9] M. Bahr, J. M. Butterworth and M. H. Seymour, JHEP **0901** (2009) 065 (arXiv:0806.2949 [hep-ph]).
- [10] M. Bahr, J. M. Butterworth, S. Gieseke and M. H. Seymour, arXiv:0905.4671 [hep-ph].
- [11] T. Affolder *et al.* [CDF Collaboration], Phys. Rev. D **65** (2002) 092002.
- [12] D. Acosta *et al.* [CDF Collaboration], Phys. Rev. D **70** (2004) 072002 (arXiv:hep-ex/0404004).
- [13] J. Pumplin, D. R. Stump, J. Huston, H. L. Lai, P. M. Nadolsky and W. K. Tung, JHEP **0207** (2002) 012 (arXiv:hep-ph/0201195).
- [14] A. Sherstnev and R. S. Thorne, Eur. Phys. J. C **55** (2008) 553 (arXiv:0711.2473 [hep-ph]).
- [15] S. Gieseke, S. Platzer, A. Siodmok and C. Rohr, DESY-PROC-2010-01.
- [16] S. Gieseke, C. A. Rohr and A. Siodmok, arXiv:1110.2675 [hep-ph].
- [17] P. Bartalini, E. L. Berger, B. Blok, G. Calucci, R. Corke, M. Diehl, Y. Dokshitzer, L. Fano *et al.*, arXiv:1111.0469 [hep-ph].
- [18] S. Gieseke, C. Rohr and A. Siodmok “Multiparton Interactions in Herwig+,” these proceedings.
- [19] B. R. Webber, Nucl. Phys. B **238** (1984) 492.
- [20] Herwig++ Collaboration (<http://herwig.hepforge.org/>), “Minimum Bias and Underlying Event tune”, http://projects.hepforge.org/herwig/trac/wiki/MB_%5CUE_tunes.
- [21] A. Buckley, H. Hoeth, H. Lacker, H. Schulz and J. E. von Seggern, Eur. Phys. J. C **65** (2010) 331 (arXiv:0907.2973 [hep-ph]).
- [22] A. Buckley *et al.*, arXiv:1003.0694 [hep-ph].

The ATLAS Monte Carlo tuning system

Sebastian Wahrmund for the ATLAS Collaboration

Institut für Kern- und Teilchenphysik and der TU Dresden,
Zellescher Weg 19, 01069 Dresden, Germany

DOI: <http://dx.doi.org/10.3204/DESY-PROC-2012-03/95>

The ATLAS experiment moved the tuning of the underlying event and minimum bias event shape modeling, previously done in a manual fashion, to the automated Professor tuning tool, employed in connection with the Rivet analysis framework, when the first corresponding experimental analysis from LHC became available. The tuning effort for the Pythia 8 generator, which includes improved models for diffraction, has been started in this automated way in ATLAS, with the aim of getting a good description of the pile-up generated by multiple minimum bias interactions. The first results for these Pythia 8 tunes, as well as PYTHIA 6 shower tunes are presented, including a study of tunes for various PDFs.

1 Introduction

Monte Carlo event generators are extensively used in high-energy particle physics, allowing the simulation of scattering processes and the generation of the outgoing particle spectra. The description of low energy QCD interactions in the generation processes necessitates the introduction of phenomenological models due to the increase of the strong coupling constant. Processes which are effected by the phenomenological description are for example: multiple parton interactions (MPI), initial- and final state radiation (which, together with the MPI, are the main contributions to the underlying event) and fragmentation processes. These models introduce additional parameters, which need to be fitted to measurements in order to provide a good Monte Carlo prediction for various other analyses. The ATLAS tuning effort for the PYTHIA 6 and Pythia 8 Monte Carlo generator and the tuning framework are presented in the following.

2 Tuning procedure

The baseline for the tuning procedure is the selection of N tuning parameters p_i and their considered ranges $[p_{\min}, p_{\max}]$. Event samples are generated for random points of the previous definite N -dimensional parameter hypercube, where the number of different points is depending on the number of input parameters to ensure a well converging behavior of the final tune. Each generated event is directly piped to the Rivet [1] framework, to perform specific analyses for each parameter variation. This allows the calculation of observables for each parameter point, which builds the input for the actual tuning process. The obtained distributions of observables for each parameter variation are the starting point for the tune, which is performed using

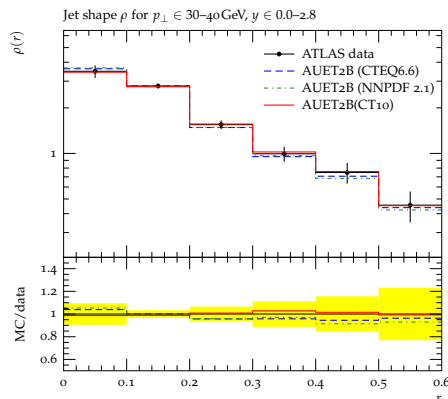


Figure 1: Comparing the PYTHIA 6 shower tune with ATLAS jet shape measurements at 7 TeV, for different next-to-leading order PDFs. Results are taken from [4].

the Professor framework [2]. Professor performs a parametrization of the generator response as a function of the parameter points and finds the set of parameters, which fits best to the given measurements of the considered observables. The user is able to influence the tuning by applying a weight for each observable, which specifies the impact of the variable for the tuning process. The whole tuning process is performed for different center-of-mass energies to obtain the energy dependence of some model parameters and for different parton density functions (PDF's), which are an extra input in the event generation step.

3 PYTHIA 6 tune

Based on the AMBT2B and AUET2B tune [3] for PYTHIA 6 a new MPI and a full shower tune were performed, using next-to-leading order PDF's and a p_T ordered shower model. The effective cutoff for space-like parton showers, the multiplier for the parton shower evolution scale and the final state radiation¹ were tuned to ATLAS measurements including jet shape studies, di-jet decorrelations and track-jet measurements. The final tune shows an excellent agreement between measurement and Monte Carlo prediction within the systematic uncertainties. Figure 1 shows the AUET2B predictions for the jet shape measurement, compared to measurements from the ATLAS experiment. All result are taken from [4].

4 Pythia 8 MPI tune

The Pythia 8 MPI tune was performed for leading order, modified leading order and next-to-leading order PDFs. The tune was accomplished using ATLAS minimum bias measurements, as well as ATLAS underlying event data based on tracks and clusters. A x dependent matter distribution was used and no rapidity order for spacelike showers was applied. The following parameters were varied for the tuning: the cutoff for MPI, the power of the energy rescaling for the min. p_T cutoff, color reconnection, and the width of the Gaussian matter function.

¹The corresponding parameter are PARP(62), PARP(64) and PARP(72) respectively.

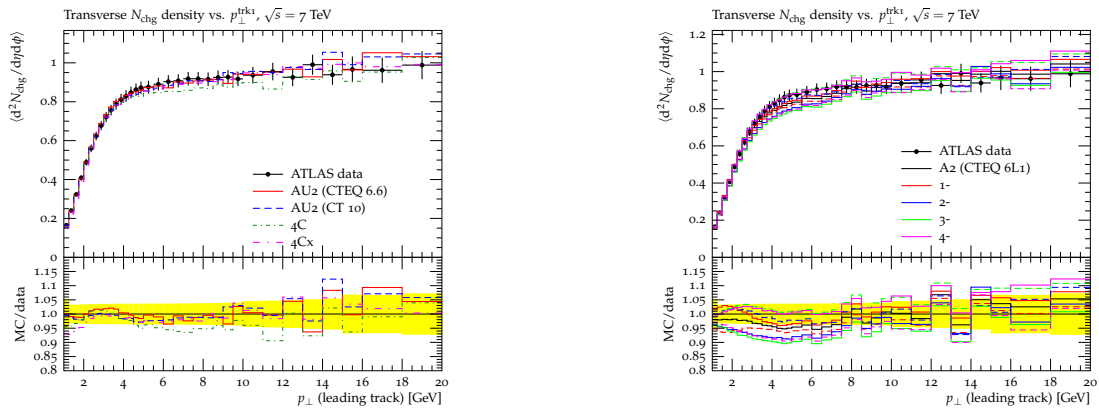


Figure 2: The average charged track number density ($p_{\text{T}} > 500 \text{ MeV}$) as a function of the leading track p_{T} is compared between prediction of Pythia 8 MPI tunes and ATLAS underlying event data, for next-to-leading order PDF's (left) and with the considerations for the eigentunes (right). Results are taken from [4].

The tunes focus mainly on distributions with $p_{\text{T}} > 500 \text{ MeV}$ and a center-of-mass energy of 7 TeV. To estimate the systematic error on the Monte Carlo prediction, the ‘‘eigentune’’ method (see [3] for details) was used, as provided by the Professor framework. The uncertainty estimation is based on variations of the parameters around the best fit value, corresponding to one standard deviation. Figure 2 shows the final tune compared to the ATLAS underlying event measurements and the corresponding eigentunes. All results are taken from [4].

5 Conclusions

The wide use of predictions from Monte Carlo generators in high energy physics makes it necessary to provide tunes to actual measurements. The ATLAS tuning framework allows a coherent and efficient setup to tune the Monte Carlo prediction to ATLAS measurements. The new AMBT2B and AUET2B tunes for PYTHIA 6 and Pythia 8 shows a good description of the measurements.

References

- [1] A. Buckley, J. Butterworth, L. Lonnblad, H. Hoeth, J. Monk, et al., *Rivet user manual*(arXiv:1003.0694 [hep-ph])
- [2] A. Buckley, H. Hoeth, H. Lacker, H. Schulz, and J. E. von Seggern, *Systematic event generator tuning for the LHC* (arXiv:0907.2973 [hep-ph])
- [3] ATLAS Collaboration, *ATLAS tunes of PYTHIA 6 and Pythia 8 for MC11*, 2010. <http://cdsweb.cern.ch/record/1363300> ATL-PHYS-PUB-2011-009
- [4] ATLAS Collaboration, *Further ATLAS tunes of PYTHIA 6 and Pythia 8*, <http://cdsweb.cern.ch/record/1395503> ATL-PHYS-PUB-2011-014

Chapter 3

Phenomenology of MPI

NLO predictions for $Wb\bar{b}$ production via double parton scattering at the LHC

Edmond L. Berger

High Energy Physics Division, Argonne National Laboratory, Argonne, IL 60439 USA

DOI: <http://dx.doi.org/10.3204/DESY-PROC-2012-03/12>

Next-to-leading order predictions in perturbative QCD are presented of various differential distributions for $pp \rightarrow Wb\bar{b}X \rightarrow \ell\nu b\bar{b}X$ at the Large Hadron Collider energy 7 TeV. Included are the contributions from both single parton scattering and double parton scattering as well as relevant backgrounds. Several kinematic variables are proposed for isolating the double parton contribution with the first 10 fb⁻¹ of integrated luminosity. Smearing associated with next-to-leading order contributions is important for a proper description of some of the observables we compute. Under specified conditions, the double parton process can be identified and measured with signal over background significance $S/\sqrt{B} \sim 10$. The work summarized here was done in collaboration with Chris Jackson, Seth Quackenbush, and Gabe Shaughnessy.

1 Introduction

With its higher energies and larger luminosities, the Large Hadron Collider (LHC) makes it possible to investigate unexplored aspects of established theories such as quantum chromodynamics (QCD). The standard single parton scattering (SPS) picture of hadron-hadron collisions is shown on the left side of Fig. 1. One parton from each proton participates in the hard scattering to produce the final state. In SPS, the differential hadronic cross section factors:

$$d\sigma_{pp}^{SPS} = \sum_{i,j} \int f_p^i(x_1, \mu) f_p^j(x'_1, \mu) d\hat{\sigma}_{ij}(x_1, x'_1, \mu) dx_1 dx'_1. \quad (1)$$

The short-distance partonic cross section $d\hat{\sigma}_{ij}$ is computed in perturbation theory, whereas the parton distribution functions (PDF) $f_p^i(x_i, \mu)$ are nonperturbative objects extracted from experiment and evolved to the appropriate hard scale μ .

The full description of hadronic collisions involves other elements including initial- and final-state soft radiation, underlying events, and multiparton interactions. Double parton scattering (DPS) describes the case in which two short-distance subprocesses occur in a given hadronic interaction, with two initial partons being active from each of the incident protons. The general picture of DPS is shown on the right side of Fig. 1. Given the small probability for single parton scattering in hadronic collisions, it is often assumed that the effects of double (or multiple) parton scattering may be ignored or subsumed into the parametrization of the underlying event. Nevertheless, it is worth exploring theoretically and investigating experimentally whether a second distinct hard component may be identified in events at the LHC. Evidence for DPS

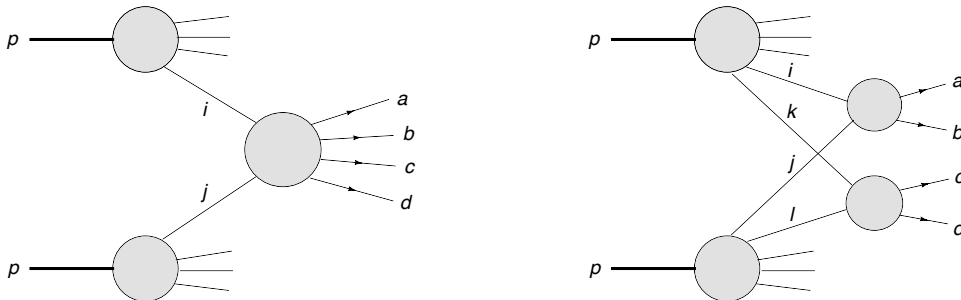


Figure 1: Schematic depiction of single parton scattering (left) and double parton scattering (right).

is reported in Refs. [1, 2, 3, 4], and many references to theoretical work may be found in Refs [5, 6, 7, 8].

In Ref. [5], we investigated the DPS and SPS contributions at the LHC for the four-parton final state $pp \rightarrow b\bar{b}jjX$ in which a $b\bar{b}$ system is produced along with two jets j . We showed that there are characteristic regions of phase space in which the DPS events are expected to concentrate, and we developed a methodology to measure the effective size of the DPS signal. Precise measurements of DPS at the LHC will provide insight into QCD dynamics beyond SPS and into parton-parton correlations, and it will help to validate a second hard component in underlying event modeling. In this contribution I summarize our next-to-leading order study in perturbative QCD of $pp \rightarrow Wb\bar{b}X \rightarrow \ell\nu b\bar{b}X$ at the Large Hadron Collider energy 7 TeV [6].

Under the assumption of weak dynamic and kinematic correlations between the two hard-scattering subprocesses, a typical approach in DPS studies is to assume the differential hadronic cross section takes a factored form in analogy to Eq. (1):

$$d\sigma_{pp}^{DPS} = \frac{m}{2\sigma_{\text{eff}}} \sum_{i,j,k,l} \int H_p^{ik}(x_1, x_2, \mu_A, \mu_B) H_p^{jl}(x'_1, x'_2, \mu_A, \mu_B) \times d\hat{\sigma}_{ij}(x_1, x'_1, \mu_A) d\hat{\sigma}_{kl}(x_2, x'_2, \mu_B) dx_1 dx_2 dx'_1 dx'_2, \quad (2)$$

where m is a symmetry factor equal to 1 (2) if the two hard-scattering subprocesses are identical (nonidentical). The joint probabilities $H_p^{ik}(x_1, x_2, \mu_A, \mu_B)$ can be approximated as the product of two single PDFs:

$$H_p^{ik}(x_1, x_2, \mu_A, \mu_B) = f_p^i(x_1, \mu_A) f_p^k(x_2, \mu_B). \quad (3)$$

Given that one hard scattering has taken place, the parameter σ_{eff} measures the size of the partonic core in which the flux of accompanying short-distance partons is confined. Typical values in phenomenological studies focus on the 10-12 mb region, consistent with measurements from the Tevatron collider [3, 4]. In writing Eqs. (2) and (3), we ignore possible strong correlations in longitudinal momentum. However, for the small values of x expected at the LHC, this should be a good approximation [5]. A detailed examination of the limitations of this approach may be found in Ref. [8].

In the DPS contribution to the production of a W boson in association with a pair of bottom quark jets, one hard scattering produces the W via the Drell-Yan mechanism, while the other hard scattering produces a $b\bar{b}$ pair. The charged lepton from the W decay (along with the

bottom quarks in the final state) provides a relatively clean signal to tag on. Our purpose is to establish whether double parton scattering can be observed as a discernible physics process in $Wb\bar{b}$ production at LHC energies. In the rest of the paper, we outline our simulation of the DPS and SPS contributions to $Wb\bar{b}$, discuss backgrounds for the same final state, and present details of our analysis. We study various single variable and two-dimensional kinematic distributions to bring out the DPS contribution more cleanly, showing that variables designed to exploit the nature of the 2 parton to 2 parton subprocesses can be used to differentiate DPS from SPS with excellent signal over background significance, $S/\sqrt{B} \sim 10$ to 15.

2 Calculation of $Wb\bar{b}$ production

We perform all calculations at center-of-mass energy $\sqrt{s} = 7$ TeV. Event rates are quoted for 10 fb^{-1} of integrated luminosity. For the DPS case, $Wb\bar{b}$ production is computed using Eq. (2) where it is assumed that one hard scattering produces the W boson via $q\bar{q} \rightarrow W^\pm X$, while the other scattering produces the $b\bar{b}$ system. The individual SPS processes which make up the DPS process are generated using the POWHEG BOX event generator [9, 10, 11] which includes next-to-leading order (NLO) QCD corrections for both, plus shower emission. In the SPS production of $Wb\bar{b}$, one hard scattering produces the complete final state. The events from this process are also generated using the POWHEG BOX [12] which implements the NLO calculation of Ref. [13].

Extracting evidence for DPS $Wb\bar{b}$ production is complicated by the fact that many standard model processes imitate the $Wb\bar{b} \rightarrow b\bar{b}l\nu$ final state. In particular, we consider contributions from (a) top quark pair production $t\bar{t}$; (b) single top quark production ($t\bar{b}$, $\bar{t}b$, tj and $\bar{t}j$ modes); (c) Wjj , where both light jets are mistagged as b jets; and (d) Wbj where the light jet is mistagged as a b jet. We also consider the following processes, which have a negligible contribution after cuts: (a) $b\bar{b}j$ where one b quark gives an isolated lepton and the light jet is tagged as a b jet; (b) $Zb\bar{b}$ where one lepton from the Z decay is missed; and (c) $b\bar{b}b\bar{b}$ ($b\bar{b}c\bar{c}$) production where at least one heavy quark gives an isolated lepton and the other does not pass the threshold cuts. The Wjj background (where both jets fake bottom quark jets) can be produced in both SPS and DPS processes.

2.1 Simulation

We concentrate on the final state in which there are two b jets, a hard lepton, and missing transverse energy \cancel{E}_T . We consider only leptonic decays of the W boson ($W \rightarrow l\nu$). We focus on the case $l = \mu$, since electrons with low transverse momentum can be easily faked by light jets. We limit the hadronic activity in our events to include exactly two hard jets, both of which must be identified as bottom quark jets. Finally, all events (DPS and SPS $Wb\bar{b}$ as well as backgrounds) are required to pass the following acceptance cuts:

$$p_{T,b} \geq 20 \text{ GeV}, \quad |\eta_b| \leq 2.5, \quad (4)$$

$$20 \text{ GeV} \leq p_{T,\mu} \leq 50 \text{ GeV}, \quad |\eta_\mu| < 2.1, \quad (5)$$

$$\cancel{E}_T \geq 20 \text{ GeV}, \quad (6)$$

$$\Delta R_{b\bar{b}} \geq 0.4, \quad \Delta R_{b\mu} \geq 0.4, \quad (7)$$

Process	Acceptance cuts	$\cancel{E}_T \leq 45$ GeV	$S'_{p_T} \leq 0.2$
$W^\pm b\bar{b}$ (DPS)	247	231	173
$W^\pm b\bar{b}$ (SPS)	1142	569	114
$t\bar{t}$	1428	290	13
$W^\pm jj$ (DPS)	43.5	37.7	27.3
$W^\pm jj$ (SPS)	101	55.7	19.6
Single top	492	168	15
$W^\pm bj$	152	53.1	8.2

Table 1: Numbers of events before and after the various cuts are applied for 10 fb^{-1} of data. After acceptance cuts, SPS $Wb\bar{b}$ production and $t\bar{t}$ production dominate the event rate. A maximum \cancel{E}_T cut reduces the background from $t\bar{t}$ significantly.

where η is the pseudorapidity and ΔR_{lk} is the separation in the azimuthal-pseudorapidity plane between the two objects l and k :

$$\Delta R_{lk} = \sqrt{(\eta_l - \eta_k)^2 + (\phi_l - \phi_k)^2}. \quad (8)$$

The cut on the missing transverse energy $\cancel{E}_T \geq 20$ GeV is motivated by the fact that the neutrino momentum in W decay is not observed. The 20 GeV cut on the b jets and the lepton is invoked to eliminate contributions from the underlying event. The upper lepton p_T cut is used to reject boosted W bosons, as in the case where a W boson originates from a t -quark decay, or when the W recoils against the $b\bar{b}$ pair in SPS. Our b jet tagging efficiencies, muon identification efficiencies, fake rates, and detector resolution effects are described in Ref. [6].

Table 1 shows the number of events from the $Wb\bar{b}$ final state (DPS and SPS) and the backgrounds after the acceptance cuts, detector effects, and mistagging effects are applied (column labeled “acceptance cuts”). In these results and those that follow, we sum the W^+ and W^- events. In evaluating the DPS processes, we assume a value $\sigma_{\text{eff}} \simeq 12$ mb for the effective cross section. However, we stress that the goal is to motivate an empirical determination of its value at LHC energies. The acceptance cuts are very effective against the Wjj final states, both for DPS and SPS. The results in Table 1 make it apparent that $Wb\bar{b}$ production from SPS and the top quark pair background are the most formidable obstacles in extracting a DPS signal. We address $t\bar{t}$ background rejection in the next section.

2.2 $t\bar{t}$ background rejection

We examine three possibilities to reduce the $t\bar{t}$ background: a cut to restrict \cancel{E}_T from above, rejection of events in which a top quark mass can be reconstructed, and a cut to restrict the transverse momentum of the leading jet. In the end, an upper cut on \cancel{E}_T in the event appears to offer the best advantage. Indeed, one would expect that \cancel{E}_T in $Wb\bar{b}$ events would be smaller than \cancel{E}_T in $t\bar{t}$ events. Top quark decays give rise to boosted W^\pm 's which, after decay, should result in larger values of missing E_T compared to the $Wb\bar{b}$ process. The DPS signal is produced in the region of relatively small \cancel{E}_T and the $t\bar{t}$ background has a harder spectrum in \cancel{E}_T . One way to suppress the $t\bar{t}$ background while leaving the DPS signal unaffected is to impose a maximum \cancel{E}_T cut in the 40-60 GeV range. In the analysis that follows, we include a

maximum \cancel{E}_T cut of 45 GeV in addition to the acceptance cuts outlined above. The effects of the maximum \cancel{E}_T cut are shown in the third column of Table 1. This cut eliminates about 80% of the $t\bar{t}$ background that remains after the initial acceptance cuts. The cut is also effective at reducing the single top quark and Wbj backgrounds, eliminating about 67% in both cases. On the other hand, 93% of the DPS $Wb\bar{b}$ events and 50% of the SPS $Wb\bar{b}$ events are retained. Of the three possibilities we consider to reduce the $t\bar{t}$ background, a cut to restrict \cancel{E}_T from above appears to offer the best advantage, and it is the only cut we impose in addition to the acceptance cuts specified above.

3 Separation of the DPS and SPS contributions

To separate the DPS contribution from the SPS and background contributions, it is valuable to use kinematic variables that take advantage of the 2 parton to 2 parton nature of the underlying DPS subprocesses. The observable S'_{p_T} exploits the transverse momentum balance of 2 to 2 scattering. It is defined as [4]:

$$S'_{p_T} = \frac{1}{\sqrt{2}} \sqrt{\left(\frac{|p_T(b_1, b_2)|}{|p_T(b_1)| + |p_T(b_2)|}\right)^2 + \left(\frac{|p_T(\ell, \cancel{E}_T)|}{|p_T(\ell)| + |\cancel{E}_T|}\right)^2}. \quad (9)$$

Here, $p_T(b_1, b_2)$ is the vector sum of the transverse momenta of the two b jets, and $p_T(\ell, \cancel{E}_T)$ is the vector sum of \cancel{E}_T and the transverse momentum of the charged lepton in the final state. In DPS production, the bottom quarks are produced roughly back-to-back such that the vector sum of their transverse momenta tends to vanish. Likewise, the vector sum of the lepton and neutrino momenta tends to be small (with corrections from the boosted W^\pm). Thus, the S'_{p_T} distribution for the DPS process exhibits an enhancement at low S'_{p_T} , as shown on the left side of Fig. 2. The peak does not occur at exactly $S'_{p_T} = 0$ owing to NLO real radiation that alters the back-to-back nature of the $b\bar{b}$ and $\ell\nu$ systems. On the other hand, SPS production of $Wb\bar{b}$ does not favor back-to-back configurations; it exhibits a peak near $S'_{p_T} = 1$, a feature linked to the fact that many $b\bar{b}$ pairs are produced from gluon splitting [5].

The clean separation in S'_{p_T} between the DPS and SPS $Wb\bar{b}$ processes is obscured by the $t\bar{t}$ background, but this background can be mitigated by a maximum \cancel{E}_T cut, as shown on the right side Fig. 2. The last column of Table 1 shows that a cut $S'_{p_T} < 0.2$ reduces the SPS $Wb\bar{b}$ rate while leaving the DPS signal relatively unaffected. In the end, the major background arises from DPS Wjj , as is expected since this process inhabits the same kinematic regions as the DPS $Wb\bar{b}$ signal. Despite this background, we find a statistical significance for the presence of DPS $Wb\bar{b}$ of $S/\sqrt{B} = 173/\sqrt{197} = 12.3$.

Azimuthal angle balance is a second notable feature of 2 parton to 2 parton scattering. Observables which take into account the angular distribution of events are also useful in the search for DPS. Figure 3 depicts two such observables. In the left plot, we show the event rates for DPS $Wb\bar{b}$ and the backgrounds (SPS $Wb\bar{b}$ included) as a function of the angle between the normals to the two planes defined by the $b\bar{b}$ and $\ell\nu$ systems. These planes are defined in the partonic center-of-mass frame and are specified by the three-momenta of the outgoing jets or leptons. The angle between the two planes is:

$$\cos \Delta\Theta_{b\bar{b}, \ell\nu} = \hat{n}_3(b_1, b_2) \cdot \hat{n}_3(\ell, \nu) \quad (10)$$

where $\hat{n}_3(i, j)$ is the unit three-vector normal to the plane defined by the $i-j$ system and $b_1(b_2)$ is the leading (next-to-leading) b jet. In order to construct the normals $\hat{n}_3(b_1, b_2)$ and $\hat{n}_3(\ell, \nu)$,

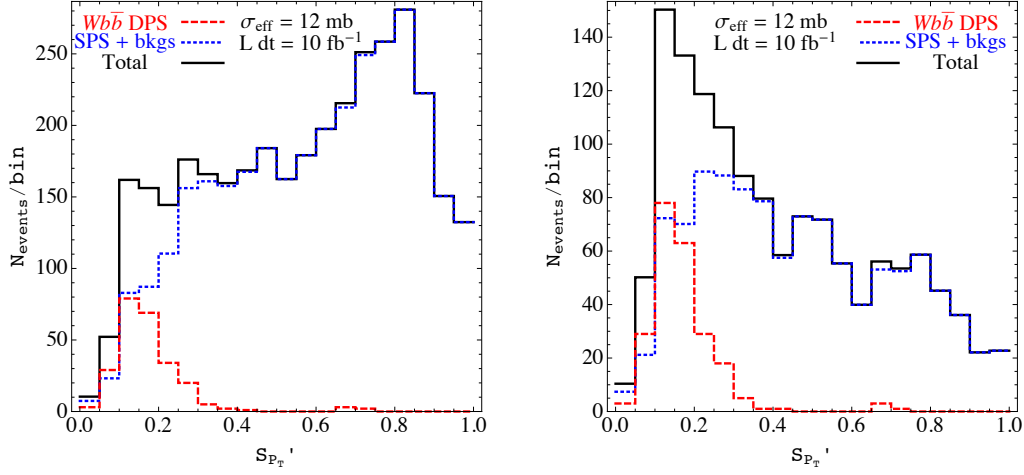


Figure 2: The S'_{p_T} distribution for DPS and SPS production of $Wb\bar{b}$ including all relevant backgrounds. On the left, only the minimal acceptance cuts are imposed, while, on the right, an additional maximum \cancel{E}_T cut is imposed ($\cancel{E}_T < 45$ GeV). A maximum \cancel{E}_T cut greatly reduces the background and produces a sharp peak in the region of small S'_{p_T} where DPS is expected to dominate.

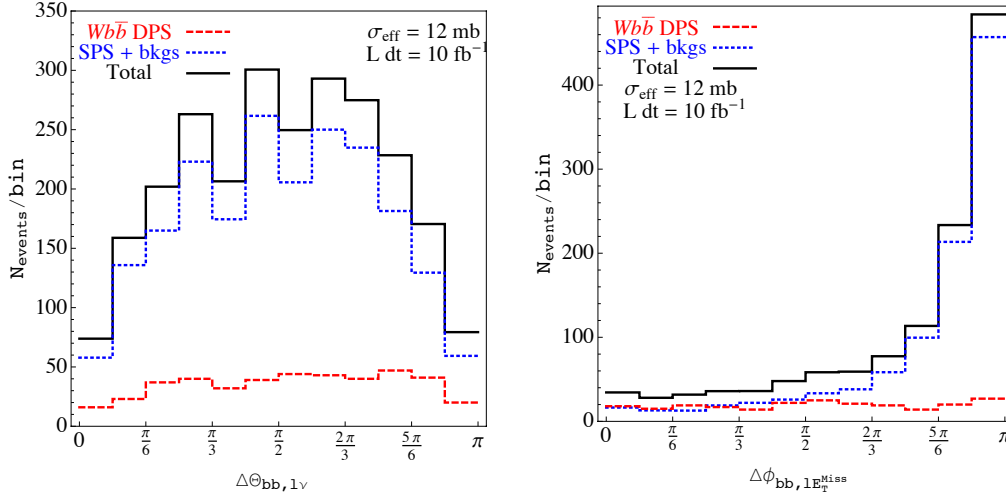


Figure 3: The event rate as a function of the angle between the normals of the two planes defined by the $b\bar{b}$ and $l\nu$ systems (left), and the azimuthal angle between the transverse momentum vectors of the $b\bar{b}$ and $l\cancel{E}_T$ systems (right). In SPS events, it is apparent that there is a strong correlation in the angles.

we require full event reconstruction using the on-shell W -boson mass relations. We see that the distribution of the DPS events is rather flat, aside from the cut-induced suppressions at

$\Theta_{b\bar{b},\ell\nu} \sim 0$ and $\sim \pi$, whereas the SPS events show a strong correlation, with a distribution that peaks near $\Delta\Theta_{b\bar{b},\ell\nu} \sim \frac{\pi}{2}$.

In the right plot of Fig. 3, we show the event rates as a function of the azimuthal angle between the transverse momentum vectors of the $b\bar{b}$ and $\ell\cancel{E}_T$ systems. Since this azimuthal angle is defined in the transverse plane, it requires only \cancel{E}_T . Full event reconstruction to determine the neutrino momentum is not needed. The DPS distribution is flat while the SPS distribution shows a strong correlation, with a preference for values toward π .

The DPS and SPS samples exhibit different behavior as a function of angular observables. However, the dominance of SPS $Wb\bar{b}$ and backgrounds over DPS $Wb\bar{b}$ for the full range of these observables makes it impossible to extract a DPS signal from these distributions by themselves. Having found interesting features in the transverse momentum variable S'_{p_T} and in the angular distributions, we now put this information together in a two-dimensional distribution.

4 Two-dimensional distributions

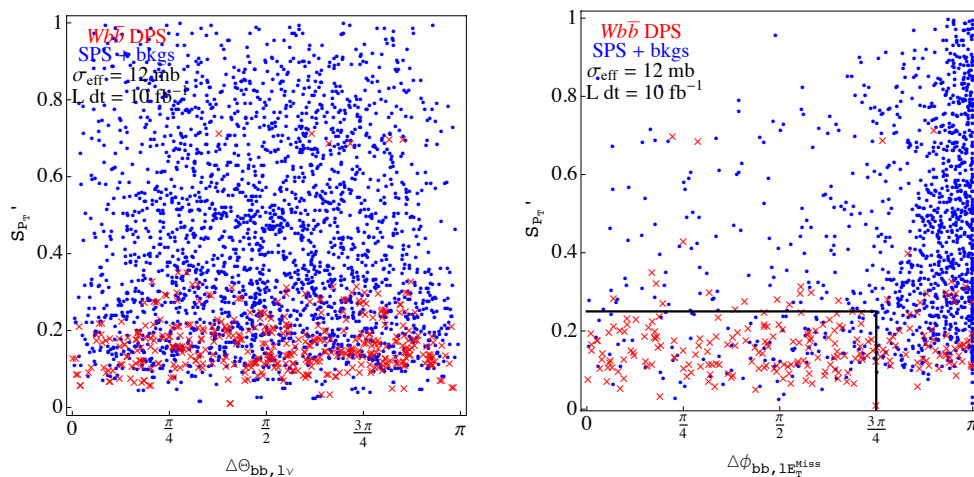


Figure 4: Two-dimensional distributions of events in the variables (left) S'_{p_T} and $\Delta\Theta_{b\bar{b},\ell\nu}$, and (right) S'_{p_T} and $\Delta\phi_{bb,\ell\cancel{E}_T}$. In both cases, the $Wb\bar{b}$ DPS events (denoted by red **x**) lie in the lower half of the plane, while the $Wb\bar{b}$ SPS and background events (denoted by blue **dots**) occupy the upper half. The plot on the right appears to achieve a cleaner separation.

Two-dimensional distributions of one variable against another show distinct regions of DPS dominance (or SPS and background dominance). In Fig. 4, we construct two such scatter plots. On the left, we show S'_{p_T} versus the angle between the normals of the two planes defined by the $b\bar{b}$ and $\ell\nu$ systems ($\Delta\Theta_{b\bar{b},\ell\nu}$). The DPS events reside predominantly in the lower half of the plane (small S'_{p_T}) and are distributed evenly in the angular variable. The separation between DPS $Wb\bar{b}$ and the SPS component is not as pronounced in the $S'_{p_T} - \Delta\Theta_{b\bar{b},\ell\nu}$ plane as we saw in our earlier study of $b\bar{b}jj$ [5]. In the $Wb\bar{b}$ case, the background events are more evenly distributed over the full plane, to some extent resulting from inclusion of both solutions for

the neutrino's longitudinal momentum in the W^\pm decay. (The greater density of points in the left plot of Fig. 4 relative to the right plot is explained by the fact that both solutions for the neutrino momentum are included in the left plot).

On the right of Fig. 4, we show the two-dimensional distribution of S'_{p_T} and $\Delta\phi_{bb,\ell \not{E}_T}$. This distribution shows a high degree of separation between the DPS $Wb\bar{b}$ and the SPS plus background samples. To quantify the degree of separation, we define a region in this plane that gives the highest statistical significance. Restricting $S'_{p_T} < 0.25$ and $\Delta\phi_{bb,\ell \not{E}_T} < 3\pi/4$, we find a sample of 154 signal and 103 background events, corresponding to a statistical significance of $S/\sqrt{B} = 15.2$. Employing the scatter plot in S'_{p_T} and $\Delta\phi_{bb,\ell \not{E}_T}$, we achieve a better significance than from S'_{p_T} alone. As long as the maximum value of $\Delta\phi_{bb,\ell \not{E}_T}$ is in the $\pi/2$ - $3\pi/4$ range, a statistically significant extraction of DPS $Wb\bar{b}$ from the other events can be obtained, given our assumed effective cross section $\sigma_{\text{eff}} = 12$ mb and luminosity.

In this study of $Wb\bar{b}$, as in our earlier study of $bbjj$, we find that DPS can be important relative to SPS in specific parts of phase space. We suggest experimental analyses of $Wb\bar{b}$ at the LHC in terms of the two-dimensional distributions presented in this section, with the goal to establish whether a discernible DPS signal is found. Assuming success, the p_T dependence of the leading object and other properties of these DPS events can be examined to establish whether the expected properties of DPS are seen. The enriched DPS event sample can be used for a direct measurement of the effective cross section σ_{eff} . Data are needed.

Acknowledgments. The work reported here was done in collaboration with Chris Jackson, Seth Quackenbush, and Gabe Shaughnessy. It was supported financially by the U. S. Department of Energy under Contract No. DE-AC02-06CH11357.

References

- [1] Axial Field Spectrometer Collaboration, Z. Phys. C **34** (1987) 163.
- [2] UA2 Collaboration, Phys. Lett. B **268** (1991) 145-154.
- [3] CDF Collaboration, Phys. Rev. D **56** (1997) 3811-3832.
- [4] D0 Collaboration, Phys. Rev. D **81** (2010) 052012 [arXiv:0912.5104 [hep-ex]].
- [5] E. L. Berger, C. B. Jackson and G. Shaughnessy, Phys. Rev. D **81** (2010) 014014 [arXiv:0911.5348 [hep-ph]].
- [6] E. L. Berger, C. B. Jackson, S. Quackenbush and G. Shaughnessy, Phys. Rev. D **84** (2011) 074021 [arXiv:1107.3150 [hep-ph]].
- [7] P. Bartalini, E. L. Berger, B. Blok, G. Calucci, R. Corke, M. Diehl, Y. L. Dokshitzer, L. Fano *et al.*, arXiv:1111.0469 [hep-ph].
- [8] M. Diehl, D. Ostermeier and A. Schafer, JHEP **1203** (2012) 089 arXiv:1111.0910 [hep-ph].
- [9] P. Nason, JHEP **0411** (2004) 040 [arXiv:hep-ph/0409146].
S. Frixione, P. Nason and C. Oleari, JHEP **0711** (2007) 070 [arXiv:0709.2092 [hep-ph]].
S. Alioli, P. Nason, C. Oleari and E. Re, JHEP **1006** (2010) 043 [arXiv:1002.2581 [hep-ph]].
- [10] S. Alioli, P. Nason, C. Oleari and E. Re, JHEP **0807** (2008) 060 [arXiv:0805.4802 [hep-ph]].
- [11] S. Frixione, P. Nason and G. Ridolfi, JHEP **0709** (2007) 126 [arXiv:0707.3088 [hep-ph]].
- [12] C. Oleari and L. Reina, JHEP **1108** (2011) 061, [Erratum-ibid. **1111**, 040 (2011)] [arXiv:1105.4488 [hep-ph]].
- [13] F. Febres Cordero, L. Reina and D. Wackerroth, Phys. Rev. D **74** (2006) 034007 [hep-ph/0606102].

Correlations in multiparton interactions

*Tomas Kasemets*¹

¹DESY, Notkestraße 85, 22607 Hamburg, Germany

DOI: <http://dx.doi.org/10.3204/DESY-PROC-2012-03/11>

Many features of multi-parton interactions are present already in double parton scattering. The two hard scatterings are connected via the double parton distributions, producing effects not present in the case of a single hard interaction. We examine the impact of correlations between initial state partons on the differential cross section for the double Drell-Yan process. The polarizations of the interacting quarks are found to induce correlations between the decay planes of the vector bosons.

1 Introduction

Interactions where more than one of the partons take part in hard collisions can provide new insights about the structure of the proton and also constitute important backgrounds to other processes, such as Higgs production [1].

In studies of multi-parton interactions an often neglected feature are the correlations between the hard collisions. Although such approximations can be partially motivated, under certain conditions, it is still necessary to examine the correlation effects in greater detail. Double parton scattering possess many properties of multi-parton interactions. As a first examination we study the double Drell-Yan process (γ^* , Z , W^\pm) [2, 3, 4]. It has the advantage of being theoretically clean and well understood in the single parton scattering case. We assume that the cross section can be factorized into hard parts, calculable by perturbation theory, and soft parts described by parton densities. The first steps towards a proof of this assumption in the context of the double Drell-Yan process has been taken in [5] and [6]. We calculate the differential cross section taking many of the correlation effects into account, in order to examine how the correlations in the distributions of the two partons propagate into measurable quantities.

2 Double parton interactions

Double parton interactions exhibit many features not present in single parton scattering. The normal parton distribution functions are replaced by double parton distributions, DPDs, and there can be interferences between the two hard collisions.

When more than one parton in the proton interacts, it is only the sum of the momenta and quantum numbers which have to match between the amplitude and the conjugate amplitude [7, 8, 9]. This is illustrated for the double Drell-Yan process in figure 1. Therefore, a parton in the amplitude can have a different momentum than its partner in the conjugate. The momentum difference r in one interaction has to be balanced by the other. Colors of the quarks can be matched in the canonical way inside each hard interaction. But there is also the possibility to

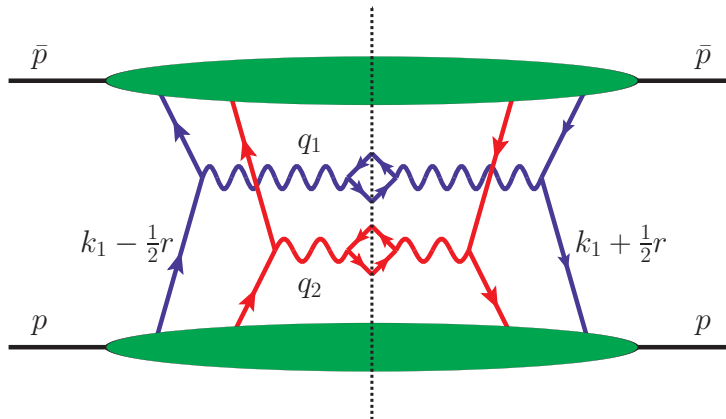


Figure 1: The double Drell-Yan process where two quarks in the right moving proton, with momentum p , interact with two anti-quarks from the left moving proton, with momentum \bar{p} . q_1 and q_2 are the momenta of the vector bosons from interaction one and two, while k_1 is the averaged momentum carried by the parton, in interaction 1, from the right moving proton. r is the momentum miss-match and has to be balanced by collision 2. Barred labels indicate that the quantities are from the left moving proton and the two interactions are labeled by the subscripts 1 and 2 respectively.

match the colors between the two collisions, producing color interference terms. Similarly there can be interference in flavor when the two colliding partons from a proton are different. There can even be fermion number interference between quarks/anti-quarks, but we will not consider this in the following. For the cross section differential in the transverse momenta of the vector bosons, \mathbf{q}_i , the double interactions are not power suppressed compared to single interactions producing the same final state [8] and are important in certain regions of phase space [10]. The power suppression arises when integrating over transverse momenta, due to the larger phase space in the case of a single interaction. k_1 and k_2 are average momenta of the partons taking part in hard interaction 1 and 2 respectively, where the average is taken over the amplitude and its conjugate. Fourier transforming the transverse momentum difference \mathbf{r} into position space, we obtain the transverse distance \mathbf{y} between the two hard interactions, i.e. from interaction 2 to 1.

3 Parton distributions

Interferences and spin correlations in double parton interactions are described by the DPDs and give rise to a large number of different double parton distributions.

The DPDs depend on the momentum fractions x_1 and x_2 carried by the partons in the two collisions, their average transverse momenta \mathbf{k}_1 , \mathbf{k}_2 and the transverse distance \mathbf{y} . Integrating over the transverse momenta yields collinear double parton distributions [11, 12, 13, 14]. The correlation between the spin of the two colliding quarks is reflected by parton distributions describing the polarization of quarks inside a proton, similar to those in single parton distributions with polarized protons [15]. We denote unpolarized quarks by q , longitudinally polarized

quarks by Δq and transversely polarized quarks by δq . We take the DPDs, in equations (1)-(3), in a right moving proton from [5]. For unpolarized and longitudinally polarized quarks the possible combinations are

$$\begin{aligned} F_{qq} &= f_{qq}(x_1, x_2, \mathbf{k}_1, \mathbf{k}_2, \mathbf{y}) \\ F_{\Delta q \Delta q} &= f_{\Delta q \Delta q}(x_1, x_2, \mathbf{k}_1, \mathbf{k}_2, \mathbf{y}) \\ F_{q \Delta q} &= g_{q \Delta q}(x_1, x_2, \mathbf{k}_1, \mathbf{k}_2, \mathbf{y}) \\ F_{\Delta q q} &= g_{\Delta q q}(x_1, x_2, \mathbf{k}_1, \mathbf{k}_2, \mathbf{y}), \end{aligned} \quad (1)$$

where f 's are scalar- and g 's are pseudo scalar-functions. For transverse polarization the parton distributions carry an open, transverse, index which corresponds to the transverse spin vector

$$\begin{aligned} F_{\Delta q \delta q}^i &= M (y^i f_{\Delta q \delta q} + \tilde{y}^i g_{\Delta q \delta q}) \\ F_{q \delta q}^i &= M (\tilde{y}^i f_{q \delta q} + y^i g_{q \delta q}). \end{aligned} \quad (2)$$

M is the proton mass and $\tilde{y}^i = y^j \epsilon^{ij}$, $i = 1, 2$ is a transverse vector orthogonal to y^i . In a left moving proton the sign changes for the pseudo scalar functions g and also of \tilde{y} , due to the change of plus/minus components in the epsilon tensor. When both interactions contain transversely polarized quarks the two open indices make the structure more involved

$$\begin{aligned} F_{\delta q \delta q}^{ij} &= \delta^{ij} f_{\delta q \delta q} + (2y^i y^j - y^2 \delta^{ij}) M^2 f_{\delta q \delta q}^t + (y^i \tilde{y}^j + \tilde{y}^i y^j) M^2 g_{\delta q \delta q}^s \\ &\quad + (y^i \tilde{y}^j - \tilde{y}^i y^j) M^2 g_{\delta q \delta q}^a. \end{aligned} \quad (3)$$

The color interference doubles the number of DPDs since they appear as color singlet distributions $^1 f_{qq}$ and as color octets $^8 f_{qq}$. Further, when the flavors of the two quarks are different, there are both flavor square f_{qq}^S and flavor interference distributions f_{qq}^I . The DPDs for the left moving protons are defined analogously and will be denoted by a bar, i.e. \bar{f}_{qq} for the unpolarized DPD. This is not to be confused with the bar appearing over subscripts which indicate anti-particles.

4 Differential cross section

The different parton distributions are contracted with the appropriate parts of a polarization dependent partonic cross section, yielding the final differential cross section for the double Drell-Yan process. We will present the results of the calculation with focus on the angular structure, and discuss how the cross section is affected by the correlations between the quarks.

To describe the final state kinematics we use a modified version of the Collins-Soper frame [16], where the arbitrary x -axis is, for definiteness, chosen to point towards the center of the LHC ring, see figure 2. The cross section is split into three parts, the first containing no transverse polarization $\sigma^{(0)}$, the second $\sigma^{(1)}$ and third $\sigma^{(2)}$ containing one and two interactions with transversely polarized quarks. The cross section with only unpolarized and longitudinally

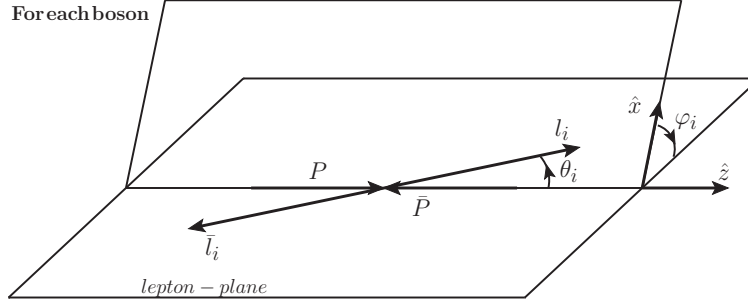


Figure 2: Reference frame for each boson, for simplicity displayed when the transverse momenta of the vector bosons are zero. P is the momentum of the right moving proton while l_i is the momentum of the lepton in interaction i . The x -axis is an arbitrary reference axis which we chose to point towards the center of the LHC ring.

polarized quarks is

$$\begin{aligned}
\frac{d\sigma^{(0)}}{dx_1 dx_2 d\bar{x}_1 d\bar{x}_2 d^2\mathbf{q}_1 d^2\mathbf{q}_2 d\Omega_1 d\Omega_2} &= \frac{\alpha^4 Q_1^2 Q_2^2}{S} \sum_{\substack{q_1, \bar{q}_1, q_2, \bar{q}_2 \\ V_1, V'_1, V_2, V'_2}} \sum_I \sum_{\substack{a_1 \bar{a}_1 = \{q_1 \bar{q}_1, \Delta q_1 \Delta \bar{q}_1, q_1 \Delta \bar{q}_1, \Delta q_1 \bar{q}_1\} \\ a_2 \bar{a}_2 = \{q_2 \bar{q}_2, \Delta q_2 \Delta \bar{q}_2, q_2 \Delta \bar{q}_2, \Delta q_2 \bar{q}_2\}}} \sum \\
&\times \frac{[K_{a_1 \bar{a}_1}^I (1 + \cos^2 \theta_1) - K'_{a_1 \bar{a}_1} \cos \theta_1]}{(Q_1^2 - m_{V_1}^2 + im_{V_1} \Gamma_{V_1}) (Q_1^2 - m_{V'_1}^2 - im_{V'_1} \Gamma_{V'_1})} \\
&\times \frac{[K_{a_2 \bar{a}_2}^I (1 + \cos^2 \theta_2) - K'_{a_2 \bar{a}_2} \cos \theta_2]}{(Q_2^2 - m_{V_2}^2 + im_{V_2} \Gamma_{V_2}) (Q_2^2 - m_{V'_2}^2 - im_{V'_2} \Gamma_{V'_2})} \\
&\times \int d^2y \mathcal{I} [F_{a_1 a_2}^I \bar{F}_{\bar{a}_1 \bar{a}_2}^I + F_{a_1 \bar{a}_2}^I \bar{F}_{\bar{a}_1 a_2}^I + F_{\bar{a}_1 a_2}^I \bar{F}_{a_1 \bar{a}_2}^I + F_{\bar{a}_1 \bar{a}_2}^I \bar{F}_{a_1 a_2}^I]
\end{aligned} \tag{4}$$

where we have used the short hand notation

$$\mathcal{I} [F_{a_1 a_2}^I \bar{F}_{\bar{a}_1 \bar{a}_2}^I] \equiv \int d^2k_1 d^2\bar{k}_1 \delta^{(2)}(\mathbf{q}_1 - \mathbf{k}_1 - \bar{\mathbf{k}}_1) \int d^2k_2 d^2\bar{k}_2 \delta^{(2)}(\mathbf{q}_2 - \mathbf{k}_2 - \bar{\mathbf{k}}_2) F_{a_1 a_2}^I \bar{F}_{\bar{a}_1 \bar{a}_2}^I \tag{5}$$

for the momentum integrals over the DPDs. Q_i^2 is the squared momentum of vector boson i , S is 2 when the final states of the two hard interactions are equal and 1 otherwise. The first sum is over the flavors of quark q_i and anti-quark \bar{q}_i for the two interactions and over the allowed vector bosons in the amplitude V_i and in the conjugated amplitude V'_i , with mass m_{V_i} and $m_{V'_i}$. The sum over I sums the color (singlet 1 and octet 8) and flavor (S_f and I_f) squares and interference terms. $a_i \bar{a}_i$ label the different combinations of unpolarized and longitudinally polarized quarks which affect not only the parton distributions but also the combinations of coupling constants K and K' , which also depend on the flavor of the quarks and vector bosons. K' is zero for photons but for a more detailed discussion we refer to [17]. Instead we want to focus upon the angular structure. θ_i is the angle between the z -axis and the momentum of the outgoing lepton from hard interaction i .

All the different terms have the same angular structures, thus, despite the proliferation of DPDs they all contribute to the same structures in the cross section. However, the relative

factors are different and hence longitudinal polarization as well as interferences in flavor and color affects both the overall rate and the angular distribution.

We now turn towards the part where one interaction involves quarks with transverse polarizations. For the production of W bosons the transversely polarized part of the cross section is zero since they only couple to left-handed particles and hence the only nonzero contribution is for γ/Z bosons in the interaction with transverse polarizations. The cross section is

$$\begin{aligned}
\frac{d\sigma^{(1)}}{dx_i d\bar{x}_i d^2\mathbf{q}_i d\Omega_i} &= \frac{\alpha^4 Q_1^2 Q_2^2}{S} \sum_{\substack{q_1, \bar{q}_1, q_2, \bar{q}_2 \\ V_1, V'_1, V_2, V'_2}} \sum_I \frac{1}{(Q_1^2 - m_{V_1}^2 + im_{V_1}\Gamma_{V_1})(Q_1^2 - m_{V'_1}^2 - im_{V'_1}\Gamma_{V'_1})} \\
&\times \frac{1}{(Q_2^2 - m_{V_2}^2 + im_{V_2}\Gamma_{V_2})(Q_2^2 - m_{V'_2}^2 - im_{V'_2}\Gamma_{V'_2})} M^2 \sin^2 \theta_2 \int d^2y \mathbf{y}^2 \\
&\times \left\{ \sum_{a_1 \bar{a}_1 = \{q_1 \bar{q}_1, \Delta q_1 \Delta \bar{q}_1\}} [K_{a_1 \bar{a}_1}^I (1 + \cos^2 \theta_1) - K_{a_1 \bar{a}_1}^{II} \cos \theta_1] \right. \\
&\quad \times \left([C^I \cos 2(\varphi_2 - \varphi_y) - C'^I \sin 2(\varphi_2 - \varphi_y)] \mathcal{I} [g_{a_1 \delta q_2}^I \bar{g}_{\bar{a}_1 \delta \bar{q}_2}^I - f_{a_1 \delta q_2}^I \bar{f}_{\bar{a}_1 \delta \bar{q}_2}^I + \text{perm.}] \right. \\
&\quad \left. \left. - [C^I \sin 2(\varphi_2 - \varphi_y) + C'^I \cos 2(\varphi_2 - \varphi_y)] \mathcal{I} [g_{a_1 \delta q_2}^I \bar{f}_{\bar{a}_1 \delta \bar{q}_2}^I + f_{a_1 \delta q_2}^I \bar{g}_{\bar{a}_1 \delta \bar{q}_2}^I + \text{perm.}] \right) \right. \quad (6) \\
&+ \sum_{a_1 \bar{a}_1 = \{q_1 \Delta \bar{q}_1, \Delta q_1 \bar{q}_1\}} [K_{a_1 \bar{a}_1}^I (1 + \cos^2 \theta_1) - K_{a_1 \bar{a}_1}^{II} \cos \theta_1] \\
&\quad \times \left([C^I \cos 2(\varphi_2 - \varphi_y) - C'^I \sin 2(\varphi_2 - \varphi_y)] \mathcal{I} [g_{a_1 \delta q_2}^I \bar{f}_{\bar{a}_1 \delta \bar{q}_2}^I - f_{a_1 \delta q_2}^I \bar{g}_{\bar{a}_1 \delta \bar{q}_2}^I + \text{perm.}] \right. \\
&\quad \left. \left. - [C^I \sin 2(\varphi_2 - \varphi_y) + C'^I \cos 2(\varphi_2 - \varphi_y)] \mathcal{I} [g_{a_1 \delta q_2}^I \bar{g}_{\bar{a}_1 \delta \bar{q}_2}^I + f_{a_1 \delta q_2}^I \bar{f}_{\bar{a}_1 \delta \bar{q}_2}^I + \text{perm.}] \right) \right. \\
&\quad \left. + \{1 \leftrightarrow 2\} \right\}
\end{aligned}$$

where C and C' are coupling factors for transverse quarks ($\delta q_2 \delta \bar{q}_2$), similar to the K 's in the previous part and 'perm.' stands for permutations of the quark/anti-quark labels. The angular dependence from interaction 1 is unchanged compared to $\sigma^{(0)}$ but for interaction 2 we now get dependence on azimuthal angles. The angular structure however stays simple and we only have dependence on one new angle, between the transverse momentum of the outgoing lepton from interaction 2 and the vector \mathbf{y} between the two hard interactions. The transverse dependence originates in the breaking of the rotation symmetry around the z -axis caused by the transverse spin of the partons. $\{1 \leftrightarrow 2\}$ represents the contribution in which interaction 1 is transversely polarized. It can be obtained by interchanging the labels for the two interactions and at the same time swapping the positions of the subscripts on the DPDs (For example: $f_{a_1 \delta q_2}$ then becomes $f_{\delta q_1, a_2}$). \mathbf{y} cannot be measured and performing the d^2y integral relates the correlations to the transverse momenta of the vector bosons. The cross section can also be displayed with the quark and final state lepton dependencies separated by aid of an arbitrary x -axis, but we have chosen to display the results in the above form since it gives formulas of shorter lengths.

The doubly transversely polarized cross section is richer in structure

$$\begin{aligned}
\frac{d\sigma^{(2)}}{dx_i d\bar{x}_i d^2\mathbf{q}_i d\Omega_i} &= \frac{\alpha^4 Q_1^2 Q_2^2}{S} \sum_{\substack{q_1, \bar{q}_1, q_2, \bar{q}_2 \\ V_1, V_1', V_2, V_2'}} \sum_I \frac{1}{(Q_1^2 - m_{V_1}^2 + im_{V_1} \Gamma_{V_1}) (Q_1^2 - m_{V_1'}^2 - im_{V_1'} \Gamma_{V_1'})} \\
&\times \frac{1}{(Q_2^2 - m_{V_2}^2 + im_{V_2} \Gamma_{V_2}) (Q_2^2 - m_{V_2'}^2 - im_{V_2'} \Gamma_{V_2'})} \sin^2 \theta_1 \sin^2 \theta_2 \int d^2y \\
&\times \left\{ [A^I \cos 2(\varphi_1 - \varphi_2) - A'^I \sin 2(\varphi_1 - \varphi_2)] \right. \\
&\quad \times \mathcal{I} [f_{\delta q_1 \delta q_2}^I \bar{f}_{\delta \bar{q}_1 \delta \bar{q}_2}^I - \mathbf{y}^4 M^4 g_{\delta q_1 \delta q_2}^{aI} \bar{g}_{\delta \bar{q}_1 \delta \bar{q}_2}^{aI} + \text{perm.}] \\
&\quad + [B^I \cos 2(\varphi_1 + \varphi_2 - 2\varphi_y) - B'^I \sin 2(\varphi_1 + \varphi_2 - 2\varphi_y)] \\
&\quad \times \mathbf{y}^4 M^4 \mathcal{I} [f_{\delta q_1 \delta q_2}^{tI} \bar{f}_{\delta \bar{q}_1 \delta \bar{q}_2}^{tI} - g_{\delta q_1 \delta q_2}^{sI} \bar{g}_{\delta \bar{q}_1 \delta \bar{q}_2}^{sI} + \text{perm.}] \\
&\quad + [A^I \sin 2(\varphi_1 - \varphi_2) + A'^I \cos 2(\varphi_1 - \varphi_2)] \\
&\quad \times \mathbf{y}^2 M^2 \mathcal{I} [f_{\delta q_1 \delta q_2}^I \bar{g}_{\delta \bar{q}_1 \delta \bar{q}_2}^{aI} + g_{\delta q_1 \delta q_2}^{aI} \bar{f}_{\delta \bar{q}_1 \delta \bar{q}_2}^I + \text{perm.}] \\
&\quad - [B^I \sin 2(\varphi_1 + \varphi_2 - 2\varphi_y) + B'^I \cos 2(\varphi_1 + \varphi_2 - 2\varphi_y)] \\
&\quad \left. \times \mathbf{y}^4 M^4 \mathcal{I} [f_{\delta q_1 \delta q_2}^{tI} \bar{g}_{\delta \bar{q}_1 \delta \bar{q}_2}^{sI} + g_{\delta q_1 \delta q_2}^{sI} \bar{f}_{\delta \bar{q}_1 \delta \bar{q}_2}^{tI} + \text{perm.}] \right\}, \tag{7}
\end{aligned}$$

where A , A' , B , and B' are coupling factors. This part of the cross section depends on θ_1 and θ_2 but also on the transverse angle between the two outgoing leptons and the angles between them and the direction \mathbf{y} . These describe transverse correlations between the decay planes of the two vector bosons and between the decay planes and the direction between the hard collisions.

5 Transverse dependence of DPDs

We employ a simple Gaussian model for the transverse dependence of the double parton distributions, and study how the interplay of longitudinal and transverse dependence affects the cross section. Even though the transverse structure of the proton is much more complicated than the model suggests, it can still provide some useful insights into what might be expected in a more complete treatment.

The transverse dependence of the proton is approximated as a three quark Fock state [18] and the wave function is separated into a purely longitudinal part and a mixed longitudinal and transverse part

$$\Psi(\hat{x}_i, \hat{\mathbf{k}}_i) = \phi(\hat{x}_i) \Omega(\hat{x}_i, \hat{\mathbf{k}}_i). \tag{8}$$

We take the Gaussian ansatz [19]

$$\Omega(\hat{x}_i, \hat{\mathbf{k}}_i) = \frac{(16\pi^2 a^2)^2}{\hat{x}_1 \hat{x}_2 \hat{x}_3} \exp \left\{ -a^2 \left(\frac{\hat{\mathbf{k}}_1^2}{\hat{x}_1} + \frac{\hat{\mathbf{k}}_2^2}{\hat{x}_2} + \frac{\hat{\mathbf{k}}_3^2}{\hat{x}_3} \right) \right\}, \tag{9}$$

where a is a positive constant of dimension GeV^{-1} , which allows us to carry out the integrations analytically. The \hat{x}_i are the longitudinal momentum fractions and $\hat{\mathbf{k}}_i$ transverse momenta of

the three quarks in the Fock state. After performing the transverse integrals, the transverse dependence of the DPDs renders the unpolarized cross section proportional to

$$\exp \left\{ -\frac{1}{8a^2} (b \mathbf{q}_1^2 + c \mathbf{q}_1 \mathbf{q}_2 + d \mathbf{q}_2^2) \right\}. \quad (10)$$

b , c and d are positive functions of $x_1, x_2, \bar{x}_1, \bar{x}_2$. The cross section decreases with transverse momenta of the two vector bosons, as expected since the quarks are more likely to be collinear to their proton. But due to the $\mathbf{q}_1 \mathbf{q}_2$ term equation (10) also shows that the cross section increases when the two bosons have opposite transverse momentum. Since already this simple model causes dependence on the azimuthal angle between the vector boson momenta, there is reason to expect such effects to be present also in more realistic descriptions.

6 Conclusions

Spin correlations, color and flavor interference proliferate the number of double parton distributions. Nevertheless, for the double Drell-Yan process many of them contribute to the same angular structures in the differential cross section. Longitudinal polarization, color and flavor interference does not introduce any new angular structures but affects both the overall rate and the angular distribution. The spin vectors of the transversely polarized quarks break the rotational invariance around the z -axis. This leads to a dependence of the cross section on the transverse angle between the decay planes of the vector bosons, different from the dependence when the two bosons are produced in one hard collision. The cross section also depends on the angles between the decay planes and the transverse direction between the two collisions. This direction is not measurable and integrating over it causes correlations with the transverse momenta of the vector bosons. Effects appearing for double Drell-Yan process are also expected in other types of processes, for example double dijet production should display similar features, but the color structure of these processes increases their complexity dramatically. Finally, we showed that even a simple model for the transverse dependence of the double parton distributions causes a dependence on the azimuthal angle between the momenta of the two vector bosons.

References

- [1] A. Del Fabbro, D. Treleani, “A Double parton scattering background to Higgs boson production at the LHC,” *Phys. Rev. D* **61** (2000) 077502 (arXiv:9911358 [hep-ph]).
- [2] M. Mekhfi, “Multiparton Processes: An Application To Double Drell-yan,” *Phys. Rev. D* **32** (1985) 2371.
- [3] J. R. Gaunt, C. -H. Kom, A. Kulesza, W. J. Stirling, “Same-sign W pair production as a probe of double parton scattering at the LHC,” *Eur. Phys. J. C* **69** (2010) 53 (arXiv:1003.3953 [hep-ph]).
- [4] C. H. Kom, A. Kulesza, W. J. Stirling, “Prospects for observation of double parton scattering with four-muon final states at LHCb,” *Eur. Phys. J. C* **71** (2011) 1802 (arXiv:1109.0309 [hep-ph]).
- [5] M. Diehl, D. Ostermeier, A. Schäfer, “Elements of a theory for multiparton interactions in QCD,” *JHEP* **1203** (2012) 089 (arXiv:1111.0910 [hep-ph]).
- [6] A. V. Manohar, W. J. Waalewijn, “A QCD Analysis of Double Parton Scattering: Color Correlations, Interference Effects and Evolution,” (arXiv:1202.3794 [hep-ph]).
- [7] M. Mekhfi, “Correlations In Color And Spin In Multiparton Processes,” *Phys. Rev. D* **32** (1985) 2380.
- [8] M. Diehl, A. Schäfer, “Theoretical considerations on multiparton interactions in QCD,” *Phys. Lett. B* **698** (2011) 389 (arXiv:1102.3081 [hep-ph]).

- [9] J. R. Gaunt, “Double Parton Splitting Diagrams and Interference and Correlation Effects in Double Parton Scattering,” (arXiv:1110.1536 [hep-ph]).
- [10] B. Blok, Y. Dokshitzer, L. Frankfurt, M. Strikman, “pQCD physics of multiparton interactions,” (arXiv:1106.5533 [hep-ph]).
- [11] F. A. Ceccopieri, “An update on the evolution of double parton distributions,” Phys. Lett. B **697** (2011) 482 (arXiv:1011.6586 [hep-ph]).
- [12] J. R. Gaunt, W. J. Stirling, “Double Parton Scattering Singularity in One-Loop Integrals,” JHEP **1106** (2011) 048 (arXiv:1103.1888 [hep-ph]).
- [13] M. G. Ryskin, A. M. Snigirev, “A Fresh look at double parton scattering,” Phys. Rev. D **83** (2011) 114047 (arXiv:1103.3495 [hep-ph]).
- [14] A. M. Snigirev, “Double-parton distributions in QCD,” Phys. Atom. Nucl. **74** (2011) 158 [Yad. Fiz. **74** (2011) 158].
- [15] D. Boer, “Investigating the origins of transverse spin asymmetries at RHIC,” Phys. Rev. D **60** (1999) 014012 (arXiv:9902255 [hep-ph]).
- [16] J. C. Collins, D. E. Soper, “Angular Distribution of Dileptons in High-Energy Hadron Collisions,” Phys. Rev. D **16** (1977) 2219.
- [17] T. Kasemets, M. Diehl, in preparation.
- [18] M. Diehl, T. Feldmann, R. Jakob, P. Kroll, “The Overlap representation of skewed quark and gluon distributions,” Nucl. Phys. B **596** (2001) 33 [Erratum-ibid. B **605** (2001) 647] (arXiv:0009255 [hep-ph]).
- [19] S. J. Brodsky, T. Huang, G. P. Lepage, “The Hadronic Wave Function In Quantum Chromodynamics,” SLAC-PUB-2540.

Fluctuations of the nucleon transverse parton densities and inelastic collisions at the LHC

Mark Strikman

Penn State University, University Park, PA 16802, USA

DOI: <http://dx.doi.org/10.3204/DESY-PROC-2012-03/9>

We consider constraints on modeling of inelastic collisions at the LHC which follow from the studies of the transverse structure of nucleon, fluctuations of the strength of the gluon field at small x and the rate of the multiparton interactions at the Tevatron. Effects due to proximity to the black disk regime are discussed. We also suggest that gluon fluctuations are maybe responsible for a number of the features of the high multiplicity events studied by CMS

1 Introduction

Modeling of the inelastic collisions at the LHC has two principal goals. One is to ensure a good description of the underlying events for the processes used to look for new particles. Another is to learn about working of QCD at ultrahigh energies. In the first case one can use a wider range of the input parameters allowing them to be outside the range dictated by the other data, ignoring effects of high gluon densities which start to be important at the LHC energies. However this way one can easily overlook emergence of new QCD phenomena.

In this talk I will focus on several challenges for building realistic description of inelastic pp collisions: including realistic transverse parton distributions in modeling pp collisions, including parton - parton correlations to describe multiparton interactions with realistic single parton transverse densities, realistic modeling of effects of black disk regime (BDR) at moderate transverse momenta both in the central and forward region, probing BDR at forward rapidities, modeling effects of diffraction for inelastic collisions.

2 Impact parameter distributions of the hard inelastic collisions

Most of the current Monte Carlo approaches model pp collisions using the impact parameter representation. This is a natural framework for description of the complete picture of the high energy interaction since in high-energy pp scattering angular momentum conservation implies that the impact parameter b becomes a good quantum number. Hence it is natural to consider amplitudes and cross sections in the impact parameter representation.

The QCD factorization theorem for hard exclusive processes [1] allows to determine in a model independent way the small x generalized diagonal parton distribution (GPD), $g(x, t|Q^2)$, where the momentum transfer to the nucleon is in the transverse direction, with $t = -\Delta_{\perp}^2$ (we

follow the notation of Refs. [2, 3]). This function reduces to the usual gluon density in the nucleon in the limit of zero momentum transfer, $g(x, t = 0|Q^2) = g(x|Q^2)$. Its two-dimensional Fourier transform

$$g(x, \rho|Q^2) \equiv \int \frac{d^2\Delta_\perp}{(2\pi)^2} e^{i(\Delta_\perp \rho)} g(x, t = -\Delta_\perp^2|Q^2) \quad (1)$$

describes the one-body density of gluons with given x in transverse space, with $\rho \equiv |\boldsymbol{\rho}|$ measuring the distance from the transverse center-of-momentum of the nucleon, and is normalized such that $\int d^2\rho g(x, \rho|Q^2) = g(x|Q^2)$. It is convenient to separate the information on the total density of gluons from their spatial distribution and parametrize the GPD in the form

$$g(x, t|Q^2) = g(x|Q^2) F_g(x, t|Q^2), \quad (2)$$

where the latter function satisfies $F_g(x, t = 0|Q^2) = 1$ and is known as the two-gluon form factor of the nucleon. Its Fourier transform describes the normalized spatial distribution of gluons with given x ,

$$F_g(x, \rho|Q^2) \equiv \int \frac{d^2\Delta_\perp}{(2\pi)^2} e^{i(\Delta_\perp \rho)} F_g(x, t = -\Delta_\perp^2|Q^2), \quad (3)$$

with $\int d^2\rho F_g(x, \rho|Q^2) = 1$ for any x .

The QCD factorization theorem predicts that the t -dependence of the vector meson (VM) production should be a universal function of t for fixed x (up to small DGLAP evolution effects). Indeed the t -slope of the J/ψ production is practically Q^2 independent, while the t -slope of the production of light vector mesons approaches that of J/ψ for large Q^2 .

The t -dependence of the measured differential cross sections of exclusive processes at $|t| < 1 \text{ GeV}^2$ is commonly described either by an exponential, or by a dipole form inspired by analogy with the nucleon elastic form factors. Correspondingly, we consider here two parametrizations of the two-gluon form factor:

$$F_g(x, t|Q^2) = \begin{cases} \exp(B_g t/2), \\ (1 - t/m_g^2)^{-2}, \end{cases} \quad (4)$$

where the parameters B_g and m_g are functions of x and Q^2 . The two parametrizations give very similar results if the functions are matched at $|t| = 0.5 \text{ GeV}^2$, where they are best constrained by present data (see Fig. 3 of Ref. [4]); this corresponds to [3]

$$B_g = 3.24/m_g^2. \quad (5)$$

The analysis of the HERA exclusive data leads to

$$B_g(x) = B_{g0} + 2\alpha'_g \ln(x_0/x), \quad (6)$$

where $x_0 = 0.0012$, $B_{g0} = 4.1 \text{ }^{(+0.3)}_{(-0.5)} \text{ GeV}^{-2}$, $\alpha'_g = 0.140 \text{ }^{(+0.08)}_{(-0.08)} \text{ GeV}^{-2}$ for $Q_0^2 \sim 3 \text{ GeV}^2$. For fixed x , $B_g(x, Q^2)$ slowly decreases with increase of Q^2 due to the DGLAP evolution [2]. The uncertainties in parentheses represent a rough estimate based on the range of values spanned by the H1 and ZEUS fits, with statistical and systematic uncertainties added linearly.

The probability distribution of pp impact parameters in events with a given hard process, $P_2(x_1, x_2, b|Q^2)$, is given by the ratio of the cross section at given b and the cross section integrated over b . As a result

$$P_2(x_1, x_2, b|Q^2) \equiv \int d^2\rho_1 \int d^2\rho_2 \delta^{(2)}(\mathbf{b} - \boldsymbol{\rho}_1 + \boldsymbol{\rho}_2) F_g(x_1, \rho_1|Q^2) F_g(x_2, \rho_2|Q^2). \quad (7)$$

This distribution represents an essential tool for phenomenological studies of the underlying event in pp collisions [2, 3].

For the two parametrizations of Eq. (4), Eq. (7) leads to (for $x \equiv x_1 = x_2$)

$$P_2(x, b|Q^2) = \begin{cases} (4\pi B_g)^{-1} \exp[-b^2/(4B_g)], \\ [m_g^2/(12\pi)] (m_g b/2)^3 K_3(m_g b), \end{cases} \quad (8)$$

where the parameters B_g and m_g are taken at the appropriate values of x and Q^2 .

Comment: The popular Monte Carlo approaches to modeling pp collisions at the collider energies – PYTHIA[5] and HERWIG[6] – use x -independent transverse distributions of partons. In PYTHIA it is given by the sum of two exponentials. This distribution is roughly equivalent to the dipole parametrization with $m^2 \approx 2 \text{ GeV}^2$ [7] which is hardly consistent with the data on J/ψ exclusive photo-production. For smaller x the difference is even larger since the transverse size increases with decrease of x – see Eq. 6. In HERWIG the dipole fit is used with m_g treated as a free parameter which is allowed to vary in a broad interval. Using parametrizations of the transverse distribution with $m_g^2 s \sim 2\text{GeV}^2$ leads to a much more narrow area in the impact parameter for events collisions with a dijet trigger – a factor of two for $x \sim 10^{-2}$ and at least of three for $x \leq 10^{-3}$. Such strong localization of the hard interactions in b strongly suppresses probability of the hard collisions at large impact parameters, leaving a much larger phase space for soft collisions. It also masks problems with s -channel unitarity for large $b \sim 1.5 \text{ fm}$ [8].

Comparison of Eq. (8) with the b dependence of the generic inelastic collisions [2, 3] leads to conclusion that there are two distinctive classes of collisions at the LHC – large b collisions with a modest dijet activity and the central events with enhanced dijet activity. Also the QCD analysis of [2, 3] has demonstrated that in the kinematics available at the LHC the distribution over b of inclusive dijet production changes very little with the variation of x 's of the colliding partons and with p_T of the produced jets. This leads to the expectation of the universal structure of the underlying events [3]. Indeed ATLAS and CMS report that for sufficiently high p_T of the leading particle ($\geq 6 - 8 \text{ GeV}/c$ for $\sqrt{s} = 7 \text{ TeV}$) the away multiplicity $|\Delta\phi| > 120^\circ$ practically does not depend on p_T . Note however that a more accurate study of the universality and possible difference between two gluon jets and $q\bar{q}$ trigger would require introducing a tighter cut on $\Delta\phi$ or subtracting the jet fragmentation contribution by fitting $\Delta\phi$ dependence of the underlying multiplicity.

Many further tests of the discussed picture which were suggested in Ref. [3] will be feasible in a near future. They include (i) Check that the transverse multiplicity does not depend on rapidities of the jets, (ii) Study of the multiplicity at $y < 0$ for events with jets at $y_1 \sim y_2 \sim 2$. This would allow to check that the transverse multiplicity is universal and that multiplicity in the away and towards regions are similar to the transverse multiplicity for $y \leq 0$. (iii) Studying whether transverse multiplicity is the same for quark and gluon induced jets. Since the gluon radiation for production of W^\pm, Z is smaller than for gluon dijets, a subtraction of the radiation effect mentioned below is very important for such a comparison.

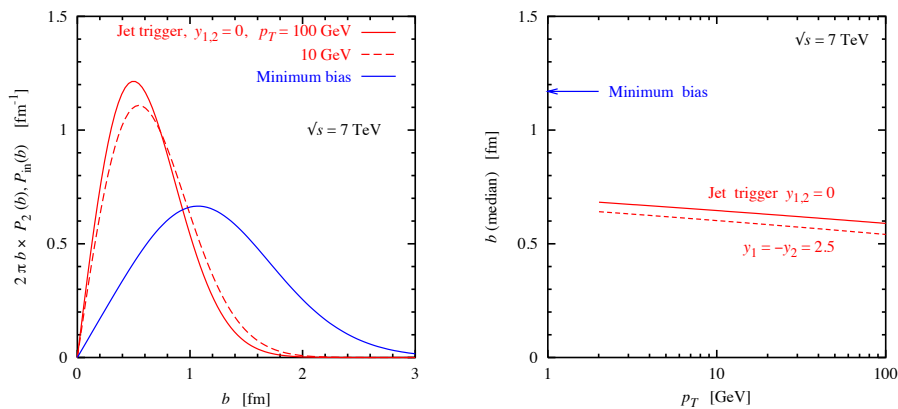


Figure 1: (a) Impact parameter distributions of inelastic pp collisions at $\sqrt{s} = 7$ TeV. *Solid (dashed) line*: Distribution of events with a dijet trigger at zero rapidity, $y_{1,2} = 0$, for $p_T = 100$ (10) GeV cf. Eq. (8). *Dotted line*: Distribution of minimum-bias inelastic events. (b) Dependence of median b on p_T for different rapidities of the dijets.

It is also worth noting that in the experimental comparisons of transverse multiplicity in the events with dijet trigger and generic inelastic events the diffractive events are often removed from the comparison. There is a strong evidence for suppression of the dijet production in the diffractive events confirming generic expectation that high energy inelastic diffraction is predominantly a large b phenomenon. Hence removing diffractive events reduces the difference between median b 's of two classes of the events. Therefore a strong increase of the transverse multiplicity occurs over somewhat smaller range of impact parameters than indicated by Fig. 1.

3 Correlations of partons and multiparton interactions

Measurements of multiparton interactions provide a unique opportunity to study parton - parton correlations in nucleons. Multiparton interactions were observed in a number of experiments at the Tevatron. The first results from the ATLAS experiment were reported at this meeting.

If we parameterize $4 \rightarrow 4$ cross section as

$$\frac{d\sigma(4 \rightarrow 4)}{d\Omega_1 d\Omega_2} = \frac{1}{S} \frac{d\sigma(2 \rightarrow 2)}{d\Omega_1} \frac{d\sigma(2 \rightarrow 2)}{d\Omega_2} \quad (9)$$

where Ω_i is the phase volume for production of a pair of jets, the Tevatron data indicate $S \sim 15$ mb. Similar S (which is often denoted as σ_{eff} or πR_{int}^2) was reported by ATLAS at this meeting.

In the independent particle approximation which is used in all Monte Carlo models with multiparton interactions, the two-parton GPD is equal to the product of single particle GPDs discussed in section 2. Using parametrization of Eq. (8) one finds [2, 9]

$$\frac{1}{S} = \int \frac{d^2\Delta}{(2\pi)^2} F_g^4(\Delta) = \frac{m_g^2}{28\pi}, \quad (10)$$

which leads to approximately a factor of two smaller cross section than the one observed at the Tevatron: $S \approx 34$ mb. This clearly shows that significant *positive* correlations should be present between partons for x 's \sim few 10^{-2} probed experimentally.

There are a priori two possibilities: (a) correlations induced via pQCD evolution which correspond to $3 \rightarrow 4$ processes [9], (b) non-perturbative correlations at the resolution scale of $Q_0^2 \sim 1$ GeV².

The analysis of [10, 11] indicates that $3 \rightarrow 4$ processes play a minor role in the Tevatron kinematics and do not allow to solve this discrepancy. Hence the only viable option seems to be presence of non-perturbative correlations. In principle they could be due to transverse or longitudinal correlations or a mix. Our studies indicate that for small x the enhancement of the cross section results from comparable contributions of the transverse and longitudinal correlations [11]. A model independent measurement of the longitudinal correlations will be possible in the pA collisions [12].

Hence in modeling inelastic collisions at the LHC one is faced with a choice between two options: ignoring information about transverse distribution of partons from hard exclusive processes and fixing it to describe four jet event – this solution is implemented in the standard versions of PYTHIA – or introducing parton-parton correlations in generating configurations for MCs, – so far not implemented in any MCs.

4 Fluctuations of the gluon field and high multiplicity events at LHC

Strength of the gluon field should depend on the size of the quark configurations. For example, the gluon field in the small configurations should be strongly screened – the gluon density much smaller than average.

The variance of the gluon strength at small x can be extracted from the comparison of the diffractive processes: $\gamma_L^* + p \rightarrow V + X$ and $\gamma_L^* + p \rightarrow V + p$ [13]:

$$\omega_g \equiv \frac{\langle G^2 \rangle - \langle G \rangle^2}{\langle G \rangle^2} = \frac{d\sigma_{\gamma^*+p \rightarrow VM+X}}{dt} \bigg/ \frac{d\sigma_{\gamma^*+p \rightarrow VM+p}}{dt} \bigg|_{t=0}. \quad (11)$$

The HERA data indicate that for $Q^2 \sim 3$ GeV² and $x \sim 10^{-3}$, $\omega_g \sim 0.15 \div 0.2$ which is rather close to the value for the analogous ratio for the soft diffraction which measures fluctuations of overall strength of the *soft* hadronic interactions.

How can one probe the gluon fluctuations in pp collisions? Let us consider multiplicity of an inclusive hard process – dijet,... as a function of some cuts – for example overall hadron multiplicity, M (trigger), and build the ratio

$$R = \frac{M(\text{trigger})}{M(\text{minimum} - \text{bias})}. \quad (12)$$

If there are no fluctuations of the parton densities, the maximal value of R is reached if the trigger selects collisions at small impact parameters $b \sim 0$. Using Eq. (8) we find [14]

$$R = P_2(0)\sigma_{in}(pp) = \frac{m_g^2}{12\pi}\sigma_{in}(pp) \approx 4.5. \quad (13)$$

A larger enhancement of R could arise only from the fluctuations of the gluon density per unit area.

The first measurement which appears to be relevant for addressing the question of fluctuations was reported by ALICE [15]. The multiplicity of J/ψ was studied as a function of the multiplicity in the central detector, namely $dN_{ch}^R/d\eta = dN_{ch}/d\eta_{\eta=0} / \langle dN_{ch}/d\eta_{\eta=0} \rangle$, for $dN_{ch}^R/d\eta \leq 5$. It was found that R increases with increase of $dN_{ch}^R/d\eta$ reaching values ≈ 5 for $dN_{ch}^R/d\eta \sim 4$. This number is close to what we estimated above. Any further increase of R would require presence of the fluctuations in transverse gluon density. An enhancement above the geometric $b = 0$ effect is given by the factor

$$R_{fl} = \frac{g_N(x_1, Q^2|n)g_N(x_2, Q^2|n) \langle S \rangle}{g_N(x_1, Q^2)g_N(x_2, Q^2) S}. \quad (14)$$

Here n labels configurations selected by the trigger, and S is the area of the transverse overlap. In principle R_{fl} could reach very large values. For example, if we consider a collision of two protons in cigar shape configurations with the same gluon density for different orientations of the protons, the enhancement would be proportional to the ratio of the principal axes of the ellipsoid. Another mechanism for the enhancement of R_{fl} is the presence of the dispersion in the gluon density with $\omega_g \sim 0.15 \div 0.2$, Eq. (11), which leads to a few percent probability for the gluon field to be a factor 1.5 larger than average.

These observations are maybe of relevance for the discussion of the high multiplicity (HM) events studied by the CMS [16]. In the analysis very rare events were selected which have the overall multiplicity for $|\eta| < 2.4$ of at least a factor of ≥ 7 larger than the minimum-bias events. Probability of such events is very small: $P_{HM} \approx 10^{-5} \div 10^{-6}$. The two-particle correlations were measured as a function of the distance in the pseudorapidity - $\Delta\eta$ and the azimuthal angle - $\Delta\phi$. Three types of correlations were observed : (a) very strong local correlation for $\Delta\eta \sim 0, \Delta\phi \sim 0$, (b) strong correlation for $\Delta\phi \sim \pi$ for a wide range of $\Delta\eta$, (c) a weak correlation for $2 < |\Delta\eta| < 4.8, \Delta\phi \sim 0$ - so called ridge.

The first question to address is how to get such a large multiplicity. It is pretty obvious that such events should originate from very central collisions. Based on our knowledge of $P_2(b)$ we find that the probability of the collisions at $b < 0.2$ fm is $\sim 2\%$. Using information about dispersion of fluctuations of the gluon fields we estimate the probability of fluctuation where **both** nucleons have $g > 1.5g_N(x)$ is $\geq 10^{-3}$. So a natural guess is that the CMS trigger selected central collisions with enhanced gluon fields in both nucleons. This should result in a much higher rate of jet production per event. Indeed inspection of the HM data indicates presence of a large total excess transverse momentum in the $\Delta\phi \sim \pi$ region. Presumably it is due to production of two back to back jets with the trigger jet generating the narrow same side correlation. Qualitatively, a large probability of the dijets is maybe due to the combination of centrality and the gluon density fluctuation. A quantitative analysis of the excess transverse momenta in the same side and away side regions is badly needed.

Note also that the increase of the multiplicity due to selection of $b \sim 0$ and selection of $b \sim 0$ and enhanced dijet production is not sufficient to generate a factor of 7 increase in the multiplicity - without of the gluon density fluctuations these two effects typically lead to $N_{ch} \sim 70$. The $g > g_N(x)$ gluon fluctuations would naturally lead to a further increase of N_{ch} .

The same side ridge could originate from the QCD string effect [17]. This could be tested by studying collisions with production of dijets with $p_T \sim 15$ GeV/c without HM trigger. Alternative mechanism would be fluctuations of the transverse shape of the colliding nucleons

plus presence of the absorptive effects for $p_t \leq 3$ GeV/c. Such a scenario appears quite natural for the high density mechanism we discuss here.

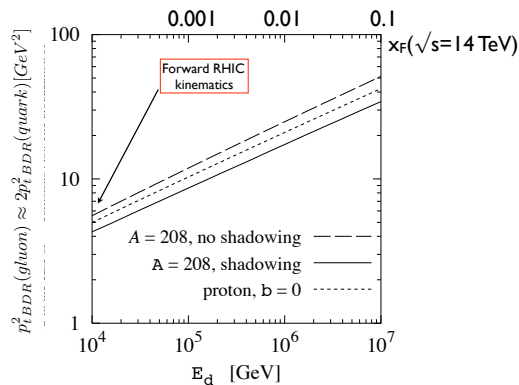


Figure 2: The p_T range where interaction is close to the BDR for the interaction of $q\bar{q}$ and color octet dipoles plotted as a function of the energy of the dipole and of x of the interacting parton for pp interactions at $\sqrt{s} = 14$ TeV.

5 Onset of nonlinear regime and suppression of minijets in pp collisions

One of the important observations of the MC models is that to reproduce the data one needs to suppress production of minijets. PYTHIA [5] introduces the energy dependent suppression factor

$$R(p_T) = p_T^4 / (p_T^2 + p_0^2(s))^2, \quad (15)$$

with $p_0(\sqrt{s} = 7 \text{ TeV}) \approx 3 \text{ GeV}/c$, corresponding to $R(p_T = 4 \text{ GeV}/c) = 0.4$. In HERWIG [6] a cutoff of similar magnitude is introduced of the form $\theta(p_T - p'_0(s))$. (Need for a cutoff of similar magnitude can be derived also by considering requirements imposed by the condition that probability of the pp collision at a given impact parameter (as determined from the data on elastic scattering) should be larger than the probability of processes with jet production. One can see that the main minijet contribution to the cross section for $\sqrt{s} = 7 \text{ TeV}$ originates from $x_i \sim 2p_T/\sqrt{s} \geq 10^{-3}$ and virtualities $Q^2 \geq 10 \text{ GeV}^2$. This is where kinematics describes well DIS scattering. So cutoff is not connected to the taming of the parton distributions at small x . This is consistent with the studies of the elastic small dipole – nucleon interaction which indicate that for this kinematics partial waves of the scattering amplitude are far from the limit of complete absorption (Black Disk Regime - BDR) even for small b , for a review see [2]. The results of this analysis for $b = 0$ are presented in Fig.2. However interaction of the colliding partons with the rest of the nucleon corresponds to much larger invariant energies and hence smaller x . This is because a parton in the nucleon with a given x_1 resolves the gluons in the second nucleon with x_2 down to $4p_T^2/x_1s$. For example, taking $x \sim 10^{-2}$, $\sqrt{s} = 14 \text{ TeV}$ and $\sim p_T^2 = 4 \text{ GeV}^2$ we find $x_2(\text{min}) = 10^{-4}$. For these x interaction is much closer to BDR, see Fig.2. Hence it appears that BDR for gluons is present in the kinematics relevant for

the presence of effective cutoff for the minijet production via interactions with the “spectator” partons. How to implement this effect in the MCs remains an open question. In any case, such a procedure has to overcome an important deficiency of the current procedure – suppression of the interaction of leading partons with media which allows a parton with large x_F to propagate through the center of the nucleon without interaction at relatively small virtualities. Such a scenario clearly contradicts the pattern of strong suppression of the leading particle production expected in the BDR. These expectations are consistent with the regularities of the leading pion production in the central deuteron-gold collisions at RHIC where local nuclear gluon density is comparable to that at the average impact parameters in pp collisions at the LHC, see [18] for the recent summary.

6 Conclusions

It is important to start developing models of inelastic pp collisions which satisfy constraints on the transverse distributions of partons from the hard exclusive processes, as well as from the measurements of MPI. This would require introducing significant correlations in the generalized double parton distributions. Effects of the BDR dynamics should be also taken into account.

It is important to perform dedicated analyses of the data to test transverse geometry of the pp collisions and to understand better dependence of the diffractive collisions on impact parameter. A number of the processes can be used to probe color fluctuations effects in pp collisions with a hard trigger. Critical tests of the underlying dynamics and in particular effects of proximity to the BDR could be performed studying hadron production in the fragmentation region and the long range correlations between hadron production in the forward and central regions.

Acknowledgements The research was supported by the DOE grant No. DE-FG02-93ER40771.

References

- [1] J. C. Collins, L. Frankfurt and M. Strikman, Phys. Rev. D **56**, 2982 (1997).
- [2] L. Frankfurt, M. Strikman and C. Weiss, Phys. Rev. D **69**, 114010 (2004).
- [3] L. Frankfurt, M. Strikman and C. Weiss, Phys. Rev. D **83**, 054012 (2011), (arXiv:1009.2559 [hep-ph]).
- [4] L. Frankfurt, C. E. Hyde, M. Strikman and C. Weiss, Phys. Rev. D **75**, 054009 (2007).
- [5] For a summary, see: T. Sjostrand and P. Z. Skands, Eur. Phys. J. C **39**, 129 (2005).
- [6] For a recent summary see M. Bahr *et al.*, Eur. Phys. J. C **58**, 639 (2008).
- [7] A. Siodmok, Proceedings of “Multi-Parton Interactions at the LHC”, arXiv:1111.0469 [hep-ph].
- [8] T. C. Rogers, A. M. Stasto, M. I. Strikman, Phys. Rev. D **77**, 114009 (2008). (arXiv:0801.0303 [hep-ph]); T. C. Rogers, M. Strikman, Phys. Rev. D **81**, 016013 (2010). (arXiv:0908.0251 [hep-ph]), T. C. Rogers, these proceedings
- [9] B. Blok, Y. Dokshitzer, L. Frankfurt, M. Strikman, Phys. Rev. D **83** 071501 (2011). (arXiv:1009.2714 [hep-ph]); Y. Dokshitzer, these proceedings.
- [10] B. Blok, Y. Dokshitzer, L. Frankfurt, M. Strikman, arXiv:1106.5533 [hep-ph].
- [11] B. Blok, Y. Dokshitzer, L. Frankfurt, M. Strikman, in preparation.
- [12] M. Strikman and D. Treleani, Phys. Rev. Lett. **88** (2002) 031801 (arXiv:0111468 [hep-ph]).
- [13] L. Frankfurt, M. Strikman, D. Treleani, C. Weiss, Phys. Rev. Lett. **101**, 202003 (2008). (arXiv:0808.0182 [hep-ph]).

- [14] M. Strikman, Phys. Rev. D **84**, 011501(R) (2011). (arXiv:1105.2285 [hep-ph]).
- [15] B. Abelev *et al.* [ALICE Collaboration], arXiv:1202.2816 [hep-ex].
- [16] V. Khachatryan *et al.* [CMS Collaboration], JHEP **1009**, 091 (2010). (arXiv:1009.4122 [hep-ex]).
- [17] Y. L. Dokshitzer, V. A. Khoze, A. H. Mueller and S. I. Troian, "Basics Of Perturbative QCD", *Gif-sur-Yvette, France: Ed. Frontieres (1991) 274 p.*
- [18] M. Strikman, Acta Phys. Polon. B **42** (2011) 2607 (arXiv:1112.3834 [hep-ph]).

Double heavy meson production through double parton scattering

Sergey P. Baranov¹, Alexander M. Snigirev², Nikolai P. Zotov^{2*}

¹P.N.Lebedev Institute of Physics, 53 Lenin avenue, 119991 Moscow, Russia

² Skobeltsyn Institute of Nuclear Physics, Lomonosov Moscow State University, 119991, Moscow, Russia

DOI: <http://dx.doi.org/10.3204/DESY-PROC-2012-03/13>

We show that the contribution from double parton scattering to the inclusive production of heavy meson pairs is comparable with the conventional single parton scattering mechanism at the LHC energy. For some species of heavy mesons the double parton scattering is the dominant mode of their production.

1 Introduction

In the last years it has become obvious that multiple parton interactions play an important role in hadron-hadron collisions at high energies and are one of the most common, yet poorly understood [1], phenomenons at the LHC. The presence of such multiple parton interactions in high-energy hadronic collisions has been convincingly demonstrated by the AFS [2], UA2 [3], CDF [4, 5], and D0 [6] collaborations, using events with the four-jets and $\gamma + 3$ -jets final states, thus providing new and complementary information on the proton structure.

A greater rate of events containing multiple hard interactions is anticipated at the LHC (as compared to the experiments mentioned above) due to much higher luminosity and greater energy of the LHC. Moreover, the reactions with multiple parton interactions will represent important background to signals from the Higgs production and other interesting processes; some certain types of multiple interactions will have distinctive signatures facilitating their detailed experimental investigation.

The main purpose of this talk (based on our previous work [7]) is to bring attention to another important process: the production of heavy meson pairs through double parton scattering, that is definitely not taken into consideration in the current theoretical estimations [8, 9]. Here, however, one should mention a recent paper [10], in which the contribution from the double parton scattering to J/ψ -pair production has been discussed for the first time for the condition of the LHCb experiment.

Let us recall that, with only assuming the factorization of the two hard parton processes A and B (Fig. 1), the inclusive cross section of a double parton scattering process in hadron-hadron

*Speaker

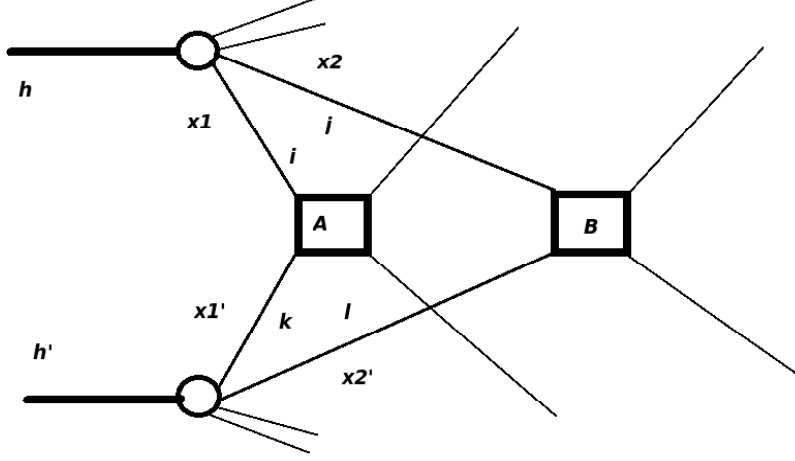


Figure 1: A schematic representation of double parton scattering mechanism.

collisions can be written in the following form [11, 12]

$$\begin{aligned} \sigma_{\text{DPS}}^{\text{AB}} &= \frac{m}{2} \sum_{i,j,k,l} \int \Gamma_{ij}(x_1, x_2; \mathbf{b}_1, \mathbf{b}_2; Q_1^2, Q_2^2) \hat{\sigma}_{ik}^A(x_1, x'_1, Q_1^2) \hat{\sigma}_{jl}^B(x_2, x'_2, Q_2^2) \\ &\times \Gamma_{kl}(x'_1, x'_2; \mathbf{b}_1 - \mathbf{b}, \mathbf{b}_2 - \mathbf{b}; Q_1^2, Q_2^2) dx_1 dx_2 dx'_1 dx'_2 d^2 b_1 d^2 b_2 d^2 b, \end{aligned} \quad (1)$$

where \mathbf{b} is the usual impact parameter, that is, the distance between the centers of colliding hadrons (e.g., the beam and the target) in transverse plane. $\Gamma_{ij}(x_1, x_2; \mathbf{b}_1, \mathbf{b}_2; Q_1^2, Q_2^2)$ are the double parton distribution functions, depending on the longitudinal momentum fractions x_1 and x_2 and on the transverse positions \mathbf{b}_1 and \mathbf{b}_2 of the two partons undergoing the hard processes A and B at the scales Q_1 and Q_2 ; $\hat{\sigma}_{ik}^A$ and $\hat{\sigma}_{jl}^B$ are the parton-level subprocess cross sections. The factor $m/2$ is a consequence of the symmetry with respect to the interacting parton species i and j : $m = 1$ if $A = B$, and $m = 2$ otherwise.

It is typically taken that the double parton distribution functions may be decomposed in terms of the longitudinal and transverse components as follows:

$$\Gamma_{ij}(x_1, x_2; \mathbf{b}_1, \mathbf{b}_2; Q_1^2, Q_2^2) = D_h^{ij}(x_1, x_2; Q_1^2, Q_2^2) f(\mathbf{b}_1) f(\mathbf{b}_2), \quad (2)$$

where $f(\mathbf{b}_1)$ is supposed to be an universal function for all kind of partons with its normalization fixed as

$$\int f(\mathbf{b}_1) f(\mathbf{b}_1 - \mathbf{b}) d^2 b_1 d^2 b = \int T(\mathbf{b}) d^2 b = 1, \quad (3)$$

and $T(\mathbf{b}) = \int f(\mathbf{b}_1) f(\mathbf{b}_1 - \mathbf{b}) d^2 b_1$ being the overlap function.

If one makes a further assumption that the longitudinal component $D_h^{ij}(x_1, x_2; Q_1^2, Q_2^2)$ reduces to a product of two independent one parton distributions,

$$D_h^{ij}(x_1, x_2; Q_1^2, Q_2^2) = D_h^i(x_1; Q_1^2) D_h^j(x_2; Q_2^2), \quad (4)$$

the cross section of the double parton scattering can be expressed in a simple form

$$\sigma_{\text{DPS}}^{\text{AB}} = \frac{m}{2} \frac{\sigma_{\text{SPS}}^{\text{A}} \sigma_{\text{SPS}}^{\text{B}}}{\sigma_{\text{eff}}}, \quad \text{with} \quad \sigma_{\text{eff}} = \left[\int d^2b (T(\mathbf{b}))^2 \right]^{-1}. \quad (5)$$

In this representation and at the factorization of longitudinal and transverse components, the inclusive cross section of single hard scattering reads

$$\begin{aligned} \sigma_{\text{SPS}}^{\text{A}} &= \sum_{i,k} \int D_h^i(x_1; Q_1^2) f(\mathbf{b}_1) \hat{\sigma}_{ik}^{\text{A}}(x_1, x'_1) \times D_{h'}^k(x'_1; Q_1^2) f(\mathbf{b}_1 - \mathbf{b}) dx_1 dx'_1 d^2b_1 d^2b \\ &= \sum_{i,k} \int D_h^i(x_1; Q_1^2) \hat{\sigma}_{ik}^{\text{A}}(x_1, x'_1) D_{h'}^k(x'_1; Q_1^2) dx_1 dx'_1. \end{aligned} \quad (6)$$

These simplifying assumptions, though rather customary in the literature and quite convenient from a computational point of view, are not sufficiently justified and are under revision now. However, the starting cross section formula (1) was derived in many works (see, e.g., Refs. [13, 14, 15, 16]) in the momentum representation using the light-cone variables and the same approximations as those applied to processes with a single hard scattering.

We restrict ourselves to this simple form (5) regarding it as the first estimation of the contribution from the double parton scattering to the inclusive double heavy meson production. The presence of the correlation term in the two-parton distributions results in the decrease [13, 17, 18] of the effective cross section σ_{eff} with the growth of the resolution scales Q_1 and Q_2 , while the dependence of σ_{eff} on the total energy at fixed scales is rather weak [18]. In fact, we obtain the minimal estimate for the contribution of interest. The CDF and D0 measurements give $\sigma_{\text{eff}} \simeq 15$ mb, which is roughly 20% of the total (elastic + inelastic) $p\bar{p}$ cross section at the Tevatron energy. We will use this value in our further estimations.

2 Numerical results and discussion

Let us start from the double J/ψ production, since the LHCb Collaboration has recently reported a first measurement [19] of this process

$$\sigma^{J/\psi J/\psi} = 5.6 \pm 1.1 \pm 1.2 \text{ nb} \quad (7)$$

with both J/ψ 's in the rapidity region $2 < y^{J/\psi} < 4.5$ and with the transverse momentum $p_T^{J/\psi} < 10$ GeV/c in proton-proton collisions at a center-of-mass energy of $\sqrt{s} = 7$ TeV. Earlier this collaboration has already measured [20] the single inclusive J/ψ production cross section with the same kinematic cuts as above

$$\sigma_{\text{SPS}}^{J/\psi} = 7.65 \pm 0.19 \pm 1.10_{1.27}^{+0.87} \mu\text{b}. \quad (8)$$

Using Eq. (5) we obtain immediately a simple estimation of the contribution from the double parton scattering at the same kinematic conditions

$$\sigma_{\text{DPS}}^{J/\psi J/\psi} = \frac{1}{2} \frac{\sigma_{\text{SPS}}^{J/\psi} \sigma_{\text{SPS}}^{J/\psi}}{\sigma_{\text{eff}}} \simeq 2.0 \text{ nb}. \quad (9)$$

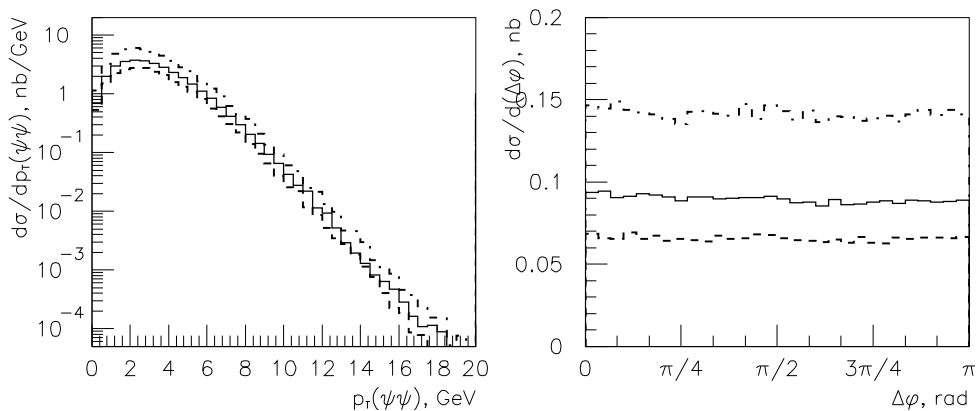


Figure 2: The distributions on the $J/\psi - J/\psi$ pair transverse momentum (left) and the azimuthal angle difference between the two J/ψ mesons (right) in the SPS process. Solid, dashed, and dash-dotted histograms represent calculations with A0, A-, and A+ gluon densities [32], respectively.

This value is quite compatible with the cross section through the “standard” mechanism of the double J/ψ production [9]

$$\sigma_{\text{SPS}}^{J/\psi J/\psi} = 4.15 \text{ nb}, \quad (10)$$

and the theoretical prediction for the summary contribution for both scattering modes is then

$$\sigma_{\text{SPS}}^{J/\psi J/\psi} + \sigma_{\text{DPS}}^{J/\psi J/\psi} = 6.15 \text{ nb}, \quad (11)$$

that is very close to the experimentally observed cross section (7) of double J/ψ production. It is worth mentioning on the other hand that the predictions on the double J/ψ production are very sensitive to the choice of the renormalization scale (because of the $\mathcal{O}(\alpha_s^4)$ dependence of the $\sigma_{\text{SPS}}^{J/\psi J/\psi}$ cross section), and so, the LHCb experimental results can also be accommodated by the SPS mechanism alone (see below).

An even better evidence for the double parton scattering process can be found in the production of χ_c pairs. The production of P -wave states is suppressed relative to the production of S -wave states because of the hierarchy of the wave functions $|\mathcal{R}_{J/\psi}(0)|^2 \gg |\mathcal{R}_{\chi_c}(0)|^2/m_\chi^2$ leading to the inequality $\sigma_{\text{SPS}}^{J/\psi J/\psi} \gg \sigma_{\text{SPS}}^{\chi_c \chi_c}$. Indeed, as one can learn from Fig. 8 in Ref. [8], the inclusive double χ_c production is suppressed in comparison with the inclusive double J/ψ production by more than two orders of magnitude.

At the same time, the inclusive production of single J/ψ and χ_c states shows nearly the same rates. The latter property is supported by both theoretical [21] and experimental [22, 23, 24] results. The reason for this is, that the χ_c mesons are produced in a direct $2 \rightarrow 1$ gluon-gluon fusion $g + g \rightarrow \chi_c$, while the J/ψ mesons are produced in a $2 \rightarrow 2$ subprocess $g + g \rightarrow J/\psi + g$, where an additional final state gluon is required by the color and charge parity conservation. As a consequence, the invariant mass of the produced system is typically much higher in the J case than in the χ_c case. (Besides that, the structure of the matrix element is such that it

vanishes when the co-produced gluon becomes soft. This further suppresses the production of low-mass states.)

Taken together, the suppression factors coming from the lower wave function on the χ_c side and from the higher final state mass and extra α_s coupling on the J/ψ side nearly compensate each other making the inclusive production cross sections comparable in size: $\sigma_{\text{SPS}}^{\chi_c} \simeq \sigma_{\text{SPS}}^{J/\psi}$. As a consequence, we get $\sigma_{\text{DPS}}^{\chi_c\chi_c} \simeq \sigma_{\text{DPS}}^{J/\psi J/\psi}$ and $\sigma_{\text{DPS}}^{\chi_c\chi_c} \gg \sigma_{\text{SPS}}^{\chi_c\chi_c}$. Thus, if observed, the production of a $\chi_c\chi_c$ pair would yield a clear and unambiguous indication of the double parton scattering process. The need in detecting the decay photon $\chi_c \rightarrow J/\psi + \gamma$ leads to certain difficulties in the experimental procedure, but the task seems still feasible as the production cross section is not small.

Another tempting possibility is to consider the simultaneous production of J/ψ and χ_c . In the SPS mode this process is forbidden at the leading order (LO) by the charge parity conservation but is possible at the next-to-leading order (NLO), $g + g \rightarrow J/\psi + \chi_c + g$. The corresponding cross section is then suppressed by one extra power of α_s and by the χ_c wave function. Alternatively, it can proceed via the soft final-state gluon radiation (the so called color octet model). The estimations of the cross section are then model dependent and rather uncertain, but even with the largest acceptable values for the color octet matrix elements one arrives at a suppression factor of about two orders of magnitude [8]. For the DPS mode we still expect no suppression, $\sigma_{\text{DPS}}^{J/\psi\chi_c} \simeq \sigma_{\text{DPS}}^{J/\psi J/\psi}$.

Yet another interesting process is the production of particles from different flavor families, say, J/ψ and Υ mesons. Once again, this process is not possible at the leading order in the SPS mode and can only occur either at the NNLO (next-to-next-to-leading order) $\mathcal{O}(\alpha_s^6)$, or via the color-octet transitions, or by means of the production and decay of P -wave mesons (i.e., $g + g \rightarrow \chi_c + \chi_b$ followed by $\chi_c \rightarrow J/\psi + \gamma$ and $\chi_b \rightarrow \Upsilon + \gamma$). So, the SPS mode is always suppressed: either by the extra powers of α_s , or by the color-octet matrix elements, or by the P -state wave function, and the DPS mode becomes the absolutely dominant one: $\sigma_{\text{DPS}}^{J/\psi \Upsilon} \gg \sigma_{\text{SPS}}^{J/\psi \Upsilon}$.

Now, to be more precise, we will derive some numerical predictions. In doing so, we rely upon perturbative QCD and nonrelativistic bound state formalism [25, 26] with only the color-singlet channels taken into consideration. Also, we accept the k_t -factorization ansatz [27, 28, 29] for the parton model. The computational technique is explained in every detail in Ref. [21], and the parameter setting is as follows. The meson masses are taken from the Particle Data Book [30], and the heavy quark masses are set equal to one half of the respective meson masses; the radial wave functions of J/ψ and Υ mesons are supposed to be known from their leptonic decay widths [30] and are set to $|\mathcal{R}_{J/\psi}(0)|^2 = 0.8 \text{ GeV}^3$ and $|\mathcal{R}_{\Upsilon}(0)|^2 = 6.48 \text{ GeV}^3$; the wave functions of the P -states are taken from the potential model [31], $|\mathcal{R}'_{\chi_c}(0)|^2 = 0.075 \text{ GeV}^5$ and $|\mathcal{R}'_{\chi_b}(0)|^2 = 1.44 \text{ GeV}^5$; the renormalization scale in the strong coupling $\alpha_s(\mu^2)$ is chosen as the meson transverse mass $\mu^2 = m^2 + p_t^2$; and we use the A0 parametrization from Ref. [32] for the unintegrated gluon density. In the present note we will restrict ourselves to the conditions of the LHCb experiment, since the Collaboration has already recorded the production of J/ψ pairs. Predictions for other experimental conditions can be made in an essentially similar way.

Within the theoretical model described above, we get for the direct inclusive J/ψ production

$$\sigma_{\text{SPS}}^{J/\psi}(\text{direct}) = 7.1 \text{ } \mu\text{b}, \quad (12)$$

and for the χ_c mesons

$$\sigma_{\text{SPS}}^{\chi_c^1} = 1.5 \text{ } \mu\text{b}, \quad \sigma_{\text{SPS}}^{\chi_c^2} = 5.1 \text{ } \mu\text{b}. \quad (13)$$

After multiplying these numbers by appropriate branching ratios [30] $Br(\chi_{c1} \rightarrow J/\psi + \gamma) = 35\%$ and $Br(\chi_{c2} \rightarrow J/\psi + \gamma) = 20\%$ and additions of the direct and indirect contributions, we get for the prompt J/ψ yield:

$$\sigma_{\text{SPS}}^{J/\psi} = \sigma_{\text{SPS}}^{J/\psi}(\text{direct}) + \sigma_{\text{SPS}}^{J/\psi}(\text{from } \chi_c) = 7.1 \mu\text{b} + 1.6 \mu\text{b} = 8.7 \mu\text{b}. \quad (14)$$

This result is in reasonable agreement with the experimental measurement (8), thus giving support to our theoretical model. Quite similarly, we get for the $b\bar{b}$ mesons

$$\sigma_{\text{SPS}}^{\Upsilon}(\text{direct}) = 140 \text{ nb}, \quad \text{and} \quad \sigma_{\text{SPS}}^{\chi_1} = 18 \text{ nb}, \quad \sigma_{\text{SPS}}^{\chi_2} = 91 \text{ nb}. \quad (15)$$

Then one can easily obtain for the DPS mode

$$\sigma_{\text{DPS}}^{J/\psi J/\psi} = 1.7 \text{ nb}, \quad (16)$$

$$\sigma_{\text{DPS}}^{J/\psi J/\psi}(\text{both from } \chi_c) = 0.9 \text{ nb}, \quad (17)$$

$$\sigma_{\text{DPS}}^{J/\psi \Upsilon} = 0.07 \text{ nb}. \quad (18)$$

The reader can continue deriving predictions for other DPS combinations.

To calculate the background contribution $\sigma_{\text{SPS}}^{J/\psi J/\psi}$ we use the code developed in [33] and extended now [34] to the k_t -factorization approach:

$$\sigma_{\text{SPS}}^{J/\psi J/\psi} = 4 \text{ nb}. \quad (19)$$

Variations in the renormalization scale μ_R^2 within a factor of 2 around the default value $\mu_R^2 = \hat{s}/4$ result in an increase or decrease on the total production rate by a factor of 1.6. Employing some different parametrizations for the unintegrated gluon densities (A+ or A- sets from Ref. [32]) also changes the predicted cross section by a factor of 1.6 up or down. Our central prediction (19) is in reasonable agreement with the data (7).

The proportion between the visible SPS and DPS contributions can, in principle, depend on the experimental cuts on the J/ψ transverse momentum. However, in the particular case which we are considering here, the LHCb Collaboration refers to no cuts on $p_T(J/\psi)$. In fact, there are some soft restrictions on the momenta of the decay muons, $p_T(\mu) > 600 \text{ MeV}$, but they are taken into account as corrections to the acceptance. The final results reported by the collaboration to compare with are the acceptance-corrected ones.

It is also worth noting that even in the general case the sensitivity of the ratio $\sigma_{\text{DPS}}/\sigma_{\text{SPS}}$ to the p_T cuts is rather weak, because the DPS and SPS contributions show the same p_T dependence. This is explained in detail in Ref. [34]. Irrespective of the particular properties of the subprocess matrix element, the p_T of the final state is dominated by the transverse momentum of the initial gluons, and the individual J/ψ spectra behave as $1/p_T^4$ in both SPS and DPS modes. Moreover, the momenta of the two J/ψ mesons are not correlated. The latter is evident in the DPS case and was not a priori evident in the SPS case, but turned out to be true (Fig.5 in Ref. [34]). So, the SPS and DPS event topologies are rather similar to each other and can hardly be distinguished from one another.

Our calculations agree with the observation made in Ref. [10] that the effects of initial parton radiation (that are automatically present in the k_t -factorization approach) destroy the original back-to-back $J/\psi J/\psi$ kinematics completely washing out the azimuthal correlations (see Fig. 2). One can potentially distinguish the SPS and DPS modes with rapidity correlations,

but we anyway find that looking at some other meson species is more indicative. In particular, the production of $\chi_c\chi_c$, $J/\psi\chi_c$ or $J/\psi\Upsilon$ pairs is totally dominated by the DPS mechanism because the SPS mechanism is suppressed for the reasons given earlier. A similar study has been carried out in Ref.[35].

Summing up, we conclude that the processes with pairs of heavy quarkonia in the final state ($J/\psi J/\psi$, $\chi_c\chi_c$, $J/\psi\chi_c$, $J/\psi\Upsilon$) can serve as precise probes of the double parton scattering at the LHC and can stimulate important steps towards understanding the multiparticle QCD dynamics.

Acknowledgements A.S. and N.Z. wish to express their gratitude to the organizers of MPI@LHC 2011 for the warm welcome and hospitality. This work is partly supported by Russian Foundation for Basic Research Grants No. 10-02-93118 and No. 11-02-08502-z, by the President of Russian Federation for support of Leading Scientific Schools Grant No 4142.2010.2. S.B. and N.Z. are very grateful to DESY Directorate for the support in the framework of Moscow-DESY project on Monte-Carlo implementation for HERA-LHC, and they were supported by RFBR Grant 11-02-01454 and the RMES (grant the Scientific Research on High energy Physics). A.S. and N.Z. were also supported by FASI State contract 02.740.11.0244.

References

- [1] P. Bartaliny et al., “Multi-Parton interactions at the LHC”, (arXiv:1111.0469 [hep-ph]).
- [2] T. Akesson et al., AFS Collaboration, “Double parton scattering in p p collisions at $\sqrt{s} = 63$ GeV”, *Zeit. Phys. C* 34 (1987) 163.
- [3] J. Alitti et al., UA2 Collaboration, “A Study of multi-jet events at the CERN anti-p p collider and a search for double parton scattering”, *Phys. Lett. B* 268 (1991) 145.
- [4] F. Abe et al., CDF Collaboration, “Study of four-jet events and evidence for double parton interactions in $p\bar{p}$ collisions at $\sqrt{s} = 1.8$ TeV”, *Phys. Rev. D* 47 (1993) 4857.
- [5] F. Abe et al., CDF Collaboration, “Double Parton Scattering in p anti-p Collisions at $\sqrt{s} = 1.8$ TeV”, *Phys. Rev. D* 56 (1997) 3811.
- [6] V.M. Abazov et al., D0 Collaboration, “Double parton interactions in photon+3 jet events in $p\bar{p}$ collisions at $\sqrt{s} = 1.96$ TeV”, *Phys. Rev. D* 81 (2010) 052012(arXiv:0912.5104v2 [hep-ex]) .
- [7] S.P. Baranov, A.M. Snigirev, N.P. Zotov, “Double heavy meson production through double parton scattering in hadronic collisions”, *Phys. Lett. B* 705 (2011) 116(arXiv:1105.6276v3 [hep-ph]).
- [8] S.P. Baranov, “Pair production of χ_c states at collider energies”, *Phys. At. Nuclei* 60 (1997) 986[*Yad. Fiz.* 60 (1997).] 1103
- [9] A.V. Berezhnoy, A.K. Likhoded, A.V. Luchinsky and A.A. Novoselov, “Production of J/ψ meson pairs and 4-c tetraquark at the LHC” (arXiv:1101.5881 [hep-ph]).
- [10] C.-H. Kom, A. Kulesza, and W.J. Stirling, “Prospects for observation of double parton scattering with four-muon final states at LHCb”, *Phys. Rev. Lett.* 107 (2011) 082002(arXiv:1109.0309v1 [hep-ph]).
- [11] J.R. Gaunt and W.J. Stirling, “Double Parton Distributions Incorporating Perturbative QCD Evolution and Momentum and Quark Number Sum Rules”, *JHEP* 1003 (2010) 005 (arXiv:0910.4347v4 [hep-ph]).
- [12] E. Cattaruzza, A. Del Fabbro, and D. Treleani, “Fractional momentum correlations in multiple production of W bosons and of $b\bar{b}$ pairs in high energy pp collisions”, *Phys. Rev. D* 72 (2005) 034022(arXiv:0507052v1 [hep-ph]) .
- [13] M.G. Ryskin and A.M. Snigirev, “Fresh look at double parton scattering”, *Phys. Rev. D* 83 (2011) 114047(arXiv:1103.3495v2 [hep-ph]).
- [14] B. Blok, Yu. Dokshitzer, L. Frankfurt, and M. Strikman, “The Four jet production at LHC and Tevatron in QCD”, *Phys. Rev. D* 83 (2011) 071501(arXiv:1009.2714v2 [hep-ph]).

- [15] M. Diehl and A. Schafer, “Theoretical considerations on multiparton interactions in QCD”, Phys. Lett. B 698 (2011) 389(arXiv:1102.3081v2 [hep-ph]).
- [16] J.R. Gaunt and W.J. Stirling, “Double Parton Scattering Singularity in One-Loop Integrals”, JHEP 1106 (2011) 048 (arXiv:1103.1888v2 [hep-ph]).
- [17] A.M. Snigirev, “Possible indication to the QCD evolution of double parton distributions?”, Phys. Rev. D 81 (2010) 065014(arXiv:1001.0104v3 [hep-ph]) .
- [18] C. Flensburg, G. Gustafson, L. Lönnblad, and A. Ster, “Correlations in double parton distributions at small x ”, JHEP 1106 (2011) 066 (arXiv:1103.4320v3 [hep-ph]).
- [19] LHCb Collaboration, “Observation of double J/ψ production in proton-proton collisions at a centre-of-mass energy $\sqrt{s}=7$ TeV”, LHCb-CONF-2011-009.
- [20] LHCb Collaboration, “Measurement of the J/ψ production cross-section at $\sqrt{s} = 7$ TeV in LHCb”, LHCb-CONF-2010-010.
- [21] S. P. Baranov, “Highlights from the k_t -factorization approach on the quarkonium production puzzles” Phys. Rev. D 66 (2002) 114003.
- [22] F. Abe et al.,(CDF Collaboration), “Inclusive J/ψ , $\Psi(2S)$, and b-quark production in $\bar{p}p$ collisions at $\sqrt{s} = 1.8\text{TeV}$ ”, Phys. Rev. Lett. 69 (1992) 3704; 71 (1993) 2537; 75 (1995) 1451; 79 (1997) 578.
- [23] T. Affolder et al.,(CDF Collaboration), “Production of $\Upsilon(1S)$ mesons from χ_b Decays in $\bar{p}p$ collisions at $\sqrt{s} = 1.8\text{TeV}$ ”, Phys. Rev. Lett. 84 (2000) 2094; 85 (2000) 2886(arXiv:9910025v1 [hep-ex]).
- [24] F. Abe et al.,(CDF Collaboration), “Production of χ_{c1} and χ_{c2} in $\bar{p}p$ collisions at $\sqrt{s} = 1.8\text{TeV}$ ”, Phys. Rev. Lett. 86 (2001) 3963.
- [25] C.-H. Chang, “Hadronic production of J/ψ associated with a gluon”, Nucl. Phys. B 172 (1980) 425; R. Baier and R. Rückl, “Hadronic production of J/ψ and Υ : transverse momentum distributions, Phys. Lett. B 102 (1981) 364(arXiv:0404158v3 [hep-ph]) ; E. L. Berger and D. Jones, “Inelastic photoproduction of J/ψ and Υ by gluons”, Phys. Rev. D 23 (1981) 1521;
- [26] H. Krasemann, “Jets from $Q\bar{Q}$ P -waves”, Zeit. Phys. C 1 (1979) 189; G. Guberina, J. Kühn, R. Peccei, and R. Rückl, “Rare decays of the Z^0 ”, Nucl. Phys. B 174 (1980) 317.
- [27] L. Gribov, E. Levin, and M. Ryskin, “Semihard processes in QCD”, Phys. Rep. 100 (1983) 1; E. Levin and M. Ryskin, “High energy hadron collisions in QCD”, Phys. Rep. 189 (1990) 268.
- [28] S. Catani, M. Ciafaloni, and F. Hautmann, “Gluon contributions to small- x heavy flavour production”, Phys. Lett. B 242 (1990) 97; “High energy factorization and small- x heavy flavour production”, Nucl. Phys. B366 (1991) 135.
- [29] J. C. Collins and R. K. Ellis, “Heavy-quark production in very high energy hadron collisions”, Nucl. Phys. B360 (1991) 3.
- [30] K. Nakamura et al.,(Particle Data Group), “Review of Particle Properties”, J. Phys. G. 37 (2010) 075021.
- [31] E. J. Eichten and C. Quigg, “Wave functions at the origin”, Phys. Rev. D 52 (1995) 1726.
- [32] H. Jung, “A CCFM Monte-Carlo generator CASCADE”, <http://www.desy.de/~jung/cascade/updf.html>
- [33] S. P. Baranov, H. Jung, “Double J/ψ production - a probe of gluon polarization?”, Zeit. Phys. C 66 (1995) 647.
- [34] S. P. Baranov, “Pair production of J/ψ mesons in the k_t -factorization approach”, Phys. Rev. D 84 (2011) 054012.
- [35] A.A. Novoselov, “Double parton scattering as a source of quarkonia pairs in LHCb”, (arXiv:1106.2184 [hep-ph].)s

Chapter 4

Measuring MPI

Measurement of hard double-partonic interactions in $W \rightarrow l\nu + 2$ jet events using the ATLAS detector at the LHC

Eleanor Dobson for the ATLAS Collaboration

DOI: <http://dx.doi.org/10.3204/DESY-PROC-2012-03/15>

The production of W bosons in association with two jets has been investigated using proton-proton collisions at a centre-of-mass energy of $\sqrt{s} = 7$ TeV. The fraction of $W + 2$ jet events arising from double parton scattering was measured to be $f_{\text{DP}}^{\text{R}} = 0.16 \pm 0.01$ (stat) ± 0.03 (sys) for jets with transverse momentum $p_{\text{T}} > 20$ GeV and rapidity $|y| < 2.8$. This corresponds to an effective cross section for hard double partonic interactions of $\sigma_{\text{eff}} = 11 \pm 1$ (stat) $^{+3}_{-2}$ (sys) mb, which is consistent with previous measurements performed at lower centre-of-mass energies in different channels. This measurement was performed using data collected with the ATLAS detector corresponding to an integrated luminosity of 33 pb^{-1} .

1 Principle of the measurement

The aim of this analysis, described in detail in [1], is to extract the fraction of $W + 2$ jet events¹ containing hard double parton interactions (DPI) produced in proton-proton collisions recorded by the ATLAS detector. The method of extraction is to fit over the distribution of a variable that has good discrimination between a W boson produced in direct association with 2 jets ($W + 2j_{\text{D}}$) and a W boson produced in association with zero jets in addition to a double-parton scatter resulting in two jets ($W_0 + 2j_{\text{DPI}}$).

The fraction of $W_0 + 2j_{\text{DPI}}$ events in the selected $W + 2j$ sample at reconstruction level R , f_{DP}^{R} , is defined as

$$f_{\text{DP}}^{\text{R}} = \frac{N_{W_0+2j_{\text{DPI}}}}{N_{W+2j}}, \quad (1)$$

where $N_{W_0+2j_{\text{DPI}}}$ is the number of $W_0 + 2j_{\text{DPI}}$ events passing $W + 2j$ selection, and N_{W+2j} is the total number of events passing $W + 2j$ selection. Although these quantities will be measured at detector level, it is shown in Section 5.3 that f_{DP}^{R} is closely related to its parton-level (P) equivalent, f_{DP}^{P} . It is possible to define the effective cross section [2] σ_{eff}

$$\sigma_{\text{eff}} = \frac{\sigma_{W_0} \cdot \sigma_{2j}}{\sigma_{W_0+2j_{\text{DPI}}}}, \quad (2)$$

where σ_{W_0} , $\sigma_{W_0+2j_{\text{DPI}}}$ and σ_{2j} are the cross-sections of $W + 0j$, $W_0 + 2j_{\text{DPI}}$ and dijet ($2j$) events

¹ $W + n_j$ will be used to denote processes in which W is produced in association with n -jets

respectively. Each cross-section can be calculated using

$$\sigma = \frac{N}{A \epsilon \mathcal{L}}, \quad (3)$$

where N is the number of events, A is the acceptance after reconstruction and unfolding corrections, ϵ is the trigger efficiency and \mathcal{L} is the integrated luminosity. Equation (2) can therefore be rewritten as

$$\sigma_{\text{eff}} = \frac{1}{f_{\text{DP}}^{\text{R}}} \cdot \frac{N_{W_0} N_{2j}}{N_{W+2j}} \cdot \frac{A_{W_0+2j_{\text{DPI}}}}{A_{W_0} A_{2j}} \cdot \frac{\epsilon_{W_0+2j_{\text{DPI}}}}{\epsilon_{W_0} \epsilon_{2j}} \cdot \frac{\mathcal{L}_{W_0+2j_{\text{DPI}}}}{\mathcal{L}_{W_0} \mathcal{L}_{2j}}. \quad (4)$$

In this analysis, a factorisation ansatz between the W and the $2j$ systems is assumed. This leads to a number of conclusions regarding the quantities in equation (4). First, the kinematics of the W do not influence the kinematic distributions of the DPI system. This implies that

$$A_{W_0+2j_{\text{DPI}}} = A_{W_0} \cdot A_{2j_{\text{DPI}}}, \quad (5)$$

once corrections involving the impact of jets on W reconstruction and vice versa have been made (discussed in detail in Section 5.4). Secondly, the kinematics of the jets in the DPI system may be modelled by the kinematics of single-scatter dijet events, which implies that

$$A_{2j_{\text{DPI}}} = A_{2j}. \quad (6)$$

Finally, the $W_0 + 2j_{\text{DPI}}$ and W_0 events will be selected online using the same trigger selection. This results in luminosity and efficiency cancellations and equation (4) simplifies to

$$\sigma_{\text{eff}} = \frac{1}{f_{\text{DP}}^{\text{R}}} \cdot \frac{N_{W_0} N_{2j}}{N_{W+2j}} \cdot \frac{1}{\epsilon_{2j}} \cdot \frac{1}{\mathcal{L}_{2j}}. \quad (7)$$

In this analysis the terms in equation (7) are determined as separate quantities allowing the evaluation of σ_{eff} with its associated uncertainty.

2 Event selection

The measurement was performed using 33 pb⁻¹ of data taken with the ATLAS detector [3] during 2010. Events were required to contain at least one primary vertex that was reconstructed within 200 mm of the interaction point and contained at least three tracks. Additional cuts were applied to reduce the contamination from noisy calorimeter cells, beam backgrounds and cosmic rays.

The selection of the $W \rightarrow \ell\nu$ signal was similar to that used in the $W \rightarrow \ell\nu + \text{jets}$ cross-section analysis [4]. Dedicated single-electron and single-muon trigger selections were used to retain $W \rightarrow e\nu$ and $W \rightarrow \mu\nu$ events, respectively.

In the electron channel, events were required to contain one electron that satisfied tight identification criteria with transverse momentum $p_{\text{T}} > 20$ GeV and pseudorapidity $|\eta| < 2.47$. Electrons reconstructed in the transition region between the barrel and endcap calorimeters ($1.37 < |\eta| < 1.52$) were excluded from the analysis. Additional requirements were applied to remove electrons falling into inactive regions of the calorimeter.

In the muon channel, events were required to contain an isolated, prompt muon with $p_{\text{T}} > 20$ GeV and pseudorapidity $|\eta| < 2.5$. The muon was reconstructed from information from both the muon spectrometer and the inner detector.

In both channels, additional requirements were placed on E_T^{miss} and transverse mass M_T . Events were required to have transverse missing energy $E_T^{\text{miss}} > 25$ GeV and $M_T > 40$ GeV.

Jets are defined using the anti- k_t [5] algorithm with $R = 0.6$ and full four momentum recombination. The jets are reconstructed from electromagnetic scale topological clusters that are built from calorimeter cells. Each jet is subsequently corrected using p_T and η dependent jet energy scale (JES) calibration factors derived from simulated Monte Carlo (MC) events [6]. Jets were required to have $p_T > 20$ GeV and $|y| < 2.8$. All jets within $\Delta R < 0.5$ of a reconstructed electron or muon were removed from the analysis. Jets originating from pile-up interactions were removed by applying a cut on the jet-vertex fraction (JVF), which was defined for each jet in the event.

Events were subsequently divided into two orthogonal datasets. The first was a $W + 0j$ sample, in which no jets were reconstructed – in accordance with the definition above – in addition to the W decay products. The second was the $W + 2j$ sample, in which exactly two additional jets were reconstructed. The $W + 0j$ sample is only used for the evaluation of σ_{eff} .

Dijet events were selected online using a trigger selection derived from the Minimum Bias Trigger Scintillators and Zero Degree Calorimeters, which have been shown to be unbiased and fully efficient for jet-based measurements [6]. Dijet events were required to contain exactly two jets, reconstructed using the same algorithm, input objects and kinematic selection as in the previous section.

3 Monte Carlo simulation

ALPGEN [7] was used to generate $W + nj$ signal events. MLM [8] matching was used, with the matching scale cut set at 20 GeV, to prevent any double counting caused by the parton shower. ALPGEN is a matrix element generator that is interfaced to HERWIG [9] v6.510, for parton showering and hadronisation, and to JIMMY [10] v4.31, for the underlying event. The event generator tune was AUET1 [11]. SHERPA [12] v1.3.1 was also used to generate an alternative sample of $W + nj$ signal events. SHERPA is a matrix element generator that uses CKKW [13] matching to prevent double counting from the parton shower. The SHERPA samples were generated with the default underlying event tune and the CKKW matching cut at 30 GeV. As a final comparison for signal events, PYTHIA6 [14] was used to generate inclusive W events, with the AMBT1 tune [15] for the underlying event activity.

Various generators were used to simulate the effect of physics backgrounds to the W signal events. $t\bar{t}$ events were generated at next-to-leading order accuracy using the MC@NLO [16] generator. MC@NLO was interfaced to HERWIG and JIMMY, and the AUET1 tune for the underlying event was used in the sample generation. Backgrounds from dijet and inclusive Z production were simulated using PYTHIA6 with tune AMBT1 for the underlying event.

Each generated event was passed through the standard ATLAS detector simulation [17], which is based on Geant4 [18]. The MC events were reconstructed and analysed using the same chain as applied to the data.

3.1 Event generator samples without double parton scattering

In addition to the standard MC simulation, $W + 2j$ events with no multiple parton interactions were generated using SHERPA and ALPGEN+HERWIG+JIMMY. These samples model the jet-jet correlations in the non-DPI production of $W + 2j$ events and were used to extract f_{DP}^{R}

from the data. DPI was switched off in SHERPA using the `MI_HANDLER` switch. This prevents secondary parton-parton scattering with $p_T \gtrsim 5$ GeV. The initial/final state radiation from the incoming/outgoing legs of the leading-order matrix element is retained, in addition to the generation of intrinsic transverse momentum and fragmentation of beam remnants.

To create a corresponding ALPGEN+HERWIG+JIMMY sample with DPI switched off, the standard generation of $W+2j$ was used, but events were rejected if the two jets were identified as originating from a non-primary parton-parton scatter. This jet-parton matching was performed using the HERWIG event record, by identifying the parton with status code 123/124 and $p_T > 3.5$ GeV that was closest to each jet².

4 Characteristics of DPI events in data and MC

The goal of this study is to identify the fraction of $W+2j$ events that are produced via double parton scattering. It is expected that the two partonic scatters are independent and therefore the jets produced in DPI events will typically be produced more back-to-back in azimuth than those produced in single scatter events. The independence of the two scatters can also be seen in variables that parameterise the transverse momentum imbalance between the jets, such as

$$\Delta_{\text{jets}} = |\vec{p}_{T,1} + \vec{p}_{T,2}| \quad \text{and} \quad \Delta_{\text{jets}}^n = \frac{|\vec{p}_{T,1} + \vec{p}_{T,2}|}{|\vec{p}_{T,1}| + |\vec{p}_{T,2}|}, \quad (8)$$

where the indices 1 and 2 identify the two jets in the event.

The SHERPA and ALPGEN+HERWIG+JIMMY predictions for Δ_{jets} are shown in Figure 1³, with and without the contribution from double parton scattering. The effect of including the DPI in each generator is an enhancement in the region $\Delta_{\text{jets}} \sim 10$ GeV. It is concluded that this enhancement is related to the DPI contribution, for which the two jets are produced back-to-back in azimuth and with similar transverse momenta. The distribution of the Δ_{jets}^n variable is also shown in Figure 1. This variable is constructed such that the region close to $\Delta_{\text{jets}}^n=1$ contains no DPI, and that near $\Delta_{\text{jets}}^n=0$ contains a larger fraction of DPI. The Δ_{jets}^n variable is particularly useful, because, as a ratio, it has reduced sensitivity to jet energy uncertainties whilst remaining sensitive to the presence of DPI.

5 Extraction of f_{DP}^{R}

The extraction of f_{DP}^{R} from the data was performed using a χ^2 minimisation to the normalised Δ_{jets}^n distribution of the form

$$(1 - f_{\text{DP}}^{\text{R}}) \cdot A + f_{\text{DP}}^{\text{R}} \cdot B, \quad (9)$$

where template A is the normalised distribution for $W+2j_{\text{D}}$ and template B is the normalised distribution for W_0+2j_{DPI} . The construction of these templates is discussed in Section 5.1. To minimise the dependence on near-collinear jets, the two bins covering $0.933 < \Delta_{\text{jets}}^n < 1.0$ were not used in the fit.

²The threshold was chosen to be 3.5 GeV to approximately match the `PTJIM` parameter (3.86 GeV), which is used in JIMMY to set the transverse momentum scale of secondary scatters.

³as for all figures in this note, these have been reproduced from [1].

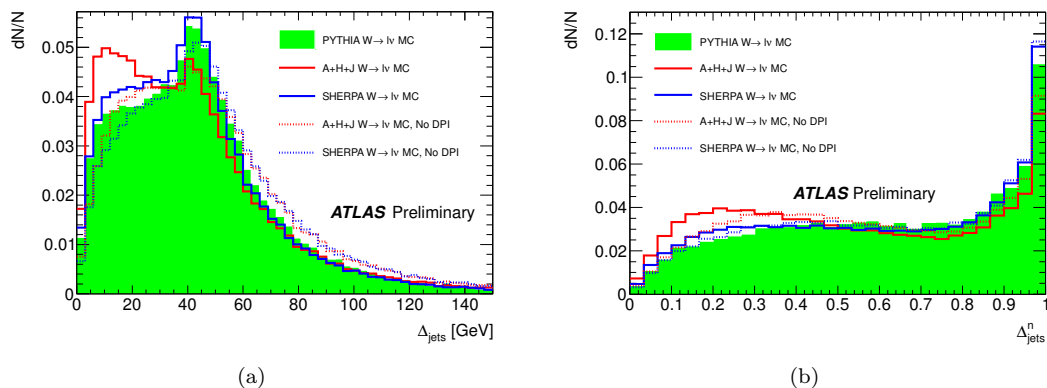


Figure 1: Predicted distributions of Δ_{jets} (a) and Δ_{jets}^n (b) in $W \rightarrow \ell\nu+2$ jet events in SHERPA and ALPGEN+HERWIG+JIMMY (A+H+J) Monte Carlo simulation when DPI is switched on and off in the manner described in Section 3. The PYTHIA prediction (with DPI switched on) is also shown for comparison. All distributions are normalised to unity.

5.1 Template construction

The model for the $W + 2j_{\text{D}}$ contribution (template A) was taken from the event generator predictions. The first model for this template was the SHERPA prediction with the MPI switched off. The second model was the ALPGEN+HERWIG+JIMMY prediction with the MPI removed. The procedure to switch off or remove MPI in the generators was discussed in Section 3. There is a small difference between the SHERPA and ALPGEN+HERWIG+JIMMY predictions, which will be used as a generator modelling uncertainty in the extraction of f_{DP}^{R} . This is discussed further in Section 5.3.

Template B, the model for $W_0 + 2j_{\text{DPI}}$ kinematics, is constructed from dijet data using the selection outlined in Section 2. The fractional difference between the extracted value of f_{DP}^{R} when using dijet MC in place of dijet data was found to be negligible.

5.2 Fit results

The result of fitting the templates to the data is shown in Figure 2. The fraction of DPI events was found to be $f_{\text{DP}}^{\text{R}} = 0.18$, using the SHERPA prediction for template A. The associated quality of the fit was $\chi^2/N_{\text{df}} = 1.4$ ($N_{\text{df}} = 27$). The fraction of DPI was observed to be $f_{\text{DP}}^{\text{R}} = 0.14$ using the ALPGEN+HERWIG+JIMMY prediction for template A, with a χ^2/N_{df} of 0.9. The final value of f_{DP}^{R} was taken to be the average of these results ($f_{\text{DP}}^{\text{R}} = 0.16$). The statistical uncertainty was obtained by varying the χ^2 by one unit and was found to be $\simeq 0.07 f_{\text{DP}}^{\text{R}}$. The systematic uncertainties on the extracted value of f_{DP}^{R} are discussed in Section 5.4.

The value f_{DP}^{R} extracted from the fit to Δ_{jets}^n can be used to normalise appropriate templates for Δ_{jets} . Figure 3 shows the distribution obtained in data compared to these normalised templates.

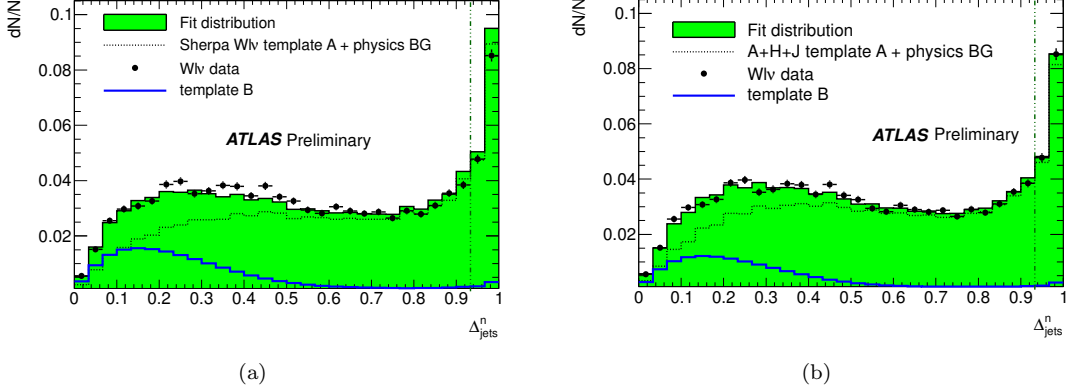


Figure 2: Comparison of Δ_{jets}^n distribution in the data with expectations after χ^2 minimisation fits of the templates to data to extract f_{DP}^{R} . The result obtained using SHERPA for template A is shown in (a) and the result obtained using ALPGEN+HERWIG+JIMMY (A+H+J) for template A is shown in (b). The physics background (physics BG) is added to template A in the figure (dotted line). The fit region is the region to the left of the dotted line. Data and the overall fit were normalised to unity, template A to $1 - f_{\text{DP}}^{\text{R}}$ and template B to f_{DP}^{R} .

5.3 Transition of results from detector to parton level

In this section, the relationship between the parton-level, f_{DP}^{P} , and reconstruction level, f_{DP}^{R} , quantities is established. The fraction of events originating from double parton scattering is defined at parton-level by

$$f_{\text{DP}}^{\text{P}} = \frac{N_{\text{W}_0+2\text{j}_{\text{DPI}}}^{\text{P}}}{N_{\text{W}_0+2\text{j}_{\text{DPI}}}^{\text{P}} + N_{\text{W}+2\text{j}_{\text{D}}}^{\text{P}}}. \quad (10)$$

where $N_{\text{W}_0+2\text{j}_{\text{DPI}}}^{\text{P}}$ is the number of events generated with the two partons originating from DPI and $N_{\text{W}+2\text{j}_{\text{D}}}^{\text{P}}$ is the number of events generated with the two partons produced directly from the $W + 2j$ matrix element. The partons are required to pass the same selection criteria as the reconstructed jets, $p_{\text{T}} > 20$ GeV and $|y| < 2.8$. The value of f_{DP}^{P} was evaluated to be 0.18 in the nominal ALPGEN+HERWIG+JIMMY settings.

DPI events were weighted with a factor x to vary this default value of f_{DP}^{P} in the sample. A χ^2 minimisation fit to this weighted sample was then performed, with the SHERPA prediction for template A and the dijet data for template B. The result of the fit yields an estimate of the fraction of DPI present in the detector level Monte Carlo, f_{DP}^{T} .

The result of the fit is shown in Figure 4(a) for $f_{\text{DP}}^{\text{P}} = 0.18$ ($x = 1$). The relationship between f_{DP}^{T} and f_{DP}^{P} is obtained by varying x and is shown in Figure 4(b). In general, there is a strong correlation between the extracted value of f_{DP}^{T} and the input value of f_{DP}^{P} . There is, however, a small bias of f_{DP}^{T} at small values of f_{DP}^{P} . This bias arises from (i) modelling differences between the two generators and (ii) physics and detector effects present in the transition from parton-level to detector-level. As the fraction of DPI is increased, the fit result becomes increasingly insensitive to the details of template A and the extracted value of f_{DP}^{T} converges towards the input value of f_{DP}^{P} .

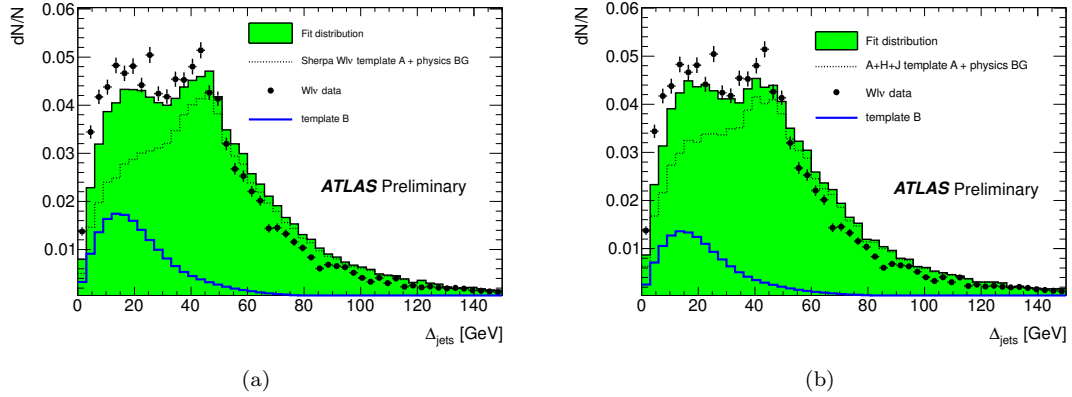


Figure 3: Comparison of Δ_{jets} distribution in the data with expectations of template *A* and *B* combined in the ratio $N_B/N_A = f_{\text{DP}}^{\text{R}}/(1-f_{\text{DP}}^{\text{R}})$, where f_{DP}^{R} is fixed to the value obtained in the fit to the $\Delta_{\text{jets}}^{\text{n}}$ distribution. The prediction using SHERPA for template *A* is shown in (a) and ALPGEN+HERWIG+JIMMY is shown in (b). The physics background (physics BG) is added to template *A* in the figure (dotted line). Data and the overall fit were normalised to unity, template *A* to $1 - f_{\text{DP}}^{\text{R}}$ and template *B* to f_{DP}^{R} .

5.4 Systematic uncertainty on f_{DP}^{R}

In Section 5.2, the final value of $f_{\text{DP}}^{\text{R}} = 0.16$ was determined using both the SHERPA and the ALPGEN+HERWIG+JIMMY predictions for template *A*. In particular, the value of f_{DP}^{R} was taken to be the average of the values extracted using the two event generators. The systematic uncertainty associated with the event generator modelling of $W + 2j_{\text{D}}$ is taken to be the difference between this average and the generator-based predictions. This is the largest systematic uncertainty in the measurement and observed to be $0.12f_{\text{DP}}^{\text{R}}$. Furthermore, in Section 5.3, the shift between f_{DP}^{P} and f_{DP}^{T} at $f_{\text{DP}}^{\text{T}} = 0.16$ was observed to be $0.1f_{\text{DP}}^{\text{R}}$. This is taken to represent the systematic uncertainty in the use of reconstructed objects to measure a quantity that is formally defined at the parton-level. It is noted that these estimates partially double count the effects of the modelling differences between SHERPA and ALPGEN+HERWIG+JIMMY.

Events in which $W + 1j_{\text{D}}$ is produced in conjunction with a DPI scatter were observed to have little impact on the analysis. At parton level, the shift in f_{DP}^{P} was found to be negligible if these events were included. Furthermore, the addition of these events at reconstruction level did not significantly alter the shape of template *A*. It is therefore concluded that the systematic uncertainty due to such combinatoric events is negligible. The impact of physics modelling was observed to be negligible for the electroweak and $t\bar{t}$ backgrounds. For the QCD background, the normalisation uncertainty derived in [4] was included, resulting in a physics background modelling uncertainty of 1% on f_{DP}^{R} .

The systematic uncertainty on f_{DP}^{R} due to jet energy scale calibration was found to be $0.1f_{\text{DP}}^{\text{R}}$. The systematic uncertainty due to the jet energy resolution was observed to be negligible. Both of these effects were calculated after varying the jet energy scale and resolution within the known uncertainties [6]. The impact of pileup was obtained by studying the fit results as a function of the number of primary vertices reconstructed in the event. The effect of removing the JVF selection criterion was studied, as an additional estimate of the uncertainty due to pile-up. The

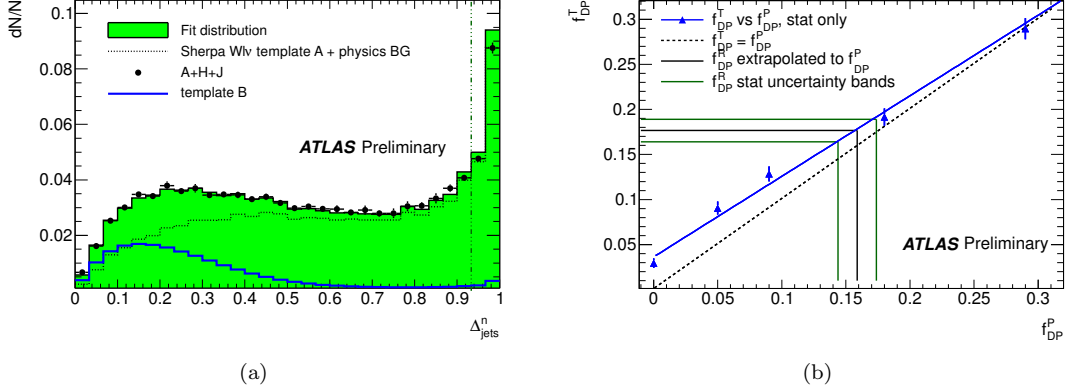


Figure 4: (a) Comparison of Δ_{jets}^n distribution predicted by the ALPGEN+HERWIG+JIMMY default ($x = 1$) with χ^2 minimisation fits of templates *A* (SHERPA) and *B*, to extract f_{DP}^T . The template construction and normalisation is the same as in Figure 2. (b) Extracted value of f_{DP}^T as a function of f_{DP}^P . A one-to-one correspondence line (dashed line) and a linear fit (unbroken line) to the points are also shown. The data extracted value f_{DP}^R (using the SHERPA prediction of template *A*) with its statistical uncertainty of $0.07 f_{\text{DP}}^R$ is also shown extrapolated to the parton level using the linear fit.

overall systematic uncertainty on f_{DP}^R due to pileup was estimated to be $0.08 f_{\text{DP}}^R$. The trigger used to select dijet events is 100% efficient in selecting dijet events and so should not bias their observed kinematics [6]. However, an additional uncertainty of 5% was included after studying the variation in the template *B* shape when the calorimeter jet trigger was used to select the events.

The sources of systematic uncertainty discussed in this section are summed in quadrature to give an overall systematic uncertainty of 21% in the measurement of f_{DP}^R .

5.5 Dependence of f_{DP}^R on phase space cuts

Figure 5 shows the values of f_{DP}^P , f_{DP}^T and f_{DP}^R as a function of the minimum jet p_T requirement. The extracted values of f_{DP}^T and f_{DP}^R are presented only for phase space regions in which the jet energy scale is well understood and the measurement is statistically feasible. The decrease of f_{DP}^R with increasing jet p_T is consistent with the MC predictions for f_{DP}^P and f_{DP}^T . This decrease reflects the fact that the partons originating from the additional scatters have a steeper p_T distribution than the partons from the primary scatter. The values of $f_{\text{DP}}^{P,T,R}$ were observed to be only weakly correlated with the maximum rapidity requirement applied to the partons/jets and is not discussed further.

6 Evaluation of σ_{eff}

The value of σ_{eff} was evaluated using equation 7. The fraction of events from double parton scattering was extracted from the data as discussed in the previous section. The exclusivity ratio, N_{W_0}/N_{W+2j} was obtained using the inclusive W dataset produced with the selection

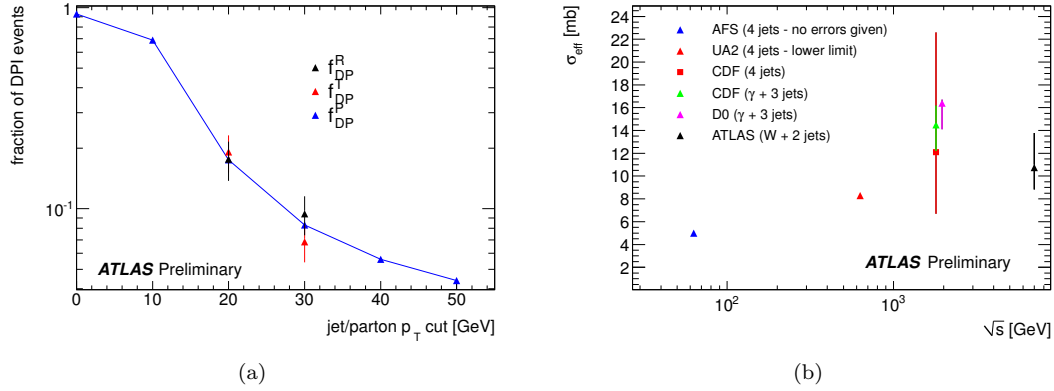


Figure 5: (a) Extracted values of $f_{\text{DPI}}^{\text{T}}$, $f_{\text{DPI}}^{\text{P}}$ and $f_{\text{DPI}}^{\text{R}}$ (using SHERPA prediction for template A) as a function of jet/parton p_{T} , and (b) the centre-of-mass \sqrt{s} dependence of σ_{eff} extracted in different processes in different experiments, for an energy range between 63 GeV and 7 TeV.

criteria outlined in Section 2. This ratio was observed to be 11, with an associated systematic uncertainty of 5% due to background modelling [4]. The statistical uncertainty was negligible. The number of (exclusive) dijet events was found to be 28820 following the event selection criteria outlined in Section 2. The integrated luminosity was $\mathcal{L} = 184 \mu\text{b}^{-1}$, with a systematic uncertainty of 3.4% [19]. The trigger selection for dijet events is fully efficient ($\epsilon_{2j} = 1$).

The lepton-jet overlap removal was only applied to jets in the $W + 2j$ sample. A small correction was applied to account for any bias in the acceptance cancellation assumed in equation 5. The effect of $E_{\text{T}}^{\text{miss}}$ resolution on the acceptance cancellation was found to be negligible.

The final result is $\sigma_{\text{eff}}(7 \text{ TeV}) = 11 \pm 1$ (stat) $^{+3}_{-2}$ (sys) mb. This is compared to results from previous experiments [20–24] as a function of centre-of-mass energy in Figure 5. The value of σ_{eff} obtained in this measurement is consistent with the Tevatron results assuming no energy dependence. However, given the quoted uncertainties on each measurement, a dependence on the centre-of-mass energy cannot be excluded.

References

- [1] ATLAS Collaboration, “A measurement of hard double-partonic interactions in $W \rightarrow l\nu + 2 \text{ jet}$ events”, ATLAS-CONF-2011-160.
- [2] B. Humpert, R. Odorico, “Multiparton scattering and QCD radiation as sources of four jet events”, Phys. Lett. B **154** (1985) 211.
- [3] ATLAS Collaboration, “The ATLAS Experiment at the CERN Large Hadron Collider”, JINST **3** S08003 (2008).
- [4] ATLAS Collaboration, “Measurement of the production cross section for W -bosons in association with jets in pp collisions using 33 pb⁻¹ of data at $\sqrt{s} = 7 \text{ TeV}$ with the ATLAS detector”, Phys. Lett. B **698** (2011) 325-345.
- [5] M. Cacciari, G. P. Salam, G. Soyez, “The anti- k_t jet clustering algorithm”, JHEP **0408** (2008) 063.
- [6] ATLAS Collaboration, “Measurement of inclusive jet and dijet cross sections in proton-proton collisions at 7 TeV centre-of-mass energy with the ATLAS detector”, Eur. Phys. J. C **71** (2011) 1512.

- [7] M. L. Mangano, M. Moretti, F. Piccinini, R. Pittau, A. D. Polosa, “ALPGEN, a generator for hard multiparton processes in hadronic collisions”, *JHEP* **0307** (2003) 001.
- [8] J. Alwall *et. al*, “Comparative study of various algorithms for the merging of parton showers and matrix elements in hadronic collisions”, *Eur. Phys. J. C* **53** (2008) 473.
- [9] G. Corcella *et. al*, “HERWIG 6: An Event generator for hadron emission reactions with interfering gluons (including supersymmetric processes)”, *JHEP* **0101** (2001) 010.
- [10] J. M. Butterworth, J. R. Forshaw, M. H. Seymour, “Multiparton interactions in photoproduction at HERA”, *Z. Phys. C* **72** (1996) 637-646.
- [11] ATLAS Collaboration, “First tuning of HERWIG/JIMMY to ATLAS data”, ATL-PHYS-PUB-2010-014, 2010.
- [12] T. Gleisberg, S. Hoeche, F. Krauss, M. Schonherr, S. Schumann, F. Siegert, J. Winter, “Event generation with SHERPA 1.1”, *JHEP* **0902** (2009) 007.
- [13] S. Catani, F. Krauss, R. Kuhn, B. R. Webber, “QCD matrix elements + parton showers”, *JHEP* **0111** (2001) 063.
- [14] T. Sjostrand, S. Mrenna, P. Z. Skands, “PYTHIA 6.4 Physics and Manual”, *JHEP* **0605** (2006) 026.
- [15] ATLAS Collaboration, “Charged particle multiplicities in pp interactions at $\sqrt{s} = 0.9$ at 7 TeV in a diffractive limited phase space measured with the ATLAS detector at the LHC and a new PYTHIA6 tune”, *Eur. Phys. J. C* **70** (2010) 823.
- [16] S. Frixione and B.R. Webber, “Matching NLO QCD computations and parton shower simulations”, *JHEP* **0206** (2002) 029.
- [17] ATLAS Collaboration, “The ATLAS simulation infrastructure”, *Eur. Phys. J. C* **70** (2010) 823.
- [18] S. Agostinelli et al. , “Geant4 - a simulation toolkit”, *Nucl. Inst. and Meth. A* **506** (2003) 250.
- [19] ATLAS Collaboration, “Updated Luminosity Determination in pp Collisions at $\sqrt{s} = 7$ TeV using the ATLAS Detector”, ATLAS-CONF-2011-011.
- [20] The AFS collaboration, “Double parton scattering in pp collisions at $\sqrt{s} = 63$ GeV”, *Z. Phys. C* **34** (1987) 163.
- [21] The UA2 Collaboration, “A Study of multi-jet events at the CERN $\bar{p}p$ collider and a search for double parton scattering”, *Phys. Lett. B* **268** (1991) 145-154.
- [22] The CDF Collaboration, “Study of four jet events and evidence for double parton interactions in $p\bar{p}$ collisions at $\sqrt{s} = 1.8$ TeV”, *Phys. Rev. D* **47** (1993) 4857-4871.
- [23] The CDF Collaboration, “Double parton scattering in $\bar{p}p$ collisions at $\sqrt{s} = 1.8$ TeV”, *Phys. Rev. D* **56** (1997) 3811-3832.
- [24] The D0 Collaboration, “Double parton interactions in photon+3 jet events in $\bar{p}p$ collisions $\sqrt{s} = 1.96$ TeV”, *Phys. Rev. D* **81** (2010) 052012.

Study of multiple partonic interactions in $D\bar{O}$

Georgy Golovanov for the $D\bar{O}$ Collaboration

Joint Institute for Nuclear Research, 6 Joliot-Curie, Dubna, Russia, 141980

DOI: <http://dx.doi.org/10.3204/DESY-PROC-2012-03/14>

The samples of inclusive $\gamma+3$ jet and $\gamma+2$ jet events collected by the $D\bar{O}$ experiment with an integrated luminosity of 1 fb^{-1} in $p\bar{p}$ collisions at $\sqrt{s} = 1.96 \text{ TeV}$ were used to study processes with multiple parton interactions (MPI). Using the sample of $\gamma+3$ jet events we measured: (a) the fraction of events with double (f_{DP}) and triple (f_{TP}) parton interactions, (b) effective cross section, σ_{eff} , a scale parameter related to the parton density inside the nucleon and (c) cross section as a function of the angle between the transverse momentum (p_{T}) of the γ +leading jet system and p_{T} sum of the two other jets. The sample of $\gamma+2$ jet events allowed us to measure the fraction of events with double parton interactions and cross sections as a function of the angle between the p_{T} of the γ +leading jet system and p_{T} of the other jet. We also estimated the contribution of events with double parton interactions as a background to the associated Higgs boson (H) and W production (with $H \rightarrow b\bar{b}$ decay) at the Tevatron.

1 Introduction

High energy inelastic scattering of nucleons occurs mainly through a single parton-parton interaction but the contribution from multiple parton interactions (MPI) can be significant. Studying the MPI at high p_{T} regime gives the important information about hadron structure and is needed for precise estimates of backgrounds to many rare processes.

2 Double parton interactions in $\gamma+3$ jet events

The cross section of a process with double parton (DP) interaction is proportional to cross sections of two partonic scatterings A and B.

$$\sigma_{DP} \equiv \frac{\sigma^A \sigma^B}{\sigma_{\text{eff}}}. \quad (1)$$

The scaling parameter σ_{eff} has the units of cross section and characterizes a size of the effective interaction region. We use a sample of $\gamma+3$ jet events collected by the $D\bar{O}$ experiment with an integrated luminosity of about 1 fb^{-1} . The $D\bar{O}$ detector is a general purpose detector described in [1]. The events should pass triggers based on the identification of high p_{T} cluster in the electromagnetic calorimeter with loose shower shape requirements for photons. Jets are reconstructed using the $D\bar{O}$ Run II iterative midpoint cone algorithm [2] with a cone size 0.7. Each event must contain at least one photon in the rapidity region $|y| < 1.0$ or $1.5 < |y| < 2.5$ and at least three jets with $|y| < 3.0$. Events are selected with photon transverse momentum

$60 < p_T^\gamma < 80$ GeV, leading (in p_T) jet $p_T > 25$ GeV, while the next-to-leading (second) and third jets must have $p_T > 15$ GeV. The DP fractions and σ_{eff} are determined in three p_T^{jet2} bins: 15–20, 20–25, and 25–30 GeV.

In order to extract σ_{eff} we compare rates of double interaction (DI) events (events with interactions at two separate $p\bar{p}$ collisions) and DP events. Assuming that scatterings in the two DP hard processes are uncorrelated, DP and DI events should be kinematically identical. The DP $\gamma + 3$ jet event sample is selected from data with a single $p\bar{p}$ collision vertex, while DI $\gamma + 3$ jet event sample contains events with two separate $p\bar{p}$ vertices. Effective cross section is extracted from the ratio of observed DP and DI $\gamma + 3$ jet event rates.

An event in DP $\gamma + 3$ jet sample can be produced by the two independent parton-parton scatterings or by a single parton-parton (SP) scattering with gluon radiation in initial or final state as well.

To identify the events with two independent parton-parton scatterings that produce $\gamma + 3$ jet final state, we use an angular distribution sensitive to the kinematics of the DP events. We define a variable:

$$\Delta S \equiv \Delta\phi\left(\vec{p}_T^{\gamma, \text{jet1}}, \vec{p}_T^{\text{jet2}, \text{jet3}}\right), \quad (2)$$

where $\Delta\phi$ is an azimuthal angle between the p_T vectors of the total transverse momenta of the two two-body systems, $\vec{p}_T^{\gamma, \text{jet1}}$ and $\vec{p}_T^{\text{jet2}, \text{jet3}}$, in $\gamma + 3$ jet events. This angle is schematically shown in Fig. 1. The distribution of ΔS variable reflects angular properties of a mixture of

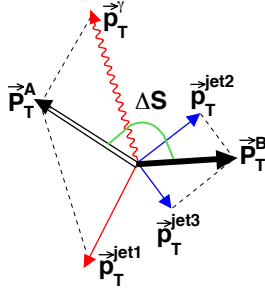


Figure 1: A possible orientation of photon and jets transverse momenta vectors in $\gamma + 3$ jet events. Vectors \vec{P}_T^A and \vec{P}_T^B are the p_T imbalance vectors of γ +jet and jet-jet pairs. The figure illustrates a general case for the production of $\gamma+3$ jets +X events.

$\gamma + 3$ jet events containing both single and double parton scatterings. To extract fraction of DP events (f_{DP}) we consider a data-driven method which uses two adjacent p_T intervals of the second jet. Since we know properties of data and DP model, the only unknown parameter is the fraction of DP events in one p_T^{jet2} bin. It is obtained from a minimization.

The found f_{DP} values with total uncertainties are 0.466 ± 0.041 for $15 < p_T^{\text{jet2}} < 20$ GeV, 0.334 ± 0.023 for $20 < p_T^{\text{jet2}} < 25$ GeV, and 0.235 ± 0.027 for $25 < p_T^{\text{jet2}} < 30$ GeV. They are shown on the left plot of Fig. 2 (three sets of the points correspond to three possible definitions for the ΔS variable [3]). The values of σ_{eff} are shown in Fig. 2 (right). The main systematic

uncertainties are caused by determinations of the DI and DP fractions giving a total systematic uncertainty of (20.5 – 32.2)%. The obtained σ_{eff} values in different $p_{\text{T}}^{\text{jet}2}$ bins agree with each other within their uncertainties. They are highly uncorrelated and are used to calculate the average value:

$$\sigma_{\text{eff}}^{\text{ave}} = 16.4 \pm 0.3(\text{stat}) \pm 2.3(\text{syst}) \text{ mb.} \quad (3)$$

This average value is in the range of those found in previous measurements [4, 5, 6, 7] performed at different energy scales of parton interactions.

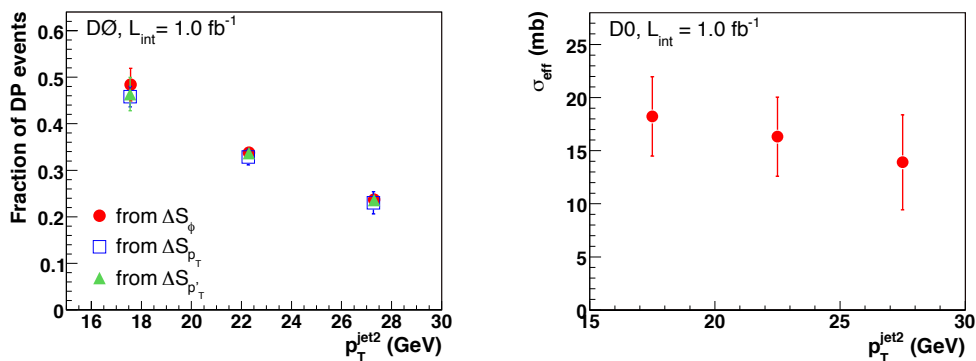


Figure 2: Left: Fractions of $\gamma + 3$ jet events with double parton interactions in the three $p_{\text{T}}^{\text{jet}2}$ intervals. Right: Effective cross section σ_{eff} (mb) measured in the three $p_{\text{T}}^{\text{jet}2}$ intervals.

3 Azimuthal decorrelations and multiple parton interactions in $\gamma + 2$ jet and $\gamma + 3$ jet events in $p\bar{p}$ collisions

As an extension of our study of $\gamma + 3$ jet events described in previous section we measure normalized differential cross sections of the azimuthal angle between the p_{T} vectors obtained by pairing the photon and leading jet and the p_{T} vector of the other one (two) jet(s) in $\gamma + 2(3)$ -jet+ X events [8]. These cross sections are very sensitive to the contribution from jets originating from additional parton hard interactions (beyond the dominant one) and can be used to tune existing MPI models and to estimate the fractions of such events.

Samples of $\gamma + 2(3)$ jet events with the same cuts as [3] are considered. The next modifications are applied: each event must contain at least one γ in the pseudorapidity region $|y| < 1.0$ or $1.5 < |y| < 2.5$ and at least two (or three) jets with $|y| < 3.5$. Events are selected with γ transverse momentum $50 < p_{\text{T}}^{\gamma} < 90$ GeV, leading jet $p_{\text{T}} > 30$ GeV, and the second jet $p_{\text{T}} > 15$ GeV. If there is a third jet with $p_{\text{T}} > 15$ GeV that passes the selection criteria, the event is also considered for the $\gamma + 3$ jet analysis.

To identify events with two independent parton-parton scatterings which produce $\gamma + 3$ jet final state we use the variable defined in (2). Analogously, to be sensitive to DP events in $\gamma + 2$ jet final state, we define an azimuthal angle between p_{T} vectors obtained by pairing

photon and leading jet p_T vectors (\vec{p}_T^A) and the second jet p_T vector:

$$\Delta\phi \equiv \Delta\phi\left(\vec{p}_T^A, \vec{p}_T^{\text{jet}2}\right), \quad (4)$$

where $\vec{p}_T^A = \vec{p}_T^\gamma + \vec{p}_T^{\text{jet}1}$. Figure 3 illustrates a possible disposition of photon and jets transverse momenta vectors in $\gamma + 2$ jet events.

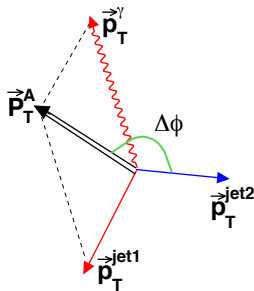


Figure 3: Diagram showing the p_T vectors of the γ +leading jet system (p_T^A), and $p_T^{\text{jet}2}$ in $\gamma + 2$ jet events.

We consider a few MPI models and two models without MPI simulated by PYTHIA [9] and SHERPA [10] MC generators. Figure 4 shows the measured cross section for the two angular variables ΔS (left plot) and $\Delta\phi$ (right plot). The data have a good sensitivity to the various MPI models, which predictions vary significantly and differ from each other by up to a factor 2 at small ΔS and $\Delta\phi$, i.e. in the region where the relative DP contribution is expected to be highest.

From these plots we may conclude that: (a) a large difference between single parton-parton interaction (SP) models and data confirms a presence of DP events in the data sample; (b) the data favor the predictions of the MPI models with Perugia-0, S0 and Sherpa MPI tunes with p_T -ordered parton showers; (c) the predictions from tune A and DW MPI models are disfavored. It is important that our preferable choice of MPI models is stable for all our measurements.

In $\gamma + 2$ jet events in which the second jet is produced in the additional independent parton interaction, the $\Delta\phi$ distribution should be flat. Using this fact and also SP prediction for $\Delta\phi$, we can get the DP fractions from a fit to data. The distributions in data, SP, and DP models, as well as a sum of the SP and DP distributions, weighted with their respective fractions for $15 < p_T^{\text{jet}2} < 20$ GeV, are shown in the left plot of Fig. 6. The DP fractions in the $\gamma + 2$ jet samples decrease in the bins of $p_T^{\text{jet}2}$ as $(11.6 \pm 1.0)\%$ for $15 - 20$ GeV, $(5.0 \pm 1.2)\%$ for $20 - 25$ GeV, and $(2.2 \pm 0.8)\%$ for $25 - 30$ GeV. To determine the fractions as a function of $\Delta\phi$, we perform a fit in the different $\Delta\phi$ regions by excluding the bins at high $\Delta\phi$. We find that they grow significantly towards the smaller angles and are higher for smaller $p_T^{\text{jet}2}$ (right plot of Fig. 6).

We also estimate the fraction of $\gamma + 3$ jet events from triple parton interactions (TP) in data as a function of $p_T^{\text{jet}2}$. In $\gamma + 3$ jet TP events, the three jets come from three different parton

STUDY OF MULTIPLE PARTONIC INTERACTIONS IN $D\bar{O}$

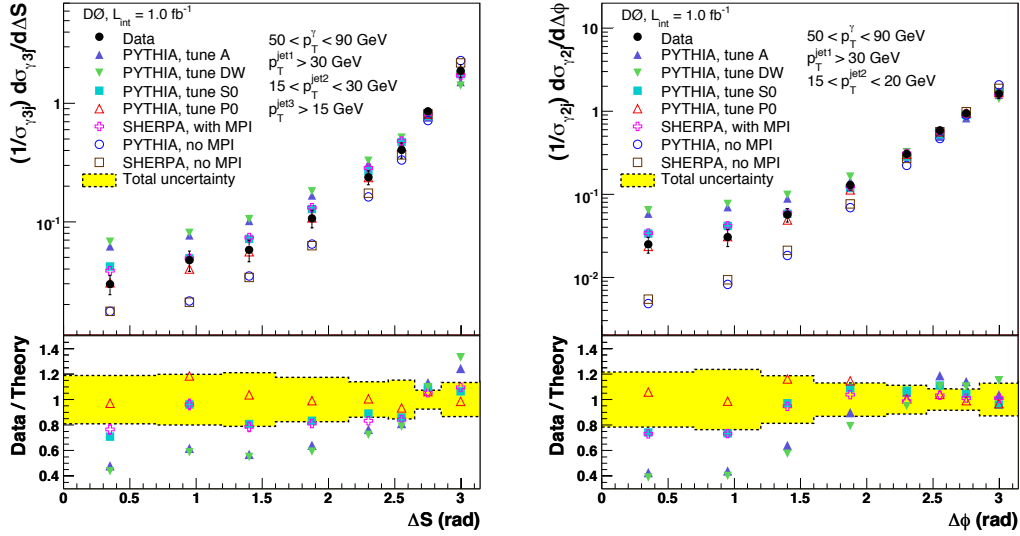


Figure 4: Left: Normalized differential cross section in the $\gamma+3$ -jet events, $(1/\sigma_{\gamma 3j}) d\sigma_{\gamma 3j}/d\Delta S$, in data compared to MC models and the ratio of data over theory, only for models including MPI, in the range $15 < p_T^{\text{jet}2} < 30$ GeV. Right: Normalized differential cross section in $\gamma+2$ -jet events, $(1/\sigma_{\gamma 2j}) d\sigma_{\gamma 2j}/d\Delta\phi$, in data compared to MC models and the ratio of data over theory, only for models including MPI, in the range $15 < p_T^{\text{jet}2} < 20$ GeV.

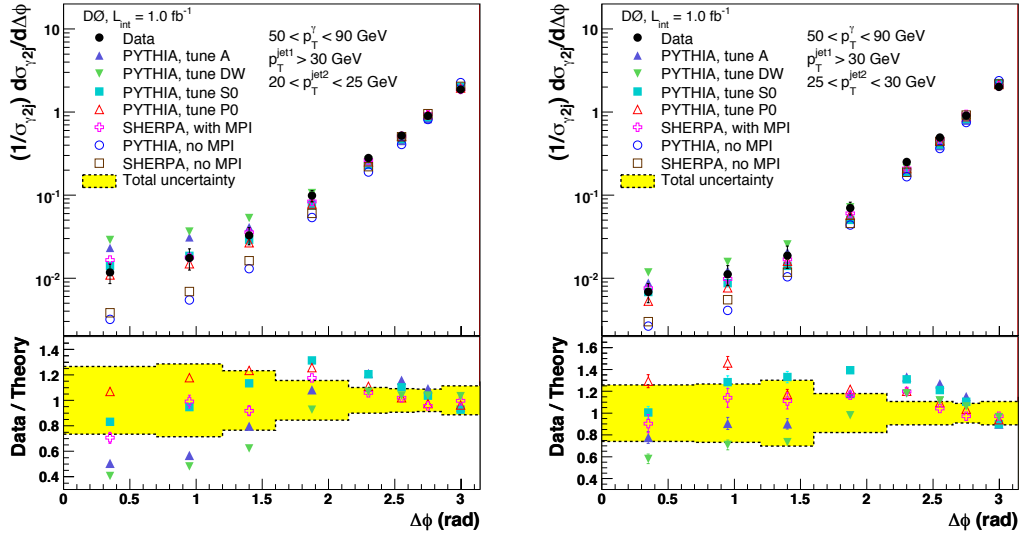


Figure 5: Normalized differential cross sections in $\gamma+2$ -jet events, $(1/\sigma_{\gamma 2j}) d\sigma_{\gamma 2j}/d\Delta\phi$, in data compared to MC models and the ratio of data over theory, only for models including MPI, in the range $20 < p_T^{\text{jet}2} < 25$ GeV (left) and $25 < p_T^{\text{jet}2} < 30$ GeV (right).

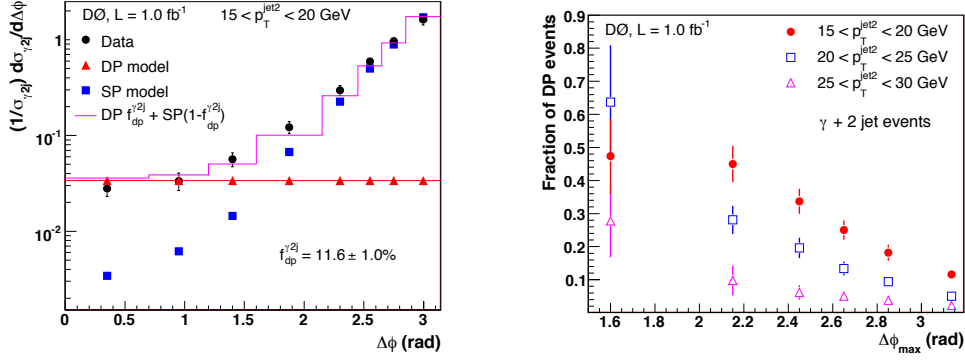


Figure 6: Left: the $\Delta\phi$ distribution in data, SP, and DP models, and the sum of the SP and DP contributions weighted with their fractions for $15 < p_T^{\text{jet}2} < 20$ GeV. Right: the fractions of DP events with total uncertainties in $\gamma + 2$ jet final state as a function of the upper limit on $\Delta\phi$ for the three $p_T^{\text{jet}2}$ intervals.

interactions, one $\gamma + \text{jet}$ and two dijet final states. In each of the two dijet events, one of the jets is either not reconstructed or below the 15 GeV p_T selection threshold. The fractions of TP events in the $\gamma + 3$ jet data have been estimated and are shown in Fig. 7. As we see, they vary in the $p_T^{\text{jet}2}$ bins as $(5.5 \pm 1.1)\%$ for 15 – 20 GeV, $(2.1 \pm 0.6)\%$ for 20 – 25 GeV, and $(0.9 \pm 0.3)\%$ for 25 – 30 GeV.

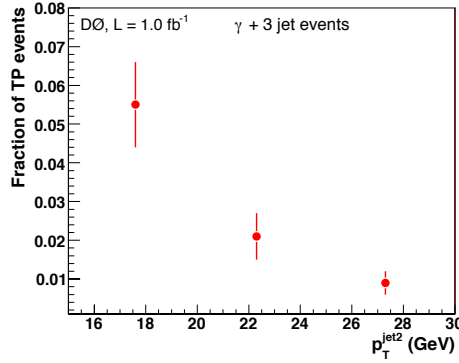


Figure 7: Fractions of $\gamma + 3$ jet events with triple parton interactions in the three $p_T^{\text{jet}2}$ intervals.

4 Conclusions

In recent $D\bar{O}$ measurements we have studied properties of events with multiple parton interactions using $\gamma + 3$ jet and $\gamma + 2$ jet final states. We measured fractions of DP events which vary from 46.6% to 23.5% in $\gamma + 3$ jet and from 11.6% to 2.2% in $\gamma + 2$ jet events at $15 < p_T^{\text{jet}2} < 20$ GeV and $25 < p_T^{\text{jet}2} < 30$ GeV respectively. For the first time the triple event fraction has been determined in $\gamma + 3$ jet events. It drops from 5.5% to 0.9% in the same $p_T^{\text{jet}2}$ intervals. The process independent parameter σ_{eff} , which defines the rate of DP events has been measured and found to be $\sigma_{\text{eff}}^{\text{ave}} = 16.4 \pm 0.3(\text{stat}) \pm 2.3(\text{syst})$ mb. Measured ΔS and $\Delta\phi$ cross sections can be useful to tune theoretical MPI models. As an application, we studied events with W +dijet final state, produced in DP interactions. We found that these events can compose quite sizable background to the associated HW production with $H \rightarrow b\bar{b}$ decay [11]. Its relative fraction is found to be 4–8% in the dijet mass region $115 < M_{jj} < 150$ GeV. A set of angular and p_T variables that are sensitive to the difference between the HW and DP kinematics was suggested. A neural network built using these variables allows to significantly suppress the DP background to a desirable level.

References

- [1] $D\bar{O}$ Collaboration, Nucl. Instrum. Methods Phys. Res. A **565** (2006) 463.
- [2] G.C. Blazey *et al.*, arXiv:hep-ex/0005012.
- [3] $D\bar{O}$ Collaboration, Phys. Rev. D **81** (2010) 052012.
- [4] AFS Collaboration, Z. Phys. C **34** (1987) 163.
- [5] UA2 Collaboration, Phys. Lett. B **268** (1991) 145.
- [6] CDF Collaboration, Phys. Rev. D **47** (1993) 4857.
- [7] CDF Collaboration, Phys. Rev. D **56** (1997) 3811.
- [8] $D\bar{O}$ Collaboration, Phys. Rev. D **83** (2011) 052008.
- [9] T. Sjöstrand *et al.*, J. High Energy Physics **0005** (2006) 026.
- [10] T. Gleisberg *et al.*, J. High Energy Physics **0902** (2009) 007.
- [11] D. Bandurin, G. Golovanov and N. Skachkov, J. High Energy Physics **1104** (2011) 054.

Chapter 5

Small- x and diffraction

Vector mesons and DVCS at HERA

Marcella Capua for the H1 and ZEUS Collaborations

Università della Calabria and INFN, Arcavacata di Rende (CS), 87036, Italy

DOI: <http://dx.doi.org/10.3204/DESY-PROC-2012-03/58>

We present a review of the latest exclusive diffraction results achieved at HERA, discussing in particular the W and t dependence of the measured cross sections in both DIS and photo-production regimes.

1 Introduction

Exclusive diffractive processes, $ep \rightarrow eXp$, where the system X is a vector meson (VM) or a real photon, have been extensively studied by the H1 and ZEUS Collaborations at HERA [1, 2, 3, 4]. These processes help to understand the transition from soft to hard Quantum Chromo-Dynamics (QCD) and to study hard diffraction at HERA at a large γp centre-of-mass energy W with a variable hard scale provided by the photon virtuality Q^2 .

Hard diffraction can be described in terms of perturbative QCD, at the leading order, by the exchange of two partons with different longitudinal and transverse momenta in a colourless configuration. In addition, at the HERA energies, the measurement of the Deeply Virtual Compton Scattering (DVCS) cross sections provide constraints on the generalised parton distributions (GPDs)[5]. The dependence of the GPDs on the four-momentum transfer squared at the proton vertex, t , gives information on the transverse distribution of partons in the proton which is not accessible through the measurements of the F_2 structure function.

In this contribution we will concentrate on the latest HERA results on exclusive diffraction discussing in particular the W and t dependence in both the Deeply Inelastic Scattering (DIS) and photo-production regimes ($Q^2 < 2 \text{ GeV}^2$).

2 W dependence

It is expected that the VM production cross section increases with increasing W energy with a power law ($\sigma \sim W^\delta$), where the power factor δ grows with Q^2 . Figure 1 (left) shows the total γp cross section together with a compilation of light and heavy VM cross section measurements in photo-production ($Q^2 \sim 0$) as a function of W . The lines with slope δ guide the eyes. The W dependence of the total γp cross section is typical of soft interactions and a similar behavior is visible also for light VMs. A different and stronger energy dependence can instead be observed for heavy VM (e.g. J/ψ) with the power δ increasing as the mass of the vector meson increases. This is interpreted as the evidence of gluon participation in the interaction, since the higher the scale at which the gluons are probed, the faster the rise with W . The power δ is shown as a function of the scale ($Q^2 + M^2$) in fig. 1 (right), for a similar compilation of exclusive processes in DIS, including also DVCS and photo-production measurements.

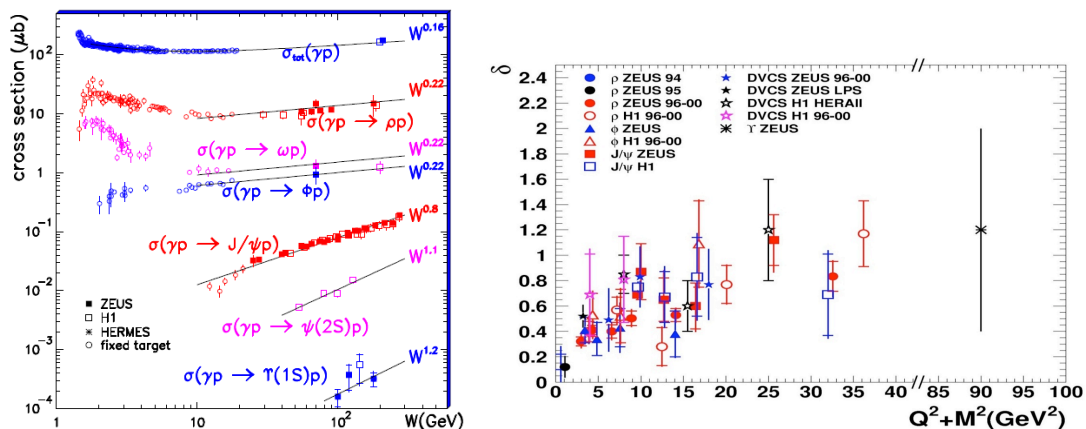


Figure 1: (left) Compilation of the total and exclusive VM photo-production cross sections as a function of W ; the curves are the result of a fit of the form W^δ . (right) Compilation of the parameter δ as a function of the scale ($Q^2 + M^2$), obtained from the measured cross sections for the exclusive VM in DIS, including also DVCS and photo-production measurements.

Still not included in fig. 1 (left) is the new preliminary H1 result on $J/\psi \rightarrow e^+e^-$ in photo-production [7], which is shown in fig. 2. This measurement is based on the last part of the HERA data taking, when three different proton beam energies were provided (920 GeV, 575 GeV and 460 GeV). The different proton beam energies allow to extend the diffractive J/ψ measurements towards lower W energies.

Figure 2 (left) shows the elastic $ep \rightarrow eJ/\psi p$ cross sections as a function of W compared with previous fixed target and H1 measurements and the resulting value of the fit of the data to W^δ is in very good agreement with previous H1 and ZEUS (not shown in the figure) measurements. In the same figure (right) the proton dissociative cross section $ep \rightarrow eJ/\psi Y$ is presented in which the proton dissociates into a low-mass state Y . The curve is the result of the fit to a power δ . The different value of the slope δ can be noticed.

3 t dependence

The t dependence of the exclusive diffractive differential cross section, $d\sigma/dt \propto e^{-bt}$, has been also investigated at HERA. We expect that because of the increasing hardness of the interaction, the t distribution becomes universal, independent of the scale and the final state observed. The asymptotic value of b , the parameter of the exponential slope of the t distribution, reflects the size of the proton.

Figure 3 shows a compilation of the b slope values obtained from an exponential fit to the differential cross sections $d\sigma/dt$ as a function of the scale ($Q^2 + M^2$) for various VMs, including the new ZEUS $\Upsilon(1S)$ [9] measurement and recent DVCS (for which $M = 0$) [2, 3, 4] measurements. A transition from the soft to the hard regime is visible, with b decreasing with the increase of the scale to an asymptotic value close to 5 GeV^{-2} , which is an indication that the gluons are well contained within the proton. In fig. 3 the ZEUS DVCS measurement [4] at $Q^2 = 3.2 \text{ GeV}^2$ has been obtained for the first time from the direct measurement of the t

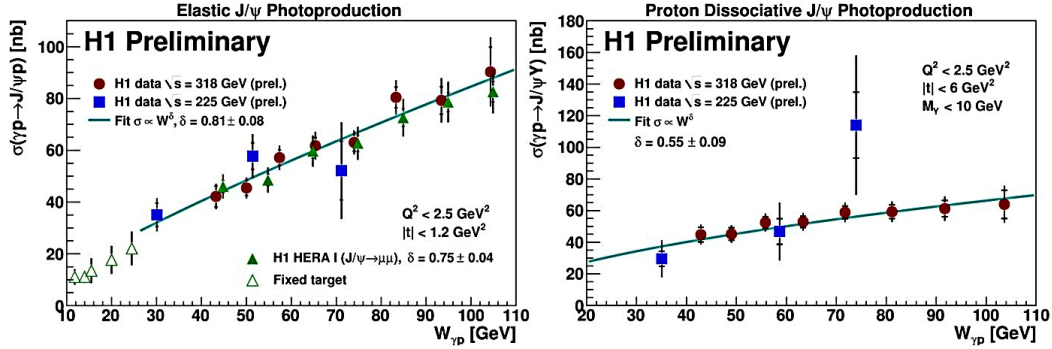


Figure 2: J/ψ photo-production cross sections as a function of W for elastic (left) and proton dissociative measurements (right). The curves are fits of the form W^δ .

variable with a dedicated spectrometer [8]. In the H1 DVCS measurements [2, 3], the t variable is computed as the vector sum of the transverse momenta of the final state photon and the scattered lepton; the kinematic region covered is $6.5 < Q^2 < 80 \text{ GeV}^2$, $30 < W < 140 \text{ GeV}$ and $t < 1 \text{ GeV}^2$. H1 has also published the differential cross section as a function of t for different values of Q^2 and W and observes a soft Q^2 dependence of the parameter b , while no dependence has been observed as a function of W .

In addition, Figure 3 shows the first determination of the b parameter for $\Upsilon(1S)$ production. The exclusive photo-production reaction $\gamma p \rightarrow \Upsilon(1S)p$ was studied by the ZEUS detector using the entire HERA data sample. The covered kinematic range is $60 < W < 220 \text{ GeV}$ and $Q^2 < 1 \text{ GeV}^2$. The measurement of b , shown in fig. 4 (top), yielded $b = 4.3^{+2.0}_{-1.3}$ (stat.) $^{+0.5}_{-0.6}$ (syst.) GeV^{-2} , consistent with predictions based on pQCD models ($b = 3.68 \text{ GeV}^{-2}$) [10]. The result is in agreement with expectations of an asymptotic behavior of the slope parameter as a function of the scale and extends the scale range to $\sim 90 \text{ GeV}^2$, the highest value achieved so far for a vector meson.

In fig. 4 (bottom) the already discussed H1 preliminary results for J/ψ are presented as differential cross section $d\sigma/dt$ for elastic photo-production, together with the results of the exponential fit, for two energy values, $\sqrt{s} = 318 \text{ GeV}$ and $\sqrt{s} = 225 \text{ GeV}$, corresponding to an higher and lower W region, respectively.

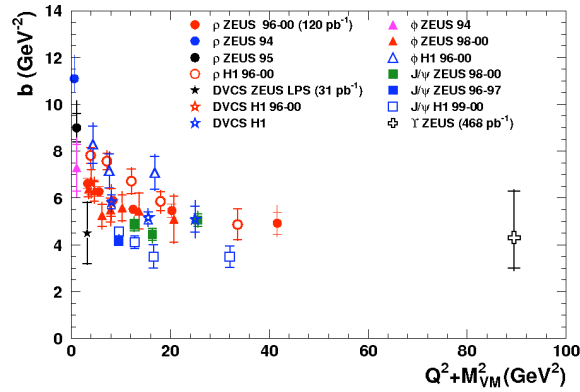


Figure 3: Comparison of the HERA measurements of the slope parameter b as a function of the scale $Q^2 + M_{VM}^2$ for exclusive VM production and for DVCS.

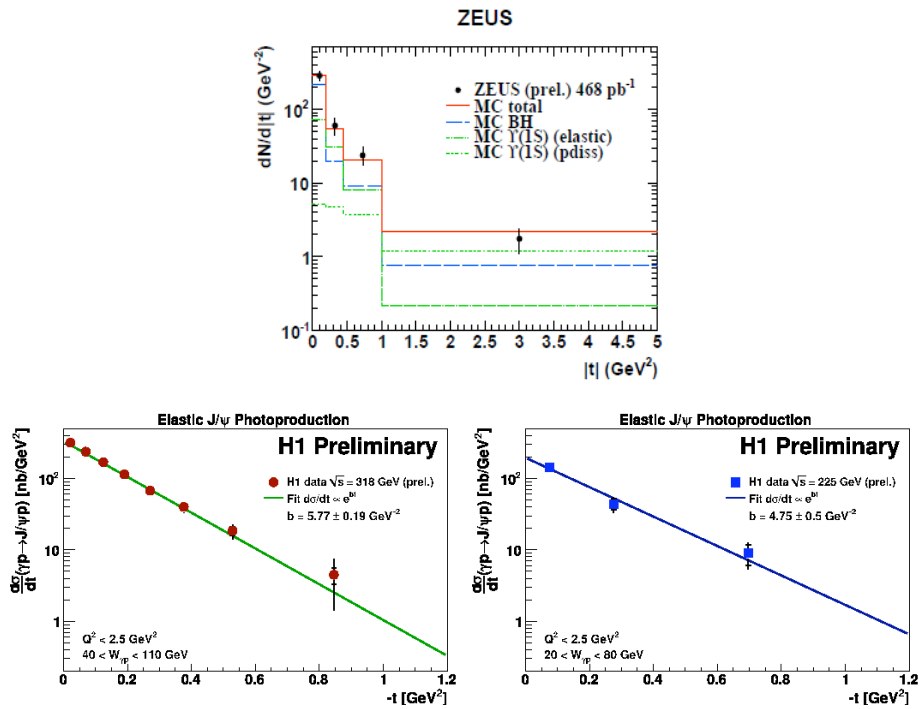


Figure 4: (top) Measured $|t|$ distribution (full dots) with error bars denoting statistical uncertainties. Fitted distributions for simulated events are shown for the Bethe-Heitler (dashed line), exclusive $\Upsilon(1S)$ (dotted line) and proton dissociative $\Upsilon(1S)$ (dash-dotted line) processes. The solid line shows the sum of all contributions. (bottom) Differential cross section for exclusive J/ψ photo-production as a function of t for two proton beam energies. The lines are the results of an exponential fit.

4 Exclusive two-pion production in DIS

A new interesting result presented by ZEUS is the exclusive DIS production of two pions [11] in the mass range $0.4 < M_{\pi\pi} < 2.5$ GeV. The measurement is performed in the kinematic range $2 < Q^2 < 80$ GeV², $32 < W < 180$ GeV and $t < 0.6$ GeV² and is shown in fig. 5 (left), where the two-pion acceptance-corrected data are compared with the pion electromagnetic form factor $|F(M_{\pi\pi})|$ assuming that the mass range includes the contribution of the ρ , $\rho'(1450)$ and $\rho''(1700)$ vector meson states.

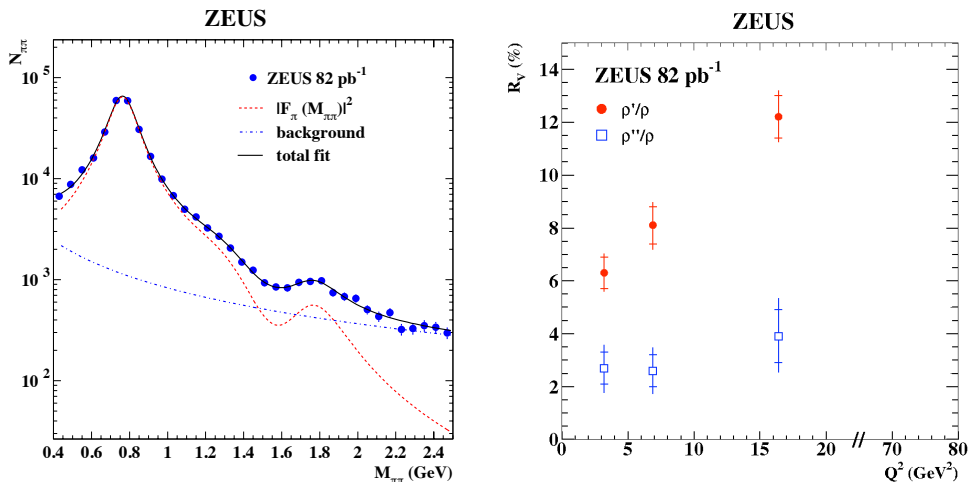


Figure 5: (left) The two-pion invariant-mass distribution $M_{\pi\pi}$, where $N_{\pi\pi}$ is the acceptance corrected number of events. The full line is the result of a fit using the Kuhn-Santamaria parameterization [12]. The dashed line is the result of the pion form factor normalized to the data and the dash-dotted line denotes the background contribution. (right) The ratio R_V as a function of Q^2 for $V = \rho'$ (full circles) and $V = \rho''$ (open squares).

The Q^2 dependence of the pion form factor has been also investigated. The data sample has been divided in three Q^2 bins and a fit to $M_{\pi\pi}$ performed. Figure 5 (right) shows the ratios $R_{\rho'} = \sigma(\rho' \rightarrow \pi\pi)/\sigma(\rho)$ and $R_{\rho''} = \sigma(\rho'' \rightarrow \pi\pi)/\sigma(\rho)$ as a function of Q^2 . We observe a strong Q^2 dependence of the ratio $R_{\rho'}$, as expected in QCD-inspired models [19]. No conclusions are possible regarding the Q^2 dependence of $R_{\rho'}$ due to the large uncertainties.

The last result presented, shown in Figure 6, is the pion form factor $|F_{\pi}|^2$ resulting from the fit for the three Q^2 regions and measurements of $e^+e^- \rightarrow \pi^+\pi^-$ in the time-like regime [13, 14, 15, 16, 17]. A Q^2 dependence of $|F_{\pi}(M_{\pi\pi})|^2$ is observed. In particular, it is visible that in the interference region between ρ' and ρ'' (left) the distribution of the γ^*p data is higher than the e^+e^- data and lower in the ρ mass range (right). The measurements are compatible for $M_{\pi\pi} > 1.8$ GeV.

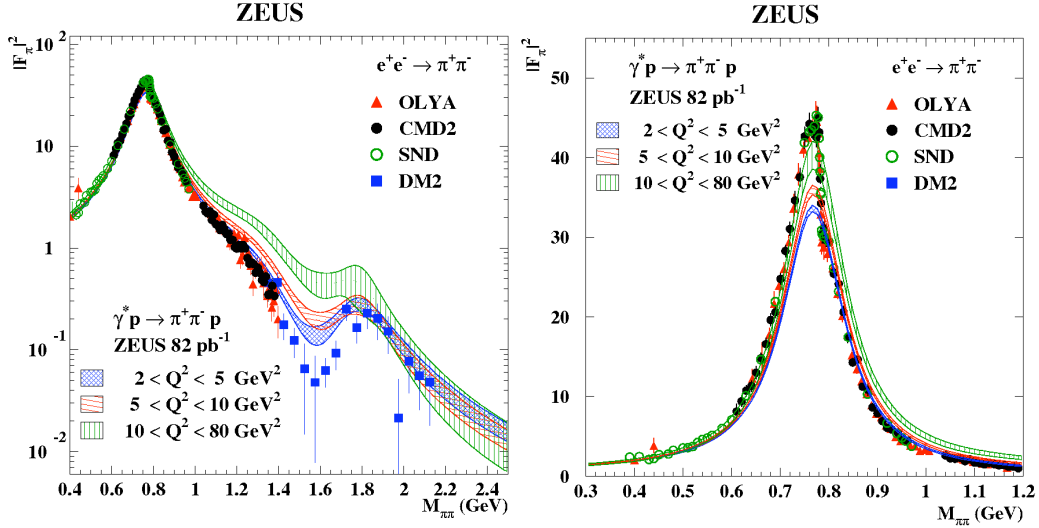


Figure 6: (left) The pion form factor squared $|F_\pi|^2$ as a function of the $\pi^+\pi^-$ invariant mass $M_{\pi\pi}$ as obtained from the reaction $e^+e^- \rightarrow \pi^+\pi^-$. The shaded bands represent the square of the pion form factor and its total uncertainty obtained in the γ^*p analysis for three ranges of Q^2 . (right) The ρ mass region of the left-hand-side figure is shown in a linear scale.

References

- [1] ZEUS Collaboration, Phys. Lett. B **487** (2000) 273; ZEUS Collaboration, Nucl. Phys. B **718** (2005) 2; ZEUS Collaboration, Nucl. Phys. B **695** (2004) 3; ZEUS Collaboration, Eur. Phys. J. C **14** (2000) 213; H1 Collaboration, Phys. Lett. B **483** (2000) 360; ZEUS Collaboration, PMC Phys. A **1** (2007) 6; H1 Collaboration, Eur. Phys. J. C **46** (2006) 585; H1 Collaboration, Eur. Phys. J. C **13** (2000) 371; ZEUS Collaboration, Eur. Phys. J. C **24** (2002) 345; H1 Collaboration, JHEP **05** (2010) 32.
- [2] H1 Collaboration, Phys. Lett. B **517** (2001) 47; ZEUS Collaboration, Phys. Lett. B **573** (2003) 45; H1 Collaboration, Eur. Phys. J. C **44** (2005) 1.
- [3] H1 Collaboration, Phys. Lett. B **681** (2009) 391; H1 Collaboration, Eur. Phys. J. C **54** (2008) 371.
- [4] ZEUS Collaboration, JHEP **05** (2009) 108.
- [5] M. Diehl, T. Gousset, B. Pire and J. Ralston, Phys. Lett. B **411** (1997) 193; M. Burkardt, Int. J. Mod. Phys. A **18** (2003) 173; M. Diehl, Eur. Phys. J. C **25** (2002) 223; V. Guzey and T. Teckentrup, Phys. Rev. D **74** (1996) 54027; K. Kumerički, Nucl. Phys. B **794** (2008) 223.
- [6] ZEUS Collaboration, Phys. Lett. B **680** (2009) 4.
- [7] H1prelim-11-011.
- [8] ZEUS Collaboration, Z. Phys. C **73** (1997) 253.
- [9] ZEUS Collaboration, Phys. Lett. **PLB-D-11-01630** (2011).
- [10] B.E. Cox, J.R. Forshaw and R. Sandapen, JHEP **906** (2009) 34.
- [11] ZEUS Collaboration, DESY-11-220, Eur. Phys. J. C **72** (2012) 1869.
- [12] J.H. Kuhn and A. Santamaria, Z. Phys. C **48** (1990) 445.
- [13] L.M. Barkov et al., Nucl. Phys. B **256** (1985) 365.
- [14] DM2 Collaboration, Phys. Lett. B **220** (1989) 312.
- [15] CMD2 Collaboration, Phys. Lett. B **527** (2002) 161.

VECTOR MESONS AND DVCS AT HERA

- [16] CMD2 Collaboration, JETP Lett. **82** (2005) 743.
- [17] SND Collaboration, J. Exp. Theor. Phys. **101** (2005) 1053.
- [18] H1 Collaboration, Phys. Lett. B **541** (2002) 251.
- [19] J. Nemchik, N.N. Nikolaev and B.G. Zakharov, Phys. Lett. B **339** (1994) 194; H. Hayashii and M. Fujikawa (for the Belle Coll.), Nucl. Phys. (Proc. Suppl.) B **198** (2010) 157; H. Abramowicz, L. Frankfurt and M. Strikman, Surveys High Energy Phys. **11** (1997) 51.

Pinning down the self-similar gluon distribution from momentum sum rule

Akbari Jahan^{1*}; Dilip K. Choudhury¹

¹Department of Physics, Gauhati University, Guwahati - 781 014, Assam, India.

DOI: <http://dx.doi.org/10.3204/DESY-PROC-2012-03/94>

The concept of self-similarity in the contemporary physics of Deep Inelastic Scattering (DIS) was introduced in 2002 when Lastovicka proposed a functional form of the structure function $F_2(x, Q^2)$ at small x . In this paper, we use the original Lastovicka's model to compute the momentum sum rule $\int_0^1 (F_2(x, Q^2) + G(x, Q^2)) dx = 1$, which relates the fraction of momentum carried by quarks and gluons inside the proton. There exists a singularity at $x \approx 0.019$ in this model. Therefore, we use Cauchy's principal value integration method to construct the fraction of momentum carried by quarks and gluons defined as $\langle x \rangle_q = \int_0^1 F_2(x, Q^2) dx$ and $\langle x \rangle_g = \int_0^1 G(x, Q^2) dx$ respectively. We suggest that the relation between quarks and gluons is given as $G(x, Q^2) = x^{-\lambda(Q^2)} F_2(x, Q^2)$, where $\lambda(Q^2)$ is the function of Q^2 .

1 Introduction

Self-similarity is a possible feature of multi-partons inside a proton at small Bjorken- x , first suggested by Lastovicka of DESY, Germany in the year 2002 [1]. Based on this notion, a form of structure function $F_2(x, Q^2)$ was proposed which could explain the H1 and ZEUS data for $6.2 \times 10^{-7} \leq x \leq 0.01$. In the present work, we use the momentum sum rule [2]

$$\int_0^1 (F_2(x, Q^2) + G(x, Q^2)) dx = 1 \quad (1)$$

and explore the possibility of pinning down the gluon distribution $G(x, Q^2)$ from it. The momentum sum rule is to be satisfied by any reasonable model of structure function. However, such requirement calls for information about the entire physical regime of x ($0 \leq x \leq 1$). It is also well-known that the gluon PDFs are, on the other hand, not directly measurable although there are several indirect ways of measuring like the longitudinal structure function or the slope and curvature of the structure function. We summarize the preliminary results of our analysis.

*Speaker, Email: akbari.jahan@gmail.com

2 Formalism

A description of the proton structure function $F_2(x, Q^2)$ reflecting self-similarity was proposed with a few parameters which were fitted from the HERA data [3, 4]. The concept of self-similarity, when applied to proton structure, leads to a simple parameterization of quark densities within the proton. The structure function (using two magnification factors $\frac{1}{x}$ and $\left(1 + \frac{k_t^2}{Q_0^2}\right)$) is subsequently obtained as:

$$F_2(x, Q^2) = \frac{e^{D_0} Q_0^2 x^{-D_2+1}}{1 + D_3 - D_1 \log x} \left(x^{-D_1 \log\left(1 + \frac{Q^2}{Q_0^2}\right)} \left(1 + \frac{Q^2}{Q_0^2}\right)^{D_3+1} - 1 \right) \quad (2)$$

where the parameters are

$$\begin{aligned} D_0 &= 0.339 \pm 0.145 \\ D_1 &= 0.073 \pm 0.001 \\ D_2 &= 1.013 \pm 0.01 \\ D_3 &= -1.287 \pm 0.01 \\ Q_0^2 &= 0.062 \pm 0.01 \text{ GeV}^2 \end{aligned} \quad (3)$$

Here D_1 , D_2 and D_3 are the parameters identified as the relevant fractal dimensions [1]. This specific parameterization provides an excellent description of the data in the region of four momentum transfer squared, $0.045 \leq Q^2 \leq 120 \text{ GeV}^2$ and Bjorken- x , $6.2 \times 10^{-7} \leq x \leq 0.01$. We assume, for simplicity, the following relation between the structure function and the gluon distribution [5]:

$$G(x, Q^2) = c(x, Q^2) \cdot F_2(x, Q^2) \quad (4)$$

where the function $G(x, Q^2)$ is to be determined from momentum sum rule. The momentum sum rule is given as:

$$\begin{aligned} 1 &= \int_0^1 \{F_2(x, Q^2) + G(x, Q^2)\} dx \\ &= \int_0^1 \{F_2(x, Q^2) + c(x, Q^2)F_2(x, Q^2)\} dx \\ &\Rightarrow \int_0^1 \{c(x, Q^2)F_2(x, Q^2)\} dx = 1 - \int_0^1 F_2(x, Q^2) dx \end{aligned} \quad (5)$$

Thus, knowing the value of $\int_0^1 F_2(x, Q^2) dx$, the gluon content of the proton can be determined. For simplicity, we assume that $c(x, Q^2)$ has the following form:

$$c(x, Q^2) = x^{-\lambda(Q^2)} \quad (6)$$

where $\lambda(Q^2)$ is to be determined from momentum sum rule. Eq. (6) conforms to the expectation that for small x gluon dominates.

Integrating the structure function of Eq. (2), we have:

$$\int_0^1 F_2(x, Q^2) dx = \int_0^1 \frac{e^{D_0} Q_0^2 x^{-D_2+1}}{1 + D_3 - D_1 \log x} \left(x^{-D_1 \log\left(1 + \frac{Q^2}{Q_0^2}\right)} \left(1 + \frac{Q^2}{Q_0^2}\right)^{D_3+1} - 1 \right) dx \quad (7)$$

Substituting the corresponding values of the parameters in the above equation, we get:

$$\int_0^1 F_2(x, Q^2) dx = \int_0^1 \frac{e^{0.339} 0.062 \left(\frac{1}{x}\right)^{0.013}}{0.073 \log\left(\frac{1}{x}\right) - 0.287} \left(\left(\frac{1}{x}\right)^{0.073 \log\left(1 + \frac{Q^2}{0.062}\right)} \left(1 + \frac{Q^2}{0.062}\right)^{-0.287} - 1 \right) dx \quad (8)$$

Using Eq. (2) and after a few steps following Cauchy's principal value integration method [6], we arrive at the following form of the integrated structure function (for any Q^2):

$$\begin{aligned} \int_0^1 F_2(x, Q^2) dx &= \frac{e^{0.339} 0.062}{0.073} \left(1 + \frac{Q^2}{0.062}\right)^{-0.287} e^{-\mu y_0} \\ &\quad \left(\log \left| \frac{y_{max} - y_0}{y_0} \right| - \mu y_{max} + \sum_{n=2}^{\infty} \frac{(-1)^n \mu^n}{n \cdot n!} \{ (y_{max} - y_0)^n + (-1)^{n+1} y_0^n \} \right) \\ &\quad - \frac{e^{0.339} 0.062}{0.073} e^{-\rho y_0} \\ &\quad \left(\log \left| \frac{y_{max} - y_0}{y_0} \right| - \rho y_{max} + \sum_{n=2}^{\infty} \frac{(-1)^n \rho^n}{n \cdot n!} \{ (y_{max} - y_0)^n + (-1)^{n+1} y_0^n \} \right) \end{aligned} \quad (9)$$

where

$$\begin{aligned} \mu &= 1 - \left(0.013 + 0.073 \log \left(1 + \frac{Q^2}{0.062} \right) \right) \\ \rho &= 0.987 \\ y_0 &= 3.93 \\ y_{max} &= \log \left(\frac{1}{x_{min}} \right) \end{aligned} \quad (10)$$

and x_{min} is introduced to take care of the end-point singularity $x = 0$ in the model. Taking only the first term in the infinite series of RHS of Eq. (9), we get [7, 8]

$$\int_0^1 F_2(x, Q^2) dx = 0.024607 \cdot \log \left| \frac{y_{max} - y_0}{y_0} \right| \cdot \frac{Q^2}{0.062} \quad (11)$$

leading to

$$x_{min} \approx 3.58 \times 10^{-4}. \quad (12)$$

Using this value of x_{min} , we calculate

$$\langle x \rangle_q = \int_{x_{min}}^1 F_2(x, Q^2) dx \quad (13)$$

and

$$\langle x \rangle_g = 1 - \langle x \rangle_q \quad (14)$$

for any Q^2 using the RHS of Eq. (9), where $\langle x \rangle_q$ and $\langle x \rangle_g$ are fraction of momentum carried by quarks and gluons respectively.

3 Results

In Table 1, we record the values of $\langle x \rangle_q$ and $\langle x \rangle_g$ for several representative values of Q^2 :

Q^2 (GeV ²)	$\langle x \rangle_q$	$\langle x \rangle_g$
10	0.0716	0.9283
20	0.1433	0.8567
30	0.2149	0.7850
35	0.2508	0.7492
40	0.2867	0.7133
45	0.3225	0.6775
50	0.3583	0.6418
55	0.3942	0.6058
60	0.4299	0.5700
65	0.4658	0.5342
70	0.5017	0.4983
75	0.5375	0.4625
80	0.5733	0.4267
85	0.6092	0.3908
90	0.6449	0.3550

Table 1: Values of $\langle x \rangle_q$ and $\langle x \rangle_g$ for a few representative values of Q^2 .

In Figure 1, it is shown that within the leading term approximation used, $\langle x \rangle_q$ increases with Q^2 while $\langle x \rangle_g$ decreases. At $Q^2 \approx 70$ GeV², both of them become nearly equal, i.e. both quarks and gluons share momentum equally.

It is to be noted that one usually expects the other pattern, i.e. $\langle x \rangle_g = \int_0^1 G(x, Q^2) dx$ should increase with Q^2 and $\langle x \rangle_q = \int_0^1 F_2(x, Q^2) dx$ should decrease [9]. This feature is presumably due to the overestimation of the large x quarks in the original Eq. (2) used and the crude approximation of taking only the first term of the infinite series in Eq. (9). The effects of large

x and higher order terms are currently under study. It will then lead to proper evaluation of the exponent λ in the definition of gluon in Eq. (6).

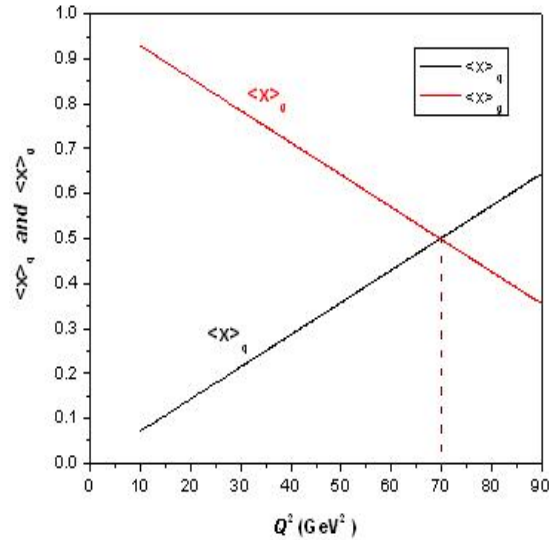


Figure 1: $\langle x \rangle_q$ and $\langle x \rangle_g$ vs Q^2 .

4 Conclusion

In this paper, we have reformulated the gluon distribution function based on momentum sum rule. We also report some preliminary results of how quark and gluon momenta are shared in the proton. Inclusion of higher order terms in the infinite series and the large x effect will hopefully pin down the gluon accurately.

References

- [1] T. Lastovicka, Euro. Phys. J. C **24** (2002) 529, (arXiv:0203260 [hep-ph])
- [2] F. E. Close, "An Introduction to Quarks and Partons", Academic Press, London, (1979) 233
- [3] H1: C. Adloff *et al.*, Eur. Phys. J. C **21** (2001) 33-61, (arXiv:0012053 [hep-ex])
- [4] ZEUS: J. Brietweg *et al.*, Phys. Lett. B **487** (2000) 53, (arXiv:0005018 [hep-ex])
- [5] J. K. Sarma, D K Choudhury and G K Medhi, Phys. Lett. B **403** (1997) 139
- [6] Gino Moretti, "Functions of a Complex Variable", Prentice Hall of India Ltd. (1968)
- [7] F. J. Yndurain, "The Theory of Quark and Gluon Interactions", Springer-Verlag, (1992) 128
- [8] J. G. De Groot *et al.*, Z. Phys. B **403** (1979) 143
- [9] H. D. Politzer, Nucl.Phys. B **122** (1977) 237

Evolution in multiple interactions: a first step beyond the 'double DGLAP' approximation

Jochen Bartels

Universität Hamburg, Germany

DOI: <http://dx.doi.org/10.3204/DESY-PROC-2012-03/19>

We discuss, for the evolution of double-parton densities, a first step beyond the double DGLAP approximation.

1 Introduction

In recent years multiple interactions have received increasing interest, both for event generators and for precision calculations of inclusive cross sections[2, 3, 4, 5, 6, 7, 8, 9]. As an example, the double inclusive cross section in the standard collinear approximation

$$d\sigma = \sum_{i_1 i_2} \int dx_1 dx_2 f_{i_1}(x_1, \mu) d\hat{\sigma}_{i_1 i_2 \rightarrow 2 jet}(x_1, x_2, \mu; \mathbf{p}_1, Y_1, \mathbf{p}_2, Y_2) f_{i_2}(x_2, \mu) \quad (1)$$

receives corrections from the two chain configuration (see fig.1, left):

$$d\sigma^{DP} = \frac{m}{\sigma_{eff}} \sum_{i_1, j_1, i_2, j_2} \int dx_1 dy_1 dx_2 dy_2 H_{i_1 j_1}(x_1, y_1, \mu_a, \mu_b) d\hat{\sigma}_{i_1 i_2 \rightarrow jet}(x_1, y_1, \mu_a; \mathbf{p}_1, Y_1) d\hat{\sigma}_{j_1 j_2 \rightarrow jet}(y_2, y_2, \mu_b; \mathbf{p}_2, Y_2) H_{i_2 j_2}(x_2, y_2, \mu_a, \mu_b) \quad (2)$$

In a popular approximation the double parton density is the product of two single parton densities (double DGLAP approximation):

$$H_{ij}(x, y, \mu_a \mu_b) = f_i(x, \mu_a) f_j(y, \mu_b) \quad (3)$$

where each parton density obeys the standard DGLAP evolution equations. On general grounds, however, one expects the evolution of multiparton densities to be more complicated: there should be correlations between the two densities and there are transitions between parton states with different parton numbers. In this contribution we want to make a few comments on aspects of multiparton evolution which go beyond this 'double DGLAP' approximation.

2 General aspects of evolution equations

In the context of deep inelastic electron proton scattering and HERA measurements it has become clear that evolution equations can be formulated either in terms of the momentum scale (DGLAP) or in rapidity (BFKL). In the former case, evolution equations can be classified

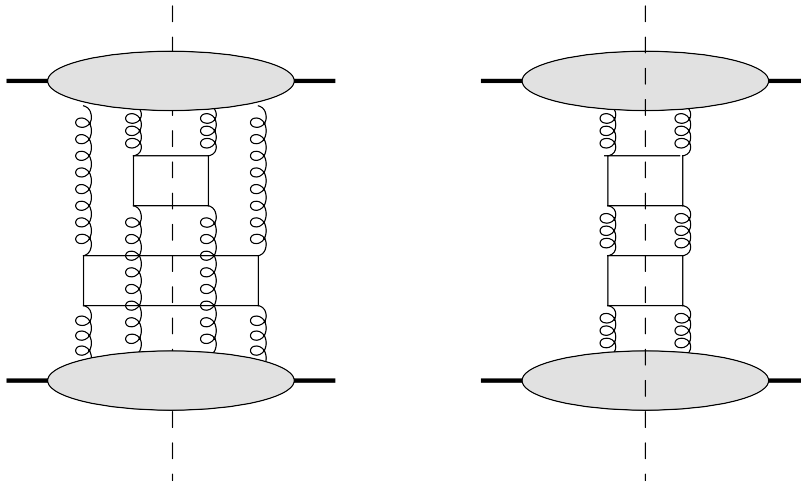


Figure 1: illustration of double and single chain cross sections.

in powers of $1/Q^2$ (twist): the DGLAP evolution equations belong to the leading twist, and they determine the scale dependence of (single) parton densities. Splitting functions are now known in NLO accuracy. Higher twist evolution equations, in the context of deep inelastic scattering, have been formulated and investigated in [10]. As an example, twist 4 introduces t -channels with four gluons, and their evolution shares many features with double parton densities. In leading order, the evolution of n -gluon states is described by the sum over pairwise $2 \rightarrow 2$ interactions, the nonforward DGLAP splitting functions. Mixing between different twist 4 operators leads to transitions from two to four-parton states. In NLO, the evolution equations will contain also three body interactions. Evolution in rapidity, on the other hand, starts from the BFKL evolution equations and describes BFKL Green's functions of reggeized gluons (sometimes also referred to as unintegrated small- x -gluon densities). Their evolution kernels (presently known in NLO accuracy) are different from the DGLAP kernels, but there exists a common region of validity. The generalization of the BFKL equation to multi-gluon Green's functions (known as the BKP equations [12]) is the analogue of the higher twist evolution, and the evolution, in leading order, is given by the sum of pairwise two-body interactions, described by the nonforward BFKL kernels. Transitions between different gluon states are described by momentum dependent transition kernels, e.g. the $2 \rightarrow 4$ transition vertex (triple Pomeron vertex). We illustrate the situation in Fig.2.

As mentioned before, the notion of higher twist has been introduced and discussed mainly in the context of deep inelastic scattering where the twist expansion is a power series expansion in $1/Q^2$. When searching for an analogous power suppression of a double parton cross section where the large momentum scale is set, for example, by the transverse momenta of the produced jets such a power counting has to be applied with care: there exist regions of momenta where the contributions from double parton scattering are of the same order as those due to single parton scattering; it is only after the integration of the outgoing momenta where a higher twist suppression holds. In contrast to the single parton density cross section no factorization theorem exists for the double scattering formula.

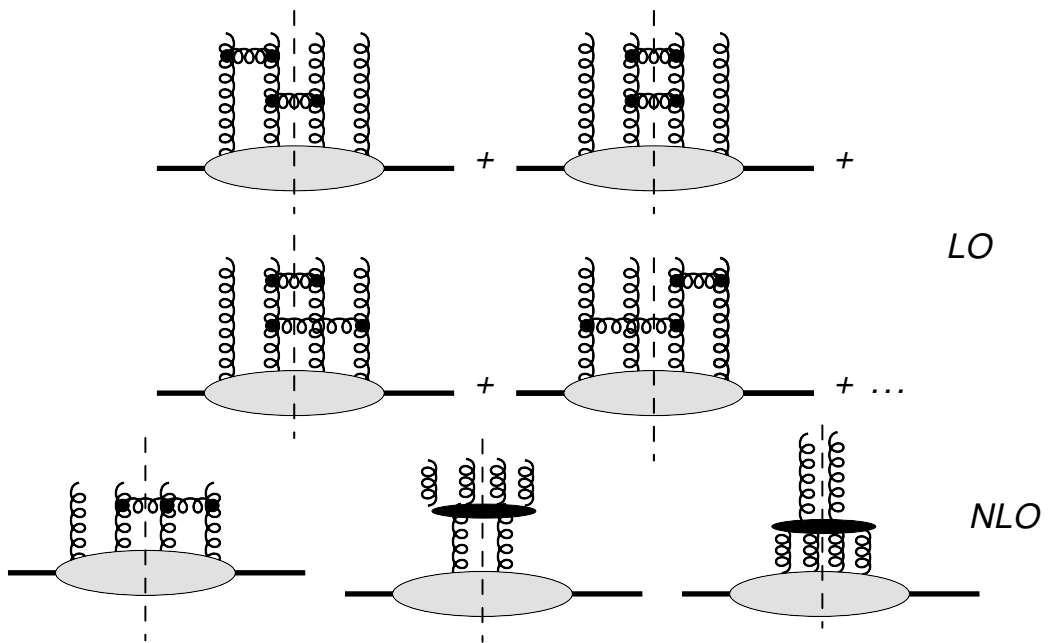


Figure 2: Building blocks of the evolution of double parton densities. The diagrams illustrate both the higher twist evolution and rapidity evolution.

From studies of deep inelastic scattering we know that, at small x , the rapidity evolution starts to compete with the momentum scale evolution equations. Furthermore, the logarithms in $1/x$ start to compensate the higher twist suppression (multi-ladder exchanges), and the twist-expansion in powers $1/Q^2$ becomes useless. The same small- x enhancement is at work also in the double parton cross section: this is why rapidity evolution (BFKL and BKP evolution equations) become increasingly important. This framework also allows to address the question of (soft) rescattering corrections to the double parton formula: from the AGK[11] rules we know that exchanges across the production vertices cancel, not only for single inclusive cross sections but also for double (and higher) inclusive cross sections. A prerequisite for the AGK rules to be valid is the symmetry of the coupling of the four gluons to the proton (Fig.2): this coupling has to be invariant under the exchange of gluons lines (color and momenta), and independent of the position of the cutting line.

3 Recombination effects in the two-chain evolution

As we have already indicated (and illustrated in Fig.2), the evolution of double parton densities contains the sum over pairwise $2 \rightarrow 2$ interactions (ignoring, for the moment, transitions from two to four gluon states). In the factorization approximation ('double DGLAP'), when viewed from the t -channel, two color singlet ladders are formed, and each ladder, evaluated at zero momentum transfer (Fig.3a) obeys the standard DGLAP evolution equation. This approximation can be justified: the color singlet two gluon system has, at least at small x , the largest anomalous dimension, and from the initial condition at the proton, there is a strong damping which suppresses large momentum transfer across the ladder. Nevertheless, it is an approximation, and there are corrections to it.

In the following we will consider a special set of corrections which we name 'recombinations'. Counting powers of the strong coupling and powers of large logarithms, this is the first correction to the double DGLAP approximation. A pair of such recombinations is illustrated in Fig.3b: starting from the lower proton we have, initially, two separate ladders, formed by gluons '1' and '4' and by gluons '2' and '3'. After a few steps, there is a recombinations of gluons: gluon '1' goes with gluon '3', and gluon '2' with gluon '4'. The first rungs after this rearrangement define the 'recombination vertex'. It is important to note that, in the double logarithmic approximation (leading power in $\ln 1/x$ and $\ln k_{\perp}^2$), this recombination is of the same order as the two independent ladders in Fig.3a, i.e. the recombination does not lose any logarithm. There is, however, a color suppression factor of the form

$$\frac{1}{N^2 - 1} \tag{4}$$

In order to become a non-negligible effect, this recombination requires a subtle interplay of momentum and rapidity dependence.

In the following we will give a brief sketch of the argument.

For the further analysis it is important to keep in mind that there are three transverse loop momenta (in Fig. 3c denoted by \mathbf{l}' , \mathbf{q} , and \mathbf{l}). Beginning with the analysis of transverse momentum integrals, one looks for configurations where transverse momenta are strongly ordered, both above and below the two production vertices. Smallest momenta are near the proton, largest near the production vertices. A straightforward analysis leads to the observation that the dependence on the loop momentum \mathbf{q} resides near the two recombination vertices above

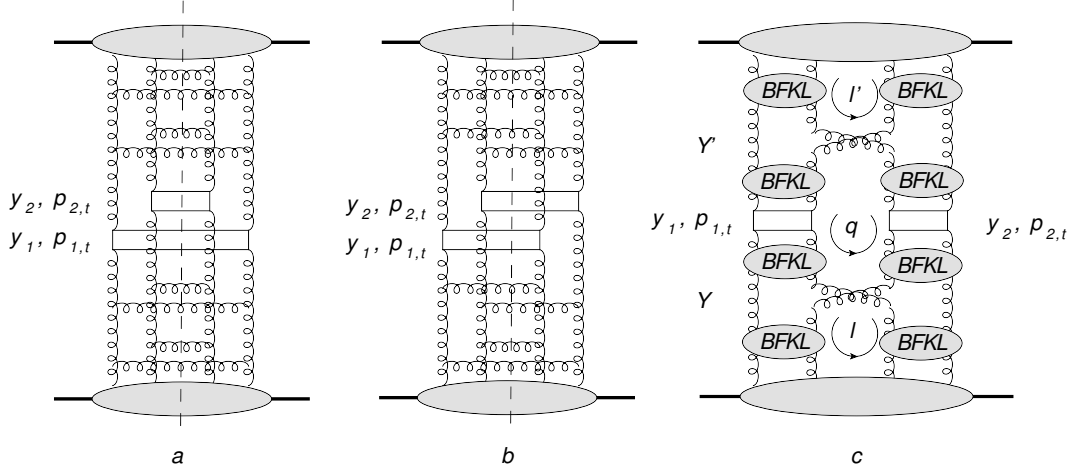


Figure 3: (a) double DGLAP evolution, (b) two recombinations, (c) and a schematic redrawing of the recombination in (b): rungs in (b) are replaced by BFKL amplitudes.

and below the production vertices, and its integral diverges in the infrared region:

$$\int \frac{d^2 q}{(q^2)^2}. \quad (5)$$

As a result, the dominant values are small, the transverse logarithms of the ladders between the recombination vertices and the protons are destroyed, and the recombination vertices become parts of the nonperturbative protons. The situation changes if we allow for small values of x and include into our analysis the rapidity dependence of the ladders. For this it is convenient to replace the rungs in Fig.3b by BFKL amplitudes, as shown in Fig.3c. The main observation is that, once rapidity intervals may become large, sizable anomalous dimensions will affect the momentum integrals, in particular the integration over q . The analysis starts from the expression of Fig.3c:

$$\begin{aligned} \frac{d\sigma}{dY_1 dY_2 d^2 p_1 d^2 p_2} &\sim \frac{1}{R_c^2} \frac{1}{R_c^2} \frac{1}{(p_1^2)^2} \frac{1}{(p_2^2)^2} \int \frac{d\mu'}{2\pi i} \int \frac{d\mu}{2\pi i} \int \frac{d\mu'_1}{2\pi i} \int \frac{d\mu_1}{2\pi i} \int \frac{d\mu'_2}{2\pi i} \int \frac{d\mu_2}{2\pi i} \\ &\int dY \int dY' \int \frac{d^2 q}{q^4} \left[\left(\frac{q^2}{Q_0^2} \right)^{\mu'} e^{(Y_{tot}-Y')\chi(\mu')} \right]^2 \\ &\left[\left(\frac{p_1^2}{q^2} \right)^{\mu'_1} e^{(Y'-Y_1)\chi(\mu'_1)} \right] \left[\left(\frac{p_1^2}{q^2} \right)^{\mu_1} e^{(Y_1-Y)\chi(\mu_1)} \right] \left[\left(\frac{p_2^2}{q^2} \right)^{\mu'_2} e^{(Y'-Y_2)\chi(\mu'_2)} \right] \left[\left(\frac{p_2^2}{q^2} \right)^{\mu_2} e^{(Y_2-Y)\chi(\mu_2)} \right] \\ &\cdot \left[\left(\frac{q^2}{Q_0^2} \right)^{\mu} e^{Y\chi(\mu)} \right]^2. \end{aligned} \quad (6)$$

Here Y_{tot} denotes the total rapidity, and Y' and Y are the rapidities of the recombination vertices above and below the production vertices, resp.. For an analysis of this formula one

searches for saddle points of the integrations. Details are described in [1] and in this contribution we only discuss a few results.

An interesting possibility is to put the recombination vertices, in rapidity, as close as possible to the high E_T dijet production matrix elements. In this case there is no BFKL or DGLAP evolution in the intervals between the produced pairs of jets and the recombination vertices. That is, in the centre of Fig.3, we simply delete the four 'BFKL blobs' nearest to the produced jet pairs. Correspondingly, in (6) we eliminate the third line, together with the integrations over $\mu_1, \mu_2, \mu'_1, \mu'_2$. The rapidities Y, Y' are close to Y_i , and the q^2 integral takes the form

$$\int \frac{d \ln q^2}{q^2} q^{4(\mu_s + \mu'_s)}, \quad (7)$$

where the saddle point values, μ_s and μ'_s , follow from the conditions:

$$0 = \chi'(\mu_s)Y + \ln \frac{q^2}{Q_0^2} \quad (8)$$

and

$$0 = \chi'(\mu'_s)(Y_{tot} - Y') + \ln \frac{q^2}{Q_0^2}. \quad (9)$$

Their approximate values are:

$$\mu_s \approx \frac{1}{2} - \frac{1}{\chi''(\frac{1}{2})} \frac{\ln \frac{q^2}{Q_0^2}}{Y}, \quad (10)$$

i.e. the integral over q^2 receives its main contribution from q^2 close to $\min\{p_1^2, p_2^2\}$.

Let us consider also a more realistic situation with $Y_1 = Y_2$ but $p_2 < p_1$. Recall that the true argument of the BFKL amplitude is not rapidity but the momentum fraction x , that is actually we have to write $\ln(1/x_i)$ instead of Y_i . When $p_2 \ll p_1$ for the same rapidities $Y_1 = Y_2$ we find, in the right ladder, the momentum fraction $x_2 \sim 2p_2/\sqrt{s} \ll x_1 \sim 2p_1/\sqrt{s}$. In other words, in this configuration we may put, in Fig.3c, the recombination vertex just into the cell nearest to the left dijet. But then there will be a large $\ln x$ (and may be $\ln q^2$) interval for the evolution of the right ladders (between the dijets on the rhs and the two recombination vertices). In other words in Fig.3c. we delete only the two 'BFKL blobs' on the lhs below and above the dijet production. Assuming that, in (6), the total rapidity interval Y_{tot} is very large, we may perform first the rapidity integral

$$\int dY \exp[-Y(\chi(\mu_2) - 2\chi(\mu))] = \frac{1}{\chi(\mu_2) - 2\chi(\mu)} \quad (11)$$

where for the BFKL blobs on the lhs we have set $\chi(\mu_1) = 0$, and for μ we put its asymptotic value $\mu = 1/2$. Now we close the contour of the μ_2 integration around the pole $\chi(\mu_2) - 2\chi(\mu) = 0$: this leads to $\mu_2 \simeq 0.18$. The same result is obtained for μ'_2 . Finally, the q^2 integral takes the form

$$\int^{p_2^2} d \ln q^2 q^{2(1-\mu_2-\mu'_2)}, \quad (12)$$

and the major contribution comes from the domain close to upper limit $q^2 \sim p_2^2$.

A closer look reveals still another detail. In the region of interest, for example in a 14 TeV pp -collision at the LHC, we observe in the central region the dijet with $p_1 \sim 20\text{GeV}$, corresponding to $x \sim 2p_1/\sqrt{s} \sim 0.003$. For such x -values, the anomalous dimension observed at HERA is not so large. For $x < 0.01$ the behaviour of the structure function $F_2(x, q^2)$ can be parametrized as

$$F_2 = c(q^2)x^{-\lambda} \quad (13)$$

with $c(q^2) \simeq \text{const}$ and $\lambda = (0.048 \pm 0.004) \cdot \ln Q^2/\Lambda^2$ [16]. This means that the effective anomalous dimension $\mu_{eff} = \lambda \ln(1/x) \sim 0.28$ for $x = 3 \cdot 10^{-3}$. This value is still large enough to provide the convergence of the q^2 integral (7) in the large q^2 domain for the case considered above where both recombination vertices are just near the dijet production cell. However it is not evident that the parametrization (13) reflects the behaviour of a *single* ladder. At not large q^2 the experimentally measured F_2 already includes some absorptive effects which reduce the growth of F_2 with x decreasing and thus leads to a lower value of λ in comparison with a single ladder contribution. In other words the true value of μ_{eff} which corresponds to a single ladder may be even larger, pushing the characteristic values of q^2 closer to the (lower) hard scale p_2^2 .

4 Generalizations

So far we have discussed the effect of two recombinations inside a two-chain contribution: one recombination on each side of the produced jet pairs. Let us first comment on the case where we have no second recombination vertex above the jet pairs: as far as only one recombination vertex is concerned, the integration over \mathbf{q} is logarithmic. However, \mathbf{q} runs also through both upper ladders and defines the low momentum scale Q_0^2 where the evolution starts: a large value of \mathbf{q} therefore kills the evolution in the upper ladders, whereas a low value prevents the evolution in the lower ladders. Therefore, a single recombination vertex is suppressed.

Next a comment on the color suppression factor (4). This suppression applies to the case when, as illustrated in Fig.2, there is evolution above and below the recombination vertex. As we have discussed before, in a preferred situation we have little or no evolution between the recombination vertices and the dijet production vertices. In this case there is no need to reconnect, between the two recombination vertices, the four t-channel gluon lines to color singlet pairs. As result, the color suppression becomes much weaker.

Next we mention another important possibility. Besides the recombination illustrated in Fig.3 there exists another configuration to which our discussion applies. We show this in Fig.4. Below the lower (or above the upper) recombination vertex, color singlet gluon ladders to the right and to the left of the cutting line allow for final states with rapidity gaps. Such configurations are absent in the double DGLAP approximation. Applying our previous discussion, we conclude that the momentum scale at the upper end of the lower rapidity gap, q^2 , will be above Q_0^2 but not too close to the jet momenta $p_1^2 = p_2^2$: this allows for 'semihard' diffraction and is in qualitative agreement with inclusive diffraction seen at HERA.

Finally we consider the case of more than two chains, say three chains with three produced pairs of jets. In this case a pair of two recombination vertices can be attributed to any pair of chains, i.e. we have three possibilities. Similarly, for n chains we have $\frac{n(n-1)}{2}$ possibilities: these counting factors can easily overcome the color suppression factor in (4). As an example, for $n = 4$, the overall counting factor is already $3/4$, and it exceeds unity for $n \geq 5$. This counting

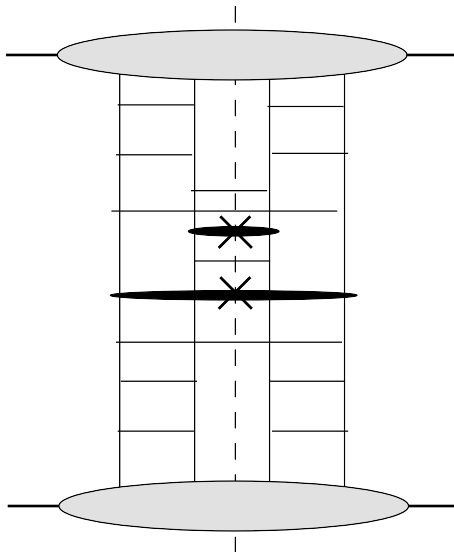


Figure 4: A recombination of two ladders which allows for diffractive states

argument is particularly important for event generators where the number of participating chains may become quite sizable.

The recombination considered in this contribution is very closely related to a recent explanation [13, 14] of the ridge effect observed in pp collisions at the LHC [15].

5 Conclusions

We view this analysis only as first step of investigating the evolution of double parton densities beyond the factorizing approximation. Clearly our analysis has to be made quantitative. Also, it is necessary to go beyond the double leading-log approximation. Work along these lines is in progress.

References

- [1] J. Bartels and M. G. Ryskin, arXiv:1105.1638 [hep-ph].
- [2] D. Treleani, Phys. Rev. D **76** (2007) 076006 [arXiv:0708.2603 [hep-ph]].
- [3] E. L. Berger, C. B. Jackson and G. Shaughnessy, Phys. Rev. D **81** (2010) 014014 [arXiv:0911.5348 [hep-ph]].
- [4] J. R. Gaunt and W. J. Stirling, JHEP **1003** (2010) 005 [arXiv:0910.4347 [hep-ph]].
- [5] J. R. Gaunt, C. H. Kom, A. Kulesza and W. J. Stirling, Eur. Phys. J. C **69** (2010) 53 [arXiv:1003.3953 [hep-ph]].
- [6] M. Strikman and W. Vogelsang, Phys. Rev. D **83** (2011) 034029 [arXiv:1009.6123 [hep-ph]].
- [7] M. Diehl and A. Schafer, Phys. Lett. B **698** (2011) 389 [arXiv:1102.3081 [hep-ph]].
- [8] C. Flensburg, G. Gustafson, L. Lonnblad and A. Ster, arXiv:1103.4320 [hep-ph].
- [9] M. G. Ryskin and A. M. Snigirev, arXiv:1103.3495 [hep-ph].

- [10] A. P. Bukhvostov, G. V. Frolov, L. N. Lipatov and E. A. Kuraev, Nucl. Phys. B **258** (1985) 601.
- [11] V. A. Abramovsky, V. N. Gribov and O. V. Kancheli, Yad. Fiz. **18** (1973) 595 [Sov. J. Nucl. Phys. **18**; M. Salvadore, J. Bartels and G. P. Vacca, arXiv:0709.3062 [hep-ph].
- [12] J. Bartels, Nucl. Phys. **B175** (1980) 365.
J. Kwiecinski, M. Praszalowicz, Phys. Lett. **B94** (1980) 413.
T. Jaroszewicz, Acta Phys. Polon. **B11** (1980) 965.
- [13] A. Dumitru, K. Dusling, F. Gelis, J. Jalilian-Marian, T. Lappi, R. Venugopalan, Phys. Lett. **B697** (2011) 21-25. [arXiv:1009.5295 [hep-ph]].
- [14] K. Dusling and R. Venugopalan, arXiv:1201.2658 [hep-ph].
- [15] V. Khachatryan *et al.* [CMS Collaboration], JHEP **1009** (2010) 091. [arXiv:1009.4122 [hep-ex]].
- [16] C. Adloff *et al.* [H1 collaboration], Phys. Lett. **B520** (2001) 183.

Low- x evolution of parton densities

Alexey Yu. Illarionov¹, Anatoly V. Kotikov^{2*}

¹Integrated Systems Laboratory, ETH, CH-8092 Zürich, Switzerland

²Bogolubov Laboratory of Theoretical Physics, JINR, 141980 Dubna, Russia

DOI: <http://dx.doi.org/10.3204/DESY-PROC-2012-03/21>

It is shown that a Bessel-like behaviour of the structure function F_2 at small x , obtained for a flat initial condition in the DGLAP evolution equations, leads to good agreement with the deep inelastic scattering experimental data from HERA.

1 Introduction

The fairly reasonable agreement between HERA data [1]-[4] and the next-to-leading-order (NLO) approximation of perturbative QCD has been observed for $Q^2 \geq 2 \text{ GeV}^2$ (see reviews in [5] and references therein) and, thus, perturbative QCD can describe the evolution of F_2 and its derivatives down to very low Q^2 values.

The standard program to study the x behaviour of quarks and gluons is carried out comparing the experimental data with the numerical solution of the DGLAP equations [6] by fitting the QCD energy scale Λ and the parameters of the x -profile of partons at some initial Q_0^2 [7, 8]. However, to investigate exclusively the small- x region, there is the alternative of doing the simpler analysis by using some of the existing analytical solutions of DGLAP in the small- x limit [9]-[12]. It was pointed out in [9] that the HERA small- x data can be well interpreted in terms of the so-called doubled asymptotic scaling (DAS) phenomenon related to the asymptotic behaviour of the DGLAP evolution discovered many years ago [13].

The study of [9] was extended in [10]-[12] to include the finite parts of anomalous dimensions (ADs) of Wilson operators and Wilson coefficients¹. This has led to predictions [11, 12] of the small- x asymptotic form of parton distribution functions (PDFs) in the framework of the DGLAP dynamics, which were obtained starting at some Q_0^2 with the flat function

$$f_a(Q_0^2) = A_a \quad (\text{hereafter } a = q, g), \quad (1)$$

where f_a are PDFs multiplied by x and A_a are unknown parameters to be determined from the data.

We refer to the approach of [10]-[12] as *generalized* DAS approximation. In this approach the flat initial conditions, Eq. (1), determine the basic role of the AD singular parts as in the standard DAS case, while the contribution from AD finite parts and from Wilson coefficients can be considered as corrections which are, however, important for better agreement with experimental data.

*Speaker

¹In the standard DAS approximation [13] only the AD singular parts were used.

The use of the flat initial condition, given in Eq. (1), is supported by the actual experimental situation: low- Q^2 data [15, 16, 3] are well described for $Q^2 \leq 0.4 \text{ GeV}^2$ by Regge theory with Pomeron intercept $\alpha_P(0) \equiv \lambda_P + 1 = 1.08$, close to the adopted ($\alpha_P(0) = 1$) one. The small rise of HERA data [1, 4, 16, 17] at low Q^2 can be explained, for example, by contributions of higher twist operators (see [12]).

The purpose of this paper is to demonstrate a good agreement [14] between the predictions of the generalized DAS approach [11] and the HERA experimental data [1] (see Fig. 1 below) for the structure function (SF) F_2 . We also compare the result of the slope $\partial \ln F_2 / \partial \ln(1/x)$ calculation with the H1 and ZEUS data [2, 3]. Looking at the H1 data [2] points shown in Fig. 2 one can conclude that $\lambda(Q^2)$ is independent on x within the experimental uncertainties for fixed Q^2 in the range $x < 0.01$. The rise of $\lambda(Q^2)$ linearly with $\ln Q^2$ could be traced in strong non-perturbative way (see [18] and references therein), i.e., $\lambda(Q^2) \sim 1/\alpha_s(Q^2)$. The analysis [19], however, demonstrated that this rise can be explained naturally in the framework of perturbative QCD.

The ZEUS and H1 Collaborations have also presented [3] the preliminary data for $\lambda(Q^2)$ at quite low values of Q^2 . The ZEUS value for $\lambda(Q^2)$ is consistent with a constant ~ 0.1 at $Q^2 < 0.6 \text{ GeV}^2$, as it is expected under the assumption of single soft Pomeron exchange within the framework of Regge phenomenology. It was important to extend the analysis of [19] to low Q^2 range with a help of well-known infrared modifications of the strong coupling constant. We used the “frozen” and analytic versions (see [14]).

2 Generalized DAS approach

The flat initial condition (1) corresponds to the case when PDFs tend to some constant value at $x \rightarrow 0$ and at some initial value Q_0^2 . The main ingredients of the results [11, 12], are:

- Both the gluon and quark singlet densities² are presented in terms of two components (“+” and “-”) which are obtained from the analytic Q^2 -dependent expressions of the corresponding (“+” and “-”) PDF moments.
- The twist-two part of the “-” component is constant at small x at any values of Q^2 , whereas the one of the “+” component grows at $Q^2 \geq Q_0^2$ as

$$\sim e^\sigma, \quad \sigma = 2\sqrt{\left[\hat{d}_+ s - \left(\hat{D}_+ + \hat{d}_+ \frac{\beta_1}{\beta_0}\right) p\right] \ln\left(\frac{1}{x}\right)}, \quad \rho = \frac{\sigma}{2 \ln(1/x)}, \quad (2)$$

where σ and ρ are the generalized Ball-Forte variables,

$$s = \ln\left(\frac{a_s(Q_0^2)}{a_s(Q^2)}\right), \quad p = a_s(Q_0^2) - a_s(Q^2), \quad \hat{d}_+ = \frac{12}{\beta_0}, \quad \hat{D}_+ = \frac{412}{27\beta_0}. \quad (3)$$

Hereafter we use the notation $a_s = \alpha_s/(4\pi)$. The first two coefficients of the QCD β -function in the $\overline{\text{MS}}$ -scheme are $\beta_0 = 11 - (2/3)f$ and $\beta_1 = 102 - (114/9)f$ with f being the number of active quark flavors.

Note here that the perturbative coupling constant $a_s(Q^2)$ is different at the leading-order (LO) and NLO approximations. Hereafter we consider for simplicity only the LO approximation³, where the variables σ and ρ are given by Eq. (2) when $p = 0$.

²The contribution of valence quarks is negligible at low x .

³The NLO results may be found in [11].

2.1 Parton distributions and the structure function F_2

The SF F_2 and PDFs have the following form

$$F_2(x, Q^2) = e f_q(x, Q^2), \quad f_a(x, Q^2) = f_a^+(x, Q^2) + f_a^-(x, Q^2), \quad (a = q, g) \quad (4)$$

where $e = (\sum_1^f e_i^2)/f$ is the average charge square.

The small- x asymptotic results for PDFs f_a^\pm are

$$\begin{aligned} f_g^+(x, Q^2) &= \left(A_g + \frac{4}{9} A_q \right) \tilde{I}_0(\sigma) e^{-\bar{d}_+(1)s} + O(\rho), & f_q^+(x, Q^2) &= \frac{f}{9} \frac{\rho \tilde{I}_1(\sigma)}{\tilde{I}_0(\sigma)} + O(\rho), \\ f_g^-(x, Q^2) &= -\frac{4}{9} A_q e^{-d_-(1)s} + O(x), & f_q^-(x, Q^2) &= A_q e^{-d_-(1)s} + O(x), \end{aligned} \quad (5)$$

where $d_-(1) = 16f/(27\beta_0)$ and $\bar{d}_+(1) = 1 + 20f/(27\beta_0)$ is the regular part of AD $d_+(n)$ in the limit $n \rightarrow 1^4$. Here n is the variable in Mellin space. The functions \tilde{I}_ν ($\nu = 0, 1$) are related to the modified Bessel function I_ν and to the Bessel function J_ν by:

$$\tilde{I}_\nu(\sigma) = \begin{cases} I_\nu(\sigma), & \text{if } s \geq 0 \\ i^{-\nu} J_\nu(i\sigma), & i^2 = -1, \text{ if } s \leq 0 \end{cases} \quad (6)$$

2.2 Effective slopes

As it has been shown in [11], the behaviour of PDFs and F_2 given in the Bessel-like form by generalized DAS approach can mimic a power law shape over a limited region of x and Q^2

$$f_a(x, Q^2) \sim x^{-\lambda_a^{\text{eff}}(x, Q^2)} \quad \text{and} \quad F_2(x, Q^2) \sim x^{-\lambda_{F_2}^{\text{eff}}(x, Q^2)}.$$

The effective slopes $\lambda_a^{\text{eff}}(x, Q^2)$ and $\lambda_{F_2}^{\text{eff}}(x, Q^2)$ have the form:

$$\begin{aligned} \lambda_{F_2}^{\text{eff}}(x, Q^2) &= \lambda_g^{\text{eff}}(x, Q^2) = \frac{f_g^+(x, Q^2)}{f_g(x, Q^2)} \rho \frac{\tilde{I}_1(\sigma)}{\tilde{I}_0(\sigma)} \approx \rho - \frac{1}{4 \ln(1/x)}, \\ \lambda_q^{\text{eff}}(x, Q^2) &= \frac{f_q^+(x, Q^2)}{f_q(x, Q^2)} \rho \frac{\tilde{I}_2(\sigma)}{\tilde{I}_1(\sigma)} \approx \rho - \frac{3}{4 \ln(1/x)}, \end{aligned} \quad (7)$$

where the symbol \approx marks the approximation obtained in the expansion of the modified Bessel functions, when the “-” component is negligible. These approximations are accurate only at very large σ values (i.e. at very large Q^2 and/or very small x).

3 Comparison with experimental data

Using the results of previous section we have analyzed HERA data for F_2 [1] and the slope $\partial \ln F_2 / \partial \ln(1/x)$ [2, 3] at small x from the H1 and ZEUS Collaborations. In order to keep the analysis as simple as possible, we fix $f = 4$ and $\alpha_s(M_Z^2) = 0.1166$ (i.e., $\Lambda^{(4)} = 284$ MeV) in agreement with the recent ZEUS results in [1].

⁴We denote the singular and regular parts of a given quantity $k(n)$ in the limit $n \rightarrow 1$ by $\hat{k}(n)$ and $\bar{k}(n)$, respectively.

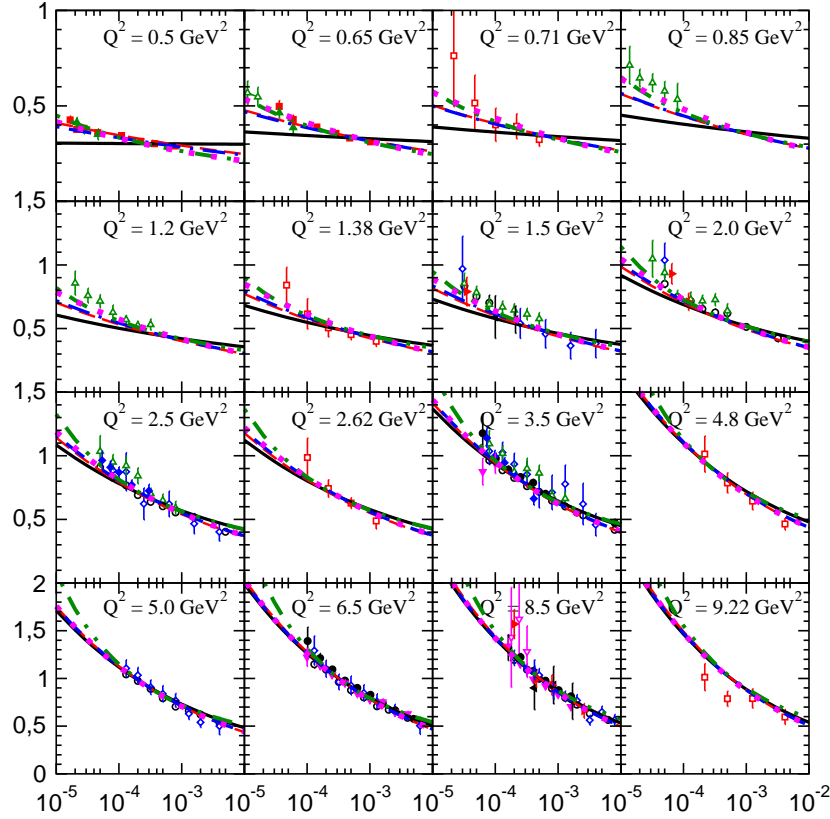


Figure 1: x dependence of $F_2(x, Q^2)$ in bins of Q^2 . The experimental data from H1 (open points) and ZEUS (solid points) [1] are compared with the NLO fits for $Q^2 \geq 0.5 \text{ GeV}^2$ implemented with the canonical (solid lines), frozen (dot-dashed lines), and analytic (dashed lines) versions of the strong-coupling constant.

As it is possible to see in Figs. 1 and 2, the twist-two approximation is reasonable at $Q^2 \geq 2 \div 4 \text{ GeV}^2$. At smaller Q^2 , some modification of the approximation should be considered. In Ref. [12] we have added the higher twist corrections. For renormalon model of higher twists, we have found a good agreement with experimental data at essentially lower Q^2 values: $Q^2 \geq 0.5 \text{ GeV}^2$ (see Figs. 4 and 5 in [12]).

In Ref. [14], to improve the agreement at small Q^2 values, we modified the QCD coupling constant. We consider two modifications.

In one case, which is more phenomenological, we introduce freezing of the coupling constant by changing its argument $Q^2 \rightarrow Q^2 + M_\rho^2$, where M_ρ is the ρ -meson mass (see [14] and references therein). Thus, in the formulae of the Section 2 we should do the following replacement:

$$a_s(Q^2) \rightarrow a_{\text{fr}}(Q^2) \equiv a_s(Q^2 + M_\rho^2) \quad (8)$$

The second possibility incorporates the Shirkov–Solovtsov idea [20] about analyticity of the coupling constant that leads to the additional its power dependence. Then, in the formulae of

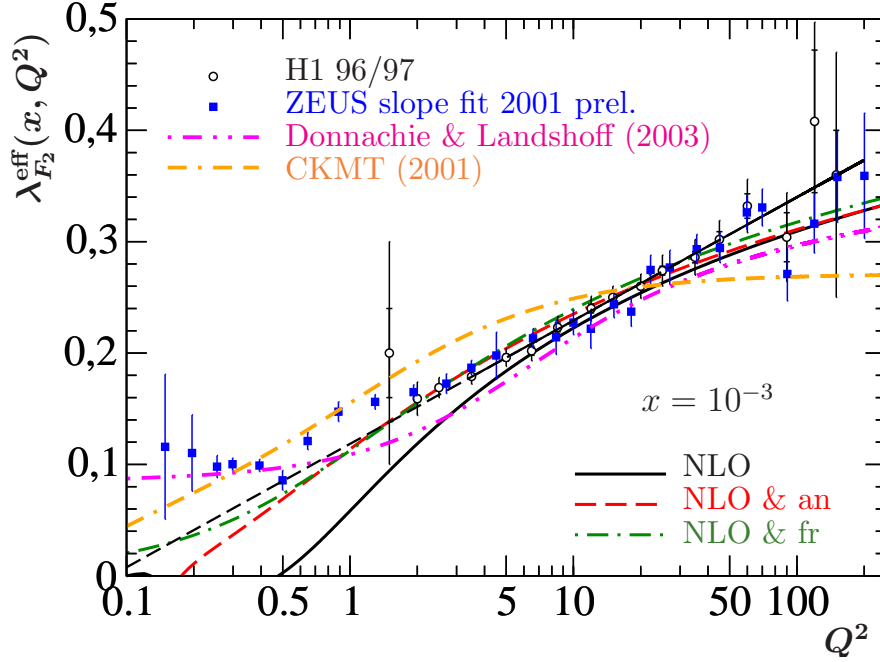


Figure 2: As in Fig. 1 but for the Q^2 dependence of $\lambda_{F_2}^{\text{eff}}(x, Q^2)$ for an average small- x value of $x = 10^{-3}$. The linear rise of $\lambda_{F_2}^{\text{eff}}(x, Q^2)$ with $\ln Q^2$ [2] is indicated by the straight dashed line. For comparison, also the results obtained in the phenomenological models by Kaidalov et al. [22] (dash-dash-dotted line) and by Donnachie and Landshoff [23] (dot-dot-dashed line) are shown.

the previous section the coupling constant $a_s(Q^2)$ should be replaced as follows: ($k = 1$ and 2 at LO and NLO)

$$a_{\text{an}}(Q^2) = a_s(Q^2) - \frac{1}{k\beta_0} \frac{\Lambda^2}{Q^2 - \Lambda^2} + \dots, \quad (9)$$

where the symbol \dots stands for terms which are zero and negligible at $Q \geq 1$ GeV [20] at LO and NLO, respectively.

Figure 2 shows the experimental data for $\lambda_{F_2}^{\text{eff}}(x, Q^2)$ at $x \sim 10^{-3}$, which represents an average of the x -values of HERA experimental data. The top dashed line represents the aforementioned linear rise of $\lambda(Q^2)$ with $\ln(Q^2)$. The Figs. 1 and 2 demonstrate that the theoretical description of the small- Q^2 ZEUS data for $\lambda_{F_2}^{\text{eff}}(x, Q^2)$ by NLO QCD is significantly improved by implementing the “frozen” and analytic coupling constants $\alpha_{\text{fr}}(Q^2)$ and $\alpha_{\text{an}}(Q^2)$, respectively, which in turn lead to very close results (see also [21]).

Indeed, the fits for $F_2(x, Q^2)$ in [12] yielded $Q_0^2 \approx 0.5\text{--}0.8$ GeV 2 . So, initially we had $\lambda_{F_2}^{\text{eff}}(x, Q_0^2) = 0$, as suggested by Eq. (1). The replacements of Eqs. (8) and (9) modify the value of $\lambda_{F_2}^{\text{eff}}(x, Q_0^2)$. For the “frozen” and analytic coupling constants $\alpha_{\text{fr}}(Q^2)$ and $\alpha_{\text{an}}(Q^2)$, the value of $\lambda_{F_2}^{\text{eff}}(x, Q_0^2)$ is nonzero and the slopes are quite close to the experimental data at $Q^2 \approx 0.5$ GeV 2 . Nevertheless, for $Q^2 \leq 0.5$ GeV 2 , there is still some disagreement with the data, which needs additional investigation.

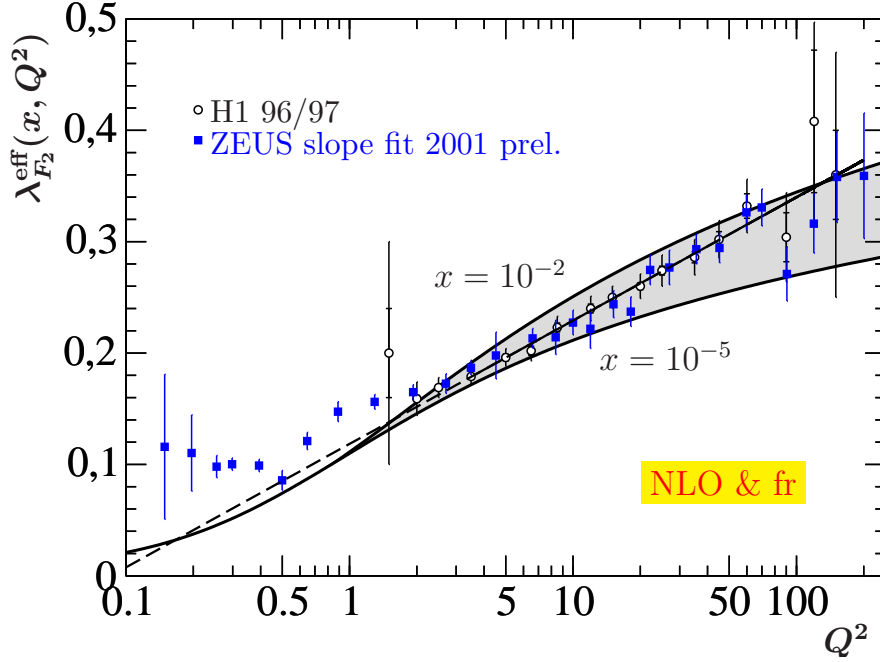


Figure 3: The values of effective slope $\lambda_{F_2}^{\text{eff}}$ as a function of Q^2 . The experimental points are same as in Fig. 2. The dashed line represents the fit from [2]. The solid curves represent the NLO fits with “frozen” coupling constant at $x = 10^{-2}$ and $x = 10^{-5}$.

For comparison, we display in Fig. 2 also the results obtained by Kaidalov et al. [22] and by Donnachie and Landshoff [23] adopting phenomenological models based on Regge theory. While they yield an improved description of the experimental data for $Q^2 \leq 0.4 \text{ GeV}^2$, the agreement generally worsens in the range $2 \text{ GeV}^2 \leq Q^2 \leq 8 \text{ GeV}^2$.

The results of fits in [12, 14] have an important property: they are very similar in LO and NLO approximations of perturbation theory. The similarity is related to the fact that the small- x asymptotics of the NLO corrections are usually large and negative (see, for example, α_s -corrections [24] to BFKL approach [25]⁵). Then, the LO form $\sim \alpha_s(Q^2)$ for some observable and the NLO one $\sim \alpha_s(Q^2)(1 - K\alpha_s(Q^2))$ with a large value of K , are similar because $\Lambda \gg \Lambda_{\text{LO}}$ ⁶ and, thus, $\alpha_s(Q^2)$ at LO is considerably smaller than $\alpha_s(Q^2)$ at NLO for HERA Q^2 values.

In other words, performing some resummation procedure (such as Grunberg’s effective-charge method [26]), one can see that the NLO form may be represented as $\sim \alpha_s(Q_{\text{eff}}^2)$, where $Q_{\text{eff}}^2 \gg Q^2$. Indeed, from different studies [27], it is well known that at small- x values the effective argument of the coupling constant is higher than Q^2 .

In the generalized DAS approach the small effect of the NLO corrections can be explained by separated contributions of the singular and regular AD parts. Indeed, the singular parts modify the argument of the Bessel functions (see Eq.(2)) and the regular parts contribute to

⁵It seems that it is a property of any processes in which gluons, but not quarks, play a basic role.

⁶The equality of $\alpha_s(M_Z^2)$ at LO and NLO approximations, where M_Z is the Z -boson mass, relates Λ and Λ_{LO} : $\Lambda^{(4)} = 284 \text{ MeV}$ (as in ZEUS paper on [1]) corresponds to $\Lambda_{\text{LO}} = 112 \text{ MeV}$ (see [12]).

the front of Bessel functions [11].

Figure 3 shows the x -dependence of the slope $\lambda_{F_2}^{\text{eff}}(x, Q^2)$. One observes good agreement between the experimental data and the generalized DAS approach for a broad range of small- x values. The absence of a variation with x of $\lambda_{F_2}^{\text{eff}}(x, Q^2)$ at small Q^2 values is related to the small values of the variable ρ there.

From Figs. 2 and 6 in [12], one can see that HERA experimental data exists at $x \sim 10^{-4} \div 10^{-5}$ for $Q^2 = 4 \text{ GeV}^2$ and at $x \sim 10^{-2}$ for $Q^2 = 100 \text{ GeV}^2$. Indeed, the correlations between x and Q^2 in the form $x_{\text{eff}} = a \times 10^{-4} \times Q^2$ with $a = 0.1$ and 1 lead to a modification of the Q^2 evolution which starts to resemble $\ln Q^2$, rather than $\ln \ln Q^2$ as is standard [19].

4 Conclusions

We have shown the Q^2 -dependence of the SF F_2 and the slope $\lambda_{F_2}^{\text{eff}} = \partial \ln F_2 / \partial \ln(1/x)$ at small- x values in the framework of perturbative QCD. Our twist-two results are in very good agreement with the precise HERA data at $Q^2 \geq 2 \text{ GeV}^2$, where the perturbative theory is applicable. The application of the “frozen” and analytic coupling constants $\alpha_{\text{fr}}(Q^2)$ and $\alpha_{\text{an}}(Q^2)$ improves the agreement for smaller Q^2 values, down to $Q^2 \geq 0.5 \text{ GeV}^2$.

As a next step of investigations, we plan to fit the H1&ZEUS data [4] and to extend the generalized DAS approach to evaluate the double PDFs which are very popular now (see [28] and references therein). Also we plan to use our approach to analyze the cross sections of processes studied at LHC by analogy with our investigations [29] of the total cross section of ultrahigh-energy deep-inelastic neutrino-nucleon scattering.

A.V.K. thanks the Organizing Committee of the 3rd International Workshop on Multiple Partonic Interactions at the LHC for invitation and support. This work was supported in part by RFBR grant 11-02-01454-a.

References

- [1] C. Adloff *et al.*, H1 Coll., Nucl.Phys. B **497** (1997) 3; Eur.Phys.J. C **21** (2001) 33; S. Chekanov *et al.*, ZEUS Coll., Eur.Phys.J. C **21** (2001) 443.
- [2] C. Adloff *et al.*, H1 Coll., Phys.Lett. B **520** (2001) 183.
- [3] T. Lastovicka, H1 Coll., Acta Phys.Polon. B **33** (2002) 2835; B. Surrow, ZEUS Coll., arXiv:0201025 [hep-ph].
- [4] F.D. Aaron *et al.*, H1 and ZEUS Coll., JHEP **1001** (2010) 109.
- [5] A.M. Cooper-Sarkar *et al.*, Int.J.Mod.Phys. A **13** (1998) 3385; A.V. Kotikov, Phys.Part.Nucl. **38** (2007) 1; [Erratum-ibid. **38** (2007) 828].
- [6] V.N. Gribov and L.N. Lipatov, Sov.J.Nucl.Phys. **15** (1972) 438, 675; L.N. Lipatov, Sov. J. Nucl. Phys. **20** (1975) 94; G. Altarelli and G. Parisi, Nucl.Phys. B **126** (1977) 298; Yu.L. Dokshitzer, Sov. Phys. JETP **46** (1977) 641.
- [7] W.K. Tung *et al.*, STEQ Coll., JHEP **0702** (2007) 053; A.D. Martin *et al.*, Phys.Lett. B **652** (2007) 292; M. Gluck *et al.*, Phys.Rev. D **77** (2008) 074002; S. Alekhin *et al.*, Phys.Rev. D **81** (2010) 014032.
- [8] A.V. Kotikov *et al.*, Z.Phys. C **58** (1993) 465; G. Parente *et al.*, Phys.Lett. B **333** (1994) 190; A.L. Kataev *et al.*, Phys.Lett. B **388** (1996) 179; Phys.Lett. B **417** (1998) 374; Nucl.Phys. B **573** (2000) 405; A.V. Kotikov and V.G. Krivokhijine, Phys.At.Nucl. **68** (2005) 1873; B.G. Shaikhmatdenov *et al.*, Phys.Rev. D **81** (2010) 034008.
- [9] R.D. Ball and S. Forte, Phys.Lett. B **336** (1994) 77.
- [10] L. Mankiewicz *et al.*, Phys.Lett. B **393** (1997) 175.

- [11] A. V. Kotikov and G. Parente, Nucl.Phys. B **549** (1999) 242; Nucl.Phys.(Proc.Suppl.) A **99** (2001) 196.
- [12] A. Yu. Illarionov *et al.*, Phys.Part.Nucl. **39** (2008) 307; Nucl.Phys.(Proc.Suppl.) **146** (2005) 234.
- [13] A. De Rújula *et al.*, Phys.Rev. D **10** (1974) 1649.
- [14] G. Cvetič *et al.*, Phys.Lett. B **679** (2009) 350.
- [15] M. Arneodo *et al.*, NM Coll., Phys.Lett. B **364** (1995) 107; Nucl.Phys. B483 (1997) 3; M.R. Adams *et al.*, E665 Coll., Phys.Rev. D **54** (1996) 3006; A. Donnachie and P. V. Landshoff, Nucl.Phys. B **244** (1984) 322; B **267** (1986) 690; Z.Phys. C61 (1994) 139.
- [16] J. Breitweg *et al.*, ZEUS Coll., Phys.Lett. B **407** (1997) 432.
- [17] J. Breitweg *et al.*, ZEUS Coll., Phys.Lett. B **487** (2000) 53; Eur.Phys.J. C **21** (2001) 443.
- [18] F. Schrempp, hep-ph/0507160.
- [19] A.V. Kotikov and G. Parente, J. Exp. Theor. Phys. **97** (2003) 859.
- [20] D.V. Shirkov and I.L. Solovtsov, Phys.Rev.Lett **79** (1997) 1209; Theor.Math.Phys. **120** (1999) 1220.
- [21] A.V. Kotikov *et al.*, J. Exp. Theor. Phys. **101** (2005) 811; (arXiv:1008.0545 [hep-ph]).
- [22] A.B. Kaidalov *et al.*, Eur.Phys.J. C **20** (2001) 301;
- [23] A. Donnachie and P.V. Landshoff, Acta Phys.Polon. B **34** (2003) 2989.
- [24] V. S. Fadin and L. N. Lipatov, Phys.Lett. B **429** (1998) 127; G. Camici and M. Ciafaloni, Phys.Lett. B **430** (1998) 349; A.V. Kotikov and L.N. Lipatov, Nucl.Phys. B **582** (2000) 19.
- [25] L.N. Lipatov, Sov.J.Nucl.Phys. **23** (1976) 338; V.S. Fadin *et al.*, Phys.Lett. B **60** (1975) 50; E.A. Kuraev *et al.*, Sov. Phys. JETP **44** (1976) 443; **45** (1977) 199; I.I. Balitsky and L.N. Lipatov, Sov.J.Nucl.Phys. **28** (1978) 822; JETP Lett. **30** (1979) 355.
- [26] G. Grunberg, Phys.Rev. D **29** (1984) 2315; Phys.Lett. B **95** (1980) 70.
- [27] Yu.L. Dokshitzer and D.V. Shirkov, Z.Phys. C **67** (1995) 449; A.V. Kotikov, Phys.Lett. B **338** (1994) 349; W.K. Wong, Phys.Rev. D **54** (1996) 1094; S.J. Brodsky *et al.*, JETP. Lett. **70** (1999) 155; M. Ciafaloni *et al.*, Phys.Rev. D **60** (1999) 114036; G. Altarelli *et al.*, Nucl.Phys. B **621** (2002) 359; Bo Andersson *et al.*, Eur.Phys.J. C **25** (2002) 77.
- [28] A.M. Snigirev, Phys.Atom.Nucl. **74** (2011) 158 M.G. Ryskin and A.M. Snigirev, Phys.Rev. D **83** (2011) 114047.
- [29] R. Fiore *et al.*, Phys.Rev. D **73** (2006) 053012; Phys.Rev. D **71** (2005) 033002; Phys.Rev. D **68** (2003) 093010; A. Y. Illarionov *et al.*, Phys.Rev.Lett. **106** (2011) 231802.

Unintegrated gluon distribution and soft pp collisions at LHC

Andrei Grinyuk¹, Hannes Jung^{2,3}, Gennady Lykasov^{1*}, Artem Lipatov⁴, Nikolay Zotov⁴

¹JINR, 141980, Dubna, Moscow region, Russia

²DESY, Notkestraße 85, 22607 Hamburg, Germany

³CERN, 1211 Genève 23, Switzerland

⁴Skobeltsyn Institute of Nuclear Physics, Lomonosov Moscow State University, 119991, Moscow, Russia

DOI: <http://dx.doi.org/10.3204/DESY-PROC-2012-03/25>

We found the parameterization of the unintegrated gluon distribution from the best description of the LHC data on the inclusive spectra of hadrons produced in pp collisions at the mid-rapidity region and small transverse momenta. It is different from the one obtained within perturbative QCD only at low intrinsic transverse momenta k_t . The application of this distribution to analysis of the $e - p$ DIS allows us to get the results which do not contradict the H1 and ZEUS data on the structure functions at low x . So, the connection between the soft processes at LHC and low- x physics at HERA is found.

1 Introduction

As is well known, hard processes involving incoming protons, such as deep-inelastic lepton-proton scattering (DIS), are described using the scale-dependent parton density functions. Usually, these quantities are calculated as a function of the Bjorken variable x and the square of the four-momentum transfer $q^2 = -Q^2$ within the framework of popular collinear QCD factorization based on the DGLAP evolution equations [1]. However, for semi-inclusive processes (such as inclusive jet production in DIS, electroweak boson production [2], etc.) at high energies it is more appropriate to use the parton distributions unintegrated over the transverse momentum k_t in the framework of k_t -factorization QCD approach [3]¹. The k_t -factorization formalism is based on the BFKL [6] or CCFM [7] evolution equations and provides solid theoretical grounds for the effects of initial gluon radiation and intrinsic parton transverse momentum k_t . The theoretical analysis of the unintegrated quark $q(x, k_t)$ distribution (u.q.d.) and gluon $g(x, k_t)$ distribution (u.g.d.) can be found, for example, in [8]- [22]. According to [11], the u.g.d. $g(x, k_t)$ at fixed Q^2 has the very interesting behavior at small $x \leq 0.01$, it increases very fast starting from almost zero values of k_t and decreases smoothly at large k_t . In contrast, the u.q.d. $q(x, k_t)$ is almost constant in the whole region of k_t up to $k_t \sim 100$ GeV/ c and much smaller than $g(x, k_t)$. These distributions were obtained using the so-called KMR formalism within the leading order (LO) and next-to-leading order of QCD (NLO) at large Q^2 from the

*Speaker

¹See, for example, reviews [4, 5] for more information.

known (DGLAP-evolved [1]) parton densities determined from the global data analysis. The unintegrated parton distributions were successfully applied to analyze the DIS data at low x and the number of processes studied at LHC (see, for example, [13]- [21]). However, at small values of Q^2 the nonperturbative effects should be included to evaluate these distributions. The non-perturbative effects can arise from the complex structure of the QCD vacuum. For example, within the instanton approach [12] the very fast increase of the unintegrated gluon distribution function at $0 \leq k_t \leq 0.5 \text{ GeV}/c$ and $Q^2 = 1 \text{ (GeV}/c)^2$ is also shown. These results stimulated us to assume, that the unintegrated gluon distribution in the proton can be included by analyzing also the soft hadron production in pp collisions. In this paper we analyze the inclusive spectra of the hadrons produced in pp collisions at LHC energies in the mid-rapidity region including the possible creation of soft gluons in the proton. We estimate the u.g.d. at low intrinsic transverse momenta $k_t \leq 1.5 - 1.6 \text{ GeV}/c$ and its parameters extracted from the best description of the LHC data at low transverse momenta p_t of the produced hadrons. We also show that our u.g.d. similar to the u.g.d. obtained in [9,10] at large k_t and different from it at low k_t .

2 Inclusive spectra of hadrons in pp collisions

2.1 Unintegrated gluon distributions

As was mentioned above, the unintegrated gluon densities $g(x, k_t^2)$ can be generally described by the BFKL [6] evolution equation, where the leading $\ln(1/x)$ contributions are summed. The conventional integrated gluon distribution $g(x, Q^2)$ can be approximately related to the unintegrated one by [13]

$$g(x, Q^2) \sim g(x, Q_0^2) + \int_{Q_0^2}^{Q^2} dk_t^2 g(x, k_t^2) \quad (1)$$

where Q_0^2 is a starting nonzero value of Q^2 . An appropriate description valid for small and large x is given by the CCFM [7] evolution equation that results in the u.g.d. $g(x, k_t^2, \bar{q}^2)$ as a function of x, k_t^2 and the additional scale \bar{q} (see details in [4,10] and references therein). The another u.g.d. $g(x, k_t^2)$ satisfies the DGLAP-type evolution equation with respect to k_t^2 [2,11].

A simple parameterization of the u.g.d. was obtained, for example, within the color-dipole approach in [8,9] on the assumption of a saturation of the gluon density at low Q^2 which successfully described both inclusive and diffractive $e - p$ scattering. The u.g.d. $xg(x, k_t^2, Q_0^2)$ is given by [9,10]

$$xg(x, k_t, Q_0) = \frac{3\sigma_0}{4\pi^2\alpha_s(Q_0)} R_0^2 k_t^2 \exp(-R_0^2(x)k_t^2) ; R_0 = \frac{1}{Q_0} \left(\frac{x}{x_0}\right)^{\lambda/2}, \quad (2)$$

where $\sigma_0 = 29.12 \text{ mb}$, $\alpha_s = 0.2$, $Q_0 = 1 \text{ GeV}/c$, $\lambda = 0.277$ and $x_0 = 4.1 \cdot 10^{-5}$. The form for $xg(x, k_t, Q_0)$ given by Eq.(2) was obtained in [9] within the model of the $(q\bar{q})$ dipole [22,23] on the assumption of the saturation effect for the gluon density, e.g., the cross section σ_{γ^*N} of the interaction of the transverse virtual photons γ^* with a nucleon N is assumed to be a constant at low Q^2 (and low x too). It corresponds to the Gaussian form for the effective dipole cross section $\hat{\sigma}(x, r)$ as a function of x and the relative transverse separation \mathbf{r} of the $q\bar{q}$ pair [9]. In fact, this form could be more complicated. In this paper we study this point and try to find the parameterization for $xg(x, k_t, Q_0)$, which is related to $\hat{\sigma}(x, r)$, from the best description of the

inclusive spectra of charge hadrons produced in pp collisions at LHC energies and mid-rapidity region.

2.2 Quark-gluon string model (QGSM) including gluons

As is well known, the soft hadron production in pp collisions at not large transfer can be analyzed within the soft QCD models, namely, the quark-gluon string model (QGSM) [24]-[26] or the dual parton model (DPM) [27]. The cut n-pomeron graphs calculated within these models result in a reasonable contribution at small but nonzero rapidities. However, it has been shown recently [28] that there are some difficulties in using the QGSM to analyze the inclusive spectra in pp collisions in the mid-rapidity region and at the initial energies above the ISR one. However, it is due to the according to Abramovskiy-Gribov-Kancheli cutting rules (AGK) [29] at mid-rapidity ($y \simeq 0$), when only one-pomeron Mueller-Kancheli diagrams contribute to the inclusive spectrum $\rho_h(y \simeq 0, p_t)$. To overcome these difficulties it was assumed in [28] that there are soft gluons in the proton, which are split into $q\bar{q}$ pairs and should vanish at the zero intrinsic transverse momentum ($k_t \sim 0$). The total spectrum $\rho_h(y \simeq 0, p_t)$ was split into two parts, the quark contribution $\rho_q(y \simeq 0, p_t)$ and the gluon one and their energy dependence was calculated [28]

$$\rho(p_t) = \rho_q(x=0, p_t) + \rho_g(x=0, p_t) = g(s/s_0)^\Delta \bar{\phi}_q(0, p_t) + (g(s/s_0)^\Delta - \sigma_{nd}) \bar{\phi}_g(0, p_t). \quad (3)$$

The following parameterization for $\bar{\phi}_q(0, p_t)$ and $\bar{\phi}_g(0, p_t)$ was found [28]:

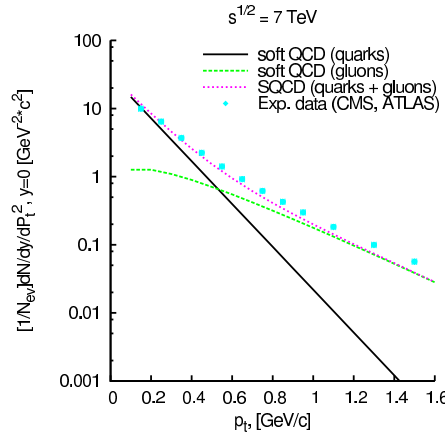


Figure 1: The inclusive spectrum of the charged hadrons as a function of p_t (GeV/c) in the central rapidity region ($y = 0$) at $\sqrt{s} = 7$ TeV at $p_t \leq 1.6$ GeV/c compared with the CMS [30] which are very close to the ATLAS data [31].

$$\begin{aligned} \bar{\phi}_q(0, p_t) &= A_q \exp(-b_q p_t) \\ \bar{\phi}_g(0, p_t) &= A_g \sqrt{p_t} \exp(-b_g p_t), \end{aligned} \quad (4)$$

where $s_0 = 1 \text{ GeV}^2$, $g = 21 \text{ mb}$, $\Delta = 0.12$. The parameters are fixed from the fit to the data on the p_t distribution of charged particles at $y = 0$ [28]: $A_q = 4.78 \pm 0.16 \text{ (GeV/c)}^{-2}$, $b_q = 7.24 \pm 0.11$

$(\text{GeV}/c)^{-1}$ and $A_g = 1.42 \pm 0.05 (\text{GeV}/c)^{-2}$; $b_g = 3.46 \pm 0.02 (\text{GeV}/c)^{-1}$. Figure 1 illustrates the best fit of the inclusive spectrum of charged hadrons produced in pp collisions at $\sqrt{s} = 7$ TeV and the central rapidity region at the hadron transverse momenta $p_t \leq 1.6 \text{ GeV}/c$; the solid line corresponds to the quark contribution ρ_q , the dashed line is the gluon contribution ρ_g , and the dotted curve is the sum of these contributions ρ_h given by Eq.(3).

2.3 Modified unintegrated gluon distributions

Let us assume the existence of the intrinsic gluons in proton, as was suggested in [32], which can be presented as the $q\bar{q}$ pairs similar to the sea $q\bar{q}$ considered in the QGSM [24]. Then, we can calculate the gluon contribution $\tilde{\phi}_g(0, p_t)$ entering into Eq.(4) as the cut graph (Fig.2, right) of the one-pomeron exchange in the gluon-gluon interaction (Fig.2, left) using the splitting of the gluons into the $q\bar{q}$ pair. Actually, the calculation can be made in a way similar to the calculation of the sea quark contribution to the inclusive spectrum within the QGSM, see Eqs.(4,5) in [28] at $n = 2$.

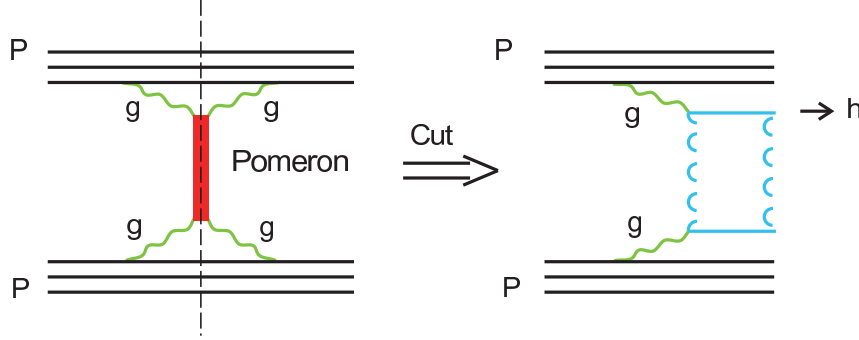


Figure 2: The one-pomeron exchange graph between two gluons in the elastic pp scattering (left) and the cut one-pomeron due to the creation of two colorless strings between quarks/antiquarks (right) [24].

$$\rho_g(x_{\pm}, p_{ht}) = F(x_+, p_{ht})F(x_-, p_{ht}) , \quad (5)$$

where the function $F(x_{\pm}, p_t; p_{ht})$ corresponds to the production of final hadrons from decay of $q\bar{q}$ string. It is calculated as the following convolution:

$$F(x_{\pm}, p_t; p_{ht}) = \int_{x_{\pm}}^1 dx_1 \int d^2 k_{1t} f_{q(\bar{q})}(x_1, k_{1t}) G_{q(\bar{q}) \rightarrow h} \left(\frac{x_{\pm}}{x_1}, p_{ht} - k_t \right) , \quad (6)$$

Here $G_{q(\bar{q}) \rightarrow h}(z, \tilde{k}_t) = z D_{q(\bar{q}) \rightarrow h}(z, \tilde{k}_t)$, $D_{q(\bar{q}) \rightarrow h}(z, \tilde{k}_t)$ is the fragmentation function (FF) of the quark (antiquark) to a hadron h , $z = x_{\pm}/x_1$, $\tilde{k}_t = p_{ht} - k_t$, $x_{\pm} = 0.5(\sqrt{x^2 + x_t^2} \pm x)$, $x_t = 2\sqrt{(m_h^2 + p_t^2)/s}$. The distribution of sea quarks (antiquark) $f_{q(\bar{q})}$ is related to the splitting function $\mathcal{P}_{g \rightarrow q\bar{q}}$ of gluons to $q\bar{q}$ by

$$f_{q(\bar{q})}(z, k_t) = \int_z^1 g(z_1, k_t, Q_0) \mathcal{P}_{g \rightarrow q\bar{q}} \left(\frac{z}{z_1} \right) \frac{dz_1}{z_1} , \quad (7)$$

where $g(z_1, k_{1t}, Q_0)$ is the u.g.d.. The gluon splitting function $\mathcal{P}_{g \rightarrow q\bar{q}}$ was calculated within the Born approximation.

Calculating the diagram of Fig.2 (right) by the use of Eqs.(5-7) for the gluon contribution ρ_g we took the FF to charged hadrons, pions, kaons, and $p\bar{p}$ pairs obtained within the QGSM [33]. From the best description of $\rho_g(x \simeq 0, p_{ht})$, see its parameterization given by Eq.(4), we found the form for the $xg(x, k_t, Q_0)$ which was fitted in the following form:

$$xg(x, k_t, Q_0) = \frac{3\sigma_0}{4\pi^2\alpha_s(Q_0)} C_1 (1-x)^{b_g} \times (R_0^2(x)k_t^2 + C_2(R_0(x)k_t)^a) \exp(-R_0(x)k_t - d(R_0(x)k_t)^3), \quad (8)$$

The coefficient C_1 was found from the following normalization:

$$g(x, Q_0^2) = \int_0^{Q_0^2} dk_t^2 g(x, k_t^2, Q_0^2), \quad (9)$$

and the parameters

$$a = 0.7; C_2 \simeq 2.3; \lambda = 0.22; b_g = 12; d = 0.2; C_1 = 0.3295$$

were found from the best fit of the LHC data on the inclusive spectrum of charged hadrons produced in pp collisions and in the mid-rapidity region at $p_t \leq 1.6$ GeV/c, see the dashed line in Fig.1 and Eq.(4).

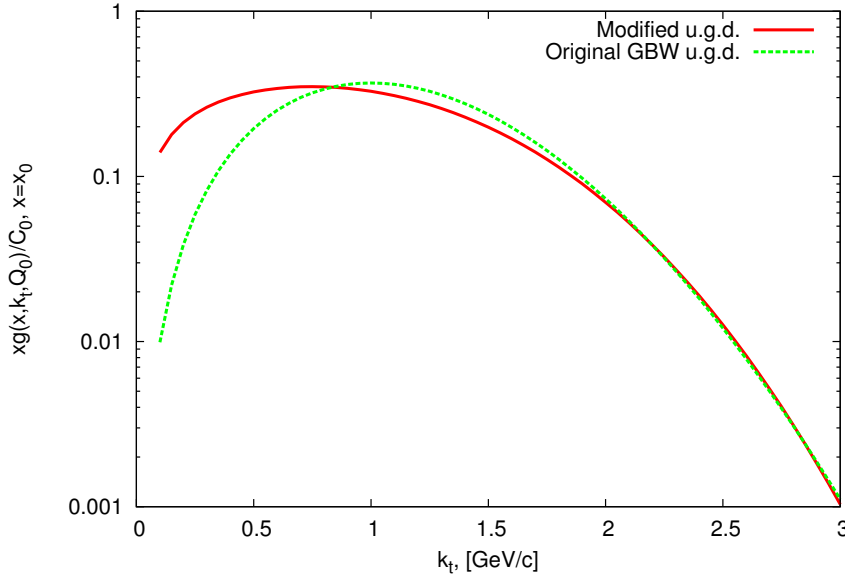


Figure 3: The unintegrated gluon distribution $xg(x, k_t, Q_0)/C_0$ as a function of k_t at $x = x_0$ and $Q_0 = 1$ GeV/c. The dashed curve corresponds to the original GBW [9, 10], Eq.(2), and the solid line is the modified u.g.d. given by Eq.(8).

Figure 3 presents the modified u.g.d. obtained by calculating the cut one-pomeron graph of Fig.2 and the original GBW u.g.d. [9,10] as a function of the transverse gluon momentum k_t . Here $C_0 = 3\sigma_0/(4\pi^2\alpha_s(Q_0))$. One can see that the modified u.g.d. (the solid line in Fig.3) is different from the original GBW u.g.d. [9,10] at $k_t < 1.5$ GeV/c and coincides with it at larger k_t . This is due to the sizable contribution of ρ_g (Eqs.(3,4)) to the inclusive spectrum $\rho(p_t)$ of charged hadrons produced in pp collisions at LHC energies and in the mid-rapidity region, see the dashed line in Fig.1.

3 Proton longitudinal structure function

Within the k_t -factorization approach, the proton longitudinal structure function $F_L(x, Q^2)$ calculated in the leading order of QCD can be presented in the following form [13]:

$$F_L(x, Q^2) = \int_x^1 \frac{dz}{z} \int^{Q^2} dk_t^2 \sum_{flavour(f)} e_f^2 \hat{C}_L^g\left(\frac{x}{z}, Q^2, m_f^2, k_t^2\right) g(x, k_t^2), \quad (10)$$

where e_f^2 is the charge of the quarks of flavor f , the functions $\hat{C}_{2,L}^g(x/z, Q^2, m_f^2, k_t^2)$ are the so called hard structure functions of the off-shell gluons with virtuality k_t^2 which correspond to the quark-box diagram for the photon-gluon interactions [13]. In the present note we calculated $F_L(x, Q^2)$ at the fixed value of the missing mass $W = 276$ GeV using the parameterization for u.g.d. at fixed Q_0^2 given by Eq.(2) and Eq.(8). The results of our calculations are presented in Fig. 4 in comparison with the H1 data [34,35].

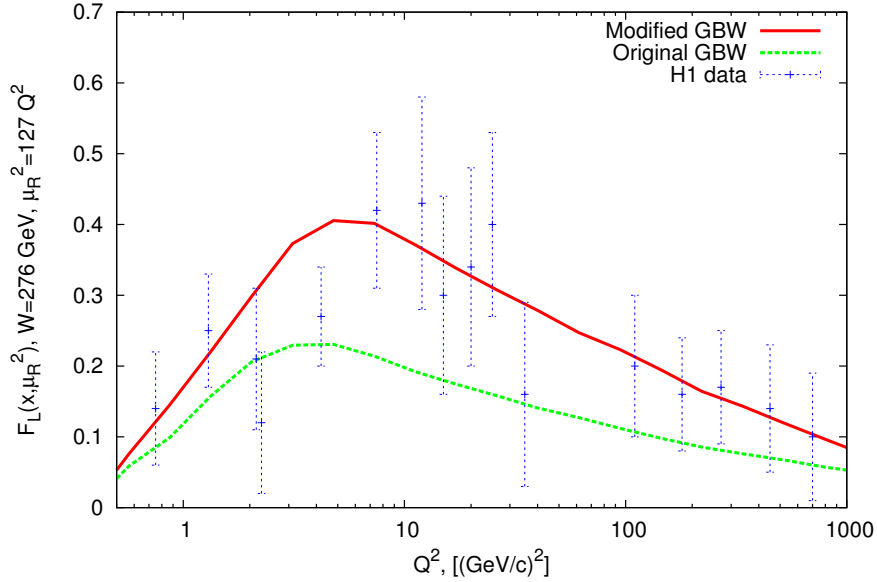


Figure 4: The longitudinal structure function $F_L(\mu_R^2)$ at $W = 276$ GeV and $\mu_R^2 = K \cdot Q^2$, where $K = 127$ [36]. The H1 data are taken from [34,35].

We find that the modified u.g.d. allows us also to describe the proton F_L . Note that in order to take into account the NLO corrections (which are important at low Q^2) in our numerical calculations we apply the method proposed in [14]. Following [14, 36], we use the shifted value of the renormalization scale $\mu_R^2 = K Q^2$, where $K = 127$. As is was shown in [36], this shifted scale in the DGLAP approach at LO approximation leads to the results which are very close to the NLO ones.

4 Conclusion

We fitted the experimental data on the inclusive spectra of charged particles produced in the central pp collisions at energies larger than the ISR starting with the sum of the quark contribution ρ_q and the gluon contribution ρ_g (see Eqs.(3,4)). The parameters of this fit do not depend on the initial energy in that energy interval. Assuming creation of soft gluons in the proton at low transverse momenta k_t and calculating the cut one-pomeron graph between two gluons in colliding protons we found the form for the unintegrated gluon distribution (modified u.g.d) as a function of x and k_t at the fixed value of Q_0^2 . The parameters of this u.g.d. were found from the best description of the LHC data on the inclusive spectra of the charged hadrons produced in the mid-rapidity pp collisions at low p_t . It was shown that the modified u.g.d. is different from the original GBW u.g.d. obtained in [9, 10] at $k_t \leq 1.6$ GeV/c and it coincides with the GBW u.g.d. at $k_t > 1.6$ GeV/c. It was also shown that the modified u.g.d. allows us to describe the longitudinal structure function $F_L(Q^2)$ at the fixed missing mass W better than the original GBW u.g.d. Therefore, some link between soft processes at the LHC and low- x physics at HERA is found.

Acknowledgments The authors are grateful to S.P. Baranov, B.I. Ermolaev, E.A. Kuraev, L.N. Lipatov, M. Mangano, C. Merino, M.G. Ryskin and Yu.M. Shabelskiy for useful discussions and comments. A.V.L. and N.P.Z. are very grateful to the DESY Directorate for the support within the Moscow — DESY project on Monte-Carlo implementation for HERA — LHC. A.V.L. was supported in part by the grant of the President of the Russian Federation (MK-3977.2011.2). This research was also supported by the FASI of the Russian Federation (grant NS-3920.2012.2), FASI state contract 02.740.11.0244, RFBR grants 11-02-01454-a and 11-02-01538-a, and the RMES (grant the Scientific Research on High Energy Physics).

References

- [1] V.N. Gribov and L.N. Lipatov, Sov.J.Nucl.Phys. **15** (1972) 438; G. Altarelli, G. Parisi, Nucl.Phys. B **126** (1997) 298; Yu.L. Dokshitzer, Sov.Phys. JETP, **46** (1977) 641.
- [2] G. Watt, A.D. Martin, M.G. Ryskin, Eur.Phys.J. C31 (2003) 73 [arXiv:hep-ph/0306169];
- [3] L.V. Gribov, E.M. Levin, M.G. Ryskin, Phys. Rep. **100** (1983) 1; E.M. Levin, M.G. Ryskin, Yu.M. Shabelsky, A.G. Shuvaev, Sov. J. Nucl. Phys. **53** (1991) 657; S. Catani, M. Ciafaloni, F. Hautmann, Nucl. Phys. B **366** (1991) 135; J.C. Collins, R.K. Ellis, Nucl. Phys. B **360** (1991) 3.
- [4] Bo Andersson., et.al., Eur.Phys.J. C**25** (2002) 77.
- [5] J. Andersen *et al.* (Small- x Collaboration), Eur. Phys. J. C **35** (2004) 67; J. Andersen *et al.* (Small- x Collaboration), Eur. Phys. J. C **48** (2006) 53.
- [6] L.N. Lipatov, Sov.J.Nucl.Phys., **23** (1976) 338; E.A. Kuraev, L.N. Lipatov, V.S. Fadin, Sov.Phys. JETP **44** (1976) 443; *ibid* **45** (1977) 199; Ya.Ya. Balitzki, L.N. Lipatov, Sov.J. Nucl.Phys. **28** (1978) 822; L.N. Lipatov, Sov.Phys. JETP **63** (1986) 904.

- [7] M. Ciafaloni, Nucl.Phys. B **296** (1988) 49; C. Catani, F. Fiorani, G. Marchesini, Phys.Lett. B **234** (1990) 339; *ibid* Nucl.Phys. B **336** (1990) 18; G. Marchesini, Nucl.Phys., B **445** (1995) 49; *ibid* Phys.Rev. D **70** (2004) 014012; [Erratum-*ibid*. D **70** (2004) 079902] [arXiv:hep-ph/0309096].
- [8] K. Golec-Biernat, M. Wusthof, Phys.Rev. D **59** (1998) 014017.
- [9] K. Golec-Biernat, M. Wusthof, Phys.Rev. D **60** (1999) 114023.
- [10] H. Jung, Proc. of the DIS'2004, Strbaske' Pleso, Slovakia, arXiv:0411287 [hep-ph].
- [11] A. D. Martin, M.G. Ryskin, G. Watt, Eur.Phys.J. C **66** (2010) 163; arXiv:/0909.5529 [hep-ph].
- [12] N.I. Kochelev, Phys.Lett. B **426** (1998) 149;
- [13] A.V. Kotikov, A.V. Lipatov, N.P. Zotov, Eur.Phys.J. C **27** (2003) 219.
- [14] A.V. Kotikov, A.V. Lipatov, N.P. Zotov, J.Exp.Theor.Phys. **101** (2005) 811.
- [15] B.I. Ermolaev, V. Greco, S.I. Troyan, Eur.Phys.J. C **71** (2011) 1750.
- [16] B.I. Ermolaev, V. Greco, S.I. Troyan, arXiv:1112.1854 [hep-ph].
- [17] S.P. Baranov, A.V. Lipatov, N.P. Zotov, Phys. Rev. D **81** (2010) 094034.
- [18] A.V. Lipatov, N.P. Zotov, Phys. Lett. B **704** (2011) 189.
- [19] A.V. Lipatov, M.A. Malyshev, N.P. Zotov, Phys. Lett. B **699** (2011) 93.
- [20] H. Jung, M. Kraemer, A.V. Lipatov, N.P. Zotov, JHEP **1101** (2011) 085.
- [21] S.P. Baranov, A.V. Lipatov, N.P. Zotov, Phys. Rev. D **85** (2012) 014034.
- [22] N.N. Nikolaev and B.G. Zakharov, Z.Phys. C **49** (1991) 607.
- [23] I.P. Ivanov, N.N. Nikolaev, Phys.Rev. D **65** (2002) 054004.
- [24] A.B. Kaidalov, Z.Phys. C **12** (1982) 63; Sarveys High Energy Phys. **13** (1999) 265. A.B. Kaidalov, O.I. Piskunova, Z.Phys. C **30** (1986) 145; Yad.Fiz. **43** (1986) 1545.
- [25] G.I. Lykasov, M.N. Sergeenko, Z.Phys. C **56** (1992) 697; *ibid* Z.Phys. C **52** (1991) 635; *ibid* Z.Phys. C **70** (1996) 455.
- [26] V.A. Bednyakov, G.I. Lykasov, V.V. Lyubushkin, Europhys.Lett. **92** (2010) 31001; arXiv:hep-ph/1005.0559.
- [27] A. Capella, U. Sukhatme, C.J.Tan, J, Tran Thanh Van, Phys.Rev. D**36**, 109 (1987); *ibid* Adv.Ser.Direct.High Energy Phys. **2** (1988) 428.
- [28] V.A. Bednyakov, A.A. Grinyuk, G.I. Lykasov, M. Poghosyan, Nucl.Phys. B **219-220** [Proc.Suppl.] (2011) 225; *ibid* Int.J.Mod.Phys. A **27** (2012) 1250042.
- [29] V. Abramovsky, V.N. Gribov, O. Kancheli, Sov.J.Nucl.Phys. **18** (1973) 308 .
- [30] CMS Colaloration, Vadrn Kachatryan, et al., Phys.Rev.Lett. **105** (2010) 022002; arXiv:1005.3299 [hep-ex]; CMS-QCD, CERN-PH-EP-2010-003, Feb.2010.
- [31] ATLAS Collaboration, G. Aad, et al., New J.Phys. **13** (2011) 053033; arXiv:1012.5104v2 [hep-ex].
- [32] S. Brodsky, C. Peterson, N. Sakai, Phys.Rev. D, **23** (1981) 2745.
- [33] Yu.M. Shabelsky, Sov.J.Nucl.Phys. **56** (1992) 2512.
- [34] P. Newman, J.Mod.Phys. A **19** (2004) 1061, arXiv:0312018 [hep-ex];
- [35] E.M. Lododzinska, arXiv:03111180 [hep-ph].
- [36] S.J Brodsky, V.S. Fadin, V.T. Kim, L.N. Lipatov, G.B. Pivovarov, JETP. Lett. **70** (1999) 155.

Isolated jet production with multi-Regge kinematics at Tevatron and LHC

Bernd Kniehl¹, Vladimir Saleev^{2*}, Alexandra Shipilova²

¹II. Institut für Theoretische Physik, Universität Hamburg,
Luruper Chaussee 149, 22761 Hamburg, Germany

²Samara State University, Ac. Pavlov, 1, 443011, Samara, Russia

DOI: <http://dx.doi.org/10.3204/DESY-PROC-2012-03/26>

We study isolated jet hadroproduction with multi-Regge kinematics invoking the hypothesis of parton Reggeization in t -channel exchanges at high energy. In this approach, the leading contribution is due to the fusion of two Reggeized gluons into a Yang-Mills gluon. Adopting the Kimber-Martin-Ryskin and Blümlein prescriptions to derive unintegrated gluon distribution function of the proton from their collinear counterparts, we evaluate cross section distributions in transverse momentum (p_T) and rapidity (y). Without adjusting any free parameters, we find good agreement with measurements by the CDF and D0 Collaborations at the Tevatron and by the ATLAS Collaboration at the LHC in a wide region of p_T , especially using Blümlein's unintegrated gluon distribution function.

1 Introduction

The study of jet inclusive production at high-energy colliders, such as the Fermilab Tevatron and the CERN LHC, is of great interest because it allows us to test perturbative quantum chromodynamics (QCD) and to extract information on the parton distribution functions (PDFs) of the proton.

The total collision energies, $\sqrt{s} = 1.8$ TeV and 1.96 TeV in Tevatron runs I and II, respectively, and $\sqrt{s} = 7$ TeV or 14 TeV at the LHC, sufficiently exceed the characteristic scale μ of the relevant hard processes, which is of order of p_T , *i.e.* we have $\Lambda_{\text{QCD}} \ll \mu \ll \sqrt{s}$. In this high-energy regime, the contribution of partonic subprocesses involving t -channel parton exchanges to the production cross section can become dominant. Then the transverse momenta of the incoming partons and their off-shell properties can no longer be neglected, and we deal with “Reggeized” t -channel partons. If the particles produced in the collision are strongly separated in rapidity, they obey multi-Regge kinematics (MRK). In the case of isolated jet inclusive production, this means the following: A single jet is produced in the central region of rapidity, while other particles are produced with large modula of rapidities.

Previously, in Ref. [1], single jet inclusive production was studied in the Regge limit of QCD using the Balitsky-Fadin-Kuraev-Lipatov (BFKL) framework [2], and it was shown that the discrepancy between data and theory in the region of small values of $x_T = 2p_T/\sqrt{S}$ may be accounted for by the BFKL Pomeron. However, Pomeron exchange should be a dominant

*Speaker

mechanism only at asymptotically large energies. In fact, in the energy range of the Tevatron and the LHC, the mechanism of Reggeized gluon and quark exchanges should be more adequate [3].

The parton Reggeization framework [4] is particularly appropriate for this kind of high-energy phenomenology. It is based on an effective quantum field theory implemented with the non-Abelian gauge-invariant action including fields of Reggeized gluons [5] and Reggeized quarks [6].

In this paper, we assume the MRK production mechanism to be the dominant one at small x_T values. We compare our results with experimental data taken by the CDF [7] and D0 [8] Collaborations at the Tevatron with $\sqrt{s} = 1.8$ TeV and 1.96 TeV and by the ATLAS Collaboration [9] at the LHC with $\sqrt{s} = 7$ TeV. We also present predictions for the p_T and y distributions of isolated jet inclusive production at the LHC with $\sqrt{s} = 14$ TeV.

2 Gluon-gluon fusion amplitude with multi-Regge kinematics

We examine isolated jet inclusive production in proton-antiproton collisions at the Tevatron and in proton-proton collisions at the LHC. To leading order (LO) in the parton Reggeization framework, the relevant hard-scattering process is $\mathcal{R} + \mathcal{R} \rightarrow g$, where \mathcal{R} is a Reggeized gluon and g is a Yang-Mills gluon. Working in the center-of-mass (c.m.) frame, we write the four-momenta of the incoming hadrons as $P_{1,2}^\mu = (\sqrt{s}/2)(1, 0, 0, \pm 1)$ and those of the Reggeized partons as $q_i^\mu = x_i P_i^\mu + q_{iT}^\mu$ ($i = 1, 2$), where x_i are the longitudinal momentum fractions and $q_{iT}^\mu = (0, \mathbf{q}_{iT}, 0)$, with \mathbf{q}_{iT} being transverse two-momenta, and we define $t_i = -q_{iT}^2 = \mathbf{q}_{iT}^2$. The gluon produced in the $2 \rightarrow 1$ partonic subprocess has four-momentum $p^\mu = q_1^\mu + q_2^\mu = (p^0, \mathbf{p}_T, p^3)$, with $\mathbf{p}_T^2 = t_1 + t_2 + 2\sqrt{t_1 t_2} \cos \phi_{12}$, where ϕ_{12} is the azimuthal angle enclosed between \mathbf{q}_{1T} and \mathbf{q}_{2T} . Introducing the light-cone vectors $n_\mu^\pm = (1, 0, 0, \pm 1)$, we define $k^\pm = k \cdot n^\pm$ for any four-vector k^μ .

The Fadin-Kuraev-Lipatov effective $\mathcal{R}\mathcal{R}g$ vertex reads [2, 10]:

$$C_{\mathcal{R}\mathcal{R}}^{g,\mu}(q_1, q_2) = -g_s f^{abc} \frac{q_1^+ q_2^-}{2\sqrt{t_1 t_2}} \left[(q_1 - q_2)^\mu + \frac{(n^+)^\mu}{q_1^+} (q_2^2 + q_1^+ q_2^-) - \frac{(n^-)^\mu}{q_2^-} (q_1^2 + q_1^+ q_2^-) \right], \quad (1)$$

where $g_s = \sqrt{4\pi\alpha_s}$, α_s is the strong-coupling constant, a and b are the color indices of the Reggeized gluons with incoming four-momenta q_1 and q_2 , and f^{abc} are the structure constants of the color group SU(3). The squared amplitude of the partonic subprocess $\mathcal{R} + \mathcal{R} \rightarrow g$ is straightforwardly found from Eq. (1) to be

$$|\overline{\mathcal{M}(\mathcal{R}\mathcal{R} \rightarrow g)}|^2 = \frac{3}{2} \pi \alpha_s \mathbf{p}_T^2. \quad (2)$$

3 Cross sections in high-energy factorization

Exploiting the hypothesis of high-energy factorization, we may write the hadronic cross sections $d\sigma$ as convolutions of partonic cross sections $d\hat{\sigma}$ with unintegrated PDFs Φ_a^h of Reggeized

partons a in the hadrons h , as

$$d\sigma(p\bar{p} \rightarrow jX) = \int \frac{dx_1}{x_1} \int \frac{d^2q_{1T}}{\pi} \int \frac{dx_2}{x_2} \int \frac{d^2q_{2T}}{\pi} \Phi_g^p(x_1, t_1, \mu^2) \Phi_g^{\bar{p}}(x_2, t_2, \mu^2) d\hat{\sigma}(\mathcal{R}\mathcal{R} \rightarrow g), \quad (3)$$

and similarly for pp collisions. We also present here a compact formula for the double differential distribution in $p_T = |\mathbf{p}_T|$ and y , which follows from Eq. (3) and reads:

$$\frac{d\sigma}{dp_T dy}(p\bar{p} \rightarrow jX) = \frac{1}{p_T^3} \int d\phi_1 \int dt_1 \Phi_g^p(x_1, t_1, \mu^2) \Phi_g^{\bar{p}}(x_2, t_2, \mu^2) \overline{|\mathcal{M}(\mathcal{R}\mathcal{R} \rightarrow g)|^2}, \quad (4)$$

where ϕ_1 is the azimuthal angle enclosed between \mathbf{q}_{1T} and \mathbf{p}_T ,

$$x_{1,2} = \frac{p_T \exp(\pm y)}{\sqrt{s}}, \quad t_2 = t_1 + p_T^2 - 2p_T \sqrt{t_1} \cos \phi_1. \quad (5)$$

Since we work at LO, the produced jet has zero invariant mass m , so that transverse energy E_T and transverse momentum p_T coincide and so do rapidity y and pseudorapidity η .

In our numerical analysis, we adopt the Kimber-Martin-Ryskin (KMR) [11] and Blümlein (B) [12] prescriptions to obtain the unintegrated gluon PDF of the proton from the conventional integrated one. As input for this procedure, we use the LO set of the Martin-Roberts-Stirling-Thorne (MRST) [13] proton PDFs as our default.

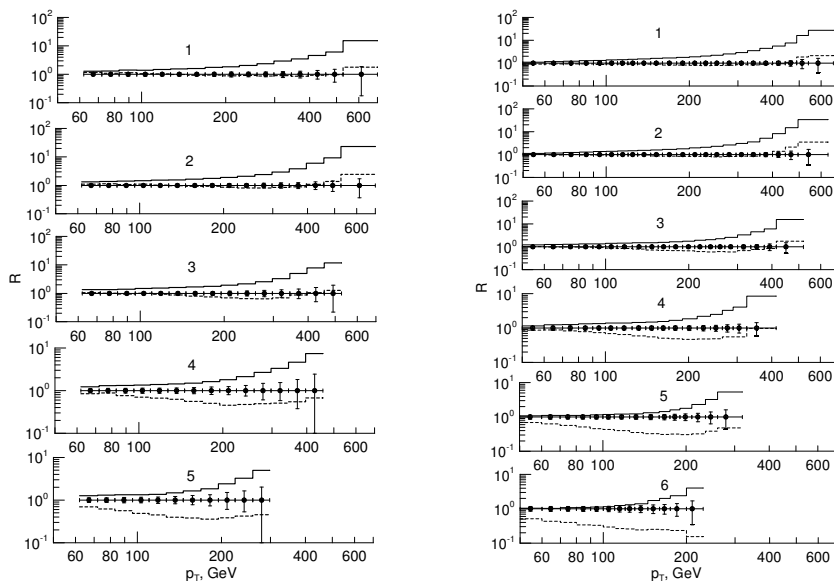


Figure 1: Ratio ($Theory/Experiment$) for p_T distributions of single jet inclusive hadroproduction in $p\bar{p}$ collisions at $\sqrt{s} = 1.96$ TeV evaluated at LO in the MRK approach using the KMR (solid histograms) and B (dashed histograms) unintegrated PDFs normalized to the CDF [7] (left panel) and D0 [8] (right panel) data.

4 Results

Recently, the CDF [7] (D0 [8]) Collaboration presented new data from Tevatron run II, which correspond to an integrated luminosity of 1.13 fb^{-1} (0.70 fb^{-1}) and cover the kinematic range $62 \text{ GeV} < p_T < 700 \text{ GeV}$ ($50 \text{ GeV} < p_T < 600 \text{ GeV}$) and $|y| < 2.1$ ($|y| < 2.4$). The CDF and D0 data are compared with our MRK predictions in Fig. 1 for the following rapidity intervals:

1. $|y| < 0.1$ (CDF) and $|y| < 0.4$ (D0)
2. $0.1 < |y| < 0.7$ (CDF) and $0.4 < |y| < 0.8$ (D0)
3. $0.7 < |y| < 1.1$ (CDF) and $0.8 < |y| < 1.2$ (D0)
4. $1.1 < |y| < 1.6$ (CDF) and $1.2 < |y| < 1.6$ (D0)
5. $1.6 < |y| < 2.1$ (CDF) and $1.6 < |y| < 2.0$ (D0)
6. $2.0 < |y| < 2.4$ (D0)

In case of the KMR unintegrated gluon PDF, we find agreement with the data for $p_T < 100 \text{ GeV}$ in all rapidity intervals, which corresponds to $x_T < 0.1$, while our predictions overshoot the data for higher values of p_T . In case of the B unintegrated gluon PDF, we find good agreement for $p_T < 500 \text{ GeV}$, but only at small absolute values of rapidity, for $|y| < 1.1$.

This may be understood by observing that the average values of the scaling variables x_1 and x_2 in Eq. (4) are of order x_T , and the MRK picture ceases to be valid for $x_i \geq 0.1$. For $x_T \geq 0.1$, one needs to resort to the collinear parton model, which starts with $2 \rightarrow 2$ partonic subprocesses at LO.

The solid and dashed curves in Fig. 1 clearly demonstrate the main theoretical uncertainties in the present study. The theoretical uncertainties due to the freedom in the choices of the renormalization and factorization scales are about 10–20 % and are not shown.

Moving on from the Tevatron to the LHC, which is currently running at $\sqrt{S} = 7 \text{ TeV}$, being about 3.5 times larger than at the Tevatron, one expects the p_T range of validity of the MRK picture to be extended by the same factor, to $p_T < 350 \text{ GeV}$. This expectation is nicely confirmed in Fig. 2, where a recent measurement by the ATLAS Collaboration [9], which is based on an integrated luminosity of 17 nb^{-1} and covers the kinematic range $60 \text{ GeV} < p_T < 600 \text{ GeV}$ and $|y| < 2.8$, is compared with our MRK predictions for the p_T and y distributions. In fact, useful agreement is found even up to the largest p_T values accessed by this measurement. The difference between the theoretical predictions based on the MRK and B unintegrated gluon PDFs are insignificant, as the average values of the scaling variables x_1 and x_2 are smaller at the LHC.

Note that, in Ref. [9], jets are identified using the anti- k_t jet-clustering algorithm with two different values of the jet-size parameter $R = \sqrt{(\Delta y)^2 + (\Delta \phi)^2}$. The ATLAS data shown in Fig. 2 refer to $R = 0.6$. The agreement is somewhat worse for $R = 0.4$. Our LO prediction does not yet depend on R .

In Fig. 3, we repeat the MRK analyses of Figs. 1 and 2 for the LHC design c.m. energy $\sqrt{s} = 14 \text{ TeV}$, where we expect the p_T range of validity to be roughly $p_T < 700 \text{ GeV}$.

5 Conclusions

The Tevatron and, even more so, the LHC are currently probing particle physics at terascale c.m. energies \sqrt{s} , so that the hierarchy $\Lambda_{\text{QCD}} \ll \mu \ll \sqrt{s}$, which defines the MRK regime, is satisfied for a wealth of QCD processes of typical energy scale μ .

In this report, we studied a QCD process of particular interest, namely single jet inclusive hadroproduction, at LO in the MRK approach, in which it is mediated by a $2 \rightarrow 1$ partonic subprocess initiated by Reggeized gluons. Despite the great simplicity of our analytic expressions, we found excellent agreement with single jet [9] data taken just recently by the ATLAS Collaboration in pp collisions with $\sqrt{s} = 7$ TeV at the LHC. By contrast, in the collinear parton model of QCD, it is necessary to take into account NLO corrections and to perform soft-gluon resummation in order to obtain a comparable degree of agreement with the data for jet inclusive production.

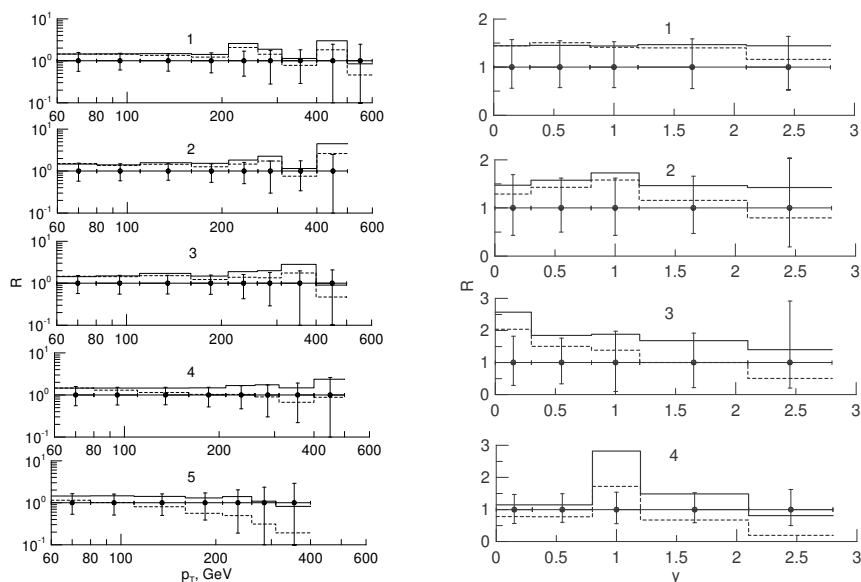


Figure 2: Ratio ($Theory/Experiment$) for p_T (left panel) and y (right panel) distributions of single jet inclusive hadroproduction in pp collisions at $\sqrt{s} = 7$ TeV evaluated at LO in the MRK approach using the KMR (solid histograms) and B (dashed histograms) unintegrated PDFs normalized to the ATLAS [9] data.

On the other hand, comparisons with data taken by the CDF and D0 Collaborations at the Tevatron in $p\bar{p}$ collisions with $\sqrt{s} = 1.8$ TeV and 1.96 TeV, which is roughly a factor of 3.5 below the value presently reached by the LHC, disclosed the limits of applicability of the MRK picture. In fact, the MRK approximation appears to break down for $x_T > 0.1$ in the case of single jet production.

These findings are in line with our previous studies of the MRK approach, applied to the production of prompt photons, diphotons, charmed mesons, bottom-flavored jets, charmonia, and bottomonia [14]. Here and in Ref. [14], parton Reggeization was demonstrated to be a powerful tool for the theoretical description of QCD processes in the high-energy limit.

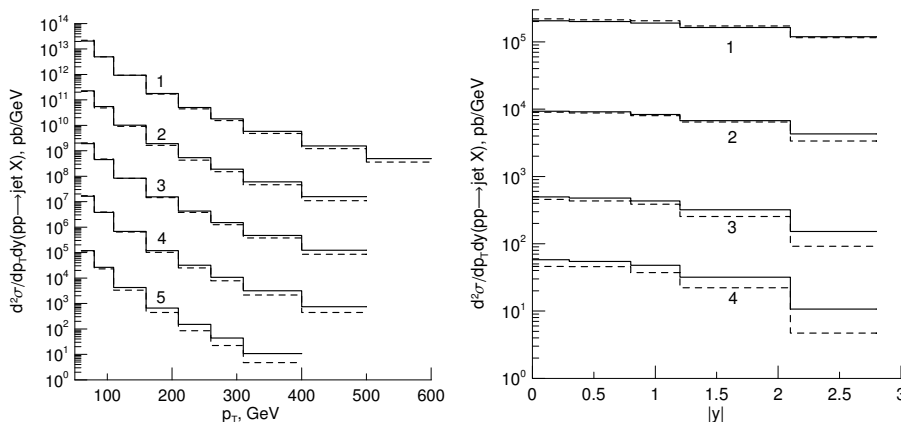


Figure 3: p_T distributions (left panel) integrated over the y intervals (1) $|y| < 0.3$ ($\times 10^8$), (2) $0.3 < |y| < 0.8$ ($\times 10^6$), (3) $0.8 < |y| < 1.2$ ($\times 10^4$), (4) $1.2 < |y| < 2.1$ ($\times 10^2$), and (5) $2.1 < |y| < 2.6$ and y distributions (right panel) integrated over the p_T intervals (1) $60 \text{ GeV} < p_T < 80 \text{ GeV}$, (2) $110 \text{ GeV} < p_T < 160 \text{ GeV}$, (3) $210 \text{ GeV} < p_T < 250 \text{ GeV}$, and (4) $310 \text{ GeV} < p_T < 400 \text{ GeV}$ of single jet inclusive hadroproduction in pp collisions at $\sqrt{s} = 14 \text{ TeV}$ evaluated at LO in the MRK approach using the KMR (solid histograms) and B (dashed histograms) unintegrated PDFs.

Acknowledgments We are grateful to V.S. Fadin, E.A. Kuraev, and L.N. Lipatov for useful discussions. The work of B.A.K. is supported in part by BMBF Grant No. 05 HT6GUA, by HGF Grant No. Ha 101, by NSF Grant No. NSF PHY05-51164, and by the Claussen-Simon-Stiftung. The work of V.A.S. and A.V.S. is supported in part by the Russian Foundation for Basic Research under Grant No. 11-02-00769-a and by the Federal Ministry for Science and Education of the Russian Federation under Contract No. 14.740.11.0894.

References

- [1] V. T. Kim and G. B. Pivovarov, “A BFKL pomeron manifestation in inclusive single jet production at high-energy hadron collisions,” *Phys. Rev. D* **57**, 1341 (1998) (arXiv:hep-ph/9709433v2).
- [2] L. N. Lipatov, “Reggeization Of The Vector Meson And The Vacuum Singularity In Nonabelian Gauge Theories,” *Sov. J. Nucl. Phys.* **23**, 338 (1976) [*Yad. Fiz.* **23**, 642 (1976)]; E. A. Kuraev, L. N. Lipatov, and V. S. Fadin, “Multi - Reggeon Processes In The Yang-Mills Theory,” *Sov. Phys. JETP* **44**, 443 (1976) [*Zh. Eksp. Teor. Fiz.* **71**, 840 (1976)]; E. A. Kuraev, L. N. Lipatov and V. S. Fadin, “The Pomeron Singularity In Nonabelian Gauge Theories,” *Sov. Phys. JETP* **45**, 199 (1977) [*Zh. Eksp. Teor. Fiz.* **72**, 377 (1977)]; I. I. Balitsky and L. N. Lipatov, “The Pomeron Singularity In Quantum Chromodynamics,” *Sov. J. Nucl. Phys.* **28**, 822 (1978) [*Yad. Fiz.* **28**, 1597 (1978)]; L. N. Lipatov, “The Bare Pomeron In Quantum Chromodynamics,” *Sov. Phys. JETP* **63**, 904 (1986) [*Zh. Eksp. Teor. Fiz.* **90**, 1536 (1986)].
- [3] B. A. Kniehl, V. A. Saleev, A. V. Shipilova, E. V. Yatsenko, “Single jet and prompt-photon inclusive production with multi-Regge kinematics: From Tevatron to LHC,” *Phys. Rev.* **D84** 074017 (2011) (arXiv:11071462 [hep-ph]). (arXiv:1107.1462 [hep-ph]).
- [4] V. S. Fadin and L. N. Lipatov, “Radiative corrections to QCD scattering amplitudes in a multi - Regge kinematics,” *Nucl. Phys.* **B406**, 259 (1993); **B477**, 767 (1996) .
- [5] L. N. Lipatov, “Gauge invariant effective action for high-energy processes in QCD,” *Nucl. Phys.* **B452**, 369 (1995) (arXiv:hep-ph/9502308v2) .

- [6] L. N. Lipatov and M. I. Vyazovsky, “Quasi-multi-Regge processes with a quark exchange in the t-channel,” Nucl. Phys. **B597**, 399 (2001) .
- [7] CDF Collaboration, T. Aaltonen *et al.*, “Measurement of the Inclusive Jet Cross Section at the Fermilab Tevatron p-pbar Collider Using a Cone-Based Jet Algorithm,” Phys. Rev. D **78**, 052006 (2008); **79**, 119902(E) (2009) (arXiv:0807.2204v4 [hep-ex]) .
- [8] D0 Collaboration, V. M. Abazov *et al.*, “Measurement of the inclusive jet cross-section in p anti-p collisions at $s^{*1/2} = 1.96$ -TeV,” Phys. Rev. Lett. **101**, 062001 (2008) .
- [9] ATLAS Collaboration, G. Aad *et al.*, “Measurement of inclusive jet and dijet cross sections in proton-proton collisions at 7 TeV centre-of-mass energy with the ATLAS detector,” Eur. Phys. J. C **71**, 1512 (2011) (arXiv:1009.5908v2 [hep-ex]) .
- [10] V. S. Fadin and L. N. Lipatov, “High-Energy Production of Gluons in a Quasi-Multi-Regge Kinematics,” JETP Lett. **49**, 352 (1989) [Pis'ma Zh. Eksp. Teor. Fiz. **49**, 311 (1989)]; Sov. J. Nucl. Phys. **50**, 712 (1989) [Yad. Fiz. **50**, 1141 (1989)] (arXiv:hep-ph/9704267v2).
- [11] M. A. Kimber, A. D. Martin, and M. G. Ryskin, Phys. Rev. D **63**, 114027 (2001); G. Watt, A. D. Martin, and M. G. Ryskin, Eur. Phys. J. C **31**, 73 (2003); Phys. Rev. D **70**, 014012 (2004); **70**, 079902(E) (2004) .
- [12] J. Blümlein, “On the k(T) dependent gluon density of the proton,” Preprint DESY 95-121 (1995) (arXiv:9506403 [hep-ph]).
- [13] A. D. Martin, R. G. Roberts, W. J. Stirling, and R. S. Thorne, “NNLO global parton analysis,” Phys. Lett. B **531**, 216 (2002) (arXiv:0201127v1 [hep-ph]) .
- [14] V. A. Saleev, Phys. Rev. D **78**, 034033 (2008); Phys. Rev. D **78**, 114031 (2008); Phys. Rev. D **80**, 114016 (2009); B. A. Kniehl, A. V. Shipilova and V. A. Saleev, Phys. Rev. D **79**, 034007 (2009); Phys. Rev. D **81**, 094010 (2010); B. A. Kniehl, D. V. Vasin, and V. A. Saleev, Phys. Rev. D **73**, 074022 (2006); Phys. Rev. D **74**, 014024 (2006); V. A. Saleev, M. A. Nefedov, A. V. Shipilova, Phys. Rev. D **85**, 074013 (2012).

Chapter 6

Theoretical considerations for the description of MPI

A new look at multiple parton collisions

Yuri L. Dokshitzer

LPTHE, Paris-VI, France and PNPI, Gatchina, Russia

DOI: <http://dx.doi.org/10.3204/DESY-PROC-2012-03/33>

Key ingredients of systematic QCD analysis of MPI are discussed.

1 Introduction

This contribution presents the QCD approach to studying MPI that I am involved in together with Boris Blok, Lonya Frankfurt and Mark Strikman. The basic new ideas of our approach have been announced in a short article [1]. A detailed pQCD analysis of the main contributions to double hard parton collisions, as well as evolution of the emerging generalized double parton distributions, $_2\text{GPD}$'s, can be found in [2].

An excess of *jets + photon* events in the back-to-back kinematics have signaled the presence of double parton collisions in the Tevatron experiments [3, 4, 5]. This phenomenon cannot be explained within a naive independent parton approximation. A model of two-proton correlations inside the proton that is capable of explaining the magnitude of the MPI contribution will be presented in [6].

Our approach to the problem of MPI is in certain sense opposite to that developed by Tevatron experiments. The CDF group in the pioneering study [3] has formulated a noble quest of extracting the MPI contribution without referring to either QCD theory or even to MC event generators. Such a puristic approach has successfully performed a noble task of establishing the presence of double hard collisions. However, it does not help much in developing the *theory* of the phenomenon that would stem from the first QCD principles at the “hard” end, and exploit known phenomenology of hadron interactions at the “soft” end. Meantime, such a theory is necessary for quantifying two-parton correlations in the proton and for better understanding of the underlying physics of collider experiments.

Following the pioneering work of Refs. [7, 8], a number of theoretical papers on multiparton interactions appeared in recent years [9, 10, 11, 12, 13]. They were based on the parton model and geometrical picture of collisions in the impact parameter space. This topic is being intensively discussed in view of the LHC program [14, 15]; Monte Carlo event generators that produce multiple parton collisions are being developed [16, 17, 18]. In our view, however, important elements of QCD that are necessary for theoretical understanding of the multiple hard interactions issue have not been properly taken into account by above-mentioned intuitive approaches.

More recently, theoretical papers exploring the nature and properties of double parton distributions and discussing their QCD evolution have appeared [1, 19, 20, 21].

The problem of theoretical approach to MPI is, sort of, educational: both the probabilistic picture, the MC generator technology is based upon, and even the Feynman diagram tech-

nique, when used in the momentum space, prove to be inadequate for careful analysis and understanding of the physics of multiple collisions.

2 Hidden reefs of MPI analysis

A careful approach to MPI phenomena uncovers a number of unconventional features.

Thus, in order to be able to trace the relative distance between the partons, one has to use the mixed longitudinal momentum–impact parameter representation which, in the momentum language, reduces to introduction of a mismatch between the transverse momentum of the parton in the amplitude and that of the same parton in the amplitude conjugated.

Another unusual feature of the multiple collision analysis may look confusing at the first sight. It is the fact that, even at the tree level, *the amplitude* describing the double hard interaction contains additional integrations over longitudinal momentum components; more precisely — over the difference of the (large) light-cone momentum components of the two partons originating from the same incident hadron (see Section 2.2).

2.1 Transverse structure

Cross section of two-parton collision can be cast in the following intuitively clear form:

$$d\sigma^{(h)} = \int d^2\rho_1 \int d^2\rho_2 f(x_1, \rho_1) f(x_2, \rho_2) \cdot d\sigma^{(p)}; \quad B = \rho_2 - \rho_1. \quad (1)$$

Here vectors ρ are the transverse positions of incident hadrons 1 and 2 with respect to the point where the two partons interact; their difference is the impact parameter of the hadron collision B . Local parton density f is the square of the wave function: $f(x_1, \rho_1) = \psi(x_1, \rho_1) \psi^\dagger(x_1, \rho_1)$, or, in the momentum representation,

$$f(x_1, \rho_1) = \int \frac{d^2k_{1\perp}}{(2\pi^2)} \psi(x_1, k_{1\perp}) \int \frac{d^2k'_{1\perp}}{(2\pi^2)} \psi^\dagger(x_1, k'_{1\perp}) \cdot e^{i\rho_1(k_{1\perp} - k'_{1\perp})}. \quad (2)$$

Substituting into (1) and integrating over transverse coordinates gives

$$\int \frac{d^2k_\perp}{(2\pi)^2} \psi(x, k_\perp) \int \frac{d^2k'_\perp}{(2\pi)^2} \psi^\dagger(x, k'_\perp) \times \int d^2\rho e^{i\rho(k_\perp - k'_\perp)} = \int \frac{d^2k_\perp}{(2\pi)^2} \psi(x, k_\perp) \psi^\dagger(x, k_\perp). \quad (3)$$

This shows that one could have written an answer for the cross section in terms of momenta from the start, treating incident objects as plane waves with given (longitudinal and transverse) momentum components.

The situation is different when two pairs of partons collide. Indeed, in this case the transverse coordinates of four partons are not independent but are related, see Fig. 1:

$$\rho_1 - \rho_3 = \rho_2 - \rho_4 = B.$$

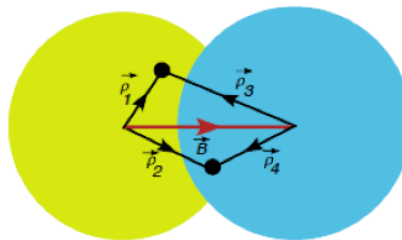


Figure 1: Geometry of four-parton collision

To see how this condition affects the momentum picture, we introduce inclusive two-parton probability density distribution, and turn to the momentum representation in analogy with Eq. (2).

$$D(x_1, x_2; \rho_1, \rho_2) = \sum_{n=3}^{\infty} \int \prod_{k=3}^n [d^2 \rho_k dx_k] \cdot \delta(\sum_{i=1}^n x_i \rho_i) \cdot \psi(x_1, \rho_1; x_2, \rho_2; x_3, \rho_3; \dots x_n, \rho_n) \psi^\dagger(x_1, \rho_1; x_2, \rho_2; x_3, \rho_3; \dots x_n, \rho_n), \quad (4)$$

Then, integrations over $(\rho_1 + \rho_2)$, $(\rho_3 + \rho_4)$ and $(\rho_1 - \rho_2) + (\rho_3 - \rho_4)$ produce, respectively,

$$k_{1\perp} - k'_{1\perp} = -(k_{2\perp} - k'_{2\perp}) \equiv \Delta, \quad k_{3\perp} - k'_{3\perp} = -(k_{4\perp} - k'_{4\perp}) \equiv \tilde{\Delta} \quad \text{and} \quad \tilde{\Delta} = -\Delta. \quad (5)$$

The presence of the relation

$$\rho_1 - \rho_3 - (\rho_2 - \rho_4) = 0$$

leaves the transverse momentum parameter Δ arbitrary.

We conclude that, in the language of momenta, a mismatch appears between transverse momenta of the parton in the wave function and the wave function conjugated. This mismatch is the same for all four participating partons as shown in Fig. 2.

Thus, the new variable Δ is an intrinsic part of the two-parton correlation function in momentum space, that was dubbed in [1] “the generalized double parton distribution”, ${}_2\text{GPD}$:

$$[2]D_h^{ab}(x_1, x_2; q_1^2, q_2^2; \Delta). \quad (6)$$

Here a, b mark parton species, h — the hadron, and q_1^2, q_2^2 (within the usual logic of parton distributions) stand for the corresponding “hardness scales”: the upper limits of (logarithmic) integrations over parton transverse momenta, $k_{1\perp}^2$ and $k_{2\perp}^2$. This is what concerns the transverse space structure.

2.2 Longitudinal structure

Now we shall look at *longitudinal momenta* of participating partons.

To elucidate the problem that one encounters here, it is instructive to examine the case when a parton “0” from one hadron virtually splits into two, “1”, “2”, whose offspring partons enter two hard interactions with partons “3” and “4” from the second hadron.

This situation is shown in Fig. 3, where black blobs mark two hard interactions that

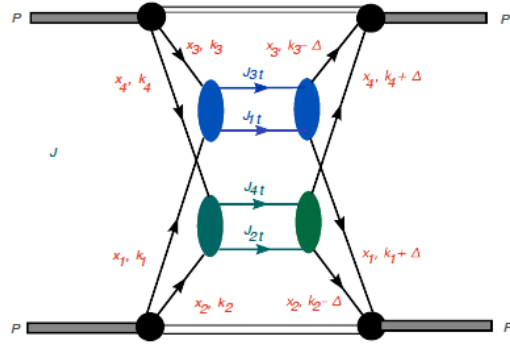


Figure 2: Shifts in parton momenta
“the generalized double parton distribution”, ${}_2\text{GPD}$:

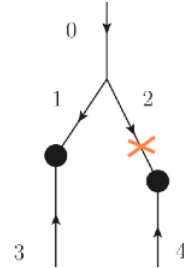


Figure 3: On-mass-shell singularity

produce some large mass final state systems (intermediate bosons, pairs of large transverse momentum jets, etc.).

Fig. 3 is a tree amplitude. This means that knowing the momenta of incident partons 0, 3, 4, and the 4-momenta of the produced final state systems Q_{13} and Q_{24} , one unambiguously determines the momenta of the virtual state partons 1 and 2.

The problem is, at certain values of longitudinal momenta of incident partons one of the intermediate partons can go *on mass shell*. For example, the parton line “2” in Fig. 3. The amplitude develops a strange singularity right inside the physical region of the external momenta ($k_0^2, k_3^2, k_4^2 \leq 0$, Q_{13}^2 and Q_{24}^2 positive).

This singularity has been discussed in the literature more than once (see, e.g., [22, 23]). However, to the best of my knowledge, its meaning and significance remained unclear before the explanation that we gave in [1].

Let us go back to the usual hard process picture, e.g., to DIS scattering. Consider perturbative splitting of an incident parton “0” into “1” and “2”, of which the former experiences hard scattering (gets hit by a lepton with a large momentum transfer Q^2), while the latter goes into the final state.

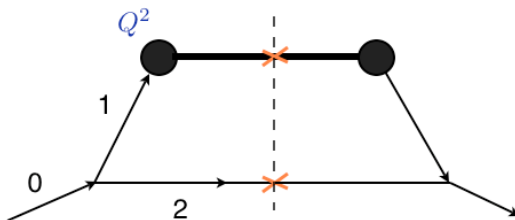


Figure 4: “On-mass-shell” partons in deep inelastic scattering

When calculating the DIS cross section (see Fig. 4) we put the parton “2” on mass shell and do not trace its fate. It may split developing a final state jet, it may propagate as a “real particle” at macroscopically large distances (confinement does not concern us here) and might eventually enter another hard interaction. This is exactly what happens with the diagram of Fig. 3 and where lies an explanation of the origin of that disturbing singularity.

What happens is the following. The singularity appears at definite momenta of incident particles and, in particular, of partons “3” and “4”. Definite momenta mean plain waves. But plain waves are not localized in space-time, so that the distance between the two hard interactions in Fig. 3 is not known and can be in fact arbitrarily large. If the hard scattering of “1” and “3” would occur in the LHC tunnel, and the collision of “2” and “4” — in, say, Gran Sasso, then the presence of the singularity is natural: it would correspond to free propagation of the particle “2” between Geneva and L’Aquila. Such a scenario is possible, but this is not what we are looking for: we intend instead to study the situation when “3” and “4” belong to the same proton!

To assure spatial localization inside one hadron, one has to construct a wave packet by smearing over the relative longitudinal momentum of the two partons. Importantly, the kinematics of the process determines only the *sum* of the light-cone momentum components ($\beta_3 + \beta_4$). So one is allowed — and has to — introduce an integration over the *difference* of the two momenta, $\beta_3 - \beta_4$, at the amplitude level. This smearing eliminates the singularity of the diagram Fig. 3:

the integral reduces to the residue at the pole of the propagator “2”.

3 Generalized double parton distributions

We have chosen to study production of two pairs of large transverse momentum jets as an example of double hard interaction. The corresponding cross section is conveniently represented as a product of cross sections of two independent collisions normalized by the factor S that has dimension of area:

$$\frac{d\sigma^{(4)}}{dt_1 dt_2} = \frac{d\sigma(x_1, x_2)}{dt_1} \frac{d\sigma(x_3, x_4)}{dt_2} \times \frac{1}{S}, \quad \frac{1}{S} = \frac{\int \frac{d^2\Delta}{(2\pi)^2} D(x_1, x_2; \Delta) D(x_3, x_4; -\Delta)}{D(x_1) D(x_2) D(x_3) D(x_4)}. \quad (7)$$

The quantity S is often referred to in the literature as “effective cross section”. However, a cross section, by definition, depends on *interaction strength*, while S characterizes transverse area of two-parton correlation in a hadron and longitudinal correlation between the partons (see [6])

$$\frac{d\sigma^{(4 \rightarrow 4)}}{dt_1 dt_2} \propto \left(\frac{\alpha_s^2}{Q^4} \right)^2 \cdot R^{-2} = \frac{\alpha_s^4}{R^2 Q^8} = \frac{\alpha_s^4}{Q^6} \cdot \frac{1}{R^2 Q^2} \propto \frac{d\sigma^{(2 \rightarrow 4)}}{dt_1 dt_2} \cdot \frac{1}{R^2 Q^2}. \quad (8)$$

So, this cross section turns out to be *power suppressed* as compared with that of the $2 \rightarrow 4$ jet production mechanism when one gets *four jets* out of 2-parton collision at an expense of two additional QCD emissions, $d\sigma^{(2 \rightarrow 4)}$.

3.1 4- and 3-parton collisions

The value of the correlation radius is determined by convergence properties of the Δ integral in (7). If two partons are taken directly from the non-perturbative hadron wave function, ${}_2\text{GPD}={}_{[2]}D(x_1, x_2)$, the correlation area is of the order of the transverse size of the hadron.

There is an additional contribution to the MPI cross section due to collision of *three* partons. In this case the numerator of (7) has a mixed structure:

$${}_{[1]}D(x_1, x_2; \Delta) {}_{[2]}D(x_3, x_4; -\Delta) + {}_{[2]}D(x_1, x_2; \Delta) {}_{[1]}D(x_3, x_4; -\Delta).$$

Here ${}_{[1]}D$ stands for 2-parton distribution involving *perturbative* parton splitting, as in the upper part of Fig 3. Being a small-distance correlation, ${}_{[1]}D$ depends on Δ only logarithmically (via parton evolution effects). As a result, the Δ integration in (7) becomes broader. In spite of this *geometrical enhancement*, the $3 \rightarrow 4$ contribution turns out to be numerically small at Tevatron energies ($x > 10^{-3}$) but may become significant at the LHC [6].

Evolution equations that incorporate into ${}_2\text{GPDs}$ all-order radiative QCD effects in the leading collinear approximation are described in [2].

3.2 A four-parton or a two-parton collision?

There were discussions in the literature whether the process of double parton splitting shown in Fig. 5 should be looked upon as a 4-parton collision.

On the one hand, it looks indeed as two hard interactions of four partons. On the other hand, such a diagram naturally appears as a loop correction to a “normal” $2 \rightarrow 4$ QCD process when one goes beyond the tree approximation. The question of potential *double counting* was raised.

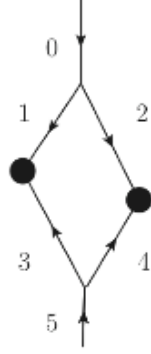


Figure 5: Loop in a double hard process

The process displayed in Fig. 5 is a “product” of two small-distance correlations, ${}_{[1]}D(x_1, x_2){}_{[1]}D(x_3, x_4)$. Since ${}_{[1]}D$ practically does not depend on Δ , the integral in (7) formally diverges.

This means that this double hard interaction is not a MPI, in our interpretation ([1, 2]). It lacks a characteristic feature of MPI, namely a power enhancement of the differential cross section in the back-to-back kinematics, $Q_{13}^2, Q_{24}^2 \ll Q^2$ (see below).

This is a loop correction that belongs to $2 \rightarrow 4$ background and has to be subtracted in a search for MPI.

3.3 Modeling ${}_2\text{GPD}$

The first natural step is an *approximation of independent partons*, which allows one to relate ${}_2\text{GPD}$ with known objects, namely

$$D(x_1, x_2, q_1^2, q_2^2; \Delta) \simeq G(x_1, q_1^2; \Delta)G(x_2, q_2^2; \Delta). \quad (9)$$

Here G is the non-forward parton correlator (known as generalized parton distribution, GPD) that determines, e.g., hard vector meson production at HERA (Fig. 6).

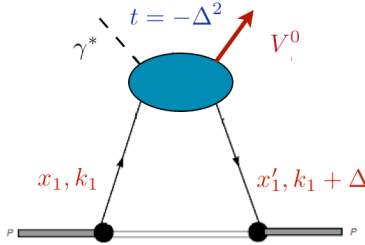


Figure 6: GPD in VM electroproduction

The GPD, on its turn, can be modeled as

$$G(x_1, q_1^2; \Delta) \simeq D(x_1, q_1^2) \times F_{2g}(\Delta^2), \quad (10)$$

with D — usual one-parton distribution determining DIS structure functions and F — the two-gluon form factor of the hadron.

The latter is a non-perturbative object; it falls fast with the “momentum transfer” Δ^2 .

This form factor can be parametrized differently, for example, by a dipole formula:

$$F_{2g}(\Delta^2) = \left(1 + \frac{\Delta^2}{m_g^2}\right)^{-2}. \quad (11)$$

Here m_g^2 is an effective parameter whose value extracted from HERA data lies in the ballpark of $m_g^2(x \sim 0.03, Q^2 \sim 3 \text{ GeV}^2) \simeq 1.1 \text{ GeV}^2$.

A simplistic approximation of independent partons does not answer the call: it fails to explain a factor 2 enhancement of back-to-back 4-jet production observed by Tevatron experiments [3, 4]. So, intra-hadron correlations between partons have to be taken into account. One does not know much about them a priori. However, certain information about non-perturbative 2-parton correlations can be extracted from phenomenology of *inelastic diffraction*, which allows one to construct a viable model for the ${}_2\text{GPD}$ of a nucleon [6].

4 Differential distribution in back-to-back kinematics

Four-parton interaction is a “higher twist” eventuality. The fact that the total MPI cross section is *power suppressed* as compared with the $2 \rightarrow 4$ cross section does not mean that $4 \rightarrow 4$ and $3 \rightarrow 4$ collisions are impossible to access at high Q^2 .

There is an essential difference between the two 4-jet production mechanisms. Namely, in $2 \rightarrow 4$ processes the final jets form a “*hedgehog*”, while double parton collisions, $4 \rightarrow 4$, produce two pairs of nearly *back-to-back jets*. Actually, in the *back-to-back kinematics* the two channels become comparable.

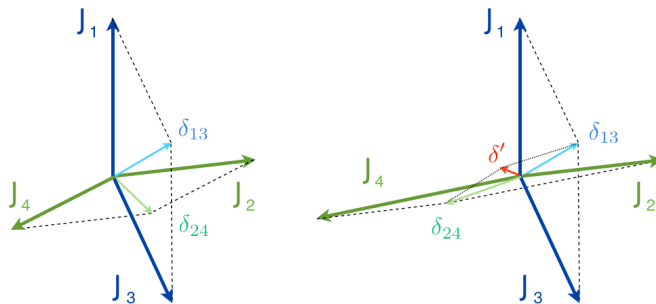


Figure 7: Enhanced kinematical configurations of four jets

Differential distributions due to $4 \rightarrow 4$ and $3 \rightarrow 4$ processes exhibit *double collinear enhancement*: they peak at small *jet imbalances*, $\delta_{ik}^2 \ll p_{i\perp}^2 \simeq p_{k\perp}^2$, Fig. 7.

$$\frac{d\sigma}{dt_1 dt_2 d^2\delta_{13} d^2\delta_{24}} \Big/ \frac{d\sigma}{dt_1 dt_2} \propto \frac{\alpha_s^2}{\delta_{13}^2 \delta_{24}^2}, \quad \delta_{ik} = p_{i\perp} + p_{k\perp}; \quad (12a)$$

$$\frac{d\sigma}{dt_1 dt_2 d^2\delta_{13} d^2\delta_{24}} \Big/ \frac{d\sigma}{dt_1 dt_2} \propto \frac{\alpha_s^2}{\delta'^2 \delta^2}, \quad \delta^2 = \delta_{13}^2 \simeq \delta_{24}^2 \gg (\delta_{13} + \delta_{24})^2 \equiv \delta'^2. \quad (12b)$$

Structure of singularities displayed in (12a) — independent enhancements in two pair imbalances — is typical for $4 \rightarrow 4$ processes.

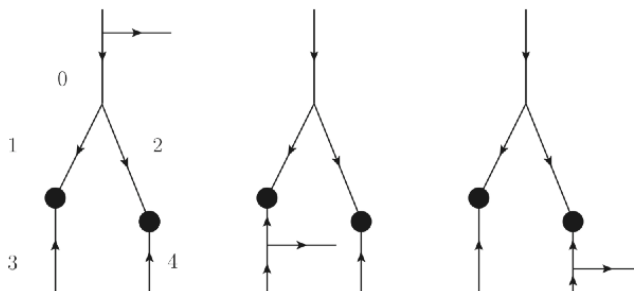


Figure 8: Origin of δ'^2 singularity in Eq. (12b)

The “end-point” contributions due to $3 \rightarrow 4$ configurations with no QCD emissions between the parton splitting ($0 \rightarrow 1 + 2$ in Fig. 8) and the two hard vertices is enhanced as (12b).

Singularities in Eqs. (12) get smeared by double logarithmic Sudakov form factors of the partons involved, depending on ratios of proper scales, see [2].

5 Conclusions

The QCD approach to MPI leads to the notion of generalized double parton distributions, ${}_2$ GPDs. Higher order logarithmic QCD corrections to ${}_2$ GPDs can be assembled via parton evolution equations derived in [1, 2] in the leading collinear approximation. Detailed formulae for total cross sections and differential distributions of four jet production in the back-to-back kinematics can be found in [2].

In order to reliably extract MPI contributions and get hold of parton correlations inside nucleon, one has to use a different strategy from that developed and promoted by Tevatron experiments [3, 4, 5]. Tevatron methods were based on measurement of *angular* correlations between jet imbalance momenta proposed in [24]. Such characteristics, however, are sensitive to non-perturbative physics and are strongly affected by experimental efficiencies of jet reconstruction. They are difficult (if at all possible) to control theoretically and should be replaced by studies of correlations in transverse momenta rather than angles.

References

- [1] B. Blok, Yu. Dokshitzer, L. Frankfurt and M. Strikman, Phys. Rev. D **83** (2011) 071501 [arXiv:1009.2714 [hep-ph]].
- [2] B. Blok, Yu. Dokshitzer, L. Frankfurt and M. Strikman, arXiv:1106.5533v2 [hep-ph].
- [3] CDF Collaboration, Phys. Rev. D **56** (1997) 3811.
- [4] D0 Collaboration, Phys. Rev. D **81** (2010) 052012 [arXiv:0912.5104 [hep-ex]].
- [5] D0 Collaboration, Phys. Rev. D **83** (2011) 052008 [arXiv:1101.1509 [hep-ex]].
- [6] B. Blok, Yu. Dokshitzer, L. Frankfurt and M. Strikman, [arXiv:1206.5594 [hep-ph]].
- [7] N. Paver and D. Treleani, Z. Phys. C **28** (1985) 187.
- [8] M. Mekhfi, Phys. Rev. D **32** (1985) 2371.
- [9] A. Del Fabbro and D. Treleani, Phys. Rev. D **61** (2000) 077502 (2000) [arXiv:hep-ph/9911358]; Phys. Rev. D **63** (2001) 057901 [arXiv:hep-ph/0005273];
A. Accardi and D. Treleani, Phys. Rev. D **63** (2001) 116002 [arXiv:hep-ph/0009234].
- [10] S. Domdey, H. J. Pirner and U. A. Wiedemann, Eur. Phys. J. C **65** (2010) 153 [arXiv:0906.4335 [hep-ph]].
- [11] L. Frankfurt, M. Strikman and C. Weiss, Phys. Rev. D **69** (2004) 114010 [arXiv:hep-ph/0311231]; Ann. Rev. Nucl. Part. Sci. **55** (2005) 403 [arXiv:hep-ph/0507286].
- [12] L. Frankfurt, M. Strikman, D. Treleani and C. Weiss, Phys. Rev. Lett. **101** (2008) 202003 [arXiv:0808.0182 [hep-ph]].
- [13] T. C. Rogers, A. M. Stasto and M. I. Strikman, Phys. Rev. D **77** (2008) 114009 [arXiv:0801.0303 [hep-ph]].
- [14] Proceedings of the 1st International Workshop on Multiple Partonic Interactions at the LHC, Verlag Deutsches Elektronen Synchrotron (2010).
- [15] P. Bartalini and L. Fano, arXiv:1103.6201 [hep-ex].
- [16] for a recent summary see T. Sjostrand and P. Z. Skands, Eur. Phys. J. C **39** (2005) 129 [arXiv:hep-ph/0408302].
- [17] for a recent summary see M. Bahr *et al.*, Eur. Phys. J. C **58** (2008) 639 [arXiv:0803.0883 [hep-ph]].

- [18] C. Flensburg, G. Gustafson, L. Lonnblad and A. Ster, arXiv:1103.4320 [hep-ph].
- [19] M. Diehl, PoS D **IS2010** (2010) 223 [arXiv:1007.5477 [hep-ph]].
- [20] M. Diehl and A. Schafer, Phys. Lett. B **698** (2011) 389 [arXiv:1102.3081 [hep-ph]].
- [21] M. G. Ryskin and A. M. Snigirev, arXiv:1103.3495 [hep-ph].
- [22] J. R. Gaunt and W. J. Stirling, JHEP **1003** (2010) 005 [arXiv:0910.4347 [hep-ph]];
J. R. Gaunt, C. H. Kom, A. Kulesza and W. J. Stirling, Eur. Phys. J. C **69** (2010) 53 [arXiv:1003.3953 [hep-ph]].
- [23] J. R. Gaunt and W. J. Stirling, arXiv:1103.1888 [hep-ph].
- [24] E. L. Berger, C. B. Jackson, G. Shaughnessy, Phys. Rev. D **81** (2010) 014014 [arXiv:0911.5348 [hep-ph]].

Single and double perturbative splitting diagrams in double parton scattering

Jonathan R. Gaunt^{1*}, W. James Stirling¹

¹Cavendish Laboratory, J J Thomson Avenue, Cambridge CB3 0HE, UK

DOI: <http://dx.doi.org/10.3204/DESY-PROC-2012-03/30>

We discuss the role of two different types of diagram in the proton-proton double parton scattering (DPS) cross section – single and double perturbative splitting graphs. Using explicit calculations of simple graphs from these classes we show that the treatment of these graphs by the ‘double PDF’ framework for describing the DPS cross section, introduced a number of years ago by Snigirev and collaborators, is unsatisfactory. We suggest that a contribution from single perturbative splitting graphs should be included in the DPS cross section, albeit with a different geometrical prefactor to the contribution from ‘zero perturbative splitting’ graphs.

1 ‘Double perturbative splitting’ diagrams in double parton scattering

We define double parton scattering (DPS) as the process in which two pairs of partons participate in hard interactions in a single proton-proton (p-p) collision. DPS processes can constitute important backgrounds to Higgs and other interesting signals (see e.g. [1]), and can themselves be considered as interesting signal processes, since they reveal information about parton pair correlations in the proton.

Making the assumption that the hard processes A and B may be factorised, the cross section for p-p DPS may be written as follows:

$$\sigma_{(A,B)}^D \propto \sum_{i,j,k,l} \int \prod_{a=1}^4 dx_a d^2\mathbf{b} \hat{\sigma}_{ik \rightarrow A}(\hat{s} = x_1 x_3 s) \hat{\sigma}_{jl \rightarrow B}(\hat{s} = x_2 x_4 s) \quad (1)$$
$$\times \Gamma_{ij}(x_1, x_2, \mathbf{b}; Q_A^2, Q_B^2) \Gamma_{kl}(x_3, x_4, \mathbf{b}; Q_A^2, Q_B^2)$$

The cross section formula is somewhat similar to that used for single parton scattering (SPS), except that two parton-level cross sections $\hat{\sigma}$ appear, and the PDF factors are two-parton generalised PDFs Γ (2pGPDs) rather than single PDFs. Note that in this formula the two 2pGPDs are integrated over a common parton pair transverse separation \mathbf{b} .

In many extant studies of DPS, it is assumed that the 2pGPD can be approximately factorised into a product of a longitudinal piece and a (typically flavour and scale independent) transverse piece:

$$\Gamma_{ij}(x_1, x_2, \mathbf{b}; Q_A^2, Q_B^2) \simeq D_p^{ij}(x_1, x_2; Q_A^2, Q_B^2) F(\mathbf{b}) \quad (2)$$

*Speaker

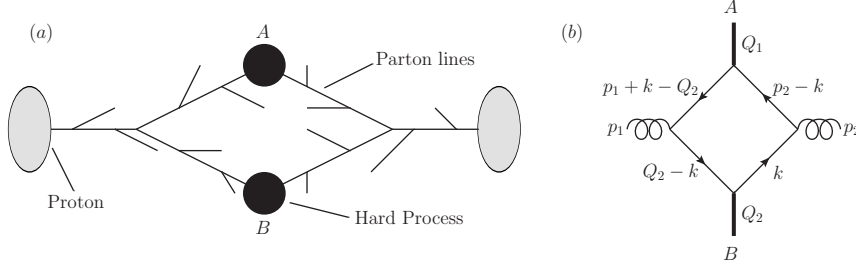


Figure 1: (a) A diagram that apparently contributes to the leading order DPS cross section according to the framework of [3]. The partons emerging from the grey proton blobs in the figure are nonperturbatively generated partons – i.e. ones existing at a low scale $\sim \Lambda_{QCD}$. (b) The ‘crossed box’ graph. In this part of the figure, A and B are arbitrary single particle final states with $Q_1^2 = Q_2^2 = Q^2 > 0$.

Then, if one introduces the quantity σ_{eff} via $\sigma_{eff} \equiv 1/[\int F(\mathbf{b})^2 d^2\mathbf{b}]$, one finds that one may write $\sigma_{(A,B)}^D$ entirely in terms of the longitudinal piece and σ_{eff} :

$$\sigma_{(A,B)}^D \propto \frac{1}{\sigma_{eff}} \sum_{i,j,k,l} \int \prod_{a=1}^4 dx_a D_p^{ij}(x_1, x_2; Q_A^2, Q_B^2) D_p^{kl}(x_3, x_4; Q_A^2, Q_B^2) \hat{\sigma}_{ik \rightarrow A} \hat{\sigma}_{jl \rightarrow B} \quad (3)$$

In [2] a quantity $D_p^{ij}(x_1, x_2; Q^2)$ is introduced, and an evolution equation for this quantity is given. We shall refer to the quantity and its evolution equation as the double PDF (dPDF) and the dDGLAP equation respectively. It is asserted in [3] that the dPDF is equal to the factorised longitudinal part of the 2pGPD in the case in which the two hard scales Q_A^2 and Q_B^2 are equal to a common value Q^2 .

The dDGLAP equation contains two types of terms on the right hand side – ‘independent branching’ terms corresponding to emission of partons from a pre-existing pair, and ‘single parton feed’ terms corresponding to the perturbative generation of a pair from the splitting of a single parton. The single feed terms involve the leading twist single parton distributions as one might expect. Given this structure of the dDGLAP equation, with single feed terms included on the right hand side, a prediction of the ‘dPDF framework’ suggested in [3] for calculating the p-p DPS cross section is that a part of the ‘double perturbative splitting’ or ‘1v1’ graph drawn in figure 1(a) should be included in the LO p-p DPS cross section. The part that should be included is proportional to $[\log(Q^2/\Lambda^2)]^n/\sigma_{eff}$ at the cross section level, where Λ is some IR cutoff of order Λ_{QCD} , and n is equal to the total number of QCD branchings in figure 1(a) (including the two that only produce internal particles). This piece should be associated with the region of transverse momentum integration for the graph in which the transverse momenta of the branchings on either side of the ‘hard processes’ in the graph are strongly ordered.

The question that then arises is whether such a structure in fact exists in the cross section expression for the loop of figure 1(a). Starting from the conventional ‘Feynman rules’ expression for the loop, it is not immediately obvious what the answer to this question is. Here we will focus on answering this question for the specific very simple ‘crossed box’ loop shown in figure 1(b), which is predicted by the dPDF framework to contain a piece proportional to $[\log(Q^2/\Lambda^2)]^2/\sigma_{eff}$. The issues raised in the treatment of this example carry over to the more general loop of figure 1(a).

We expect the $[\log(Q^2/\Lambda^2)]^2/\sigma_{eff}$ piece in figure 1(b) to be predominantly contained in the portion of the cross section integration in which the external transverse momenta, as well as the transverse momenta and virtualities of the internal particles, are all small. This is actually the region around a certain pinch singularity in the loop integral known as the double parton scattering singularity [4]. In [5], we obtained an analytic expression for the part of an arbitrary loop containing a DPS singularity associated with the loop particles emerging from the initial state particles being nearly on-shell and collinear, in the limit in which the external transverse momenta are small. Applied to the loop of figure 1(b) this reads (schematically, suppressing helicity and colour labels):

$$L_{DPS, \text{fig 1(b)}} \propto \frac{1}{Q^2} \int d^2\mathbf{k} \Phi_{g \rightarrow q\bar{q}}(x, \mathbf{k} - \mathbf{Q}_2) \Phi_{g \rightarrow \bar{q}q}(1-x, -\mathbf{k}) \quad (4)$$

$$\times \mathcal{M}_{q\bar{q} \rightarrow A}(\hat{s} = x(1-x)s) \mathcal{M}_{q\bar{q} \rightarrow B}(\hat{s} = x(1-x)s) + (q \leftrightarrow \bar{q})$$

In this formula, $x = p_2 \cdot Q_1/p_1 \cdot p_2$, $s = (p_1 + p_2)^2$, and \mathbf{k} (\mathbf{Q}_2) is the component of k (Q_2) transverse to the axis defined by the directions of the incoming particles. $\Phi_{g \rightarrow q\bar{q}}(x, \mathbf{k})$ is the $\mathcal{O}(\alpha_S)$ light cone wavefunction (LCWF) to produce a $q\bar{q}$ pair from a g [6], with the quark having lightcone momentum fraction x and transverse momentum \mathbf{k} with respect to the parent gluon. It can be factored into a \mathbf{k} and x dependent part, where the \mathbf{k} dependent part is proportional to $\epsilon \cdot \mathbf{k}/\mathbf{k}^2$, ϵ being the transverse part of the gluon polarisation vector. It is generally true that any QCD $1 \rightarrow 2$ splitting with physically polarised external particles has a corresponding LCWF that is proportional to $1/\mathbf{k}$. Provided one uses a physical gauge for the gluon, all LCWFs corresponding to a $1 \rightarrow 2$ QCD splitting are then proportional to $1/\mathbf{k}$.

Inserting (4) into the standard $2 \rightarrow 2$ cross section expression, and performing a number of changes of variable, we arrive at the following expression for the DPS singular part of the $gg \rightarrow AB$ cross section:

$$\sigma_{DPS, \text{fig 1(b)}} \propto \int \prod_{i=1}^2 dx_i d\bar{x}_i \hat{\sigma}_{q\bar{q} \rightarrow A}(\hat{s} = x_1 \bar{x}_1 s) \hat{\sigma}_{q\bar{q} \rightarrow B}(\hat{s} = x_2 \bar{x}_2 s) \quad (5)$$

$$\times \int \frac{d^2\mathbf{r}}{(2\pi)^2} \Gamma_{g \rightarrow q\bar{q}}(x_1, x_2, \mathbf{r}) \Gamma_{g \rightarrow \bar{q}q}(\bar{x}_1, \bar{x}_2, -\mathbf{r})$$

$$\Gamma_{g \rightarrow q\bar{q}}(x_1, x_2, \mathbf{r}) \propto \frac{\alpha_S}{2\pi} \delta(1 - x_1 - x_2) T^{ij}(x_1, x_2) \int^{\mathbf{k}^2 < \mathcal{O}(Q^2)} d^2\tilde{\mathbf{k}} \frac{[\tilde{\mathbf{k}} + \frac{1}{2}\mathbf{r}]^i [\tilde{\mathbf{k}} - \frac{1}{2}\mathbf{r}]^j}{[\tilde{\mathbf{k}} + \frac{1}{2}\mathbf{r}]^2 [\tilde{\mathbf{k}} - \frac{1}{2}\mathbf{r}]^2}. \quad (6)$$

$T^{ij}(x_1, x_2)$ contains a function of x_1 and x_2 that may be regarded as a ‘ $1 \rightarrow 2$ ’ splitting function, multiplied by a constant matrix in transverse space¹. \mathbf{r} is equal to the transverse momentum imbalance of one of the quarks/antiquarks in the loop between amplitude and conjugate, and is the Fourier transform of the parton pair separation \mathbf{b} in the $q\bar{q}$ pair emerging from either gluon. $\Gamma_{g \rightarrow q\bar{q}}(x_1, x_2, \mathbf{r})$ can therefore be thought of as the $\mathcal{O}(\alpha_S)$ transverse momentum-space 2pGPD to find a $q\bar{q}$ pair inside a gluon. Note that the expression here effectively coincides with that of [7], in which a cross section expression for the box of 1(b) is obtained starting from a pure DPS view of the box.

¹Note that the cross section is really a sum of terms with different $T^{ij}(x_1, x_2)$ factors in the $g \rightarrow q\bar{q}$ 2pGPDs. This is associated with the fact that, from the point of view of the quarks, there is an unpolarised diagonal contribution to the process plus polarised and interference contributions in colour, spin, and flavour space. See e.g. [7, 8] for a discussion of correlation and interference effects in DPS processes.

Let us consider the part of the integral (5) that is associated with the magnitude of the imbalance \mathbf{r} being smaller than some small cut-off Λ that is of the order of Λ_{QCD} . The contribution to the cross section from this portion contains a $\log^2(Q^2/\Lambda^2)$ factor multiplied by Λ^2 (which can be thought of as an effective ‘ $1/\sigma_{eff}$ ’ factor for this contribution). The majority of this contribution comes from the region in which the transverse momenta and virtualities of the quarks and antiquarks in the $gg \rightarrow AB$ loop are much smaller in magnitude than $\sqrt{Q^2}$ (i.e. the region in which the assumptions used to derive (4) apply), which is a necessary feature of a contribution to be able to regard it as a DPS-type contribution. By making a specific choice of Λ (let us call this Λ_S), one could obtain an expression which is exactly in accord with the expectations of [3] – that is, a product of two large DGLAP logarithms multiplied by the same $1/\sigma_{eff}$ factor that appears in diagrams in which the parton pair from neither proton has arisen as a result of one parton perturbatively splitting into two (‘ $2v2$ ’ or ‘zero perturbative splitting’ diagrams). The $1/\sigma_{eff}$ factor for the $2v2$ diagrams presumably has a natural value of the order of $1/R_p^2$ that is set by the nonperturbative dynamics ($R_p =$ proton radius).

The fact that we have to make a somewhat arbitrary choice for Λ in order to arrive at the result anticipated by the dPDF framework is concerning. There is nothing in the calculation of figure 1(b) to indicate that we should take the region of it with $|\mathbf{r}| < \Lambda_S$ as the ‘DPS part’ – the scale Λ_S does not naturally appear at any stage of the calculation. There is no more justification for taking the part of the box with $|\mathbf{r}| < \Lambda_S$ to be the DPS part than there is for, say, taking the piece with $|\mathbf{r}| < 2\Lambda_S$, or that with $|\mathbf{r}| < \Lambda_S/2$, to be the DPS part.

There therefore appear to be some unsatisfactory features of the dPDF framework with regards to its treatment of the box in figure 1(b). In a physical gauge, precisely the same issues will be encountered for the case of the arbitrary ‘ $1v1$ ’ graph in figure 1(a). One obtains a result that is consistent with the dPDF framework if one demarcates the portion of the cross section integral in which the transverse loop momentum imbalance between amplitude and conjugate is less than Λ_S as DPS, but there is no natural reason to do this. There is no distinct piece of figure 1(a) that contains a natural scale of order Λ_{QCD} and is associated with the transverse momenta inside the loop being strongly ordered on either side of the diagram. In fact, most of the contribution to the total cross section expression for the graph comes from the region of integration in which the transverse momenta of particles inside the loop are of $\mathcal{O}(\sqrt{Q^2})^2$. This fact suggests that at the level of total cross sections, we should perhaps remove ‘ $1v1$ ’ graphs entirely from the DPS contribution, and regard them as pure SPS (this approach is advocated in [10], for both the total and the differential cross sections). Treating the graphs in this way would have the advantage that we would not perform any double counting between DPS and SPS – the graph of figure 1(a) is in principle also included in the SPS $pp \rightarrow AB$ cross section (albeit as a very high order correction that will not be included in practical low order calculations, if the number of QCD emissions from inside the loop of the graph is large).

Very similar conclusions may be reached if one uses a covariant gauge such as the Feynman gauge for the gluon fields in figure 1(a), although these conclusions are perhaps not obtained so readily. In a covariant gauge, gluons with unphysical ‘scalar’ polarisation can exist in loop diagrams. Such scalar-polarised gluons can give rise to power-law DPS divergences rather than logarithmic ones, and additional ‘super-leading’ contributions to the AB production process (in terms of powers of Q) – the two phenomena are related. On the other hand one generally

²One should bear in mind however that the same is not true for the cross section expression differential in the transverse momenta of A and B for $p_{T,A}^2, p_{T,B}^2 \ll Q^2$. Here, the major contribution is associated with transverse momenta in the loop $\ll \sqrt{Q^2}$ if there is one emission or more from inside the loop, or with a range of transverse momenta between $\sim |p_{T,A}|, |p_{T,B}|$ and $\sim \sqrt{Q^2}$ if there are no such emissions [8].

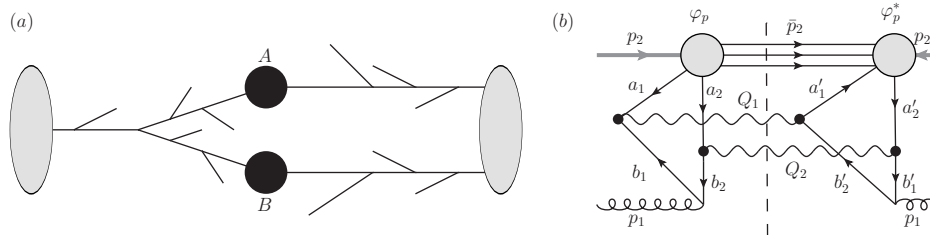


Figure 2: (a) A generic graph from the ‘2v1’ class. (b) A simple ‘2v1’ graph in which a gluon splits into a $q\bar{q}$ pair, and these partons then interact in two separate Drell-Yan interactions with a ‘nonperturbatively generated’ $q\bar{q}$ pair from a proton.

expects the ‘super-leading’ contribution to cancel in a suitable sum over graphs (as in [9]), which effectively leaves one with the same logarithmic DPS divergences that are encountered in a physical gauge.

One can gain some insight into the source of the problems in the dPDF framework by looking at the \mathbf{b} -space 2pGPD corresponding to (6). This comes out as being proportional to $1/\mathbf{b}^2$ – this behaviour (which was first spotted in [7]) can be traced to the fact that the $g \rightarrow q\bar{q}$ LCWF in \mathbf{b} space (like any any LCWF corresponding to a QCD $1 \rightarrow 2$ splitting with physically polarised external particles) is proportional to $1/\mathbf{b}$, and $\Gamma(\mathbf{b}) \sim \Phi(\mathbf{b})^2$. Note that this behaviour is very different from the behaviour of all 2pGPDs that is anticipated by the dPDF framework (i.e. smooth function of size R_p). There is no natural feature in the product of two ‘perturbative splitting’ 2pGPDs that is of size R_p and can be naturally identified as DPS. A key error then in the formulation of the dPDF framework seems to be the assumption that all 2pGPDs can be approximately factorised into dPDFs and smooth transverse functions of size R_p . A sound theoretical framework for describing p-p DPS needs to carefully take account of the different \mathbf{b} dependence of pairs of partons emerging from perturbative splittings, whilst simultaneously avoiding double counting between SPS and DPS.

2 ‘Single perturbative splitting’ diagrams

Aside from the ‘1v1’ graphs that were the focus of the previous section, and the ‘2v2’ graphs that were also briefly mentioned, there is a further class of graph that can potentially contribute to the p-p DPS cross section. These are graphs in which one proton provides one parton to the double scattering, and the other two, at the nonperturbative level – a representative graph is sketched in figure 2(a). For obvious reasons, we will refer to the graphs as ‘2v1’ or ‘single perturbative splitting’ graphs.

It seems clear that we should include contributions from the 2v2 graphs as part of the DPS cross section. An important question is whether we should also include contributions from the 2v1 graphs, and if so, what form these contributions should take (in particular, how does the effective σ_{eff} factor for the 2v1 graphs differ from that for the 2v2 graphs?).

To answer this question, let us take a similar approach as we did for the 1v1 graphs in the previous section. That is, we take the graph drawn in figure 2(b) that has the simplest possible 2v1 structure, and see whether there is a ‘natural’ part of the cross section expression for it that is proportional to $1/R_p^2$, and also contains a large logarithm associated with the $1 \rightarrow 2$

splitting. If there is such a structure in the 2v1 graph, then this part of this graph should be included in the LO DPS cross section, and we also expect there to be a $\log(Q^2/\Lambda^2)^n/R_p^2$ piece in the more general 2v1 diagram of figure 2(a) that should also be included in the LO DPS cross section.

In the calculation of the cross section for figure 2(b), it is necessary to include a hadronic amplitude or wavefunction factor ψ_p to find two nonperturbatively generated (‘independent’) partons in the proton, at the amplitude level in the calculation. It would be inappropriate to try and calculate a 2v1 cross section in a naive ‘fully parton-level’ way omitting the proton on the ‘nonperturbative pair’ side because then one has three particles in the initial state (whereas the standard framework for calculating a cross section requires two particles in the initial state). Furthermore, by deleting the proton on the ‘nonperturbative pair’ side one is then neglecting the important fact that the nonperturbatively generated partons are tied together in the same proton (as was pointed out in [10]). The use of proton wavefunctions or hadronic amplitudes in the calculation of DPS-type graphs was discussed long ago in [11], and has been discussed more recently in [8, 10].

After a lengthy calculation, one finds that the cross section for figure 2(b) contains the following expression:

$$\begin{aligned} \sigma_{1v2}(s) &= \hat{\sigma}_{\bar{q}q \rightarrow \gamma^*}(\hat{s} = x_1 y_1 s) \hat{\sigma}_{q\bar{q} \rightarrow \gamma^*}(\hat{s} = x_2 y_2 s) \\ &\times \frac{m}{2} \left[\int \frac{d^2 \mathbf{r}}{(2\pi)^2} \Gamma_{p;q\bar{q}}(x_1, x_2; \mathbf{r}) \right] \left[\frac{\alpha_s}{2\pi} P_{g \rightarrow q\bar{q}}(y_2) \delta(1 - y_1 - y_2) \int_{\Lambda^2}^{Q^2} \frac{d\mathbf{Q}_1^2}{\mathbf{Q}_1^2} \right] \end{aligned} \quad (7)$$

In this expression we have omitted helicity and colour labels and sums for simplicity. The quantity $\Gamma_{p;q\bar{q}}(x_1, x_2; \mathbf{r})$ is the 2pGPD of the nonperturbatively generated parton pair, whilst $P_{g \rightarrow q\bar{q}}$ is the LO $1 \rightarrow 2$ splitting function for the process $g \rightarrow q\bar{q}$. m is a symmetry factor that is equal to 1 if the two hard processes are the same, and is equal to 2 otherwise (for the double Drell-Yan process under consideration, it equals 1).

The integral over \mathbf{Q}_1 in (7) gives rise to a large transverse momentum logarithm $\log(Q^2/\Lambda^2)$, whilst the integral over \mathbf{r} supplies a prefactor of order $\Lambda^2 \sim 1/R_p^2$ (we assume $\Gamma_{p;q\bar{q}}(\mathbf{r})$ only has support for $|\mathbf{r}|$ values of order Λ_{QCD} – see later). Thus, there is a part of the cross section expression for figure 2(b) that is proportional to $\log(Q^2/\Lambda^2)/R_p^2$ and should be included in the LO DPS cross section.

When we generalise the result (7) to the leading logarithmic part of the arbitrary 2v1 diagram in figure 2(a), and then sum up all of the diagrams to obtain the contribution of 2v1 graphs to the LO DPS cross section, then we obtain the result below³:

$$\begin{aligned} \sigma_{(A,B)}^{D,1v2}(s) &= 2 \times \frac{m}{2} \int dx_1 dx_2 dy_1 dy_2 \hat{\sigma}_{ik \rightarrow A}(\hat{s} = x_1 y_1 s) \hat{\sigma}_{jl \rightarrow B}(\hat{s} = x_2 y_2 s) \\ &\times \check{D}_p^{ij}(x_1, x_2; Q^2) \int \frac{d^2 \mathbf{r}}{(2\pi)^2} \Gamma_{p, indep}^{kl}(y_1, y_2, \mathbf{r}; Q^2) \end{aligned} \quad (8)$$

The quantity $\check{D}_p^{ij}(x_1, x_2; Q^2)$ is the ‘accumulated sPDF feed’ contribution to the dPDF. This evolves from a zero initial value at a nonperturbative scale $Q_0 \sim \Lambda_{QCD}$ according to the full

³Note that for simplicity we take the two hard scales to be equal here, $Q_A^2 = Q_B^2 = Q^2$, and only write down the unpolarised diagonal contribution in colour, flavour and spin space. The contributions associated with spin polarisation (longitudinal or transverse) are expected to have a similar structure. On the other hand, it is known that the colour and quark number interference contributions will contain Sudakov logarithms – see e.g. [7, 8].

dDGLAP equation. $\Gamma_{p,ind\epsilon}^{kl}(y_1, y_2, \mathbf{r}; Q^2)$ is the ‘independent branching’ 2pGPD. This sums up the effect of independent strongly ordered parton emissions from a nonperturbatively generated parton pair. It evolves according to the dDGLAP equation with the sPDF feed term removed. There is an additional prefactor of 2 in (8) because there are two sets of 1v2 graphs that give equivalent contributions – in one set the nonperturbatively generated parton pair emerges from the ‘left’ proton, whilst in the other it emerges from the ‘right’ proton.

A critical requirement for the derivations of (7) and (8) to be valid is that parton pairs connected only via nonperturbative interactions should have an \mathbf{r} -space distribution that is cut off at values of order Λ_{QCD} (or equivalently a \mathbf{b} -space distribution that is smooth on scales of size $\ll R_p$). This appears to be a somewhat reasonable requirement – at a low scale $Q_0 \sim \Lambda_{QCD}$ there is only the scale Λ_{QCD} available to set the size of the \mathbf{r} profile for $\Gamma_{p,ind\epsilon}^{kl}$, and the evolution of $\Gamma_{p,ind\epsilon}$ essentially preserves the transverse profile to higher scales. What is more, such behaviour for $\Gamma_{p,ind\epsilon}$ would appear to be required in order to get the necessary prefactor of order $1/R_p^2$ in the 2v2 contribution to DPS, which is calculated according to the following expression (for the diagonal unpolarised contribution):

$$\begin{aligned}
 \sigma_{(A,B)}^{D,2v2}(s) &= \frac{m}{2} \int dx_1 dx_2 dy_1 dy_2 \hat{\sigma}_{ik \rightarrow A}(\hat{s} = x_1 y_1 s) \hat{\sigma}_{jl \rightarrow B}(\hat{s} = x_2 y_2 s) \\
 &\times \int \frac{d^2 \mathbf{r}}{(2\pi)^2} \Gamma_{p,ind\epsilon}^{ij}(x_1, x_2, \mathbf{r}; Q^2) \Gamma_{p,ind\epsilon}^{kl}(y_1, y_2, -\mathbf{r}; Q^2)
 \end{aligned} \tag{9}$$

Note that the quantity $(2\pi)^{-2} \int d^2 \mathbf{r} \Gamma_{p,ind\epsilon}^{kl}(y_1, y_2, \mathbf{r}; Q^2)$ in (8) is equal to $\Gamma_{p,ind\epsilon}^{kl}(y_1, y_2, \mathbf{b} = \mathbf{0}; Q^2)$. This appears to indicate that the 2v1 contribution to DPS probes independent branching 2pGPDs at zero parton separation. In fact, the result (8) corresponds to a broad logarithmic integral over values of \mathbf{b}^2 that are $\ll R_p^2$ but $\gg 1/Q^2$. The quantity $\Gamma_{p,ind\epsilon}^{kl}(y_1, y_2, \mathbf{b} = \mathbf{0}; Q^2)$ appears as a result of our smoothness assumption on $\Gamma_{p,ind\epsilon}^{kl}(y_1, y_2, \mathbf{b}; Q^2)$.

If one assumes that the independent branching 2pGPD can be approximately factorised according to the prescription in (2), then the contribution to the DPS cross section from 2v1 graphs is similar to that predicted by the dPDF framework, albeit with a different associated ‘ σ_{eff} ’. Indeed we find that $(\sigma_{eff,2v2})^{-1} = \int d^2 \mathbf{b} [F(\mathbf{b})]^2$, whilst $(\sigma_{eff,1v2})^{-1} = F(\mathbf{b} = \mathbf{0})$. If one then makes the further assumption that $F(\mathbf{b})$ is approximately Gaussian, one finds that each 2v1 contribution to DPS receives a factor of 2 enhancement over the 2v2 contribution from the $(\sigma_{eff})^{-1}$ geometrical prefactor (as is also noted in [10]). One should perhaps not put too much trust into this exact figure, however – it clearly relies on a number of assumptions whose validity is somewhat uncertain.

3 The total cross section for DPS

If one were to take the suggestions outlined earlier in this report at face value, then one would obtain the following expression for (the unpolarised diagonal contribution to) the total LO DPS cross section:

$$\sigma_{(A,B)}^D(s) = \sigma_{(A,B)}^{D,2v2}(s) + \sigma_{(A,B)}^{D,1v2}(s) \tag{10}$$

with $\sigma_{(A,B)}^{D,1v2}(s)$ and $\sigma_{(A,B)}^{D,2v2}(s)$ being given by the expressions (8) and (9) respectively. This expression shares some common terms with the DPS cross section formulae proposed in [10] and [12]. Looking closely at (10) however, one can identify a number of concerning issues with

regard to this equation, which indicate that modifications to it may be required in order to correctly describe the DPS cross section.

The first issue is that we were originally expecting to obtain an expression for the DPS cross section looking something like (1), with the 2pGPDs in these formulae each having an interpretation in terms of hadronic operator matrix elements. Our proposed expression (10) deviates somewhat in structure from these expectations (in particular, one would struggle to come up with a matrix element representation for $\check{D}_p^{ij}(x_1, x_2; Q^2)$). This feature is related to the fact that we have entirely removed the ‘1v1’ contribution from the DPS cross section.

The second issue is that there is a rather sharp distinction in (10) between perturbatively and nonperturbatively generated parton pairs, with the 2pGPD for the latter $\Gamma_{p, indep}^{kl}$ having a natural width in \mathbf{r} space of order Λ . Does there exist some scale at which we can (approximately) regard all parton pairs in the proton as being ‘nonperturbatively generated’ in this sense (as is assumed in (10))? If so, what is the appropriate value for the scale (presumably it should be rather close to Λ_{QCD})?

A final issue is that in the above, we have largely ignored the interesting and potentially important interference and correlated parton contributions to DPS catalogued in [7, 8].

In this report, we have shown that the treatment of 1v1 and 2v1 contributions to DPS by the dPDF framework of Snigirev et al. appears to be unsatisfactory, and presented the results of a calculation that indicates that we should include a contribution to the DPS cross section from 2v1 graphs, if we include a contribution from 2v2 graphs. There appear to be some unsatisfactory features in our alternative suggestion for the DPS cross section (10), which perhaps indicates that completely removing any contribution from 1v1 graphs from the DPS cross section is not quite the correct prescription.

References

- [1] A. Del Fabbro and D. Treleani, “A Double parton scattering background to Higgs boson production at the LHC”, *Phys. Rev. D* **61** (2000) 077502 [hep-ph/9911358].
- [2] G. M. Zinovev, A. M. Snigirev and V. P. Shelest, “Equations For Many Parton Distributions In Quantum Chromodynamics”, *Theor. Math. Phys.* **51** (1982) 523 [*Teor. Mat. Fiz.* **51** (1982) 317].
- [3] A. M. Snigirev, “Double parton distributions in the leading logarithm approximation of perturbative QCD”, *Phys. Rev. D* **68** (2003) 114012 [hep-ph/0304172].
- [4] Z. Nagy and D. E. Soper, “Numerical integration of one-loop Feynman diagrams for N-photon amplitudes”, *Phys. Rev. D* **74** (2006) 093006 [hep-ph/0610028].
- [5] J. R. Gaunt and W. J. Stirling, “Double Parton Scattering Singularity in One-Loop Integrals”, *JHEP* **1106** (2011) 048 [arXiv:1103.1888 [hep-ph]].
- [6] A. Harindranath, R. Kundu and W. -M. Zhang, “Deep inelastic structure functions in light front QCD: Radiative corrections”, *Phys. Rev. D* **59** (1999) 094013 [hep-ph/9806221].
- [7] M. Diehl and A. Schafer, “Theoretical considerations on multiparton interactions in QCD”, *Phys. Lett. B* **698** (2011) 389 [arXiv:1102.3081 [hep-ph]].
- [8] M. Diehl, D. Ostermeier and A. Schafer, “Elements of a theory for multiparton interactions in QCD”, arXiv:1111.0910 [hep-ph].
- [9] J. M. F. Labastida and G. F. Sterman, “Inclusive Hadron - Hadron Scattering In The Feynman Gauge”, *Nucl. Phys. B* **254** (1985) 425.
- [10] B. Blok, Y. L. Dokshitzer, L. Frankfurt and M. Strikman, “pQCD physics of multiparton interactions”, arXiv:1106.5533 [hep-ph].
- [11] N. Paver and D. Treleani, “Multi - Quark Scattering And Large P(t) Jet Production In Hadronic Collisions”, *Nuovo Cim. A* **70** (1982) 215.
- [12] M. G. Ryskin and A. M. Snigirev, “A Fresh look at double parton scattering”, *Phys. Rev. D* **83** (2011) 114047 [arXiv:1103.3495 [hep-ph]].

Multi-gluon correlations in the color glass condensate

Tuomas Lappi

Department of Physics, P.O. Box 35, 40014 University of Jyväskylä, Finland and
Helsinki Institute of Physics, P.O. Box 64, 00014 University of Helsinki, Finland

DOI: <http://dx.doi.org/10.3204/DESY-PROC-2012-03/29>

We discuss recent work on gluon correlations in high energy collisions and argue that they are most naturally understood in the Color Glass Condensate framework. We discuss first the dense-dense regime which is relevant for, e.g., the “ridge”-correlation observed at midrapidity in AA and pp collisions. We then describe recent progress in understanding two-particle correlations in the dilute-dense system, relevant for forward dihadron production in deuteron-gold collisions. This requires computing the energy dependence of higher point Wilson line correlators from the JIMWLK renormalization group equation. We find that the large N_c approximation used so far in the phenomenological literature is not very accurate. On the other hand a Gaussian finite N_c approximation is a surprisingly good approximation of the result from the full JIMWLK equation.

1 Introduction

The physics of high energy hadronic or nuclear collisions is dominated by the gluonic degrees of freedom of the colliding particles. These small x gluons form a dense nonlinear system that is, at high enough \sqrt{s} , best described as a classical color field and quantum fluctuations around it. The Color Glass Condensate (CGC, for reviews see [1, 2, 3, 4]) is an effective theory developed around this idea. It gives an universal description that can equally well be applied to small- x DIS as to dilute-dense (pA or forward AA) and dense-dense (AA or very high energy pp) hadronic collisions. The CGC is based on an effective description of large- x partons as a color charge density and small- x ones as a classical field radiated by these charges. The most convenient parametrization of the dominant gauge field is in terms of Wilson lines that describe the eikonal propagation of a projectile through it. The cutoff separating the large- x and small- x degrees of freedom is an arbitrary factorization scale, thus the requirement that physical observables cannot depend on it leads to a renormalization group equation. This nonlinear equation, known by the acronym JIMWLK [5, 6, 7, 11, 12], describes the evolution in rapidity of the probability distribution of the Wilson lines. It reduces, in a large N_c - mean field approximation, to the BK [13, 14] equation and further, in the dilute linear regime, to the BFKL one.

The nonlinear interactions of the small- x gluons generate dynamically a new transverse momentum scale, the saturation scale Q_s . The saturation scale grows with energy, as the increased density of gluons makes their interactions nonlinear at higher transverse momenta. At high enough energy the color glass condensate is thus a one-scale system, characterized by a dominant momentum scale Q_s that is hard enough to justify a weak coupling calculation.

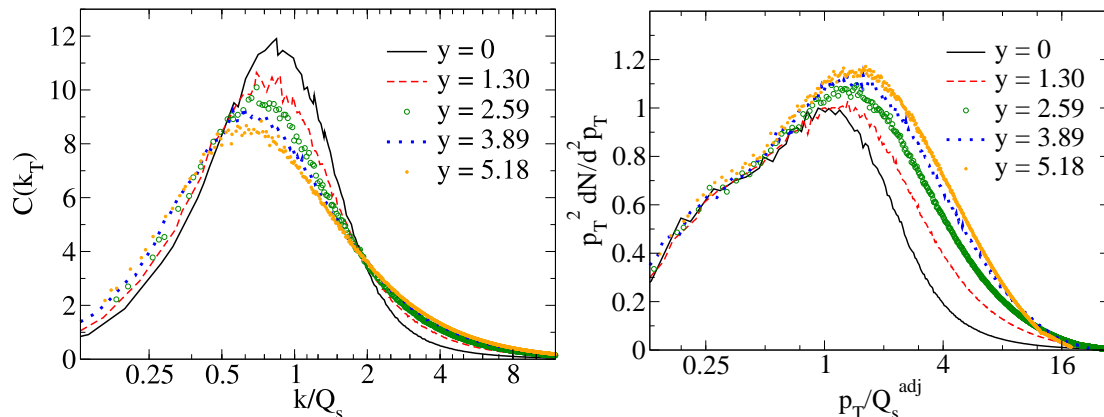


Figure 1: Left: evolution of unintegrated (“dipole”) gluon distribution starting from an MV model initial condition. Right: The resulting gluon spectrum produced in a heavy ion collision. Note that this should be thought of as the gluon spectrum at midrapidity with y representing the logarithm of \sqrt{s} .

The scale Q_s dominates both the gluon spectrum and multigluon correlations. The nature of a unique saturation scale as both the typical gluon transverse momentum and as the correlation length $1/Q_s$ differentiates the CGC qualitatively from the high- x part of the wavefunction.

2 Bulk particle production

One of the most unique aspects of the CGC framework is the prospect of understanding bulk quantities, such as particle multiplicities integrated over the whole p_T spectrum, in weak coupling. At leading order in α_s , calculating the spectrum of gluons produced in the initial stages of a heavy ion collision requires solving the time evolution of the non-perturbative strong classical gauge field (known as the glasma field [15]). This field is then, at late enough times, Fourier-decomposed and the modes interpreted as on-shell gluons. This calculation needs the Wilson lines corresponding to the individual colliding nuclei to provide the initial condition for the glasma fields [16], whose equations of motion must then be solved numerically [17, 18, 19]. In most of the numerical studies in the literature, the Wilson lines have been taken from the MV model [20, 21, 22], which is straightforward to implement numerically.

Only very recently [23] an actual numerical solution of the JIMWLK equation has been used to provide the initial condition for the evolution of the glasma fields. The JIMWLK equation is solved, in practice, by reformulating the RGE for the probability distribution of Wilson lines as a Langevin equation [24, 25, 26] for the rapidity dependence of an ensemble of Wilson lines. These configurations can then directly be used in the initial condition for the glasma fields. The results of this calculation are summarized in Fig. 1. On the left is plotted the correlation function of Wilson lines $U(\mathbf{x}_T)$ (i.e. dipole cross section or dipole gluon distribution) in momentum space:

$$C(\mathbf{k}_T) = \mathbf{k}_T^2 \int d^2\mathbf{x}_T e^{i\mathbf{k}_T \cdot (\mathbf{x}_T - \mathbf{y}_T)} \frac{1}{N_c} \langle \text{Tr} U^\dagger(\mathbf{x}_T) U(\mathbf{y}_T) \rangle, \quad (1)$$

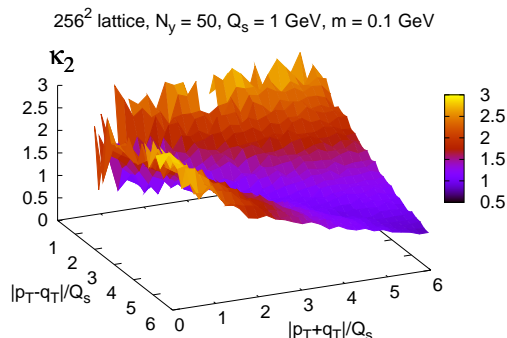


Figure 2: The two gluon correlation function in the MV model, from a full non-perturbative classical field calculation [27]. The near side $\mathbf{p}_T \approx \mathbf{q}_T$ and away side $\mathbf{p}_T \approx -\mathbf{q}_T$ peak structure is clearly seen.

starting from an MV model initial condition at $y = 0$. The main effect of the evolution (as expected from BK evolution) is the hardening of the unintegrated gluon distribution due to the development of a geometric scaling region for $k_T \gtrsim Q_s$. The effect on the gluon spectrum in the glasma is shown in Fig. 1 (right): also the spectrum of gluons in the glasma gets harder with increasing energy. Note that, as advocated above, the spectrum is integrable and the total gluon multiplicity finite without any additional cut-offs. This is a non-trivial consequence of the non-linear interactions of the gluonic field.

3 Correlations in the dense-dense limit

The classical color field is a multi-gluon system, and as such has naturally built in correlations that are long range in rapidity. The formalism for computing the observable correlations in a collision of two high density gluonic systems in the CGC framework was developed in [28, 29, 30]. The essential power-counting argument can be summarized as follows. In the CGC, and the glasma, the gluon fields are non-perturbatively strong; $A_\mu \sim 1/g$. Therefore the correlations arising from quantum fluctuations around the field, which give the typical correlations in a perturbative calculation, are actually subleading compared to the ones arising from the probability distribution of Wilson lines. Physically this means that the dominant correlations are those that are enhanced by large logarithms of x , present already in the wavefunctions of the colliding projectiles and re-summed by the JIMWLK evolution.

The only nonperturbative calculation of the double inclusive gluon spectrum has been performed in Ref. [27]. The main result is shown in Fig. 2 in terms of the quantity

$$\kappa_2(\mathbf{p}_T, \mathbf{q}_T) = S_\perp Q_s^2 \frac{C_2(\mathbf{p}_T, \mathbf{q}_T)}{\left\langle \frac{dN}{dy_p d^2\mathbf{p}_T} \right\rangle \left\langle \frac{dN}{dy_q d^2\mathbf{q}_T} \right\rangle}, \quad (2)$$

where the correlated double inclusive gluon spectrum is defined as

$$C_2(\mathbf{p}_T, \mathbf{q}_T) = \left\langle \frac{dN}{dy_p d^2\mathbf{p}_T} \frac{dN}{dy_q d^2\mathbf{q}_T} \right\rangle - \left\langle \frac{dN}{dy_p d^2\mathbf{p}_T} \right\rangle \left\langle \frac{dN}{dy_q d^2\mathbf{q}_T} \right\rangle. \quad (3)$$

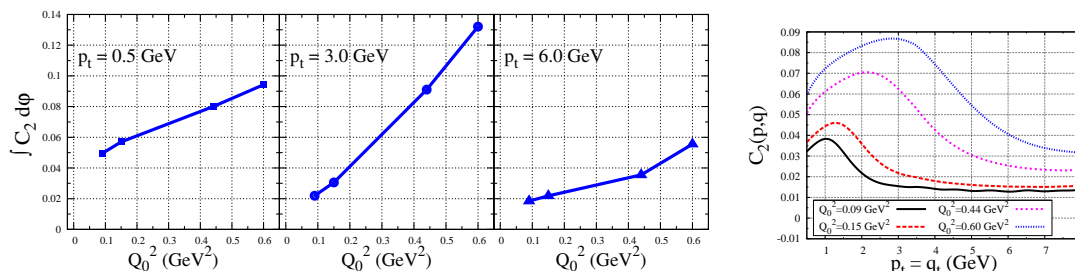


Figure 3: Left: Near side correlated multiplicity (integrated over azimuthal angle) as a function of the saturation scale the CGC calculation. Right: transverse momentum spectrum of the correlated secondary particles. Figures from Ref. [31].

Here S_\perp is the transverse area of the collision system. The result displays two characteristic main features. Firstly the double inclusive spectrum, scaled with the number of correlation regions $S_\perp Q_s^2$, is of order one. Secondly one observes a characteristic enhancement in the back-to-back $\mathbf{p}_T \sim -\mathbf{q}_T$ and near side $\mathbf{p}_T \sim \mathbf{q}_T$ regions. While the former is present also in the dilute limit, due to momentum conservation, the latter is a genuine nontrivial high gluon density effect that has no counterpart in a purely perturbative (or string fragmentation, for that matter) picture. This is the basis of the CGC contribution to the "ridge" correlation, a structure at small azimuthal angle and large rapidity separation, that has been observed in AA and pp collisions at high energy.

The calculation of Ref. [27] uses the MV model for the Wilson line distribution. Work on repeating the calculation using the Wilson line configurations from JIMWLK evolution is still ongoing. In the meanwhile the effects of high energy evolution have been analyzed in a k_T -factorized approximation [31, 32], which is valid for particle production at $p_T \gtrsim Q_s$ [33]. The k_T -factorized approximation for the double inclusive gluon spectrum is

$$\begin{aligned}
 C(\mathbf{p}_T, \mathbf{q}_T) &= \frac{\alpha_s^2}{4\pi^{10}} \frac{N_c^2 S_\perp}{(N_c^2 - 1)^3 \mathbf{p}_T^2 \mathbf{q}_T^2} \\
 &\times \left\{ \int d^2 \mathbf{k}_T \Phi_{A_1}^2(y_p, \mathbf{k}_T) \Phi_{A_2}(y_p, \mathbf{p}_T - \mathbf{k}_T) \left[\Phi_{A_2}(y_q, \mathbf{q}_T + \mathbf{k}_T) + \Phi_{A_2}(y_q, \mathbf{q}_T - \mathbf{k}_T) \right] \right. \\
 &\quad \left. + \Phi_{A_2}^2(y_q, \mathbf{k}_T) \Phi_{A_1}(y_p, \mathbf{p}_T - \mathbf{k}_T) \left[\Phi_{A_1}(y_q, \mathbf{q}_T + \mathbf{k}_T) + \Phi_{A_1}(y_q, \mathbf{q}_T - \mathbf{k}_T) \right] \right\}. \quad (4)
 \end{aligned}$$

Here Φ_{A_i} , the unintegrated gluon distribution in nucleus i , is related to the correlator $C(\mathbf{k}_T)$ of Eq. (1) simply by $\Phi(\mathbf{k}_T) = C(\mathbf{k}_T)/(4\alpha_s N_c)$. In [31, 32] it is obtained from the mean field BK equation. The qualitative features of the correlation obtained using Eq. (4) are illustrated in Fig. 3. What is shown is the correlation integrated over $\Delta\varphi$, the azimuthal angle separation between the two produced gluons. It rises for increasing Q_s , which corresponds to increasing centrality. Also the dependence of the correlation on the p_T -cutoff, first rising and then decreasing, matches that seen in the CMS data [34]. A more recent detailed analysis [35] confirms the conclusions reached here on a more quantitative level.

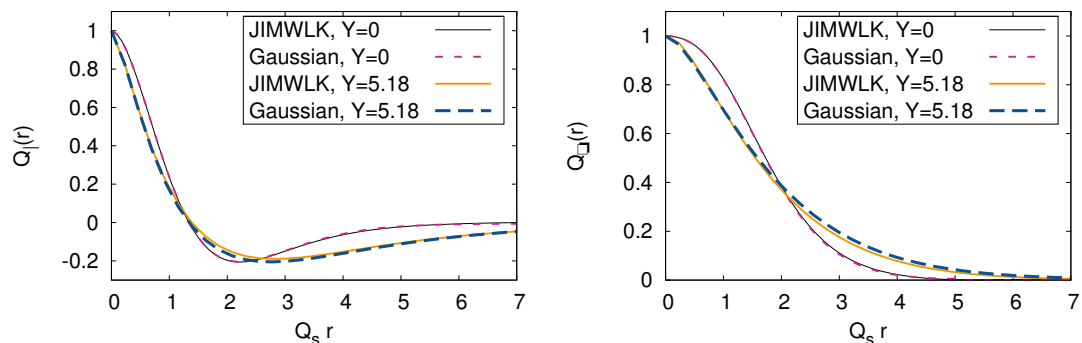


Figure 4: The JIMWLK result for the quadrupole correlator compared to the Gaussian approximation. Shown are the initial condition (MV model) at $y = 0$ and the result after 5.18 units of evolution in rapidity, for the “line” (left) and “square” (right) coordinate configurations. Figures from Ref. [36].

4 Correlations in the dense-dilute limit

One of the more striking signals of saturation physics at RHIC is the observed broadening of the away-side peak in di-hadron correlations in forward deuteron-gold scattering [37, 38]. Our theoretical starting point in analyzing these correlations is to consider the high- x parton from the proton required to produce two relatively large p_T particles at forward rapidity in the final state. We assume the high- x particle to be a quark, since the valence distribution dominates at high x . In order to have a correlated production of two particles this quark must then radiate a gluon, carrying a fraction z of its longitudinal momentum. To leading order we then have a picture of a quark-gluon system propagating (eikonally in our high energy approximation) through the target nucleus. The eikonal matrix element is given by Wilson lines in the appropriate representation for the two particles, leading to a double inclusive cross section

$$\begin{aligned} \frac{d\sigma^{qA \rightarrow qgX}}{d^3k_1 d^3k_2} &\propto \frac{\alpha_s N_c}{2} \int_{\mathbf{x}_T, \bar{\mathbf{x}}_T, \mathbf{y}_T, \bar{\mathbf{y}}_T} e^{-i\mathbf{k}_{T1} \cdot (\mathbf{x}_T - \bar{\mathbf{x}}_T)} e^{-i\mathbf{k}_{T2} \cdot (\mathbf{y}_T - \bar{\mathbf{y}}_T)} \mathcal{F}(\bar{\mathbf{x}}_T - \bar{\mathbf{y}}_T, \mathbf{x}_T - \mathbf{y}_T) \\ &\left\langle \hat{Q}(\mathbf{y}_T, \bar{\mathbf{y}}_T, \bar{\mathbf{x}}_T, \mathbf{x}_T) \hat{D}(\mathbf{x}_T, \bar{\mathbf{x}}_T) - \hat{D}(\mathbf{y}_T, \mathbf{x}_T) \hat{D}(\mathbf{x}_T, \bar{\mathbf{z}}_T) - \hat{D}(\mathbf{z}_T, \bar{\mathbf{x}}_T) \hat{D}(\bar{\mathbf{x}}_T, \bar{\mathbf{y}}_T) \right. \\ &\quad \left. + \frac{C_F}{N_c} \hat{D}(\mathbf{z}_T, \bar{\mathbf{z}}_T) + \frac{1}{N_c^2} \left(\hat{D}(\mathbf{y}_T, \bar{\mathbf{z}}_T) + \hat{D}(\mathbf{z}_T, \bar{\mathbf{y}}_T) - \hat{D}(\mathbf{y}_T, \bar{\mathbf{y}}_T) \right) \right\rangle, \quad (5) \end{aligned}$$

with $\mathbf{z}_T = z\mathbf{x}_T + (1-z)\mathbf{y}_T$ and likewise, $\bar{\mathbf{z}}_T = z\bar{\mathbf{x}}_T + (1-z)\bar{\mathbf{y}}_T$. The kinematical factors denoted by \mathcal{F} can be calculated in light cone perturbation theory [39]. What is then needed to describe the target are the expectation values of the dipole, quadrupole, and sextupole Wilson

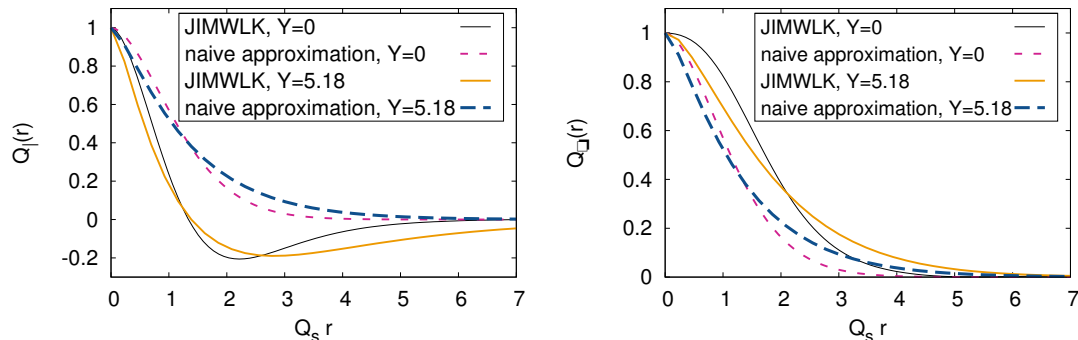


Figure 5: The JIMWLK result for the quadrupole correlator compared to the “naive large N_c ” approximation. Shown are the initial condition (MV model) at $y = 0$ and the result after 5.18 units of evolution in rapidity, for the “line” (left) and “square” (right) coordinate configurations. Figures from Ref. [36].

line operators $D = \langle \hat{D} \rangle$, $Q = \langle \hat{Q} \rangle$, and $\langle \hat{D} \hat{Q} \rangle$ defined by

$$\hat{D}(\mathbf{x}_T, \mathbf{y}_T) = \frac{1}{N_c} \text{Tr} U(\mathbf{x}_T) U^\dagger(\mathbf{y}_T), \quad \hat{Q}(\mathbf{x}_T, \mathbf{y}_T, \mathbf{u}_T, \mathbf{v}_T) = \frac{1}{N_c} \text{Tr} U(\mathbf{x}_T) U^\dagger(\mathbf{y}_T) U(\mathbf{u}_T) U^\dagger(\mathbf{v}_T). \quad (6)$$

For practical phenomenological work it would be extremely convenient to be able to express these higher point correlators in terms of the dipole, which is straightforward to obtain from the BK equation. In the phenomenological literature so far [40, 41] this has been done using a “naive large N_c ” approximation as

$$Q(\mathbf{x}_T, \mathbf{y}_T, \mathbf{u}_T, \mathbf{v}_T) \underset{N_c \rightarrow \infty}{\approx} \frac{1}{2} (D(\mathbf{x}_T, \mathbf{y}_T) D(\mathbf{u}_T, \mathbf{v}_T) + D(\mathbf{x}_T, \mathbf{v}_T) D(\mathbf{u}_T, \mathbf{y}_T)). \quad (7)$$

A more elaborate scheme would be a “Gaussian” approximation (“Gaussian truncation” in [42]), where one assumes the relation between the higher point functions and the dipole to be the same as in the (Gaussian) MV model. The expectation value of the quadrupole operator in the MV model has been derived e.g. in Ref. [43]; the one for the 6-point function is unfortunately not known yet.

In Ref. [36] we have studied the validity of these approximations by comparing them numerically to the solution of the JIMWLK equation, following the conjecture of Ref. [44] that the JIMWLK result should significantly deviate from both of them. As studying the full 8-dimensional phase space for the quadrupole operator would be cumbersome, we have concentrated on two special coordinate configurations. The “line” configuration is defined by taking $\mathbf{u}_T = \mathbf{x}_T$ and $\mathbf{v}_T = \mathbf{y}_T$, with $r = |\mathbf{x}_T - \mathbf{y}_T|$ and the “square” by taking $\mathbf{x}_T, \mathbf{y}_T, \mathbf{u}_T, \mathbf{v}_T$ as the corners of a square with side r . For these particular configurations the “naive large N_c ” approximation reduces to

$$Q_{\square}^{\text{naive}}(r) \approx Q_{\square}^{\text{naive}}(r) \approx D(r)^2 \quad (8)$$

and the Gaussian approximation to

$$Q_{|}(r) \approx \frac{N_c + 1}{2} \left(D(r) \right)^{2 \frac{N_c + 2}{N_c + 1}} - \frac{N_c - 1}{2} \left(D(r) \right)^{2 \frac{N_c - 2}{N_c - 1}} \quad (9)$$

$$Q_{\square}(r) \approx (D(r))^2 \left[\frac{N_c + 1}{2} \left(\frac{D(r)}{D(\sqrt{2}r)} \right)^{\frac{2}{N_c + 1}} - \frac{N_c - 1}{2} \left(\frac{D(\sqrt{2}r)}{D(r)} \right)^{\frac{2}{N_c - 1}} \right]. \quad (10)$$

Our results [36] for the quadrupole expectation value are shown in Figs. 4 and 5, with a comparison of the initial and evolved (for 5.18 units in y) results to the approximations. The MV-model initial condition $y = 0$ satisfies the Gaussian approximation by construction. Figure 4 shows that the Gaussian approximation is still surprisingly well conserved by the evolution. A possible explanation for this based on the structure of the JIMWLK equation has recently been proposed in [45, 46]. The naive large N_c approximation used in some phenomenological works, on the other hand, fails already at the initial condition, as shown in Fig. 5. This stresses the importance the various $SU(3)$ group structure constraints violated in this approach. Crucially for the phenomenological consequences, even the characteristic length/momentum scale differs by factor ~ 2 from the actual result.

This result does not yet fully address the effect on the measurable cross section. For that one must perform the integrals in (5) to go from the position space correlator to the momentum space one. Also additional effects such as inelastic contributions [47] and high- x effects in the deuteron (as compared to the proton) must be included, as discussed in [48]. This full calculation is still a work in progress.

Acknowledgments The author has been supported by the Academy of Finland, project 141555, and by computing resources from CSC – IT Center for Science in Espoo, Finland.

References

- [1] E. Iancu and R. Venugopalan, “The Color glass condensate and high-energy scattering in QCD,” In *Hwa, R.C. (ed.) et al.: Quark gluon plasma* 249-3363 (arXiv:hep-ph/0303204).
- [2] H. Weigert, “Evolution at small $x(bj)$: The Color glass condensate,” *Prog. Part. Nucl. Phys.* **55** (2005) 461 (arXiv:hep-ph/0501087).
- [3] F. Gelis, E. Iancu, J. Jalilian-Marian and R. Venugopalan, “The Color Glass Condensate,” *Ann. Rev. Nucl. Part. Sci.* **60** (2010) 463 (arXiv:1002.0333 [hep-ph]).
- [4] T. LAPPI, “Small x physics and RHIC data,” *Int. J. Mod. Phys. E* **20** (2011) 1 (arXiv:1003.1852 [hep-ph]).
- [5] J. Jalilian-Marian, A. Kovner, L. D. McLerran and H. Weigert, “The Intrinsic glue distribution at very small x ,” *Phys. Rev. D* **55** (1997) 5414 (arXiv:hep-ph/9606337).
- [6] J. Jalilian-Marian, A. Kovner, A. Leonidov and H. Weigert, “The BFKL equation from the Wilson renormalization group,” *Nucl. Phys. B* **504** (1997) 415 (arXiv:hep-ph/9701284).
- [7] J. Jalilian-Marian, A. Kovner, A. Leonidov and H. Weigert, “The Wilson renormalization group for low x physics: Towards the high density regime,” *Phys. Rev. D* **59** (1999) 014014 (arXiv:hep-ph/9706377).
- [8] J. Jalilian-Marian, A. Kovner and H. Weigert, “The Wilson renormalization group for low x physics: Gluon evolution at finite parton density,” *Phys. Rev. D* **59** (1999) 014015 (arXiv:hep-ph/9709432).
- [9] J. Jalilian-Marian, A. Kovner, A. Leonidov and H. Weigert, “Unitarization of gluon distribution in the doubly logarithmic regime at high density,” *Phys. Rev. D* **59** (1999) 034007 [Erratum-ibid. *D* **59** (1999) 099903] (arXiv:hep-ph/9807462).
- [10] E. Iancu, A. Leonidov and L. D. McLerran, “Nonlinear gluon evolution in the color glass condensate. 1.,” *Nucl. Phys. A* **692** (2001) 583 (arXiv:hep-ph/0011241).

- [11] E. Ferreiro, E. Iancu, A. Leonidov and L. McLerran, “Nonlinear gluon evolution in the color glass condensate. 2,” Nucl. Phys. A **703** (2002) 489 (arXiv:hep-ph/0109115).
- [12] A. H. Mueller, “A Simple derivation of the JIMWLK equation,” Phys. Lett. B **523** (2001) 243 (arXiv:hep-ph/0110169).
- [13] I. Balitsky, “Operator expansion for high-energy scattering,” Nucl. Phys. B **463** (1996) 99 (arXiv:hep-ph/9509348).
- [14] Y. V. Kovchegov, “Small x $F(2)$ structure function of a nucleus including multiple pomeron exchanges,” Phys. Rev. D **60** (1999) 034008 (arXiv:hep-ph/9901281).
- [15] T. Lappi and L. McLerran, “Some features of the glasma,” Nucl. Phys. A **772** (2006) 200 (arXiv:hep-ph/0602189).
- [16] A. Kovner, L. D. McLerran and H. Weigert, “Gluon production at high transverse momentum in the McLerran-Venugopalan model of nuclear structure functions,” Phys. Rev. D **52** (1995) 3809 (arXiv:hep-ph/9505320).
- [17] A. Krasnitz and R. Venugopalan, “Nonperturbative computation of gluon minijet production in nuclear collisions at very high-energies,” Nucl. Phys. B **557** (1999) 237 (arXiv:hep-ph/9809433).
- [18] A. Krasnitz, Y. Nara and R. Venugopalan, “Coherent gluon production in very high-energy heavy ion collisions,” Phys. Rev. Lett. **87** (2001) 192302 (arXiv:hep-ph/0108092).
- [19] T. Lappi, “Production of gluons in the classical field model for heavy ion collisions,” Phys. Rev. C **67** (2003) 054903 (arXiv:hep-ph/0303076).
- [20] L. D. McLerran and R. Venugopalan, “Computing quark and gluon distribution functions for very large nuclei,” Phys. Rev. D **49** (1994) 2233 (arXiv:hep-ph/9309289).
- [21] L. D. McLerran and R. Venugopalan, “Gluon distribution functions for very large nuclei at small transverse momentum,” Phys. Rev. D **49** (1994) 3352 (arXiv:hep-ph/9311205).
- [22] L. D. McLerran and R. Venugopalan, “Green’s functions in the color field of a large nucleus,” Phys. Rev. D **50** (1994) 2225 (hep-ph/9402335).
- [23] T. Lappi, “Gluon spectrum in the glasma from JIMWLK evolution,” Phys. Lett. B **703** (2011) 325 (arXiv:1105.5511 [hep-ph]).
- [24] H. Weigert, “Unitarity at small Bjorken x ,” Nucl. Phys. A **703** (2002) 823 (arXiv:hep-ph/0004044).
- [25] J. -P. Blaizot, E. Iancu and H. Weigert, “Nonlinear gluon evolution in path integral form,” Nucl. Phys. A **713** (2003) 441 (arXiv:hep-ph/0206279).
- [26] K. Rummukainen and H. Weigert, “Universal features of JIMWLK and BK evolution at small x ,” Nucl. Phys. A **739** (2004) 183 (arXiv:hep-ph/0309306).
- [27] T. Lappi, S. Srednyak and R. Venugopalan, “Non-perturbative computation of double inclusive gluon production in the Glasma,” JHEP **1001** (2010) 066 (arXiv:0911.2068 [hep-ph]).
- [28] F. Gelis, T. Lappi and R. Venugopalan, “High energy factorization in nucleus-nucleus collisions,” Phys. Rev. D **78** (2008) 054019 (arXiv:0804.2630 [hep-ph]).
- [29] F. Gelis, T. Lappi and R. Venugopalan, “High energy factorization in nucleus-nucleus collisions. II. Multigluon correlations,” Phys. Rev. D **78** (2008) 054020 (arXiv:0807.1306 [hep-ph]).
- [30] F. Gelis, T. Lappi and R. Venugopalan, “High energy factorization in nucleus-nucleus collisions. 3. Long range rapidity correlations,” Phys. Rev. D **79** (2009) 094017 (arXiv:0810.4829 [hep-ph]).
- [31] A. Dumitru, K. Dusling, F. Gelis, J. Jalilian-Marian, T. Lappi and R. Venugopalan, “The Ridge in proton-proton collisions at the LHC,” Phys. Lett. B **697** (2011) 21 (arXiv:1009.5295 [hep-ph]).
- [32] K. Dusling, F. Gelis, T. Lappi and R. Venugopalan, “Long range two-particle rapidity correlations in A+A collisions from high energy QCD evolution,” Nucl. Phys. A **836** (2010) 159 (arXiv:0911.2720 [hep-ph]).
- [33] J. -P. Blaizot, T. Lappi and Y. Mehtar-Tani, “On the gluon spectrum in the glasma,” Nucl. Phys. A **846** (2010) 63 (arXiv:1005.0955 [hep-ph]).
- [34] V. Khachatryan *et al.* [CMS Collaboration], “Observation of Long-Range Near-Side Angular Correlations in Proton-Proton Collisions at the LHC,” JHEP **1009** (2010) 091 (arXiv:1009.4122 [hep-ex]).
- [35] K. Dusling and R. Venugopalan, “Azimuthal collimation of long range rapidity correlations by strong color fields in high multiplicity hadron-hadron collisions,” (arXiv:1201.2658 [hep-ph]).

- [36] A. Dumitru, J. Jalilian-Marian, T. Lappi, B. Schenke and R. Venugopalan, “Renormalization group evolution of multi-gluon correlators in high energy QCD,” *Phys. Lett. B* **706** (2011) 219 (arXiv:1108.4764 [hep-ph]).
- [37] A. Adare *et al.* [PHENIX Collaboration], “Suppression of back-to-back hadron pairs at forward rapidity in $d+Au$ Collisions at $\sqrt{s_{NN}} = 200$ GeV,” *Phys. Rev. Lett.* **107** (2011) 172301 (arXiv:1105.5112 [nucl-ex]).
- [38] E. Braidot, “Two-particle azimuthal correlations at forward rapidity in STAR,” (arXiv:1102.0931 [nucl-ex]).
- [39] C. Marquet, “Forward inclusive dijet production and azimuthal correlations in p(A) collisions,” *Nucl. Phys. A* **796** (2007) 41 (arXiv:0708.0231 [hep-ph]).
- [40] K. Tuchin, “Nonlinear pair production in scattering of photons on ultra-short laser pulses at high energy,” *Phys. Lett. B* **686** (2010) 29 (arXiv:0911.4964 [hep-ph]).
- [41] J. L. Albacete and C. Marquet, “Azimuthal correlations of forward di-hadrons in $d+Au$ collisions at RHIC in the Color Glass Condensate,” *Phys. Rev. Lett.* **105** (2010) 162301 (arXiv:1005.4065 [hep-ph]).
- [42] J. Kuokkanen, K. Rummukainen and H. Weigert, “HERA-data in the light of small x evolution with state of the art NLO input,” *Nucl. Phys. A* **875** (2012) 29 (arXiv:1108.1867 [hep-ph]).
- [43] F. Dominguez, C. Marquet, B. -W. Xiao and F. Yuan, “Universality of Unintegrated Gluon Distributions at small x ,” *Phys. Rev. D* **83** (2011) 105005 (arXiv:1101.0715 [hep-ph]).
- [44] A. Dumitru and J. Jalilian-Marian, “Forward dijets in high-energy collisions: Evolution of QCD n -point functions beyond the dipole approximation,” *Phys. Rev. D* **82** (2010) 074023 (arXiv:1008.0480 [hep-ph]).
- [45] E. Iancu and D. N. Triantafyllopoulos, “Higher-point correlations from the JIMWLK evolution,” *JHEP* **1111** (2011) 105 (arXiv:1109.0302 [hep-ph]).
- [46] E. Iancu and D. N. Triantafyllopoulos, “JIMWLK evolution in the Gaussian approximation,” *JHEP* **1204** (2012) 025 (arXiv:1112.1104 [hep-ph]).
- [47] T. Altinoluk and A. Kovner, “Particle Production at High Energy and Large Transverse Momentum - ‘The Hybrid Formalism’ Revisited,” *Phys. Rev. D* **83** (2011) 105004 (arXiv:1102.5327 [hep-ph]).
- [48] M. Strikman and W. Vogelsang, “Multiple parton interactions and forward double pion production in pp and dA scattering,” *Phys. Rev. D* **83** (2011) 034029 (arXiv:1009.6123 [hep-ph]).

Unitarity and consistency in multiple hard collisions

Ted C. Rogers^{1*}, Mark Strikman²

¹*C.N. Yang Institute for Theoretical Physics, Stony Brook University, Stony Brook NY 11794, USA*

²*Department of Physics, Pennsylvania State University, University Park, PA 16802, USA*

DOI: <http://dx.doi.org/10.3204/DESY-PROC-2012-03/31>

We address the question of how to simultaneously account for unitarity constraints in a variety of different types of very high energy cross sections wherein a description of multiple hard partonic collisions is important. It is shown how models and extrapolations that utilize the concept of multiple hard partonic scatterings can be made consistent with one another while still adequately describing existing experimental data.

1 Introduction

1.1 s -channel unitarity

The procedure to account for s -channel unitarity in very high energy hadronic collisions has been understood for many years now; one defines a profile function for the limit of $s \gg -t$ in terms of the amplitude $A(s, t)$ for elastic hadron-hadron scattering in the high energy limit $t \approx -\mathbf{q}_t^2$:

$$\Gamma(s, b_t) \equiv \frac{1}{2is(2\pi)^2} \int d^2\mathbf{q}_t e^{i\mathbf{q}_t \cdot \mathbf{b}_t} A(s, t), \quad (1)$$

Imposing unitarity and analyticity leads to the following set of well known relations between the elastic, total, and inelastic cross sections:

$$\sigma_{tot}(s) = 2 \int d^2\mathbf{b}_t \operatorname{Re} \Gamma(s, b_t), \quad (2)$$

$$\sigma_{el}(s) = \int d^2\mathbf{b}_t |\Gamma(s, b_t)|^2, \quad (3)$$

$$\sigma_{inel}(s) = \int d^2\mathbf{b}_t \left(2 \operatorname{Re} \Gamma(s, b_t) - |\Gamma(s, b_t)|^2 \right). \quad (4)$$

Defining an inelastic profile function,

$$\Gamma^{inel}(s, b_t) \equiv \left(2 \operatorname{Re} \Gamma(s, b_t) - |\Gamma(s, b_t)|^2 \right), \quad (5)$$

*Speaker

a description of the total cross section must obey

$$\Gamma^{\text{inel}}(s, b), \Gamma(s, b) \leq 1. \quad (6)$$

(Here it is assumed that the amplitude is entirely imaginary which is appropriate in the $s \gg -t$ limit.) Generally, the profile function grows with energy. When $\Gamma^{\text{inel}}(s, b_t) \approx 1$ in some region $b_t < b_{\text{max}}$ then it is said to have reached the “black disk limit” (BDL).

1.2 Minijets and multiple hard collisions

It has become common to combine the s -channel picture with treatments of multiple hard partonic collisions (e.g., [1] and references therein) thereby relating descriptions of minimum bias events, the underlying event, and other complex aspects of hadron-hadron collisions to the treatment of the total cross section. One common approach is to describe the production of semi-hard minijets using the standard perturbative QCD expression while modeling the contribution from soft physics (using for example Regge theory) and using an eikonal model of multiple scattering to reconstruct from this the total cross section:

$$\Gamma(s, b) = 1 - e^{-\chi_h(s, b) - \chi_s(s, b_t)}, \quad (7)$$

where $\chi_h(s, b)$ and $\chi_s(s, b_t)$ are eikonals that describe the hard and soft partonic collisions respectively.

For the case of just one hard collision the inclusive cross section can be calculated directly from the standard perturbative QCD factorization formula:

$$\begin{aligned} \sigma_{\text{pQCD}}^{\text{inc}}(s; p_t^c) &= \sum_{i,j,k,l} \frac{K}{1 + \delta_{kl}} \int dx_1 dx_2 \int dp_t^2 \times \\ &\times \frac{d\hat{\sigma}_{ij \rightarrow kl}}{dp_t^2} f_{i/p_1}(x_1; p_t) f_{j/p_2}(x_2; p_t) \theta(p_t - p_t^c), \end{aligned} \quad (8)$$

where $f_{i/p_1}(x_1; p_t)$ and $f_{j/p_2}(x_2; p_t)$ are the ordinary parton distribution functions. The perturbative expression is only valid for sufficiently large jet transverse momentum p_t , so a lower cutoff p_t^c must be imposed on the integral in Eq. 8. In practice, the value of $\sigma_{\text{pQCD}}^{\text{inc}}(s; p_t^c)$ is quite sensitive to the precise choice of p_t^c , and the cross section grows rapidly with energy [2]. This has been a persistent complication in attempts to incorporate Eq. (8) into complete descriptions of multiple partonic scattering, such as the eikonal description in Eq. (7). One naturally hopes to be guided by considerations like unitarity to determine the most appropriate value for p_t^c . However, constraints like the Froissart bound do not apply directly to inclusive cross sections like Eq. (8) which are proportional to particle multiplicity.

One way to tame the rapid growth of the cross section while lowering p_t^c is to adjust the width of the distribution of hard partons in impact parameter space, so that the unitarization effects built into the eikonal description of Eq. (7) become stronger. However, this does not actually increase the range of validity of the perturbative expression, as illustrated in Fig. 1. Moreover, it conflicts with direct measurements of the impact parameter distribution of hard partons, as we will discuss later.

2 Total cross section from multiple hard collisions

Given a description of hard multiple partonic scatterings, one can directly reconstruct their contribution to the total inelastic cross section from basic combinatorial arguments [3]. Following

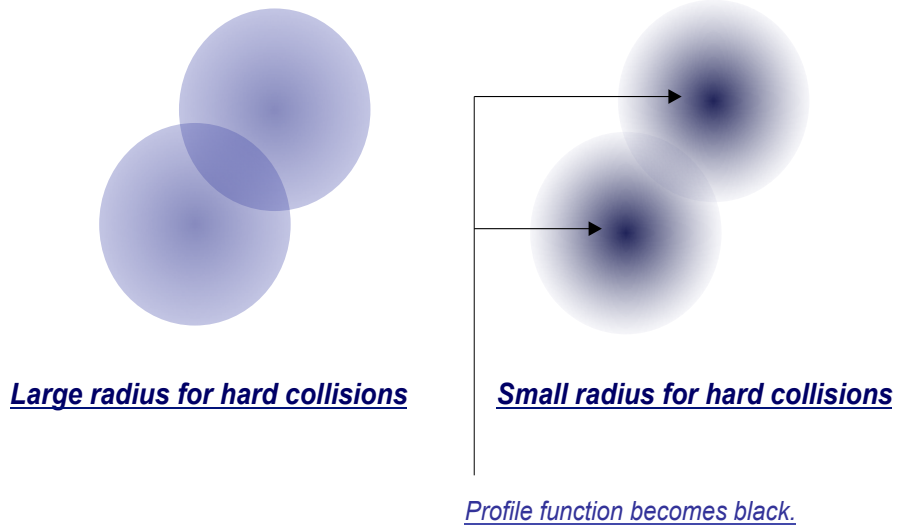


Figure 1: If the distribution of hard partons in transverse coordinate space is narrow, the cross section is tamed, but the approach to the black disk limit is faster, signaling a more rapid breakdown of normal QCD factorization.

the reasoning of Ref. [4], one finds

$$\Gamma_{\text{dijets}}^{\text{inel}}(s, b_t; p_t^c) = \sum_{n=1}^{\infty} (-1)^{n-1} \chi_{2n}(s, b_t; p_t^c), \quad (9)$$

where $\chi_{2n}(s, b_t; p_t^c)$ is the impact parameter dependent probability for n hard scatterings at impact parameter b_t . Overall consistency with Sect. 1.1 therefore requires that

$$\Gamma_{\text{dijets}}^{\text{inel}}(s, b; p_t^c) \leq \Gamma_{\text{actual}}^{\text{inel}}(s, b). \quad (10)$$

If it is assumed that the partons are identical and correlations are totally ignored, then

$$\chi_{2n}(s, b_t; p_t^c) = \frac{1}{n!} \chi_2(s, b_t; p_t^c)^n, \quad (11)$$

and the contribution to the total inelastic cross section in Eq. (9) becomes

$$\Gamma_{\text{dijets}}^{\text{inel}}(s, b_t; p_t^c) = 1 - \exp[-\chi_2(s, b_t; p_t^c)]. \quad (12)$$

Note that Eq. (12) has the same form as the eikonal expression in Eq. (7), though the reasoning that leads to it is quite different. $\chi_2(s, b_t; p_t^c)$ represents the distribution in transverse coordinate space of hard partons. Therefore, a description of the b_t -dependence of $\chi_2(s, b_t; p_t^c)$ is required to completely reproduce the total inelastic profile function.

3 Two-gluon form factor

Fortunately, the b_t -dependence in $\chi_2(s, b_t; p_t^c)$ can be extracted directly from experiments that probe impact parameter dependence. In Ref. [5], for instance, the following form was fitted to the two-gluon form factor in exclusive deeply inelastic vector meson production:

$$F_g(x, t; \mu) = \frac{1}{\left(1 - \frac{t}{m_g(x, \mu)^2}\right)^2}, \quad (13)$$

where the x and μ dependence in the parameter $m_g(x, \mu)$ account for some of the effects of evolution. Using this result allows $\chi_2(s, b_t; p_t^c)$ to be written as

$$\chi_2(s, b_t; p_t^c) = \sigma_{\text{pQCD}}^{\text{inc}}(s; p_t^c) P_2(s, b_t; p_t^c) \quad (14)$$

where

$$P_2(s, b_t; p_t^c) \equiv \frac{m_g^2(x; p_t^c)}{12\pi} \left(\frac{m_g(x; p_t^c) b_t}{2}\right)^3 K_3(m_g(x; p_t^c) b_t). \quad (15)$$

Expressed in this way, the total inclusive dijet cross section $\sigma_{\text{pQCD}}^{\text{inc}}(s; p_t^c)$ is

$$\sigma_{\text{pQCD}}^{\text{inc}}(s; p_t^c) = \int d^2\mathbf{b}_t \chi_2(s, b_t; p_t^c). \quad (16)$$

Using Eq. (14) in Eq. (12) then gives the contribution from dijet production to the left side of Eq. (10). The comparison in Eq. (10) was performed in Ref. [6] against typical extrapolations of $\Gamma_{\text{actual}}^{\text{inel}}(s, b)$ to high energy, and the inequality was found to be violated even for $b_t \gtrsim 1$ fm where multiple hard collisions are expected to be rarer. Since the impact parameter distribution is fixed by other measurements, this suggests that there is a problem with the uncorrelated scattering ansatz of Eq. (11).

4 General correlations

Reconciling the descriptions of the total cross section from Sect. 1.1 and 1.2 with the requirements of unitarity requires an account of non-perturbative correlations between the initial state partons. We note that the sizes of correlations can be extracted from measurements of observables like σ_{eff} [7] (Also, see E. Dobson, these proceedings). Therefore, in Ref. [6] the role of correlations was organized so that their effect on $\Gamma_{\text{dijets}}^{\text{inel}}(s, b; p_t^c)$ is easy to analyze.

Starting with the $n = 2$ contribution in the uncorrelated ansatz Eq. (11), a shift parametrized by $\eta_2(s, b)$ is introduced to account for correlations between two initial state partons. That is, we write

$$\chi_4(s, b; p_t^c) \rightarrow \frac{1}{2} (1 + \eta_4(s, b_t)) \chi_2(s, b; p_t^c)^2, \quad (17)$$

and similarly for larger n to account for triple and higher correlations. We call $\eta_{2n}(s, b_t)$ the n -correlation correction. Using Eq. (9) then gives

$$\Gamma_{\text{jets}}^{\text{inel}}(s, b_t; p_t^c) = 1 - \exp[-\chi_2(s, b_t; p_t^c)] - \sum_{n=2}^{\infty} \frac{(-1)^n \eta_{2n}(s, b_t)}{n!} \chi_2(s, b_t; p_t^c)^n \exp[-\chi_2(s, b_t; p_t^c)]. \quad (18)$$

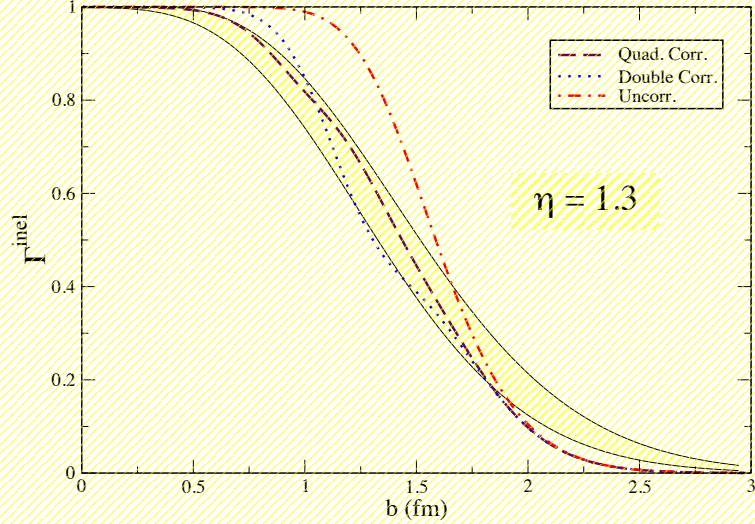


Figure 2: $\Gamma_{\text{dijets}}^{\text{inel}}(s, b_t; p_t^c)$ with correlation corrections imposed.

The $1 - \exp[-\chi_2(s, b; p_t^c)]$ part of Eq. 18 is the uncorrelated approximation. It also matches the commonly used eikonal model, though the reasoning used to arrive at it is rather different. Accounting for the $\eta_{2n}(s, b_t)$ functions for increasingly large n allows one to extend $\Gamma_{\text{jets}}^{\text{inel}}(s, b; p_t^c)$ to larger b_t before encountering a problem with Eq. (10).

The effect of double correlation corrections was estimated in Ref. [6], using the measured value of $\sigma_{eff} \approx 14.5$ mb from [8] which suggests a value for η_2 around ~ 1.3 . As a first try, we ignore the impact parameter dependence of the correction. Using this in Eq. (18) gives the $\Gamma_{\text{jets}}^{\text{inel}}(s, b_t; p_t^c)$ shown in Fig. 2. For $\Gamma_{\text{actual}}^{\text{inel}}(s, b_t)$ we use a collection of Regge-like extrapolations [9], indicated in the figure by the yellow band. The dashed curve approximates all correlations by $\eta \approx 1.3$, while the dotted curve keeps only the double correlations. The energy is chosen to be the upper limit for the LHC, $\sqrt{s} = 14$ TeV and the transverse momentum cutoff is a typical value of $p_t^c = 2.5$ GeV. From the figure, it is clear that the large impact parameter region becomes much more consistent with Eq. (10) when the effect of non-perturbative correlations is included.

5 Conclusions

Taken together, existing measurements of inclusive cross sections and the impact parameter dependence of exclusive processes imply that non-perturbative correlations are needed in models of multiple hard scatterings in order to maintain reasonable consistency with unitarity while describing the growth of the total cross section, particularly at large impact parameters. The next step is to determine a method for estimating or calculating the correlation corrections in Eq. (18). Ideally, this will follow from a complete perturbative QCD factorization treatment that describes scattering with multi-parton correlation functions. Promising work in this direction has recently been presented in Ref. [10, 11]. General considerations of how to extract the sizes

of correlations from observables in high energy collisions (e.g., Ref. [12]) are also needed.

Acknowledgments We are very thankful to the organizers of this stimulating workshop for their kind invitation. T. Rogers was also supported in part by the National Science Foundation, grant PHY-0969739. M. Strikman was supported by the US Department of Energy under grant number DE-FG02-93ER-40771.

References

- [1] R. Engel, “Models of primary interactions,” Nucl. Phys. Proc. Suppl. **122**, 40 (2003).
- [2] R. Engel, T. K. Gaisser and T. Stanev, “Extrapolation Of Hadron Production Models To Ultra-High Energy,” *Prepared for 27th International Cosmic Ray Conference (ICRC 2001), Hamburg, Germany, 7-15 Aug 2001*
- [3] L. Ametller and D. Treleani, “Shadowing In Semihard Interactions,” Int. J. Mod. Phys. A **3**, 521 (1988).
- [4] T. C. Rogers, A. M. Stasto and M. I. Strikman, “Unitarity Constraints on Semi-hard Jet Production in Impact Parameter Space,” Phys. Rev. D **77**, 114009 (2008) (arXiv:0801.0303 [hep-ph]).
- [5] L. Frankfurt, M. Strikman and C. Weiss, “Dijet production as a centrality trigger for pp collisions at CERN LHC,” Phys. Rev. D **69** (2004) 114010 (arXiv:hep-ph/0311231).
- [6] T. C. Rogers and M. Strikman, “Multiple Hard Partonic Collisions with Correlations in Proton-Proton Scattering,” Phys. Rev. D **81**, 016013 (2010) (arXiv:0908.0251 [hep-ph]).
- [7] L. Sonnenschein, “Photon + jets at D0,” (arXiv:0906.2636 [hep-ex]).
- [8] F. Abe *et al.* [CDF Collaboration], “Double parton scattering in $\bar{p}p$ collisions at $\sqrt{s} = 1.8\text{TeV}$,” Phys. Rev. D **56**, 3811 (1997).
- [9] M. M. Block, F. Halzen and B. Margolis, “How large is the total cross-section at supercollider energies?,” Phys. Rev. D **45**, 839 (1992).
M. M. Block, F. Halzen and T. Stanev, “Extending the frontiers: Reconciling accelerator and cosmic ray p p cross sections,” Phys. Rev. D **62**, 077501 (2000) (arXiv:hep-ph/0004232).
V. A. Khoze, A. D. Martin and M. G. Ryskin, “Soft diffraction and the elastic slope at Tevatron and LHC energies: A MultiPomeron approach,” Eur. Phys. J. C **18**, 167 (2000) (arXiv:hep-ph/0007359).
TOTEM Collaboration (1997), Letter of Intent, CERN/LHCC 97-49.
<http://totem.web.cern.ch/Totem/>
S. Lami, “TOTEM: The experiment to measure the total proton proton cross section at LHC,” Nucl. Phys. Proc. Suppl. **175-176**, 42 (2008) (arXiv:hep-ex/0612049).
R. M. Godbole, A. Grau, G. Pancheri and Y. N. Srivastava, “Soft gluon radiation and energy dependence of total hadronic cross-sections,” Phys. Rev. D **72**, 076001 (2005) (arXiv:hep-ph/0408355).
- [10] M. Diehl and A. Schafer, “Theoretical considerations on multiparton interactions in QCD,” Phys. Lett. B **698**, 389 (2011) (arXiv:1102.3081 [hep-ph]).
- [11] M. Diehl, D. Ostermeier and A. Schafer, “Elements of a theory for multiparton interactions in QCD,” (arXiv:1111.0910 [hep-ph]).
- [12] G. Calucci and D. Treleani, “Disentangling correlations in Multiple Parton Interactions,” Phys. Rev. D **83**, 016012 (2011) (arXiv:1009.5881 [hep-ph]).

Energy flow observables in hadronic collisions

Francesco Hautmann

Department of Theoretical Physics, University of Oxford, Oxford OX1 3NP

DOI: <http://dx.doi.org/10.3204/DESY-PROC-2012-03/52>

We present recent QCD calculations of energy flow distributions associated with the production of jets at wide rapidity separations in high-energy hadron collisions, and discuss the role of these observables to analyze contributions from parton showering and from multiple parton collisions.

Jet rates and event shape variables have long been used [1] to characterize QCD final states from hard scatter events at high-energy colliders and to describe the event's energy flow. Jet shape variables describing the jet's internal structure and the energy flow within a jet have also been studied, and are being proposed [2] as diagnostic tools at the LHC in searches for potential new physics signals from highly boosted massive states. In the last year first LHC measurements of event shapes [3] and jet shapes [4] have been performed.

In all these cases, the interpretation of results depends on a good understanding of the overall structure of the final states. This in turn implies controlling effects due to strong interaction dynamics in the initial state. Thus for instance jet shape observables such as [5, 6] that are sensitive to the jet's substructure are also sensitive to soft physics effects, including the underlying event, pile-up, and multiple parton interactions [7, 8]. Hadronic event shapes measured at the LHC [3] suggest that parton showering effects dominate contributions of hard matrix elements evaluated at high multiplicity.

In this article we focus on parton showering and multi-parton interactions (for recent discussions reviewing these topics, see respectively [9] and [10, 11]), and we discuss energy flow observables [12] which become measurable, essentially for the first time, at the LHC, and may be used for studies of showering and of multiple collisions. The main focus is on the region of high rapidities, where production of final states with sizeable momentum transfers presents new features at the LHC compared to previous collider experiments [7]. Thus we consider final states associated with the production of two jets widely separated in rapidity [13, 14]. To be specific, we consider correlations of a forward and a central jet (Fig. 1), and investigate the associated transverse energy flow as a function of pseudorapidity and azimuthal angle in the transverse plane [12].

The region of high rapidities is critical. While first measurements of forward jet spectra at the LHC [15] are roughly in agreement with predictions from different Monte Carlo simulations, detailed aspects of production rates and correlations [15, 16] are not well understood yet. From the underlying event standpoint [17, 18], energy flow measurements [19] in minimum bias and dijet events emphasize the difficulty [20] in achieving a unified underlying event description from central to forward rapidities based on PYTHIA [21] Monte Carlo tuning.

Ref. [12] considers production of central and forward jets (taking e.g. central and forward

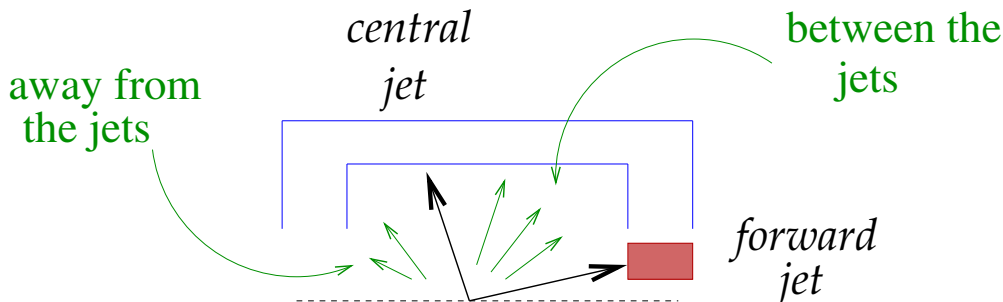


Figure 1: *Production of forward and central jets: energy flow in the inter-jet and outside regions.*

jet pseudorapidities in the range $1 < \eta_c < 2$, $-5 < \eta_f < -4$), and the transverse energy flow

$$\frac{dE_{\perp}}{d\eta} = \frac{1}{\sigma} \int dq_{\perp} q_{\perp} \frac{d\sigma}{dq_{\perp} d\eta} .$$

While the measurements [19] are designed to investigate properties of the soft underlying event, this energy flow observable is sensitive to harder color radiation. Also, it enables one to access more details on the structure of the final states associated with the jet production processes observed in [15, 16]. The transverse factor q_{\perp} in the above energy flow distribution enhances matrix element corrections due to extra hard-parton emission at short distances, and gives contributions which break the transverse momentum ordering approximation in the long-distance evolution of the parton showers. Ref. [12] computes these effects in the high-energy factorization framework [14, 22].

The transverse energy flow, obtained by summing the energies over all particles in the final states, is naturally also sensitive to soft particles being produced into the final states. In order to study hard radiation one may rather consider the associated charged particle p_T spectra. However, at the LHC it is possible to control the infrared sensitivity of the energy flow by looking at an alternative observable, defined in a different manner [12] as follows. One may first cluster particles into jets by means of a jet algorithm, and then construct the associated energy flow from jets with transverse energy above a given lower bound q_0 . Infrared safety is ensured by running a jet algorithm, as opposed to applying the bound on the energy flow integral. The question is which value of q_0 is phenomenologically meaningful. At the LHC the transverse energy per unit rapidity is large enough across a wide rapidity range that a mini-jet type of bound $q_0 \approx 5$ GeV should be feasible. This is to be contrasted with previous collider experiments, where one either did not have the detector capabilities to go very forward in rapidity (as at the Tevatron) or did not have enough transverse energy per unit rapidity (as at HERA, about $1 \div 2$ GeV per unit rapidity). Calorimetric measurements of this mini-jet energy flow at the LHC will be interesting.

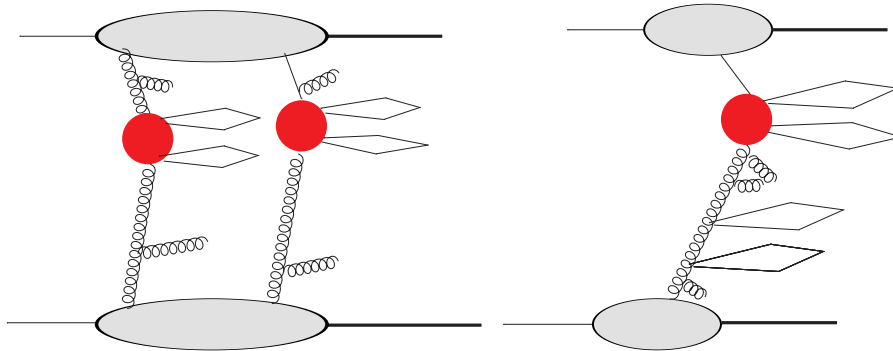


Figure 2: *Multi-jet production by (left) multiple parton collisions; (right) single parton collision.*

Multiple parton collisions (Fig. 2) form one of the major motivations for such energy flow studies. Multiple collisions become increasingly important with energy as parton densities grow [23], contributing primarily to highly differential cross sections sensitive to the detailed distribution of the states produced by parton evolution. Their role at the LHC is being studied very actively both by experiment [8, 18, 20] and theory [8, 10, 11, 24]. Since multi-parton interactions depend on the growth of parton densities and probe the detailed final-state structure, their treatment should be affected by corrections to parton shower evolution. Collinear ordering is known to give an effective picture of parton evolution for inclusive observables; however, it is not expected to represent the detailed final states reliably when longitudinal momentum fractions x become small and parton densities increase. So, in particular, noncollinear high-energy corrections to QCD showers could affect the analysis of multiple interactions significantly [7, 25]. The energy flow in forward-central jet production may provide a first step to analyze this issue.

Figs. 3 and 4 report results for the energy flow [12] from three Monte Carlo event generators: the k_{\perp} -shower CASCADE generator [26], to evaluate contributions of high-energy logarithmic corrections; the NLO matched POWHEG generator [27], to evaluate the effects of NLO corrections to matrix elements; PYTHIA Monte Carlo [21], used in two different modes: with the LHC tune Z1 [28] (PYTHIA-mpi) to evaluate contributions of multi-parton interactions, and without any multi-parton interactions (PYTHIA-nompi).

Fig. 3 shows the pseudorapidity dependence of the transverse energy flow in the region between the central and forward jets. The particle energy flow plot on the left in Fig. 3 shows the jet profile picture, and indicates enhancements of the energy flow in the inter-jet region with respect to the PYTHIA-nompi result from higher order emissions in CASCADE and from multiple parton collisions in PYTHIA-mpi. On the other hand, there is little effect from the next-to-leading hard correction in POWHEG with respect to PYTHIA-nompi. The energy flow is dominated by multiple-radiation, parton-shower effects. The mini-jet energy flow plot on the right in Fig. 3 indicates similar effects, with reduced sensitivity to infrared radiation. As the mini-jet flow definition suppresses the contribution of soft radiation, the CASCADE and PYTHIA-mpi results become more similar in the inter-jet region. Distinctive effects are also found in [12] by computations in the region away from the jets.

Fig. 4 illustrates the azimuthal dependence of the mini-jet transverse energy flow. Here $\Delta\phi$ is measured with respect to the central jet. The $\Delta\phi$ distribution is shown for three different

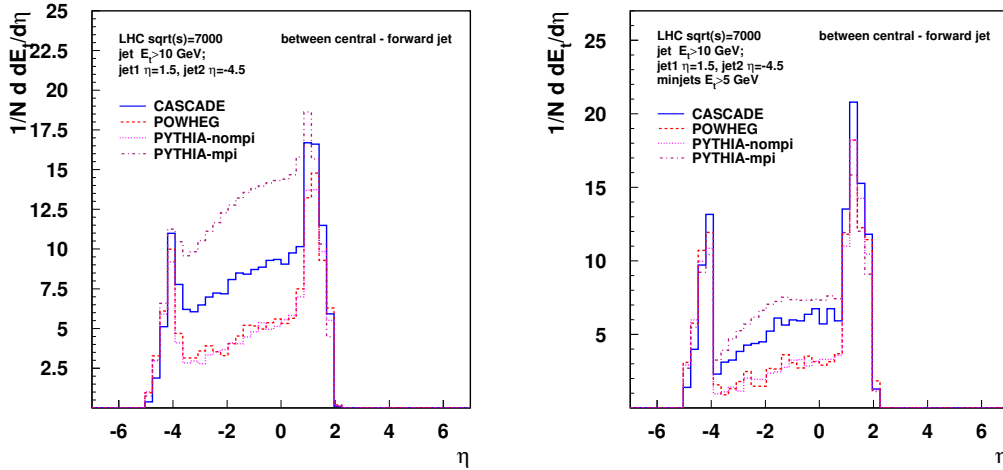


Figure 3: *Transverse energy flow [12] in the inter-jet region: (left) particle flow; (right) mini-jet flow.*

rapidity ranges, corresponding to the central-jet, forward-jet, and intermediate rapidities. As we go toward forward rapidity, the CASCADE and PYTHIA-mpi calculations give a more pronounced flattening of the $\Delta\phi$ distribution compared to POWHEG and PYTHIA-nompi, corresponding to increased decorrelation between the jets.

The above numerical results indicate that quite distinctive behaviors should be expected from measurements of particle and mini-jet energy flows associated with production of forward and central jets. They will tell us about several soft-physics effects, from the structure of underlying events to multiple parton collisions to QCD showering, which are relevant to a range of subjects in LHC physics: from studies of color flow in the QCD tuning of Monte Carlo event generators to searches for new physics signals based on the structure of jets. One feature emerging already from the above studies is that gluon emission over large rapidity intervals gives sizeable contribution to the inter-jet energy flow. As a result, the rates for multi-parton interactions may be influenced significantly by non-collinear corrections to single-chain showering. From the theory viewpoint, it underlines the relevance of approaches which aim at a more accurate and complete description of initial state dynamics by generalizing the notion of parton distributions, both for quark-dominated [29] and gluon-dominated [30] processes.

Acknowledgments. I thank the convenors for the invitation to a very nice workshop. The results in this article have been obtained in collaboration with M. Deak, H. Jung and K. Kutak.

References

- [1] B.R. Webber, arXiv:1009.5871 [hep-ph].
- [2] A. Altheimer et al., arXiv:1201.0008 [hep-ph].

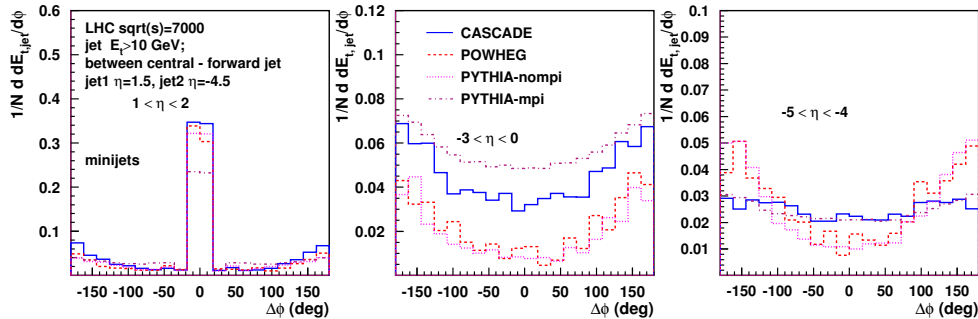


Figure 4: Azimuthal dependence of the mini-jet energy flow [12] for different rapidity ranges: (left) central-jet; (middle) intermediate; (right) forward-jet.

- [3] CMS Coll. (V. Khachatryan et al.), Phys. Lett. **B699** (2011) 48.
- [4] ATLAS Coll. (G. Aad et al.), Phys. Rev. **D83** (2011) 052003; arXiv:1203.4606 [hep-ex]; CMS Coll. (S. Chatrchyan et al.), arXiv:1204.3170 [hep-ex].
- [5] S.D. Ellis, A. Hornig, C. Lee, C.K. Vermilion and J.R. Walsh, JHEP **1011** (2010) 101; A. Banfi, M. Dasgupta, K. Khelifa-Kerfa and S. Marzani, JHEP **1008** (2010) 064; C.F. Berger, T. Kucs and G. Sterman, Phys. Rev. **D68** (2003) 014012.
- [6] J. Thaler and K. Van Tilburg, JHEP **1103** (2011) 015; J.H. Kim, Phys. Rev. **D83** (2011) 011502.
- [7] Z. Ajaltouni et al., arXiv:0903.3861 [hep-ph]; D. d’Enterria, arXiv:0911.1273 [hep-ex]; M. Grothe et al., arXiv:1103.6008 [hep-ph].
- [8] P. Bartalini and L. Fanò (eds.), Proc. 1st MPI Workshop (Perugia, 2008), arXiv:1003.4220 [hep-ex]; P. Bartalini et al., arXiv:1111.0469 [hep-ph].
- [9] S. Höche, SLAC preprint SLAC-PUB-14498 (2011).
- [10] M. Diehl, arXiv:1111.0272 [hep-ph].
- [11] Yu.L. Dokshitzer, arXiv:1203.0716 [hep-ph].
- [12] M. Deak, F. Hautmann, H. Jung and K. Kutak, Eur. Phys. J. C **72** (2012) 1982.
- [13] A.H. Mueller and H. Navelet, Nucl. Phys. **B282** (1987) 727; C. Ewerz et al., J. Phys. **G26** (2000) 696; S. Catani et al., Nucl. Phys. B Proc. Suppl. **29A** (1992) 182; D. Colferai et al., JHEP **1012** (2010) 026.
- [14] M. Deak, F. Hautmann, H. Jung and K. Kutak, arXiv:1012.6037 [hep-ph]; arXiv:1112.6386 [hep-ph]; JHEP **0909** (2009) 121; arXiv:0908.1870; F. Hautmann, arXiv:1101.2656 [hep-ph]; PoS ICHEP2010 (2010) 108.
- [15] CMS Coll. (S. Chatrchyan et al.), arXiv:1202.0704 [hep-ex].
- [16] ATLAS Coll. (G. Aad et al.), JHEP **1109** (2011) 053; CMS Coll. (S. Chatrchyan et al.), arXiv:1204.0696 [hep-ex].
- [17] ATLAS Coll. (G. Aad et al.), Eur. Phys. J. C **71** (2011) 1636; Phys. Rev. **D83** (2011) 112001.
- [18] H. Van Haevermaet, talk at DIS2012; CMS Coll. (S. Chatrchyan et al.), JHEP **1109** (2011) 109; CMS-PAS-FWD-11-003.
- [19] CMS Coll. (S. Chatrchyan et al.), JHEP **1111** (2011) 148.
- [20] P. Bartalini and L. Fanò, arXiv:1103.6201 [hep-ex].
- [21] P. Skands, Phys. Rev. **D82** (2010) 074018.
- [22] S. Catani et al., Phys. Lett. **B242** (1990) 97; Nucl. Phys. **B366** (1991) 135; Phys. Lett. **B307** (1993) 147; S. Catani and F. Hautmann, Phys. Lett. **B315** (1993) 157; Nucl. Phys. **B427** (1994) 475.

- [23] N. Paver and D. Treleani, *Nuovo Cim.* **A70** (1982) 215; T. Sjöstrand and M. van Zijl, *Phys. Rev.* **D36** (1987) 2019.
- [24] J.R. Gaunt and W.J. Stirling, arXiv:1202.3056 [hep-ph]; *JHEP* **1106** (2011) 048; *JHEP* **1003** (2010) 005; B. Blok, Yu. Dokshitzer, L. Frankfurt and M. Strikman, *Eur. Phys. J. C* **72** (2012) 1963; *Phys. Rev.* **D83** (2011) 071501; M. Strikman and W. Vogelsang, *Phys. Rev.* **D83** (2011) 034029; T.C. Rogers and M. Strikman, *Phys. Rev.* **D81** (2010) 016013; G. Calucci and D. Treleani, arXiv:1204.6403 [hep-ph]; *Phys. Rev.* **D83** (2011) 016012; *Phys. Rev.* **D80** (2009) 054025; *Phys. Rev.* **D79** (2009) 074013; D. Treleani, *Phys. Rev.* **D76** (2007) 076006; M. Diehl and A. Schäfer, *Phys. Lett.* **B698** (2011) 389; M. Diehl, D. Ostermaier and A. Schäfer, *JHEP* **1203** (2012) 089; A.V. Manohar and W.J. Waalewijn, arXiv:1202.5034 [hep-ph]; arXiv:1202.3794 [hep-ph]; F.A. Ceccopieri, *Phys. Lett.* **B697** (2011) 482; S. Domdey, H.-J. Pirner and U.A. Wiedemann, *Eur. Phys. J. C* **65** (2010) 153; S.P. Baranov, A.M. Snigirev and N.P. Zotov, *Phys. Lett.* **B705** (2011) 116; C.H. Kom, A. Kulesza and W.J. Stirling, *Eur. Phys. J. C* **71** (2011) 1802; *Phys. Rev. Lett.* **107** (2011) 082002; A.M. Snigirev, *Phys. Rev.* **D83** (2011) 034028; M.G. Ryskin and A.M. Snigirev, arXiv:1203.2330 [hep-ph]; *Phys. Rev.* **D83** (2011) 114047; E. Maina, *JHEP* **1101** (2011) 061; *JHEP* **0909** (2009) 081; *JHEP* **0904** (2009) 098; D. Bandurin, G. Golovanov and N. Skachkov, *JHEP* **1104** (2011) 054; E.L. Berger, C.B. Jackson, S. Quackenbush and G. Shaughnessy, *Phys. Rev.* **D84** (2011) 074021; E.L. Berger, C.B. Jackson and G. Shaughnessy, *Phys. Rev.* **D81** (2010) 014014.
- [25] F. Hautmann, *Acta Phys. Polon. B* **40** (2009) 2139; PoS ICHEP2010 (2010) 150; in J. Bartels et al., arXiv:0902.0377 [hep-ph], Proc. ISMD2008; F. Hautmann and H. Jung, *Nucl. Phys. Proc. Suppl.* **184** (2008) 64; arXiv:0812.3026; arXiv:0808.0873; *JHEP* **0810** (2008) 113; arXiv:0804.1746; arXiv:0805.4786.
- [26] H. Jung et al., *Eur. Phys. J. C* **70** (2010) 1237.
- [27] S. Alioli, P. Nason, C. Oleari and E. Re, *JHEP* **1104** (2011) 081.
- [28] R.D. Field, arXiv:1010.3558 [hep-ph]; arXiv:1202.0901 [hep-ph]; *Acta Phys. Polon. B* **42** (2011) 2631.
- [29] S. Mert Aybat and T.C. Rogers, *Phys. Rev.* **D83** (2011) 114042; P.J. Mulders and T.C. Rogers, *Phys. Rev.* **D81** (2010) 094006; S. Mantry and F. Petriello, *Phys. Rev.* **D84** (2011) 014030; *Phys. Rev.* **D83** (2011) 053007; arXiv:1108.3609 [hep-ph]; Y. Li, S. Mantry and F. Petriello, *Phys. Rev.* **D84** (2011) 094014; T. Becher and M. Neubert, *Eur. Phys. J. C* **71** (2011) 1665; I.W. Stewart, F.J. Tackmann and W.J. Waalewijn, *JHEP* **1009** (2010) 005; A. Idilbi and I. Scimemi, *Phys. Lett.* **B695** (2011) 463; arXiv:1012.4419 [hep-ph]; M. Garcia-Echevarria, A. Idilbi and I. Scimemi, arXiv:1111.4996 [hep-ph]; arXiv:1104.0686 [hep-ph]; F. Hautmann, M. Hentschinski and H. Jung, arXiv:1205.1759 [hep-ph]; F.A. Ceccopieri, *Mod. Phys. Lett. A* **24** (2009) 3025; arXiv:1006.4731 [hep-ph]; I. Cherednikov and N. Stefanis, arXiv:1104.0168 [hep-ph]; *Phys. Rev.* **D80** (2009) 054008; *Mod. Phys. Lett. A* **24** (2009) 2913; *Nucl. Phys.* **B802** (2008) 146; *Phys. Rev.* **D77** (2008) 094001; J.C. Collins and F. Hautmann, *JHEP* **0103** (2001) 016; *Phys. Lett.* **B472** (2000) 129; F. Hautmann, *Nucl. Phys.* **B604** (2001) 391; *Phys. Lett.* **B655** (2007) 26; arXiv:0708.1319; hep-ph/0011381; hep-ph/0105098; hep-ph/0101006.
- [30] F. Dominguez, J.W. Qiu, B.W. Xiao and F. Yuan, arXiv:1109.6293 [hep-ph]; F. Dominguez, A.H. Mueller, S. Munier and B.W. Xiao, arXiv:1108.1752 [hep-ph]; E. Avsar, arXiv:1108.1181 [hep-ph]; arXiv:1203.1916 [hep-ph]; F. Dominguez, C. Marquet, B.W. Xiao and F. Yuan, *Phys. Rev.* **D83** (2011) 105005; B.W. Xiao and F. Yuan, *Phys. Rev.* **D82** (2010) 114009; *Phys. Rev. Lett.* **105** (2010) 062001; F. Dominguez, B.W. Xiao and F. Yuan, arXiv:1009.2141 [hep-ph]; F. Hautmann and D.E. Soper, *Phys. Rev.* **D75** (2007) 074020; *Phys. Rev.* **D63** (2000) 011501; F. Hautmann, arXiv:0812.2873 [hep-ph]; *Phys. Lett.* **B643** (2006) 171; hep-ph/0209320; hep-ph/0105082; F. Hautmann, Z. Kunszt and D.E. Soper, hep-ph/9906284; hep-ph/9806298.

Collinear distributions in double parton scattering

Mikhail G. Ryskin¹, Alexander M. Snigirev^{2*}

¹ Petersburg Nuclear Physics Institute, Gatchina, St. Petersburg, 188300, Russia

² Skobeltsyn Institute of Nuclear Physics, Lomonosov Moscow State University, 119991, Moscow, Russia

DOI: <http://dx.doi.org/10.3204/DESY-PROC-2012-03/28>

In this talk we consider revised formulas which operate with the modified collinear two-parton distributions extracted from deep inelastic scattering to describe the inclusive cross section of a double parton scattering in a hadron collision. The related phenomenological effects are discussed.

1 Introduction and customary formalism

Now it has become clear that multiple parton interactions play an important role in high energy hadronic collisions and are one of the most common, yet poorly understood [1], phenomenon at the LHC. Experimental evidence for double hard scattering has been found in the production of multijets [2, 3, 4] and of single photons associated with three jets [5, 6]. The theoretical investigation of multiple parton interactions has a long history and has experienced a renewed interest in more recent times (see, for instance, [1] and references therein), driven by the need to understand the hadronic activity at the LHC.

Nevertheless, the phenomenology of multiple parton interactions relies on the models which are essentially intuitive and involve substantial simplifying assumptions. Therefore, it is extremely desirable to combine theoretical efforts in order to achieve a better description of multiple interactions, in particular, double scattering, which is very likely to be an important multiple scattering mode at the LHC. In this talk we consider some steps towards this purpose basing on our previous work [7]. The cross section formulas currently used to calculate the double scattering processes are revised basing on the modified collinear two-parton distributions extracted from deep inelastic scattering (DIS).

Using only the assumption of factorization of the two hard parton processes A and B , the inclusive cross section of a double parton scattering process in a hadron collision may be written in the following form

$$\begin{aligned} \sigma_{(A,B)}^D = & \frac{m}{2} \sum_{i,j,k,l} \int \Gamma_{ij}(x_1, x_2; \mathbf{b}_1, \mathbf{b}_2; Q_1^2, Q_2^2) \times \hat{\sigma}_{ik}^A(x_1, x'_1, Q_1^2) \hat{\sigma}_{jl}^B(x_2, x'_2, Q_2^2) \\ & \times \Gamma_{kl}(x'_1, x'_2; \mathbf{b}_1 - \mathbf{b}, \mathbf{b}_2 - \mathbf{b}; Q_1^2, Q_2^2) dx_1 dx_2 dx'_1 dx'_2 d^2 b_1 d^2 b_2 d^2 b, \end{aligned} \quad (1)$$

*Speaker

where \mathbf{b} is the impact parameter — the distance between centers of colliding hadrons (e.g., the beam and the target) in transverse plane. $\Gamma_{ij}(x_1, x_2; \mathbf{b}_1, \mathbf{b}_2; Q_1^2, Q_2^2)$ are the double parton distribution functions, which depend on the longitudinal momentum fractions x_1 and x_2 , and on the transverse position \mathbf{b}_1 and \mathbf{b}_2 of the two partons undergoing the hard processes A and B at the scales Q_1 and Q_2 . $\hat{\sigma}_{ik}^A$ and $\hat{\sigma}_{jl}^B$ are the parton-level subprocess cross sections. The factor $m/2$ appears due to the symmetry of the expression for interchanging parton species i and j . $m = 1$ if $A = B$, and $m = 2$ otherwise.

It is typically assumed that the double parton distribution functions may be decomposed in terms of longitudinal and transverse components as follows:

$$\Gamma_{ij}(x_1, x_2; \mathbf{b}_1, \mathbf{b}_2; Q_1^2, Q_2^2) = D_h^{ij}(x_1, x_2; Q_1^2, Q_2^2) f(\mathbf{b}_1) f(\mathbf{b}_2), \quad (2)$$

where $f(\mathbf{b}_1)$ is supposed to be a universal function for all kinds of partons with its normalization fixed as

$$\int f(\mathbf{b}_1) f(\mathbf{b}_1 - \mathbf{b}) d^2 b_1 d^2 b = \int T(\mathbf{b}) d^2 b = 1, \quad (3)$$

and $T(\mathbf{b}) = \int f(\mathbf{b}_1) f(\mathbf{b}_1 - \mathbf{b}) d^2 b_1$ is the overlap function.

If one also makes the assumption that the longitudinal components $D_h^{ij}(x_1, x_2; Q_1^2, Q_2^2)$ reduce to the product of two independent one parton distributions,

$$D_h^{ij}(x_1, x_2; Q_1^2, Q_2^2) = D_h^i(x_1; Q_1^2) D_h^j(x_2; Q_2^2), \quad (4)$$

the cross section of double parton scattering can be expressed in the simple form

$$\sigma_{(A,B)}^D = \frac{m}{2} \frac{\sigma_{(A)}^S \sigma_{(B)}^S}{\sigma_{\text{eff}}}, \quad (5)$$

$$\sigma_{\text{eff}} = [\int d^2 b (T(\mathbf{b}))^2]^{-1}. \quad (6)$$

In this representation and at the factorization of longitudinal and transverse components, the inclusive cross section of single hard scattering is written as

$$\begin{aligned} \sigma_{(A)}^S &= \sum_{i,k} \int D_h^i(x_1; Q_1^2) f(\mathbf{b}_1) \hat{\sigma}_{ik}^A(x_1, x'_1) D_{h'}^k(x'_1; Q_1^2) f(\mathbf{b}_1 - \mathbf{b}) dx_1 dx'_1 d^2 b_1 d^2 b \\ &= \sum_{i,k} \int D_h^i(x_1; Q_1^2) \hat{\sigma}_{ik}^A(x_1, x'_1) D_{h'}^k(x'_1; Q_1^2) dx_1 dx'_1. \end{aligned} \quad (7)$$

These simplifying assumptions, though rather customary in the literature and quite convenient from a computational point of view, are not sufficiently justified and should be revised [7, 8, 9, 10]. However, the starting cross section formula (1) was found (derived) in many works (see, e.g., Refs. [8, 9, 10]) using the light-cone variables and the same approximations as those applied to the processes with a single hard scattering.

2 Revised formulas in momentum representation

All the previous formulas were written in the mixed (momentum and coordinate) representation. Recall that in general, for the case of the multiple parton interactions, we have to use

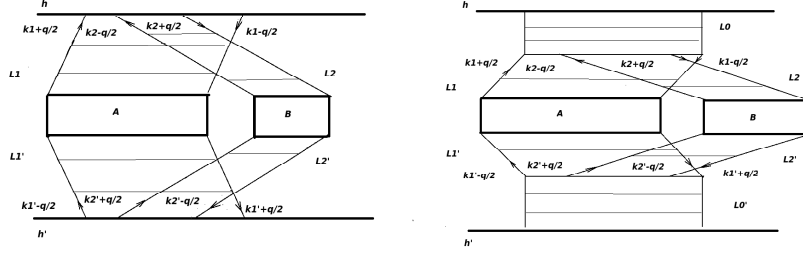


Figure 1: Graphs for double parton scattering according to the first term in Eq. (9) (left) and according to the second evolution term in Eq. (9) (right). A and B are the hard parton subprocesses. q is the momentum transfer through the ladders $L1, L2, L1'$ and $L2'$.

the *Generalized* Parton Distribution Functions (GPDF). In other words, in the Feynman diagram (ladder) which describes the GPDF, the parton momenta k_L (in the left part of diagram corresponding to the amplitude A^*) and k_R (in the right part of the diagram corresponding to amplitude A) may be different. Let us denote $k_L = k + q/2$ and $k_R = k - q/2$, where q is the momentum transfer through the whole ladder. Since the ladders in Figure 1 form a loop we will call q the loop momentum. In the previous formulas, instead of transverse momentum q_t , we used the conjugate coordinate \mathbf{b} ¹.

For our further goal the momentum representation is more convenient:

$$\begin{aligned} \sigma_{(A,B)}^D = & \frac{m}{2} \sum_{i,j,k,l} \int \Gamma_{ij}(x_1, x_2; \mathbf{q}; Q_1^2, Q_2^2) \hat{\sigma}_{ik}^A(x_1, x_1') \hat{\sigma}_{jl}^B(x_2, x_2') \\ & \times \Gamma_{kl}(x_1', x_2'; -\mathbf{q}; Q_1^2, Q_2^2) dx_1 dx_2 dx_1' dx_2' \frac{d^2 q}{(2\pi)^2}. \end{aligned} \quad (8)$$

The hard subprocesses A and B originate from two different branches of the parton cascade. Note that only the sum of the parton momenta (in both branches) is conserved, while in each individual branch there may be some difference, q , between the transverse (parton) momenta in the initial state wave function and the conjugate wave function.

The main problem is to make the correct calculation of $\Gamma_{ij}(x_1, x_2; \mathbf{q}; Q_1^2, Q_2^2)$ without simplifying assumptions (2) and (4). These functions are available in the current literature [11, 12, 13, 14] only for $\mathbf{q} = 0$ in the collinear approximation. In this approximation the two-parton distribution functions, $\Gamma_{ij}(x_1, x_2; \mathbf{q} = 0; Q^2, Q^2) = D_h^{ij}(x_1, x_2; Q^2, Q^2)$ with the two hard scales set equal, satisfy the generalized Dokshitzer-Gribov-Lipatov-Altarelli-Parisi (DGLAP) evolution equations, derived initially in Refs. [13, 14].

The evolution equation for Γ_{ij} consists of two terms. The first term describes the independent (simultaneous) evolution of two branches of parton cascade: one branch contains the parton x_1 , and another branch — the parton x_2 . The second term allows for the possibility of splitting of one parton evolution (one branch k) into two different branches, i and j . It contains the usual splitting function $P_{k \rightarrow ij}(z)$. The solutions of the generalized DGLAP evolution equations with the given initial conditions at the reference scales μ^2 may be written [7, 15] in

¹In the case of conventional DIS the cross section is given by the integral over \mathbf{b} corresponding to $q_t = 0$.

the form:

$$D_h^{j_1 j_2}(x_1, x_2; \mu^2, Q_1^2, Q_2^2) = D_{h_1}^{j_1 j_2}(x_1, x_2; \mu^2, Q_1^2, Q_2^2) + D_{h_2}^{j_1 j_2}(x_1, x_2; \mu^2, Q_1^2, Q_2^2) \quad (9)$$

with

$$\begin{aligned} & D_{h_1}^{j_1 j_2}(x_1, x_2; \mu^2, Q_1^2, Q_2^2) \\ &= \sum_{j_1' j_2'} \int_{x_1}^{1-x_2} \frac{dz_1}{z_1} \int_{x_2}^{1-z_1} \frac{dz_2}{z_2} D_h^{j_1' j_2'}(z_1, z_2; \mu^2) D_{j_1'}^{j_1}\left(\frac{x_1}{z_1}; \mu^2, Q_1^2\right) D_{j_2'}^{j_2}\left(\frac{x_2}{z_2}; \mu^2, Q_2^2\right) \end{aligned} \quad (10)$$

and

$$\begin{aligned} & D_{h_2}^{j_1 j_2}(x_1, x_2; \mu^2, Q_1^2, Q_2^2) \\ &= \sum_{j' j_1' j_2'} \int_{\mu^2}^{\min(Q_1^2, Q_2^2)} dk^2 \frac{\alpha_s(k^2)}{2\pi k^2} \int_{x_1}^{1-x_2} \frac{dz_1}{z_1} \int_{x_2}^{1-z_1} \frac{dz_2}{z_2} D_h^{j'}(z_1 + z_2; \mu^2, k^2) \\ &\quad \times \frac{1}{z_1 + z_2} P_{j' \rightarrow j_1' j_2'}\left(\frac{z_1}{z_1 + z_2}\right) D_{j_1'}^{j_1}\left(\frac{x_1}{z_1}; k^2, Q_1^2\right) D_{j_2'}^{j_2}\left(\frac{x_2}{z_2}; k^2, Q_2^2\right), \end{aligned} \quad (11)$$

where $\alpha_s(k^2)$ is the QCD coupling, $D_{j_1'}^{j_1}(z; k^2, Q^2)$ are the known single distribution functions (the Green's functions) at the parton level with the specific δ -like initial conditions at $Q^2 = k^2$. $D_h^{j_1' j_2'}(z_1, z_2, \mu^2)$ is the initial (input) two-parton distribution at the relatively low scale μ . The one parton distribution (before splitting into the two branches at some scale k^2) is given by $D_h^{j'}(z_1 + z_2, \mu^2, k^2)$. Note, that in Eq. (9) we assume that the loop momentum $q < \mu$ is small and due to strong ordering of parton transverse momenta in the collinear DGLAP evolution it may be neglected.

The first term is the solution of homogeneous evolution equation (independent evolution of two branches), where the input two-parton distribution is generally not known at the low scale μ . For this nonperturbative two-parton function at low z_1, z_2 one may assume the factorization $D_h^{j_1' j_2'}(z_1, z_2, \mu^2) \simeq D_h^{j_1'}(z_1, \mu^2) D_h^{j_2'}(z_2, \mu^2)$ neglecting the constraints due to momentum conservation ($z_1 + z_2 < 1$). This leads to

$$D_{h_1}^{ij}(x_1, x_2; \mu^2, Q_1^2, Q_2^2) \simeq D_h^i(x_1; \mu^2, Q_1^2) D_h^j(x_2; \mu^2, Q_2^2). \quad (12)$$

As a rule, the multiple interactions take place at relatively low transverse momenta and low x_1, x_2 where the factorization hypothesis (12) for the first term is a good approximation. In this case, the cross section for double parton scattering can be estimated, using the two-gluon form factor of the nucleon $F_{2g}(q)$ [8, 16] for the dominant gluon-gluon scattering mode (or something similar for other parton scattering modes),

$$\begin{aligned} \sigma_{(A,B)}^{D,1 \times 1} &= \frac{m}{2} \sum_{i,j,k,l} \int D_h^i(x_1; \mu^2, Q_1^2) D_h^j(x_2; \mu^2, Q_2^2) \hat{\sigma}_{ik}^A(x_1, x_1') \hat{\sigma}_{jl}^B(x_2, x_2') \\ &\quad \times D_{h'}^k(x_1'; \mu^2, Q_1^2) D_{h'}^l(x_2'; \mu^2, Q_2^2) dx_1 dx_2 dx_1' dx_2' \int F_{2g}^A(q) \frac{d^2 q}{(2\pi)^2}. \end{aligned} \quad (13)$$

From the dipole fit $F_{2g}(q) = 1/(q^2/m_g^2 + 1)^2$ to the two-gluon form factor follows that the characteristic value of q is of the order of the “effective gluon mass” m_g . Thus the initial conditions for the single distributions can be fixed at some not large reference scale $\mu \sim m_g$, because of the weak logarithmic dependence of these distributions on the scale value. In this approach $\int F_{2g}^4(q) \frac{d^2q}{(2\pi)^2}$ gives the estimation of $[\sigma_{\text{eff}}]^{-1}$.

The second term in Eq. (9) is the solution of complete evolution equation with the evolution originating from one “nonperturbative” parton at the reference scale. Here, the independent evolution of two branches starts at the scale k^2 from a point-like parton j' . In this case the large q_t domain is not suppressed by the form factor $F_{2g}(q)$ and the corresponding contribution to the cross section reads

$$\begin{aligned}
 \sigma_{(A,B)}^{D,2 \times 2} = & \frac{m}{2} \sum_{i,j,k,l} \int dx_1 dx_2 dx'_1 dx'_2 \int^{\min(Q_1^2, Q_2^2)} \frac{d^2q}{(2\pi)^2} \\
 & \times \sum_{j'j_1'j_2'} \int^{q^2} \frac{\min(Q_1^2, Q_2^2)}{dk^2} \frac{\alpha_s(k^2)}{2\pi k^2} \int_{x_1}^{1-x_2} \frac{dz_1}{z_1} \int_{x_2}^{1-z_1} \frac{dz_2}{z_2} D_h^{j'}(z_1 + z_2; \mu^2, k^2) \\
 & \times \frac{1}{z_1 + z_2} P_{j' \rightarrow j_1' j_2'} \left(\frac{z_1}{z_1 + z_2} \right) D_{j_1'}^i \left(\frac{x_1}{z_1}; k^2, Q_1^2 \right) D_{j_2'}^j \left(\frac{x_2}{z_2}; k^2, Q_2^2 \right) \hat{\sigma}_{ik}^A(x_1, x'_1) \hat{\sigma}_{jl}^B(x_2, x'_2) \\
 & \times \sum_{j'j_1'j_2'} \int^{q^2} \frac{\min(Q_1^2, Q_2^2)}{dk'^2} \frac{\alpha_s(k'^2)}{2\pi k'^2} \int_{x'_1}^{1-x'_2} \frac{dz_1}{z_1} \int_{x'_2}^{1-z_1} \frac{dz_2}{z_2} D_{h'}^{j'}(z_1 + z_2; \mu^2, k'^2) \\
 & \times \frac{1}{z_1 + z_2} P_{j' \rightarrow j_1' j_2'} \left(\frac{z_1}{z_1 + z_2} \right) D_{j_1'}^k \left(\frac{x'_1}{z_1}; k'^2, Q_1^2 \right) D_{j_2'}^l \left(\frac{x'_2}{z_2}; k'^2, Q_2^2 \right), \quad (14)
 \end{aligned}$$

or in substantially shorter yet less transparent form:

$$\begin{aligned}
 \sigma_{(A,B)}^{D,2 \times 2} = & \frac{m}{2} \sum_{i,j,k,l} \int dx_1 dx_2 dx'_1 dx'_2 \int^{\min(Q_1^2, Q_2^2)} \frac{d^2q}{(2\pi)^2} \\
 & \times D_{h_2}^{ij}(x_1, x_2; q^2, Q_1^2, Q_2^2) \hat{\sigma}_{ik}^A(x_1, x'_1) \hat{\sigma}_{jl}^B(x_2, x'_2) D_{h'_2}^{kl}(x'_1, x'_2; q^2, Q_1^2, Q_2^2). \quad (15)
 \end{aligned}$$

By analogy, the combined (“interference”) contribution may be written as

$$\begin{aligned}
 \sigma_{(A,B)}^{D,1 \times 2} = & \frac{m}{2} \sum_{i,j,k,l} \int dx_1 dx_2 dx'_1 dx'_2 \int^{\min(Q_1^2, Q_2^2)} F_{2g}^2(q) \frac{d^2q}{(2\pi)^2} \\
 & \times [D_h^i(x_1; \mu^2, Q_1^2) D_h^j(x_2; \mu^2, Q_2^2) \hat{\sigma}_{ik}^A(x_1, x'_1) \hat{\sigma}_{jl}^B(x_2, x'_2) D_{h'_2}^{kl}(x'_1, x'_2; q^2, Q_1^2, Q_2^2) \\
 & + D_{h_2}^{ij}(x_1, x_2; q^2, Q_1^2, Q_2^2) \hat{\sigma}_{ik}^A(x_1, x'_1) \hat{\sigma}_{jl}^B(x_2, x'_2) D_{h'}^k(x'_1; \mu^2, Q_1^2) D_{h'}^l(x'_2; \mu^2, Q_2^2)]. \quad (16)
 \end{aligned}$$

The equations (13), (15) and (16) present our solution of the problem — we obtain the estimation of the inclusive cross section for double parton scattering, taking into account the

QCD evolution and based on the well-known collinear distributions extracted from deep inelastic scattering. Similar results were obtained in Ref. [17] with an emphasis on the differential cross sections. However, one should note that the input two-parton distribution $D_h^{j_1, j_2}(z_1, z_2, \mu^2)$ may be more complicated than that given by factorization ansatz (12). Now, let us discuss in more detail the second term, that is the 2×2 contribution.

3 Discussion and conclusions

The contribution to the cross section from the second term induced by the QCD evolution cannot be reduced to the form (5) with some new constant effective cross section as it was done in earlier estimations [18, 19, 20]. The QCD evolution effects for the cross section are anticipated to be larger than for the two-parton distribution functions. For those such effects were estimated in Refs. [12, 21] on the level of 10% - 30% as compared to the “factorization” components at $x \sim 0.1$ and $Q \sim 100$ GeV. Indeed, in Eq. (14) the integration over q includes no strong suppression factor $F_{2g}(q)$ and the phase space integral may be estimated as

$$\int^{Q^2} dq^2 \int_{q^2}^{Q^2} \frac{dk^2}{k^2} \int_{q^2}^{Q^2} \frac{dk'^2}{k'^2} \simeq 2Q^2, \quad Q^2 \gg \mu^2, \quad (17)$$

where within the leading order (LO) accuracy we take q^2 as the lower limit for k^2 and k'^2 integrations; at $q^2 > k^2$ the loop momentum q_t destroys the logarithmic structure of the integrals for collinear evolution from k^2 to Q^2 .

We see that at a large final scale Q^2 the contribution of the second (2×2) component should dominate being proportional to Q^2 , while the contributions of the 1×1 or 1×2 components $\sim m_g^2 \sim 1/\sigma_{eff}$ are limited by the nucleon (hadron) form factor F_{2g} ².

The real gain is, of course, smaller due to the running coupling constant and the fact that at low x distribution functions grow logarithmically on the integration variables. So we have the additional factor in favor of the first factorized term of Eq. (9), which is proportional [22] to the initial gluon and quark multiplicities: the second term evolves from *one* “nonperturbative” parton, while the first term has *two* initial independent “nonperturbative” partons at the reference scale.

As a result, the experimental effective cross section, σ_{eff}^{exp} , which is not measured directly but is extracted by means of the normalization to the product of two single cross sections:

$$\frac{\sigma_{DPS}^{\gamma+3j}}{\sigma^{\gamma j} \sigma^{jj}} = [\sigma_{eff}^{exp}]^{-1}, \quad (18)$$

appears to be dependent on the probing hard scale. It should decrease with increasing the resolution scale because all additional contributions to the cross section of double parton scattering are positive and increase. In the above formula, $\sigma^{\gamma j}$ and σ^{jj} are the inclusive $\gamma+$ jet and dijets cross sections, $\sigma_{DPS}^{\gamma+3j}$ is the inclusive cross section of the $\gamma+3$ jets events produced in the double parton process. It is worth noticing that the CDF and D0 Collaborations extract σ_{eff}^{exp} without any theoretical predictions on the $\gamma+$ jet and dijets cross sections, by comparing the number of observed double parton $\gamma+3$ jets events in one $p\bar{p}$ collision to the number of $\gamma+3$ jets events with hard interactions occurring in the case of two separate $p\bar{p}$ collisions.

²In terms of impact parameters \mathbf{b} this means that in the second (2×2) term two pairs of partons are very close to each other; $|\mathbf{b}_1 - \mathbf{b}_2| \sim 1/Q$.

The recent D0 measurements [6] represent this effective cross section, $\sigma_{\text{eff}}^{\text{exp}}$, as a function of the second (ordered in the transverse momentum p_T) jet $p_T, p_T^{\text{jet}2}$, which can serve as a resolution scale. The obtained cross sections reveal a tendency to be dependent on this scale. In Ref. [23] this observation was interpreted as the first indication to the QCD evolution of double parton distributions.

We have to emphasize that the dominant contribution to the phase space integral (17) comes from a large $q^2 \sim Q^2$ and, strictly speaking, the above reasoning makes no allowance for the collinear (DGLAP) evolution of two independent branches of the parton cascade (i.e., in the ladders $L1, L2, L1'$ and $L2'$) in the 2×2 term. Formally, in the framework of collinear approach this contribution should be considered as the result of interaction of *one* pair of partons with the $2 \rightarrow 4$ hard subprocess³. Recall, however, that when estimating (17) we neglect the anomalous dimension, γ , of the parton distributions $D_j^k(x/z, k^2, Q^2) \propto (Q^2/k^2)^\gamma$. In collinear approach the anomalous dimensions $\gamma \propto \alpha_s \ll 1$ are assumed to be small. On the other hand, in a low x region the value of anomalous dimension is enhanced by the $\ln(1/x)$ logarithm and may be rather large numerically. So the integral over q^2 is *slowly* convergent and the major contribution to the cross section is expected to come actually from some characteristic intermediate region, $m_g^2 \ll q^2 \ll Q_1^2$ ($Q_1 < Q_2$). Thus we do not expect such strong sensitivity to the upper limit of q -integration as in the case of the pure phase space integral (17). Therefore it makes sense to consider the quantitative contribution of the 2×2 term even within the collinear approach as applied to the LHC kinematics, where the large (in comparison with m_g) available values of Q_1 and Q_2 provide wide enough integration region for the characteristic loop momenta q .

Next, in a configuration with two quite different scales (say, $Q_1^2 \ll Q_2^2$) the upper limit of q^2 integral is given by a smaller scale (at $q > Q_1$ the hard matrix element corresponding to σ^A begins to diminish with q_t). In this case the collinear evolution from the scale $q = Q_1$ up to the scale Q_2 in the ladders (parton branches) $L2$ and $L2'$ seems sufficiently justified.

In summary, we suggest a practical method which makes it possible to estimate the inclusive cross section for double parton scattering, taking into account the QCD evolution and based on the well-known collinear distributions extracted from deep inelastic scattering. We also support the conclusion in Refs. [23, 24] that the experimentally measured effective cross section, $\sigma_{\text{eff}}^{\text{exp}}$, (18) should decrease with increasing the resolution scale Q^2 due to presence of the evolution (correlation) term in the two-parton distributions.

Acknowledgments A.M.S. wishes to express the gratitude to the organizers of MPI@LHC 2011 for the warm welcome and hospitality. This work is partly supported by Russian Foundation for Basic Research Grants No. 10-02-93118 and No. 11-02-08502-z, by the President of Russian Federation for support of Leading Scientific Schools Grant No 4142.2010.2, by FASI State contract No 02.740.11.0244 and by the Federal Program of the Russian State RSGSS=65751.2010.2.

References

- [1] P. Bartalini *et al.*, “Multi-Parton interactions at the LHC”, (arXiv:1111.0469 [hep-ph]).
- [2] **AFS** Collaboration, T. Akesson *et al.*, “Double parton scattering in p p collisions at $\sqrt{S} = 63$ GeV”, Z. Phys. C **34** (1987) 163.

³This is in agreement with the statement [10] that “the structure of right figure should not be included in the leading logarithmic *double* parton scattering cross section”.

- [3] **UA2** Collaboration, J. Alitti *et al.*, “A Study of multi-jet events at the CERN anti-p p collider and a search for double parton scattering”, *Phys. Lett. B* **268** (1991) 145.
- [4] **CDF** Collaboration, F. Abe *et al.*, “Study of four-jet events and evidence for double parton interactions in p p-bar collisions at $\sqrt{s} = 1.8$ TeV”, *Phys. Rev. D* **47** (1993) 4857.
- [5] **CDF** Collaboration F. Abe *et al.*, “Double Parton Scattering in p anti-p Collisions at $\sqrt{s} = 1.8$ TeV”, *Phys. Rev. D* **56** (1997) 3811.
- [6] **D0** Collaboration, V.M. Abazov *et al.*, “Double parton interactions in photon+3 jet events in p \bar{p} collisions $\sqrt{s} = 1.96$ TeV”, *Phys. Rev. D* **81** (2010) 052012 (arXiv:0912.5104v2 [hep-ex]).
- [7] M.G. Ryskin and A.M. Snigirev, “Fresh look at double parton scattering”, *Phys. Rev. D* **83** (2011) 114047 (arXiv:1103.3495v2 [hep-ph]).
- [8] B. Blok, Yu. Dokshitzer, L. Frankfurt, and M. Strikman, “The Four jet production at LHC and Tevatron in QCD”, *Phys. Rev. D* **83** (2011) 071501 (arXiv:1009.2714v2 [hep-ph]).
- [9] M. Diehl and A. Schafer, “Theoretical considerations on multiparton interactions in QCD”, *Phys. Lett. B* **698** (2011) 389 (arXiv:1102.3081v2 [hep-ph]).
- [10] J.R. Gaunt and W.J. Stirling, “Double Parton Scattering Singularity in One-Loop Integrals”, *JHEP* **1106** (2011) 048 (arXiv:1103.1888v2 [hep-ph]).
- [11] A.M. Snigirev, ‘ ‘QCD status of factorization ansatz for double parton distributions”, *Phys. Rev. D* **68** (2003) 114012.
- [12] V.L. Korotkikh and A.M. Snigirev, “Double parton correlations versus factorized distributions”, *Phys. Lett. B* **594** (2004) 171 (arXiv:0404155v1 [hep-ph]).
- [13] R. Kirschner, “Generalized Lipatov-Altarelli-Parisi equations and jet calculus rules”, *Phys. Lett.* **84B** (1979) 266.
- [14] V.P. Shelest, A.M. Snigirev, and G.M. Zinovjev, “Gazing into the multiparton distribution equations in QCD”, *Phys. Lett.* **113B** (1982) 325.
- [15] A.M. Snigirev, “Double-Parton Distributions in QCD”, *Phys. At. Nucl.* **74** (2011) 158 [*Yad. Fiz.* **74** (2011) 158].
- [16] L. Frankfurt and M. Strikman, “Two-gluon form factor of the nucleon and J/ψ photoproduction”, *Phys. Rev. D* **66** (2002) 031502.
- [17] B. Blok, Yu. Dokshitzer, L. Frankfurt, and M. Strikman, ‘ ‘pQCD physics of multiparton interactions”, (arXiv:1106.5533 [hep-ph]).
- [18] E. Cattaruzza, A. Del Fabbro, and D. Treleani, “Fractional momentum correlations in multiple production of W bosons and of $b\bar{b}$ pairs in high energy pp collisions”, *Phys. Rev. D* **72** (2005) 034022 (arXiv:hep-ph/0507052v1).
- [19] J.R. Gaunt, C.-H. Kom, A. Kulesza, and W.J. Stirling, “Same-sign W pair production as a probe of double parton scattering at the LHC”, *Eur. Phys. J. C* **69** (2010) 53 (arXiv:1003.3953v2 [hep-ph]).
- [20] E. Maina, “Multiple Parton Interactions in Z+jets production at the LHC. A comparison of factorized and non-factorized double parton distribution functions”, *JHEP* **1101** (2011) 061 (arXiv:1010.5674v2 [hep-ph]).
- [21] J.R. Gaunt and W.J. Stirling, “Double Parton Distributions Incorporating Perturbative QCD Evolution and Momentum and Quark Number Sum Rules”, *JHEP* **1003** (2010) 005 (arXiv:0910.4347v4 [hep-ph]).
- [22] A.M. Snigirev, “Asymptotic behavior of double parton distribution functions”, *Phys. Rev. D* **83** (2011) 034028 (arXiv:1010.4874v1 [hep-ph]).
- [23] A.M. Snigirev, “Possible indication to the QCD evolution of double parton distributions?”, *Phys. Rev. D* **81** (2010) 065014 (arXiv:1001.0104v3 [hep-ph]).
- [24] C. Flensburg, G. Gustafson, L. Lonnblad, and A. Ster, “Correlations in double parton distributions at small x”, *JHEP* **1106** (2011) 066 (arXiv:1103.4320v3 [hep-ph]).

Theoretical considerations on the double Drell-Yan process as a prototype for multiparton interactions

Markus Diehl¹, Daniel Ostermeier², Andreas Schäfer^{2*}

¹DESY, Notkestraße 85, 22607 Hamburg, Germany

²Universität Regensburg, 93040 Regensburg, Germany

DOI: <http://dx.doi.org/10.3204/DESY-PROC-2012-03/27>

We investigate several ingredients for a theory of multiple hard scattering in hadron-hadron collisions. Issues discussed include the space-time structure of multiple interactions, their power behavior, Sudakov logarithms, and the possibility to constrain multiparton distributions by connecting them with generalized parton distributions.

1 Introduction

The phenomenology of multiparton interactions relies on models that are physically intuitive but involve significant simplifications. So far a systematic description of multiple interactions in QCD remains elusive. Here we report on some steps towards this goal. We will see to which extent the cross section formulae currently used to calculate multiple-scattering processes can be justified in QCD and to which extent they need to be completed.

We consider the case of two hard scatters at parton level. For definiteness we analyze the production of two electroweak gauge bosons with large invariant mass (γ^* , Z , or W). Since the main interest in multiparton interactions is driven by the need to understand details of the final state, we keep the transverse momenta of the produced gauge bosons differential, rather than integrating over them. For the production of a single boson there is a powerful theoretical description based on transverse-momentum dependent parton densities [1], which we aim to extend to the case of multiparton interactions, starting from first-principle QCD. Integrating over transverse momenta gives the more familiar formulation in terms of collinear parton distributions.

The following discussion is a short summary of [2]. Detailed derivations of our results and further discussion are given in [3].

2 Tree-level analysis

We begin with the cross section formula for double parton scattering at tree level. For definiteness we take two colliding protons and consider the case where the two partons coming from

*Speaker

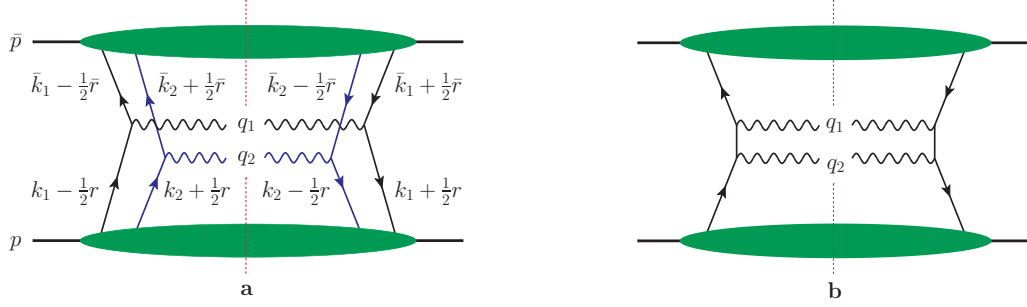


Figure 1: Graphs for the production of two gauge bosons by double (a) or single (b) hard scattering. The dotted line denotes the final-state cut. The decays of the gauge bosons into fermion-antifermion pairs are not shown for simplicity.

one of the protons are quarks. The corresponding graph is shown in Fig. 1a, which also specifies our assignment of momentum variables.

We use light-cone coordinates $v^\pm = (v^0 \pm v^3)/\sqrt{2}$ and $\mathbf{v} = (v^1, v^2)$ for any four-vector v and choose a reference frame where p moves fast to the right and \bar{p} fast to the left, with transverse momenta $\mathbf{p} = \bar{\mathbf{p}} = \mathbf{0}$. We consider kinematics where the invariant masses of the bosons are large and where their transverse momenta are much smaller, i.e. we require $q_T \ll Q$ with $q_1^2 \sim q_2^2 \sim q_T^2$ and $q_1^2 \sim q_2^2 \sim Q^2$.

The two-quark distributions required to describe graph 1a read

$$F_{a_1, a_2}(x_1, x_2, \mathbf{z}_1, \mathbf{z}_2, \mathbf{y}) = 2p^+ \int dy^- \frac{dz_1^-}{2\pi} \frac{dz_2^-}{2\pi} e^{i(x_1 z_1^- + x_2 z_2^-)p^+} \langle p | \mathcal{O}_{a_2}(0, z_2) \mathcal{O}_{a_1}(y, z_1) | p \rangle \quad (1)$$

with bilinear operators

$$\mathcal{O}_a(y, z) = \bar{q}(y - \frac{1}{2}z) \Gamma_a q(y + \frac{1}{2}z) \Big|_{z^+ = y^+ = 0}. \quad (2)$$

The transverse positions \mathbf{z}_i and \mathbf{y} are Fourier conjugate to the transverse momenta \mathbf{k}_i and \mathbf{r} in figure 1a. Furthermore, $a = q, \Delta q, \delta q$ labels the quark polarization and

$$\Gamma_q = \frac{1}{2}\gamma^+, \quad \Gamma_{\Delta q} = \frac{1}{2}\gamma^+ \gamma_5, \quad \Gamma_{\delta q}^j = \frac{1}{2}i\sigma^{j+} \gamma_5 \quad (3)$$

with $j = 1, 2$. The operators in (2) are well-known from the definitions of single-parton densities for unpolarized, longitudinally polarized and transversely polarized quarks, see e.g. [4]. Analogous definitions hold for antiquarks and for a left-moving hadron. The cross section can finally be written as

$$\begin{aligned} \frac{d\sigma|_{1a}}{\prod_{i=1}^2 dx_i d\bar{x}_i d^2\mathbf{q}_i} &= \frac{1}{C} \sum_{\substack{a_1, a_2 = q, \Delta q, \delta q \\ \bar{a}_1, \bar{a}_2 = \bar{q}, \Delta \bar{q}, \delta \bar{q}}} \left[\prod_{i=1}^2 \hat{\sigma}_{i, a_i \bar{a}_i}(q_i^2) \int \frac{d^2\mathbf{z}_i}{(2\pi)^2} e^{-i\mathbf{z}_i \mathbf{q}_i} \right] \\ &\times \int d^2\mathbf{y} F_{a_1, a_2}(x_i, \mathbf{z}_i, \mathbf{y}) F_{\bar{a}_1, \bar{a}_2}(\bar{x}_i, \mathbf{z}_i, \mathbf{y}) \end{aligned} \quad (4)$$

where here and in the following we write $F(x_i, \mathbf{z}_i, \mathbf{y})$ instead of $F(x_1, x_2, \mathbf{z}_1, \mathbf{z}_2, \mathbf{y})$ for brevity. The $\hat{\sigma}_{i, a\bar{a}}$ are the partonic cross sections and it is understood that for each $a_i = \delta q$ both F_{a_1, a_2} and $\hat{\sigma}_{i, a\bar{a}}$ carry extra indices j associated with the direction of the transverse quark polarization. Corresponding remarks hold for $\bar{a}_i = \delta \bar{q}$. C is a combinatorial factor related to identical particles in the final state.

Integration of the cross section over \mathbf{q}_1 and \mathbf{q}_2 leads to collinear (i.e. transverse-momentum integrated) two-parton densities

$$F_{a_1, a_2}(x_i, \mathbf{y}) = F_{a_1, a_2}(x_i, \mathbf{z}_i = \mathbf{0}, \mathbf{y}). \quad (5)$$

The corresponding cross section formula is the basis for the phenomenology of multiple interactions and has been used for a long time. It was derived in [5] for scalar partons and in [6] for quarks.

3 Power behavior

A pair of electroweak gauge bosons can be produced by two hard scatters, but also by a single one. An example graph is shown in figure 1b, and the corresponding cross section formula reads

$$\frac{d\sigma|_{1b}}{\prod_{i=1}^2 dx_i d\bar{x}_i d^2\mathbf{q}_i} = \frac{d\hat{\sigma}}{dx_1 d\bar{x}_1 d^2\mathbf{q}_1} \int \frac{d^2\mathbf{z}}{(2\pi)^2} e^{-iz(\mathbf{q}_1 + \mathbf{q}_2)} f_q(x, z) f_{\bar{q}}(\bar{x}, z), \quad (6)$$

where $x = x_1 + x_2$, $\bar{x} = \bar{x}_1 + \bar{x}_2$, $\hat{\sigma}$ is the cross section for $q\bar{q}$ annihilation into two gauge bosons and $f_q(x, z)$ is the analog of $F_{q, q}(x_i, z_i, \mathbf{y})$ for a single quark.

Dimensional analysis of (4) and (6) reveals that

$$\frac{d\sigma}{\prod_{i=1}^2 dx_i d\bar{x}_i d^2\mathbf{q}_i} \sim \frac{1}{Q^4 \Lambda^2} \quad (7)$$

for both the single and double hard-scattering mechanisms. Here the small scale Λ^2 represents q_T^2 or the scale of non-perturbative interactions, whichever is larger. We thus obtain an important result: multiple hard scattering is *not* power suppressed in cross sections that are sufficiently differential in transverse momenta.

The situation changes when one integrates over \mathbf{q}_1 and \mathbf{q}_2 , because single hard-scattering populates a larger phase space. In single hard-scattering, only the sum $\mathbf{q}_1 + \mathbf{q}_2$ is restricted to be of order Λ , while the individual momenta can be as large as the hard scale Q . In contrast, both boson transverse momenta are restricted to be of order Λ in double hard-scattering. Thus power counting yields

$$\frac{d\sigma|_{1a}}{\prod_{i=1}^2 dx_i d\bar{x}_i} \sim \frac{\Lambda^2}{Q^4}, \quad \frac{d\sigma|_{1b}}{\prod_{i=1}^2 dx_i d\bar{x}_i} \sim \frac{1}{Q^2}. \quad (8)$$

In the transverse-momentum integrated cross section multiple hard-scattering is thus power suppressed. This is in fact required for the validity of the usual collinear factorization formulae, which describe only the single hard-scattering contribution.

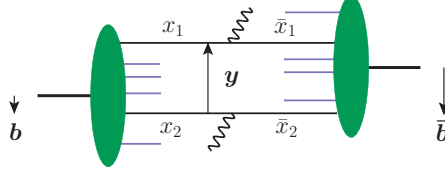


Figure 2: Visualization of the cross section formula (11) when \mathbf{q}_1 and \mathbf{q}_2 are integrated over.

4 Impact parameter

The distributions $F(x_i, \mathbf{z}_i, \mathbf{y})$ depend on spatial transverse coordinates for the quarks but still refer to a proton with definite (zero) transverse momentum. A representation purely in impact parameter space can be obtained using the methods of [7, 8, 9], where impact parameter densities for a single parton are constructed from generalized parton distributions. To this end we first define non-forward distributions $F(x_i, \mathbf{z}_i, \mathbf{y}; \mathbf{\Delta})$ with proton states $\langle p^+, \frac{1}{2}\mathbf{\Delta} |$ and $| p^+, -\frac{1}{2}\mathbf{\Delta} \rangle$ with different transverse momenta. Now we introduce the wave packet

$$|p^+, \mathbf{b}\rangle = \int \frac{d^2\mathbf{p}}{(2\pi)^2} e^{-i\mathbf{b}\mathbf{p}} |p^+, \mathbf{p}\rangle, \quad (9)$$

which describes a proton with definite transverse position \mathbf{b} , and the Fourier transform of $F(x_i, \mathbf{z}_i, \mathbf{y}; \mathbf{\Delta})$,

$$F_{a_1, a_2}(x_i, \mathbf{z}_i, \mathbf{y}; \mathbf{b}) = \int \frac{d^2\mathbf{\Delta}}{(2\pi)^2} e^{-i\mathbf{b}\mathbf{\Delta}} F_{a_1, a_2}(x_i, \mathbf{z}_i, \mathbf{y}; \mathbf{\Delta}). \quad (10)$$

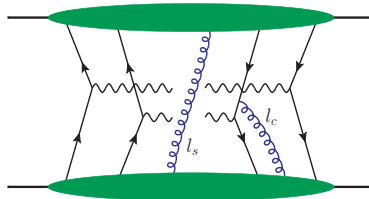
Integrating $F(x_i, \mathbf{z}_i, \mathbf{y}; \mathbf{b})$ over \mathbf{b} one recovers the distributions $F(x_i, \mathbf{z}_i, \mathbf{y})$, so that the cross section can be cast into the form

$$\begin{aligned} \frac{d\sigma|_{1a}}{\prod_{i=1}^2 dx_i d\bar{x}_i d^2\mathbf{q}_i} &= \frac{1}{C} \sum_{\substack{a_1, a_2=q, \Delta q, \delta q \\ \bar{a}_1, \bar{a}_2=\bar{q}, \Delta\bar{q}, \delta\bar{q}}} \left[\prod_{i=1}^2 \hat{\sigma}_{i, a_i \bar{a}_i}(q_i^2) \int \frac{d^2\mathbf{z}_i}{(2\pi)^2} e^{-i\mathbf{z}_i \mathbf{q}_i} \right] \int d^2\mathbf{y} d^2\mathbf{b} d^2\bar{\mathbf{b}} \\ &\times F_{a_1, a_2}(x_i, \mathbf{z}_i, \mathbf{y}; \mathbf{b}) F_{\bar{a}_1, \bar{a}_2}(\bar{x}_i, \mathbf{z}_i, \mathbf{y}; \bar{\mathbf{b}}), \end{aligned} \quad (11)$$

which has a simple geometric interpretation in impact parameter space. Taking the average of transverse positions in the amplitude and its conjugate, one identifies \mathbf{y} as the average distance between the two scattering partons, as can be seen from (2). Likewise, \mathbf{b} is the average distance between parton 2 and the right-moving proton, and $\bar{\mathbf{b}}$ is the average distance between parton 2 and the left-moving proton. This is illustrated in Fig. 2 for the case where the cross section is integrated over \mathbf{q}_i , so that $\mathbf{z}_i = \mathbf{0}$ and the positions in the amplitude and its conjugate coincide.

5 Beyond leading order

Our discussion so far has been concerned with tree graphs as in Fig. 1. At this level, our results can readily be generalized to other hard-scattering processes, in particular to jet production with the well-known subprocesses $qq \rightarrow qq$, $qg \rightarrow qg$, etc.


 Figure 3: Example graph with a collinear gluon l_c and a soft gluon l_s .

A proper factorization formula in QCD must of course include corrections to the tree-level cross section, and in particular take care of additional gluon exchange. In [3] we argue that the factorization proof for Drell-Yan production can to a large part be extended to double hard-scattering processes producing colorless states such as electroweak gauge bosons. We restrict ourselves to such processes from now on.

There are two types of additional gluon exchange that are not power suppressed by the large scale and hence need to be taken into account systematically. The first type concerns gluons which emerge from the subgraph representing the partons in the right-moving proton and which attach to a hard-scattering subgraph, see Fig. 3. To leading-power accuracy, the effect of these gluons can be represented by Wilson lines that appear in the operators defining parton distributions and make them gauge invariant. For gauge boson pair production, each quark or antiquark field is to be multiplied by a Wilson line according to

$$q_j(z) \rightarrow [W(z, v)]_{jk} q_k(z), \quad \bar{q}_j(z) \rightarrow \bar{q}_k(z) [W^\dagger(z, v)]_{kj} \quad (12)$$

with

$$W(z, v) = \text{P exp} \left[ig \int_0^\infty d\lambda v A^\alpha(z - \lambda v) t^\alpha \right], \quad (13)$$

where j and k are color indices, P denotes path ordering, and the sign convention for the coupling g is such that the covariant derivative reads $D^\mu = \partial^\mu + igA^{\mu, a} t^a$.

In order to avoid rapidity divergences in the parton distributions, we tilt v away from the light-cone [1]. This results in an additional parameter $\zeta^2 = (2pv)^2/|v^2|$ in the parton distributions for proton p . Their ζ dependence is connected with Sudakov logarithms and will be discussed in Section 7. As ζ is a measure of the plus-momentum of the proton [10], an adequate choice of ζ in cross section formulae is the hard scale Q .

The second type of unsuppressed gluon exchange is between the right- and left-moving partons as shown in Fig. 3, provided the gluons are soft and thus do not take partons far off shell. In processes with small observed transverse momenta in the final state, the effects of these gluons do not cancel. Provided that gluons in the Glauber region give no net contribution (which we currently cannot show but have to assume), soft gluon effects can be described by a so-called soft factor, which is defined in terms of vacuum expectation values of Wilson lines. Proper care needs to be taken to prevent double counting, because the Wilson lines $W(z, v)$ in the parton distributions include soft gluon momenta as well [1].

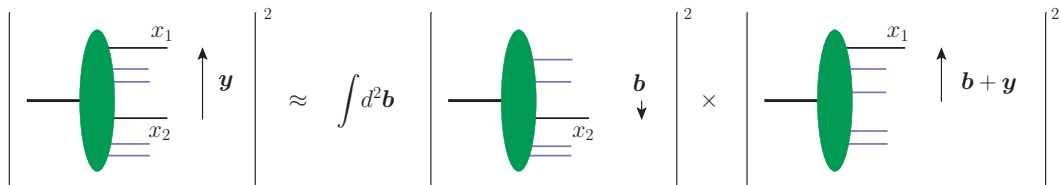


Figure 4: Illustration of the approximation (16) of a two-parton distribution in terms of single-parton distributions. Implicit in the figure is the representation of these distributions as squares of light-cone wave functions in the proton.

6 Connection with generalized parton distributions

In order to obtain a representation of the multiparton distributions in terms of GPDs, we insert a complete set of intermediate states $|X\rangle\langle X|$ between the operators \mathcal{O}_{a_2} and \mathcal{O}_{a_1} in the two-parton distributions in impact parameter space. This gives a product of single-parton operators sandwiched between a proton state and X . If we *assume* that the ground state dominates in the sum over all X and take the intermediate proton states in the impact parameter representation (9), we obtain a representation

$$F_{a_1, a_2}(x_i, z_i, \mathbf{y}; \mathbf{b}) \approx f_{a_2}(x_2, z_2; \mathbf{b} + \frac{1}{2}x_1 z_1) f_{a_1}(x_1, z_1; \mathbf{b} + \mathbf{y} - \frac{1}{2}x_2 z_2) \quad (14)$$

in terms of single-quark distributions

$$f_a(x, z; \mathbf{b}) = \int \frac{d^2\Delta}{(2\pi)^2} e^{-i\mathbf{b}\Delta} \int \frac{dz^-}{2\pi} e^{ixz^- p^+} \langle p^+, \frac{1}{2}\Delta | \mathcal{O}_a(0, z) | p^+, -\frac{1}{2}\Delta \rangle \quad (15)$$

in impact parameter space.

At $z_i = \mathbf{0}$ the relation (14) involves only collinear distributions. Integrating over \mathbf{b} we get

$$F_{a_1, a_2}(x_i, \mathbf{y}) \approx \int d^2\mathbf{b} f_{a_2}(x_2; \mathbf{b}) f_{a_1}(x_1; \mathbf{b} + \mathbf{y}), \quad (16)$$

which has a straightforward physical interpretation as sketched in Fig. 4. In different guises, this relation is at the basis of most phenomenological studies and has long been used in the literature, see e.g. [11, 12, 13] and [14, 15].

We emphasize that the relations (14) and (16) are obtained by restricting a sum over all intermediate states to a single proton in a selected helicity state. We do not have a justification or a strong physical motivation for this restriction, other than stating a posteriori that it is tantamount to neglecting any correlation between both partons in the proton. It seems plausible to assume that this is a reasonable first approximation, at least in a certain region of variables, but one should not expect such an approximation to be very precise.

7 Sudakov logarithms

As is well known, transverse momenta \mathbf{q}_i which are much smaller than the hard scale Q of a process give rise to Sudakov logarithms in the cross section. These logarithms must be

resummed to all orders in perturbation theory, which for single gauge boson production can be done using the Collins-Soper-Sterman formalism [16]. We extended this formalism to gauge boson pair production in [3] and sketch the main results of our analysis in the following.

So far we have glossed over the color structure of double parton distributions. For two quarks one has distributions 1F and 8F , which describe the cases where the two quark lines with momenta $k_1 - r/2$ and $k_1 + r/2$ in graph 1a are coupled to a color singlet or a color octet, respectively. In the cross section formulae (4) and (11) one should replace FF by ${}^1F{}^1F + {}^8F{}^8F$, with each $\hat{\sigma}_i$ including a color factor $1/3$. The relations (14) and (16) hold for 1F .

The dependence of a two-quark distribution on the rapidity parameter ζ defined in Section 5 is governed by the differential equation

$$\frac{d}{d \log \zeta} \begin{pmatrix} {}^1F \\ {}^8F \end{pmatrix} = [G(x_1 \zeta, \mu) + G(x_2 \zeta, \mu) + K(\mathbf{z}_1, \mu) + K(\mathbf{z}_2, \mu)] \begin{pmatrix} {}^1F \\ {}^8F \end{pmatrix} + \mathbf{M}(\mathbf{z}_1, \mathbf{z}_2, \mathbf{y}) \begin{pmatrix} {}^1F \\ {}^8F \end{pmatrix}, \quad (17)$$

where 1F and 8F depend on x_i , \mathbf{z}_i , \mathbf{y} and ζ . They also depend on a renormalization scale μ , but we need not discuss this dependence here. The kernels G and K in (17) already appear in the Collins-Soper equation [10] for single-quark distributions. The matrix \mathbf{M} mixes color singlet and color octet distributions and is μ independent, whereas the μ dependence of G and K is given by a renormalization group equation

$$\gamma_K(\alpha_s(\mu)) = -\frac{dK(\mathbf{z}, \mu)}{d \log \mu} = \frac{dG(x\zeta, \mu)}{d \log \mu} \quad (18)$$

and thus cancels in $G + K$. Both K and \mathbf{M} are due to soft gluon exchange and can be defined as vacuum matrix elements of Wilson line operators, similar to those discussed in Section 5. They can only be calculated perturbatively if the transverse distances on which they depend are sufficiently small.

The general solution of (17) can be written as

$$\begin{pmatrix} {}^1F(x_i, \mathbf{z}_i, \mathbf{y}; \zeta) \\ {}^8F(x_i, \mathbf{z}_i, \mathbf{y}; \zeta) \end{pmatrix} = e^{-S(x_1 \zeta, \mathbf{z}_1, \mathbf{z}_2) - S(x_2 \zeta, \mathbf{z}_1, \mathbf{z}_2)} e^{L\mathbf{M}(\mathbf{z}_1, \mathbf{z}_2, \mathbf{y})} \begin{pmatrix} {}^1F^{\mu_0}(x_i, \mathbf{z}_i, \mathbf{y}) \\ {}^8F^{\mu_0}(x_i, \mathbf{z}_i, \mathbf{y}) \end{pmatrix} \quad (19)$$

with

$$S(x\zeta, \mathbf{z}_1, \mathbf{z}_2) = -\frac{K(\mathbf{z}_1, \mu_0) + K(\mathbf{z}_2, \mu_0)}{2} \log \frac{x\zeta}{\mu_0} + \int_{\mu_0}^{x\zeta} \frac{d\mu}{\mu} \left[\gamma_K(\alpha_s(\mu)) \log \frac{x\zeta}{\mu} - G(\mu, \mu) \right] \quad (20)$$

and $L = \log(\sqrt{x_1 x_2} \zeta / \mu_0)$. The scale μ_0 specifies the initial condition of the differential equation (17), with a natural choice being $\mu_0 \propto 1/\sqrt{|\mathbf{z}_1| |\mathbf{z}_2|}$.

The leading double logarithms of ζ/μ_0 in (19) come from the second term in (20), whereas terms involving K and \mathbf{M} only contain single logarithms. The Sudakov exponent S also appears in the solution of the Collins-Soper equation for single-quark distributions [10],

$$f(x, \mathbf{z}; \zeta) = e^{-S(x\zeta, \mathbf{z}, \mathbf{z})} f^{\mu_0}(x, \mathbf{z}). \quad (21)$$

We thus obtain the important result that to double logarithmic accuracy the Sudakov factor for a multiparton distribution is the product of the Sudakov factors for single parton densities, both for color singlet and color octet distributions. A non-trivial cross talk between all partons, and in particular a mixing between color singlet and octet distributions occurs, however, at the level of single logarithms, which are known to be important for phenomenology.

8 Conclusions

We have studied several aspects of multiparton interactions in hadron-hadron collisions. Our theoretical framework is hard-scattering factorization, which requires a large virtuality or momentum transfer in each partonic scattering process but is valid in the full range of parton momentum fractions, i.e. not limited to small x .

The basic cross section formula for multiple interactions can be derived at tree level using standard hard-scattering approximations and has an intuitive geometrical interpretation in impact parameter space. We have shown that it can be formulated at the level of transverse-momentum dependent multiparton distributions, which permits a description of the transverse momenta of the particles produced in the hard scattering. This is particularly important because it is in transverse-momentum dependent cross sections that multiparton interactions are not power suppressed compared with single hard scattering.

To develop a reliable phenomenology, one needs information about the size and kinematic dependences of two-parton distributions. One can relate them to generalized parton distributions for single partons, which are experimentally accessible in exclusive scattering processes, but this requires an approximation whose reliability we cannot quantify.

To go from tree level to genuine factorization formulae, one must be able to sum certain types of collinear and soft gluon exchanges into Wilson lines. We argue in [3] that for double-scattering processes producing color-singlet particles this can be achieved using the methods that have been successfully applied to single Drell-Yan production [1, 10, 17, 18]. This also permits the resummation of Sudakov logarithms, with important results sketched in Section 7. The production of two electroweak gauge bosons thus emerges as a channel where the current perspectives for developing the theory look very good, and where different aspects of multiple interactions can hopefully be explored experimentally at LHC.

References

- [1] J. C. Collins, “The Foundations of Perturbative QCD,” Cambridge University Press, Cambridge 2011.
- [2] M. Diehl, A. Schäfer, “Theoretical considerations on multiparton interactions in QCD,” *Phys. Lett.* **B698** (2011) 389-402., arXiv:1102.3081[hep-ph]
- [3] M. Diehl, D. Ostermeier, A. Schäfer, “Elements of a theory for multiparton interactions in QCD,” *JHEP* **1203** (2012) 089, arXiv:1111.0910[hep-ph].
- [4] J. P. Ralston, D. E. Soper, “Production Of Dimuons From High-Energy Polarized Proton Proton Collisions,” *Nucl. Phys.* **B152** (1979) 109.
- [5] N. Paver, D. Treleani, “Multi - Quark Scattering And Large P(t) Jet Production In Hadronic Collisions,” *Nuovo Cim.* **A70** (1982) 215.
- [6] M. Mekhfi, “Multiparton Processes: An Application To Double Drell-yan,” *Phys. Rev.* **D32** (1985) 2371.
- [7] D. E. Soper, “The Parton Model and the Bethe-Salpeter Wave Function,” *Phys. Rev.* **D15** (1977) 1141.
- [8] M. Burkardt, “Impact parameter space interpretation for generalized parton distributions,” *Int. J. Mod. Phys.* **A18** (2003) 173, arXiv:0207047[hep-ph].
- [9] M. Diehl, “Generalized parton distributions in impact parameter space,” *Eur. Phys. J.* **C25** (2002) 223; Erratum *ibid.* **C31** (2003) 277 arXiv:0205208[hep-ph]
- [10] J. C. Collins, D. E. Soper, “Back-To-Back Jets in QCD,” *Nucl. Phys.* **B193** (1981) 381.
- [11] T. Sjöstrand, M. van Zijl, “Multiple Parton-Parton Interactions in an Impact Parameter Picture,” *Phys. Lett.* **B188** (1987) 149;
- [12] L. Durand, H. Pi, “QCD and Rising Total Cross-Sections,” *Phys. Rev. Lett.* **58** (1987) 303;

- [13] L. Ametller, D. Treleani, “Shadowing In Semihard Interactions,” *Int. J. Mod. Phys.* **A3** (1988) 521.
- [14] L. Frankfurt, M. Strikman, C. Weiss, “Dijet production as a centrality trigger for pp collisions at CERN LHC,” *Phys. Rev.* **D69** (2004) 114010, arXiv:0311231[hep-ph].
- [15] S. Domdey, H. J. Pirner, U. A. Wiedemann, “Testing the Scale Dependence of the Scale Factor in Double Dijet Production at the LHC,” *Eur. Phys. J.* **C65** (2010) 153, arXiv:0906.4335[hep-ph].
- [16] J. C. Collins, D. E. Soper, G. F. Sterman, “Transverse Momentum Distribution in Drell-Yan Pair and W and Z Boson Production,” *Nucl. Phys.* **B250** (1985) 199.
- [17] X. Ji, J.-P. Ma, F. Yuan, “QCD factorization for semi-inclusive deep-inelastic scattering at low transverse momentum,” *Phys. Rev.* **D71** (2005) 034005, arXiv:0404183[hep-ph].
- [18] J. C. Collins, T. C. Rogers, A. M. Stasto, “Fully unintegrated parton correlation functions and factorization in lowest-order hard scattering,” *Phys. Rev.* **D77** (2008) 085009, arXiv:0708.2833[hep-ph].

Chapter 7

Connections to other fields

Forward photon spectrum in 7 TeV pp collisions measured by the LHCf experiment

Koji Noda for the LHCf Collaboration

INFN - Section of Catania, Via S. Sofia 64, Catania, Italy

DOI: <http://dx.doi.org/10.3204/DESY-PROC-2012-03/43>

LHCf is an experiment designed to measure the energy and transverse momentum spectra of very forward neutral particles produced at the Interaction Point 1 of LHC. Its goal is to calibrate the hadron interaction models in air-shower simulations used for ultra-high-energy cosmic-ray (UHECR) experiments, and its results would also be useful to get a glimpse of the physics in inelastic hadronic collisions. LHCf has taken data in 2009-2010 pp runs at 0.9 and 7 TeV. Then the detector was removed from the experimental area. In this paper the forward photon spectrum obtained at 7 TeV will be presented. Results will be discussed compared to the MC models widely used in UHECR physics. Future prospects for the analysis and the data taking at 14 TeV will be also discussed.

1 Introduction

Cosmic rays with energy above 10^{15} eV have been detected on the Earth since several decades ago, but there still remain many uncertainties in understanding their properties. In particular, the properties of cosmic rays beyond 10^{18} eV, called ultra-high-energy cosmic ray (UHECR), have not been clarified yet. We do not know much about its chemical composition, the mechanism of its propagation, and thus its astrophysical origin. One reason is that it can be detected indirectly only with a particle cascade called air-shower, and that we must always care for systematic errors caused by the air-shower development.

If we try to understand the cosmic rays in a step-by-step way from the Earth side, we must understand first what the cosmic rays are, i.e., the chemical composition. For its determination, the maximum depth of the air-shower development is generally used. Recently, a measurement by Pierre Auger Observatory suggests that the chemical composition of UHECR has a gradual transition from a light chemical composition (proton) to a heavy one (iron) [1]. However, this result is different from a result by the HiRes experiment [2]. Furthermore, the depth of the shower maximum is severely dependent on the hadronic interaction models used in Monte Carlo simulations for the air-shower development. The models are based on the perturbative QCD, but they treat the non-linear effects only in phenomenology. Therefore, in order to reduce the uncertainty in the discussion of the chemical composition, we must reduce first the model dependence with experimental data obtained in colliders like Large Hadron Collider (LHC).

There are several key quantities for the air-shower development. It starts with the first interaction of the cosmic ray and a nucleus of the atmosphere, where the inelastic cross section of the first interaction is important. In LHC the TOTEM experiment has already measured the inelastic cross section [3]. Then, the energy of the cosmic ray is transferred inelastically

to secondary particles like baryons and mesons. These secondary particles in the forward direction make following particle cascades. Thus, the amount of transferred energy (inelasticity) and the energy spectrum of the forward particles are important here. The latter is the main goal of the LHCf experiment [5]. It measures the spectra of very forward neutral particles (photons, neutral pions and neutrons) emitted in high energy collisions in LHC. As for the spectrum of forward pions, available data with the highest energy is that for neutral pions by the UA7 experiment [4] in SPS, whose collision energy corresponds to 10^{14} eV in cosmic-ray energy. On the other hand, the LHCf experiment is designed to obtain data with a collision energy of 14 TeV, corresponding to 10^{17} eV in cosmic-ray energy. Thus, it will be expected to reduce the uncertainty of the model dependence close to the UHECR energy.

2 The LHCf detector

LHCf is installed at the CERN Large Hadron Collider in Geneva, Switzerland. The LHCf detector is located at 140m away from Interaction Point 1 (IP1; the ATLAS site) and at zero degree collision angle. The detector is installed in the instrumentation slots of the neutral particle absorbers (TAN). Inside the TAN the beam vacuum chamber makes a Y-shaped transition from a single beam tube facing the IP to two separate beam tubes joining to the arcs of LHC. The TAN instrumentation slot is in the crotch of the Y. Charged secondary particles from IP are swept aside by the inner beam separation dipole before reaching TAN, so only neutral particles are incident on the LHCf detectors. This location covers the pseudo-rapidity range from 8.4 to infinity. This instrumentation slot exists in each of both sides of IP1, thus we have two detectors located on opposite sides of IP1, named Arm1 and Arm2.

The overall concepts for the two Arms are the same (Fig. 1). Each of the two LHCf detectors consists of two small sampling calorimeters and four position sensitive layers inserted into the calorimeter layers. The calorimeter is made of 16 plastic scintillators sandwiched by tungsten absorbers, and it has a total length equivalent to 44 radiation lengths, and 1.55 interaction length. We call the calorimeters small & large towers. The four position sensitive layers are distributed among the layers of the calorimeters for determining the transverse shower positions. Arm1 utilizes scintillating fibers as the position-sensitive layers, while Arm2 uses silicon (Si) microstrip sensors. In addition the geometrical configurations of the two towers for each Arm are different for the purposes of redundancy and consistency check. In front of each detector, a Front Counter made of plastic scintillators is inserted. It provides useful trigger information by covering a larger aperture than the calorimeters. Many additional details of both Arms can be found in [5].

The detector can identify photons with the two calorimeters. It measures their energy spectrum beyond 100 GeV with less than 5% energy resolution, and their incident position with 0.2mm position resolution. If a photon is detected in each of the two calorimeters at the same time, it is expected to be reconstructed as an event from a neutral pion. This is the main target of the LHCf detector. Measured spectrum of neutral pions can be used to discriminate among the hadronic interaction models. Also, hadronic showers of high-energy neutrons can be measured with energy resolution of about 30%.

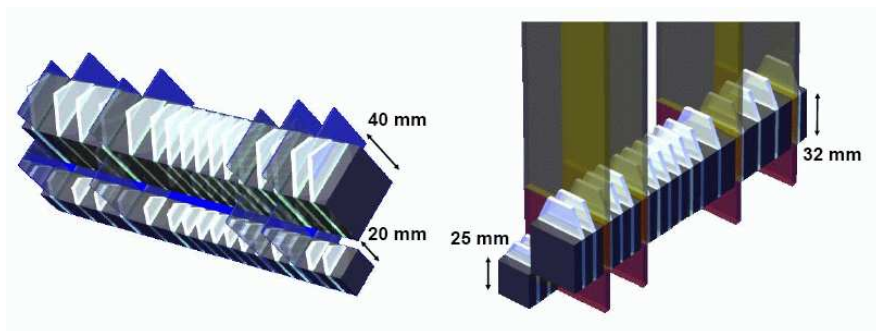


Figure 1: Schematic view of the LHCf detectors (Arm1 on the left, Arm2 on the right). Plastic scintillators (light blue color) are interleaved with tungsten blocks (dark gray color). Four position sensitive layers (scintillating fibers in Arm1, dark blue color; silicon micro-strip detectors in Arm2, purple color) are distributed in each calorimeter.

3 Data acquisition

The current LHCf detector was not designed to be a radiation hard detector. That is because the model discrimination requires just a short period during the early phase of the LHC commissioning before the high luminosity operations. For the LHC operation in 2009 and 2010, we have obtained data for pp collision with energies of $\sqrt{s} = 0.9$ and 7 TeV. The accumulated numbers of events are about 100k showers at 0.9 TeV, and about 400M showers at 7 TeV, corresponding to about 1M neutral pion events, for each of the two Arms. After the operation for several months, the detectors were removed from the slot in 2010.

In Fig. 2, we show an example of a candidate of a neutral pion event, i.e., one photon for each tower, obtained by Arm2. We can see sharp peaks from single photon events detected by the first two layers of the Si microstrip sensors. With the information we can reconstruct the invariant mass of the photon pairs. It is expected to be around the mass of the neutral pion (135 MeV) and will be used for an energy calibration. We have also obtained the energy spectra of the neutral pions for both of the Arms. A preliminary result can be seen in [6].

4 Photon analysis

The first physics result from the LHCf experiment has been published in 2011 [7]. It is dedicated to measurements of the single photon spectrum. Events by neutral hadrons are removed by a simple criteria based on the longitudinal development of the showers, obtained by the scintillators. The energy of the remained photons is determined from the same information on the light produced in the scintillators. We applied corrections to it: for non-uniformity of light collection efficiency, and for particles leaking out of the edges of the calorimeter towers. In this corrections we used the lateral positions of showers determined with the information by the position sensitive layers. The information by the position sensitive layers is also used to exclude ‘multi-hit’ events that have more than one showers inside the same tower. The two Arms have different geometrical configurations, thus in this analysis we have selected a common region for each tower in order to combine the two spectra without any acceptance correction.

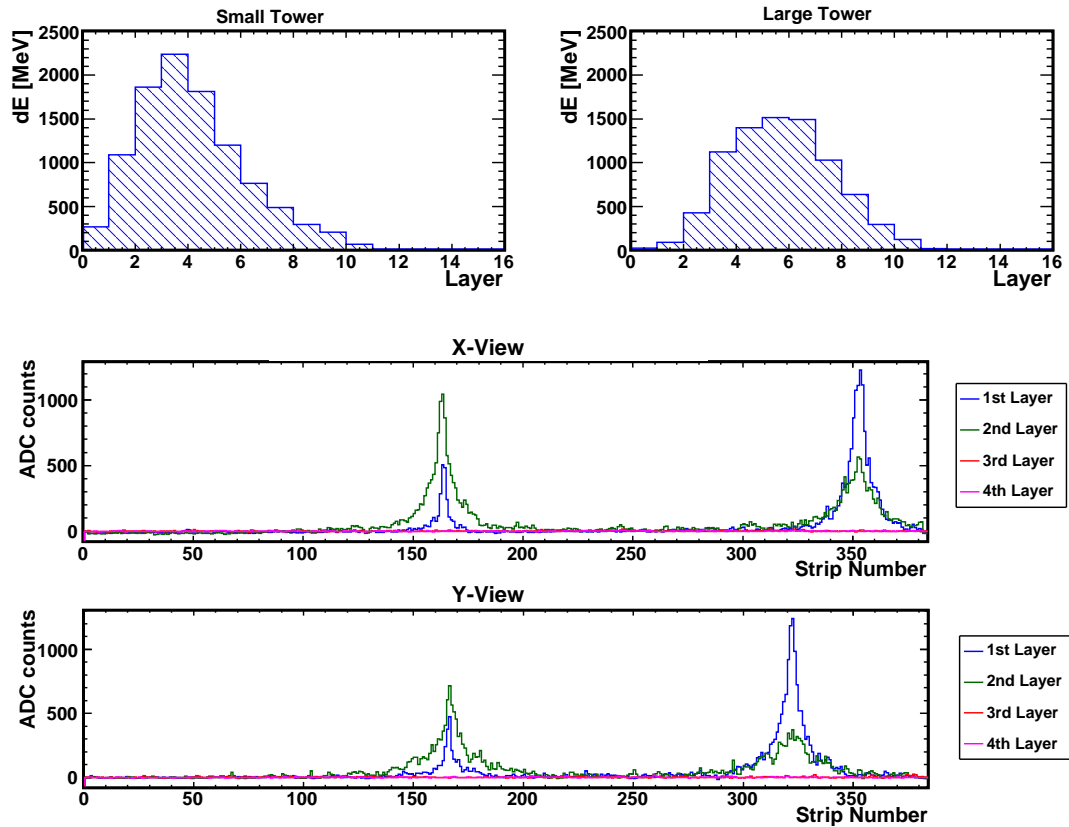


Figure 2: An example of data taken during 2010 operation [7] (a candidate for detection of two photons from the decay of a neutral pion). The upper two panels show the transition curves taken by the two calorimeters: the left is by the small tower, while the right is by the large tower. The lower two panels are the data from the Si microstrip sensors; The upper is the four x-view data, while the lower is the four y-view data. The identifiable peaks are from the 1st and 2nd layers, while the data from the 3rd and 4th layers are almost zero.

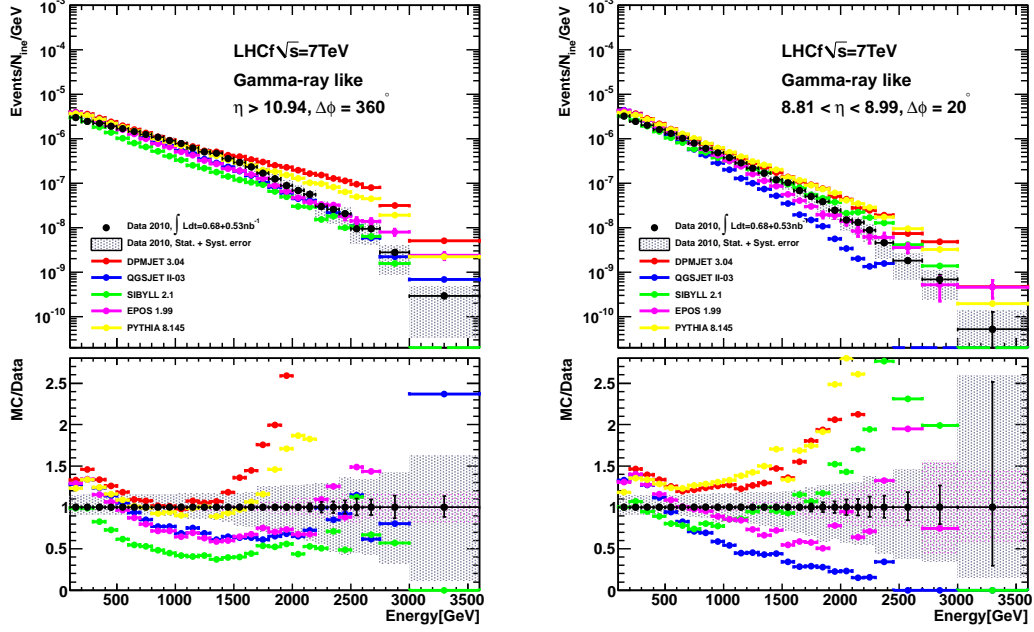


Figure 3: Comparison between the measured single-photon energy spectra (black dots) and the predictions of the following MC codes: DPMJET 3.04 (red), QGSJET II-03 (blue), SIBYLL 2.1 (green), EPOS 1.99 (magenta) and PYTHIA 8.145 (yellow), taken from [7]. Top panels show the spectra and bottom panels show the ratio of MC results to experimental data. Left and right panels refer to different pseudo-rapidity ranges. Error bars show the statistical error and gray shaded areas the systematic error for experimental data. Magenta shaded areas indicate the statistical error associated to MC simulations.

The region is pseudo-rapidity $\eta > 10.94$ and azimuthal range $\Delta\phi = 360^\circ$ for the small towers, while $8.81 < \eta < 8.99$ and $\Delta\phi = 20^\circ$ for the large towers. Further details about the analysis can be found in [7].

Figure 3 shows the single-photon energy spectra obtained from a data set taken in pp collisions at $\sqrt{s} = 7$ TeV in 2010. During the period for the data set, the integrated luminosity is estimated to be $\int Ldt = 0.68 \text{ nb}^{-1}$ and 0.53 nb^{-1} for Arm1 and Arm2, respectively. Multiplying it with an assumed inelastic cross section $\sigma_{\text{ine}} = 71.5 \text{ mb}$, we derived the number of inelastic collisions, N_{ine} , on the vertical axis. The black points are the energy spectra obtained by the combination of the two Arms, and they are compared with results predicted by MC simulations using different models: DPMJET 3.04[8], QGSJET II-03 [9], SIBYLL 2.1 [10], EPOS 1.9[11] and PYTHIA 8.145[12, 13]. Left and right panels refer to the selected regions as mentioned before.

As a result, we see that none of the model predictions nicely describe the LHCf data in the whole energy ranging from 100 GeV to 3.5 TeV. In particular there is a big discrepancy in

high energy region. Discussions about this result with the model developers have been already started. Improvements of the hadron interaction models are expected in near future.

5 Future prospects

Now we are working for the following analyses for topics such as neutral pions, 900 GeV photons, and Pt distribution of photons and hadron spectra at 7 TeV collisions. At the same time, we are preparing for foreseen data acquisitions with the proton-ion collision in 2012, and the pp collisions at $\sqrt{s} = 14$ TeV in 2014. A higher luminosity is expected for the 14 TeV runs than that in the 7 TeV runs. Thus we are planning a hardware upgrade of the plastic scintillators and the scintillating fibers to ones made of Gd_2SiO_5 (GSO), which are more radiation-hard than the plastic scintillators. The radiation hardness of the GSO scintillator was measured in a test beam, and we confirmed that it has properties good enough for our use [14].

Another upgrade is planned for the Arm2 detector. The current configuration of the Si microstrip sensors distributed in the plastic scintillators are not optimized for an energy reconstruction using the Si sensors. If we change the configuration, an improvement of the energy resolution only with the Si is expected, by a MC study, to be less than 10%. However, the Si sensors were originally not considered as a calorimeter, thus we require additional work for them. The first is the gain calibration using the test beam data and a MC simulation for the same configuration. We have obtained a gain factor from ADC counts to the energy deposit on the Si sensors. Then the incident particle energy can be reconstructed from the energy deposit, using a function obtained by a simulation for LHC configuration. A preliminary result with a MC data set shows that the energy resolution for photons is $\sim 15\%$ up to 1.5 TeV [15]. When the Si sensor is used as a calorimeter, it would help not only the calorimetry of the scintillators, but also a separation of the ‘multi-hit’ events, which could not be resolved only by the scintillators.

6 Conclusions

LHCf is a collider experiment dedicated for the cosmic-ray physics. It measures the energy spectrum of very forward particles generated in pp collisions in LHC. Its aim is to minimize systematic errors in air-shower simulations used in ultra-high-energy cosmic-ray experiments. In this paper we briefly surveyed our detector and the current status of the experiment. We have already done the data acquisition for pp collisions at $\sqrt{s} = 7$ TeV, and removed the detectors. The obtained photon spectra are not well described by the MC expectations, especially in high energies. Now we are working for following analyses and foreseen detector upgrade. The prospects about the hardware upgrade were also shown in this paper.

References

- [1] J. Abraham et al. (Auger Coll.), “Measurement of the Depth of Maximum of Extensive Air Showers above 10^{18} eV”, *Physical Review Letters* **104** (2010) 091101.
- [2] R. U. Abbasi et al. (HiRes Coll.), “Indications of Proton-Dominated Cosmic-Ray Composition above 1.6 EeV”, *Physical Review Letters* **104** (2010) 161101.
- [3] G. Antchev et al. (TOTEM Coll.), “First measurement of the total proton-proton cross section at the LHC energy of $\sqrt{s} = 7$ TeV”, *Europhysics Letters* **96** (2011) 21002.

- [4] E. Pare et al, “Inclusive production of π^0 's in the fragmentation region at the $S\bar{p}p$ S collider”, Physics Letter B **242** (1990) 531.
- [5] O. Adriani et al. (LHCf Coll.), “The LHCf detector at the CERN Large Hadron Collider”, JINST **3** (2008) S08006.
- [6] H. Menjo et al. (LHCf Coll.), “Energy spectrum of neutral pion at LHC proton-proton collisions measured by the LHCf experiment” (HE1.4, 1335), Proceedings of the 32nd International Cosmic Ray Conference (2011) in press.
- [7] O. Adriani et al. (LHCf Coll.), “Measurement of zero degree single photon energy spectra for $\sqrt{s} = 7$ TeV proton-proton collisions at LHC”, Physics Letter B **703** (2011) 128.
- [8] F. W. Bopp et al., “Antiparticle to particle production ratios in hadron-hadron and d-Au collisions in the DPMJET-III Monte Carlo model”, Physical Review C **77** (2008) 014904.
- [9] S. Ostapchenko, “Nonlinear screening effects in high energy hadronic interactions”, Physical Review D **74** (2006) 014026.
- [10] E.-J. Ahn et al., “Cosmic ray interaction event generator SIBYLL 2.1”, Physical Review D **80** (2009) 094003.
- [11] K. Werner et al., “Parton ladder splitting and the rapidity dependence of transverse momentum spectra in deuteron-gold collisions at the BNL Relativistic Heavy Ion Collider”, Physical Review C **74** (2006) 044902.
- [12] T. Sjöstrand et al., “PYTHIA 6.4 physics and manual”, JHEP **05** (2006) 026.
- [13] T. Sjöstrand et al., “A brief introduction to PYTHIA 8.1”, Computer Physics Communications **178** (2008) 852.
- [14] K. Kawade et al., “Study of radiation hardness of Gd_2SiO_5 scintillator for heavy ion beam”, JINST **6** (2011) T09004.
- [15] K. Noda et al. (LHCf Coll.), “Data analysis of the LHCf Si microstrip sensors” (HE3.1, 421), Proceedings of the 32nd International Cosmic Ray Conference (2011) in press.

Chapter 8

Outlook

Overview of experimental results presented at MPI@LHC 2011

Arthur Moraes

University of Glasgow, School of Physics and Astronomy, G12 8QQ, Glasgow, UK

DOI: <http://dx.doi.org/10.3204/DESY-PROC-2012-03/55>

This report will present a brief overview of some of the exciting experimental results presented at the 3rd International Workshop on Multiple Partonic Interactions at the LHC - MPI@LHC 2011. The experimental results presented at the conference included some of the most recent measurements from the LHC experiments as well as results from Tevatron and HERA collaborations.

1 Introduction

The Large Hadron Collider (LHC) is successfully colliding particles at the energy frontier and will remain the prime international facility for high energy physics research for the next decades. The main purpose of LHC is the study of the fundamental laws of Nature at very high energies. Besides the search for the elusive Higgs boson, the last missing piece of the Standard Model (SM) of Particle Physics, the LHC is also investigating the existence of new particles and interactions.

Recent studies on Higgs and beyond the Standard Model (BSM) searches with LHC data have not yet produced conclusive evidence proving the existence of new physics. Nevertheless, these searches reveal a common feature in the attempt to separate candidate signals from the background: the complex structure of the underlying interactions produced alongside the candidate processes of interest.

Protons, and indeed all hadrons, are made of quarks and gluons, collectively known as partons. When protons collide at high energies, their partonic constituents may undergo head-on collisions. The higher the energy involved in a proton-proton collision, the greater is the probability that a parton from one of the incoming protons will scatter off a parton from the other proton. The record high energies in proton-proton collisions at the LHC lead to an increased probability that not only one but multiple parton-parton interactions may take place in each proton-proton collision. The production of rare signals at the LHC will typically be accompanied by and correlated to several parton-parton interactions taking place in the same proton-proton collision.

This underlying structure of partonic interactions present in hadronic interactions has not been fully understood yet and early LHC results have shown that simulation models cannot satisfactorily predict many of their features either. It is known, however, that multiple partonic interactions (MPI) account for much of the underlying event associated to the production of highly energetic particles as well as to the direct background in many searches for new physics.

The MPI are experiencing a growing popularity and are currently widely invoked to account for observations that would not be explained otherwise: the global properties of particle production in proton-proton collisions at the LHC, the cross sections for multiple heavy flavour production, the survival probability of large rapidity gaps in hard diffraction, etc. At the same time, the implementation of the MPI effects in the simulation models is quickly proceeding through an increasing level of sophistication and complexity that, in perspective, achieves deep general implications for the LHC physics.

Measuring the properties of multiple partonic interactions will be crucial to understand the challenging environment present in LHC collisions, hence the relevance of these studies and the discussion of their results in forums like the MPI@LHC workshop series.

This report will briefly review and introduce some of the experimental results presented at the 3rd International Workshop on Multiple Partonic Interactions at the LHC - MPI@LHC 2011, which took place at DESY, Hamburg. Further details on individual results, including technical details and extended discussion on the physics results, can be found in the contributions published in this proceedings.

2 Experimental results presented at MPI@LHC 2011

The global properties of high-energy proton-proton collisions are deeply correlated with the dynamics of multiple partonic interactions. The rise in the total proton-proton cross-section (σ_{tot}) as a function of the centre-of-mass energy (\sqrt{s}) can be associated with the rise in multiple partonic interactions. The TOTEM Collaboration presented their measurements of the total, elastic and inelastic proton-proton cross-sections at $\sqrt{s} = 7$ TeV (fig. 1). They measured $\sigma_{tot}^{pp}(\sqrt{s} = 7 \text{ TeV}) = 98.3 \pm 0.2$ (stat) ± 0.8 (syst) mb and $\sigma_{el}^{pp}(\sqrt{s} = 7 \text{ TeV}) = 24.8 \pm 0.2$ (stat) ± 1.2 (syst) mb, from which they derived $\sigma_{inel}^{pp}(\sqrt{s} = 7 \text{ TeV}) = \sigma_{tot} - \sigma_{el} = 73.5 \pm 0.6$ (stat) ± 1.8 (syst) mb. Their results confirm the expected rises in σ_{tot} and σ_{inel} with the centre-of-mass energy and further support models predicting an increase in the MPI activity at the LHC compared to previous hadron colliders.

The diffractive component of the inelastic cross-section was also discussed in several presentations at the workshop. Newman made an extensive review of diffraction and multiple partonic interactions.

Single and double diffraction are important components of the hadronic inelastic interactions. Among other applications, determining the exact fraction of diffraction is important for phenomenology models which rely on the non-diffractive inelastic cross-section to parameterize the rate of MPI in hadron collisions. Results from the ALICE Collaboration measured at different centre-of-mass energies were discussed and showed to agree with previous data from CERN SPS experiments as well as with a wide range of model predictions (see Newman's contribution).

The differential pseudorapidity (η) gap cross-section measurement made by ATLAS was also discussed by Newman (see fig. 2). Through this measurement one is able to study the impact of MPI and hadronisation fluctuations on small gaps (small $\Delta\eta^F$). There are considerable variations between Monte Carlo (MC) model predictions for small gap production which is associated with the fluctuations in predictions for the underlying event and MPI rates. The cross-section measurement for large gap values probes the single diffractive cross-section.

Multiplicity distributions were extensively discussed by all LHC collaborations (see, for example, contributions from Leyton, Bansal, Grosse-Oetringhaus and Volyansky). Similar conclusions regarding fluctuations in the prediction of multiplicity spectra can be obtained from

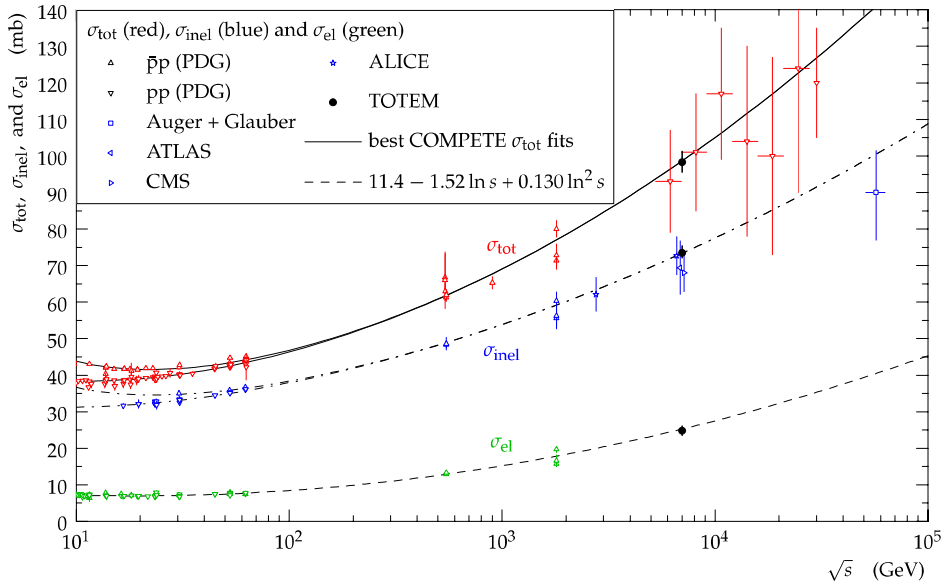


Figure 1: Total (σ_{tot}), inelastic (σ_{inel}) and elastic (σ_{el}) cross-section as a function of \sqrt{s} . Further details in contribution from Österberg in this proceedings.

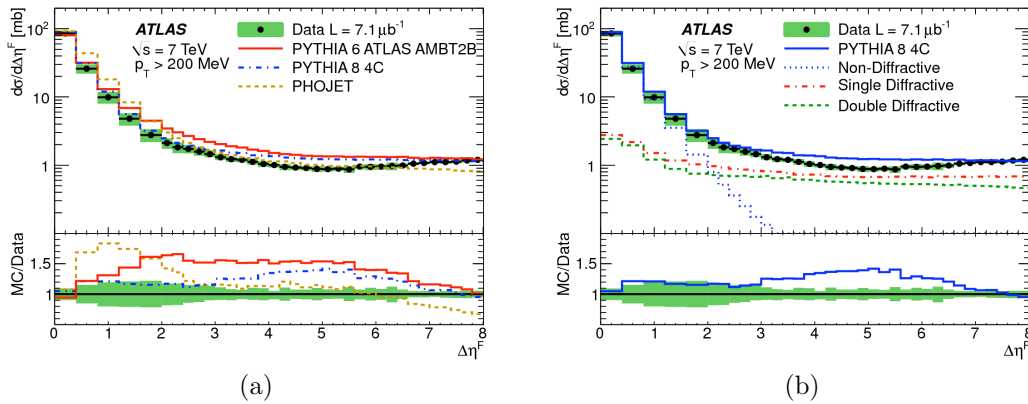


Figure 2: Inelastic cross section differential in forward gap size $\Delta\eta^F$ for particles with $p_T > 200$ MeV. The shaded bands represent the total uncertainties. The full lines in (a) show the predictions of PHOJET and versions of PYTHIA 6 and PYTHIA 8. The dashed lines in (b) represent the contributions of the non-diffractive (ND), single diffractive (SD) and double diffractive (DD) components according to PYTHIA 8.

these studies: phenomenology models employing MPI cannot adequately describe very low multiplicity events, typically dominated by soft particles (low p_T particles) and highly influenced

by diffractive interactions nor the high multiplicity tails of multiplicity distributions, usually associated to events containing hard particles (high p_T particles) and (semi-) hard multiple partonic interactions.

New results on particle correlations as well as attempts to model these observables have been presented at the workshop. These studies further extend the reach of physics effects one can investigate in order to assess the impact of MPI in different regions of the phase-space. Measurement of two-particle angular correlations (see fig. 3) and on the azimuthal ordering of charged hadrons (fig. 4) reveal interesting features which current phenomenology models still cannot describe properly.

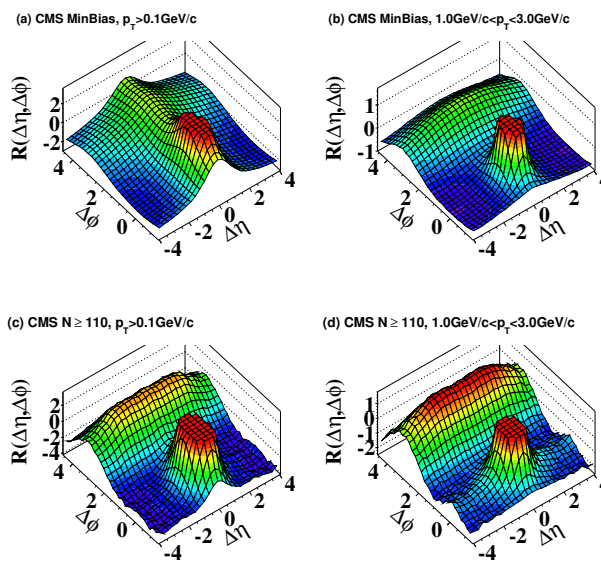


Figure 3: Two-particle angular correlations measured for various kinematic selection cuts for proton-proton collisions at $\sqrt{s} = 7$ TeV by the CMS collaboration. These measurements have inspired modifications in the implementation of MPI in some MC models. Further details in contribution from Basal and Alderweireldt in this proceedings.

The underlying event (UE) was also object of several presentations. The ALICE collaboration, amongst various interesting results, showed measurements for the transverse sphericity which indicate that data events are more spherical than MC, particularly for selection cuts focused on high multiplicity events. This suggests there is a higher MPI activity in data than what is currently generated in MC simulations (see contribution from Grosse-Oetringhaus in this proceedings). Comparisons between the rise in charged particle densities for minimum bias and underlying event as a function of the centre-of-mass energy were also presented by ALICE and highlight the crucial role played by MPI in these two classes of measurements (fig. 5): the rise in charged particle density in the UE is steeper than that seen in minimum bias indicating that MPI activity is higher in the former compared to the latter. ATLAS and CMS report similar results.

Knutsson presented an overview of several H1 and ZEUS measurements which investigate

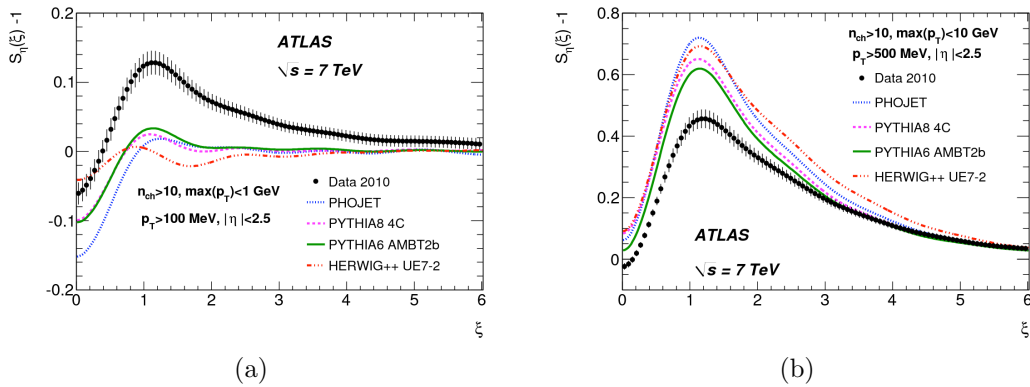


Figure 4: Spectral analysis of correlations between the longitudinal and transverse components of charged hadrons. Power spectrum S_η for the azimuthal ordering of charged hadrons measured by ATLAS for two selection cuts: (a) low- p_T enriched and (b) low- p_T depleted sample. Further details in contribution from Leyton in this proceedings.

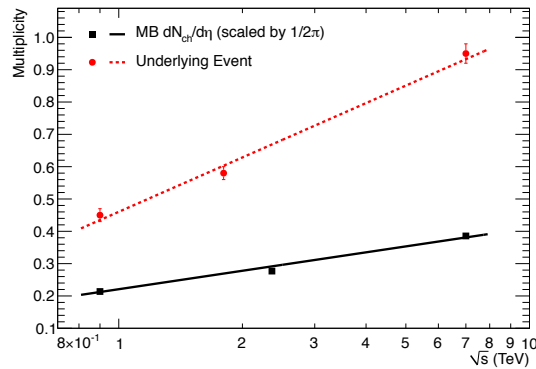


Figure 5: Comparison of number density in the plateau of the transverse region and $dN_{ch}/d\eta$ in minimum bias events (scaled by $1/2\pi$). Both are for charged particles with $p_T > 0.5$ GeV. Further details in contribution from Grosse-Oetringhaus in this proceedings.

the role of MPI in electron (or positron)-proton collisions at HERA. Recent studies on charged particle distributions and mini-jet production in photoproduction events were discussed and highlight, yet again, the relevance of MPI in the interpretation of their results. For example, fig. 6 shows the charged particle flow in photoproduction measured by H1. It is clear from the comparison between data and MC predictions that an adequate description of the data requires the inclusion of MPI in the MC models.

The D0 collaboration reported on their direct measurements of multiple partonic interactions which included results for double-parton scattering (DPS) as well as triple-parton scattering (TPS). Golanov presented their results for the measured fractions of DPS and TPS events which

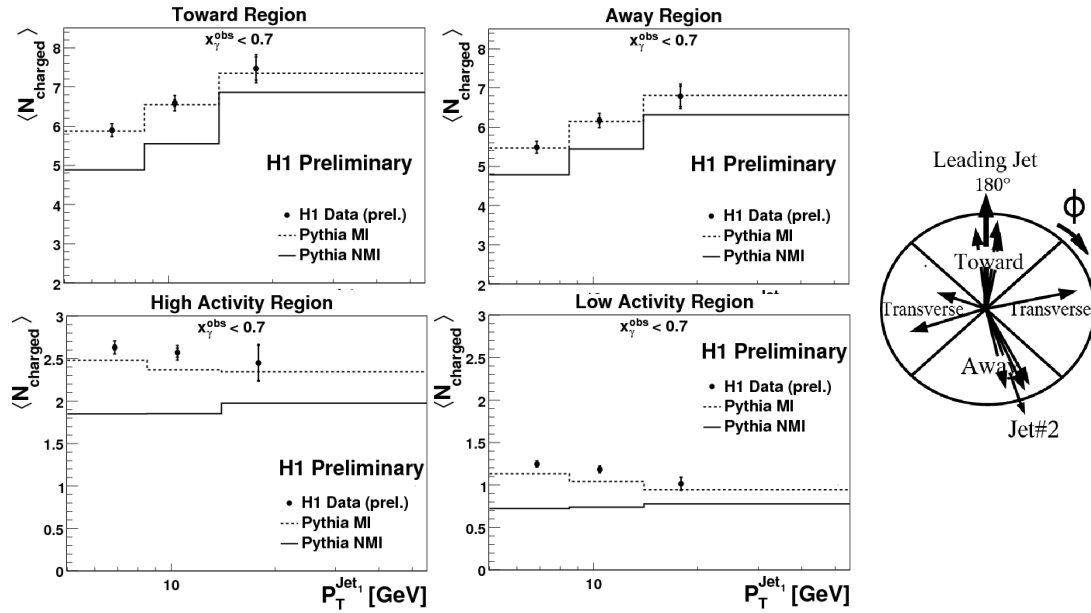


Figure 6: Charged particle flow in photoproduction: comparison between data and MC for various angular regions. Further details in contribution from Knutsson in this proceedings.

vary as a function of the second leading jet p_T (p_T^{jet2}). The DPS fraction in $\gamma + 2$ jets was 11.6% for events with $15 \text{ GeV} < p_T^{jet2} < 20 \text{ GeV}$ and drops to 2.2% for $25 \text{ GeV} < p_T^{jet2} < 30 \text{ GeV}$. The TPS fraction in $\gamma + 3$ jets, which was determined for the first time, was 5.5% for events with $15 \text{ GeV} < p_T^{jet2} < 20 \text{ GeV}$ and drops to 0.9% for $25 \text{ GeV} < p_T^{jet2} < 30 \text{ GeV}$. The measured effective cross-section (σ_{eff}) was $\sigma_{eff} = 16.4 \pm 0.3(\text{stat}) \pm 2.3(\text{syst}) \text{ mb}$, which is comparable to a similar measurement done by the CDF collaboration.

The first result on direct measurement of DPS at the LHC was presented by the ATLAS collaboration. Investigating $W+2$ jet event topologies from proton-proton collisions at $\sqrt{s}=7$ TeV they were able to measure the fraction of DPS in their sample (f_{DPS}) as well as σ_{eff} . Dobson reported the following results: $f_{DPS} = 0.16 \pm 0.01(\text{stat}) \pm 0.03(\text{syst})$ and $\sigma_{eff} = 11 \pm 1(\text{stat}) \pm 3(\text{syst}) \text{ mb}$.

3 Outlook

Measurements exploring several aspects of multiple partonic interactions were discussed at the 3rd International Workshop on Multiple Partonic Interactions at the LHC - MPI@LHC 2011. These results add to the growing body of evidence showing the impact of MPI on the QCD dynamics in high-energy collisions involving partonic initial states. Many of these results also challenge our current phenomenology used to describe the complex nature of QCD interactions at the LHC.

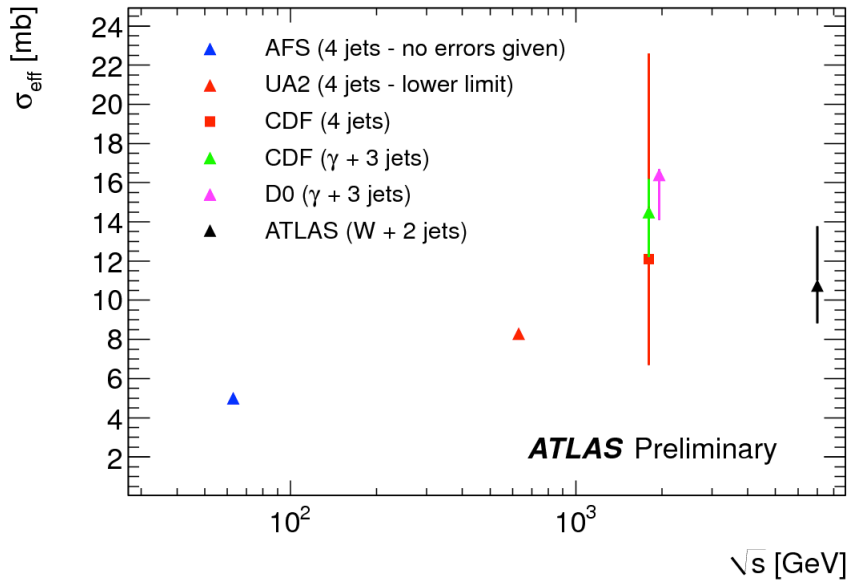


Figure 7: The centre-of-mass \sqrt{s} dependence of σ_{eff} extracted in different processes in different experiments, for an energy range between 63 GeV and 7 TeV. Further details in contribution from Dobson in this proceedings.

The future outlook for the continuation of these discussions looks very exciting and will certainly rely on new results expected to be published by the LHC collaborations in the coming months. These will include further measurements on correlations in particle production in inelastic events, underlying event measurements in different systems and with new observables (Drell-Yan and jet area studies, for example) and direct measurements of MPI processes.

Multiple interactions: summarizing remarks (theory)

Jochen Bartels

Universität Hamburg, Germany

DOI: <http://dx.doi.org/10.3204/DESY-PROC-2012-03/56>

1 Introduction

In recent years it has been more and more realized that multiple interactions play an important role for the analysis of hadron-hadron collisions. This applies to the structure of the underlying event and, most important, to the calculation of inclusive cross sections: corrections due to multiple interactions may represent an important background in the search for new physics. The analysis of multiple jet events at the Tevatron (also confirmed by HERA data) has clearly shown that double chains are at work. It is expected that, at the LHC, the number of participating chains may become quite sizable.

For inclusive cross sections it may be useful to recapitulate the simplest master formulae: the usual collinear factorization scheme leads to

$$d\sigma = \sum_{i_1 i_2} \int dx_1 dx_2 f_{i_1}(x_1, \mu) d\hat{\sigma}_{i_1 i_2 \rightarrow 2 jet}(x_1, x_2, \mu; \mathbf{p}_1, Y_1, \mathbf{p}_2, Y_2) f_{i_2}(x_2, \mu). \quad (1)$$

But in certain kinematic regions it also receives corrections from the two chain configuration:

$$d\sigma^{DP} = \frac{m}{\sigma_{eff}} \sum_{i_1, j_1, i_2, j_2} \int dx_1 dy_1 dx_2 dy_2 H_{i_1 j_1}(x_1, y_1; \mu_a, \mu_b; \vec{\Delta}) d\hat{\sigma}_{i_1 i_2 \rightarrow jet}(x_1, y_1, \mu_a; \mathbf{p}_1, Y_1) d\hat{\sigma}_{j_1 j_2 \rightarrow jet}(y_2, y_2, \mu_b; \mathbf{p}_2, Y_2) H_{i_2 j_2}(x_2, y_2; \mu_a, \mu_b; \vec{\Delta}). \quad (2)$$

(further explanations are given below, see Fig.1). For the double parton densities H_{ij} often a simple factorizing ansatz is used:

$$H_{ij}(x_1, x_2; \mu_a, \mu_b; \vec{\Delta}) = f_i(x_1, \mu_a) f_j(x_2, \mu_b). \quad (3)$$

During this meeting important contributions have been presented which lead to much deeper insight into the theory behind (2) and, more general, into the theory of multiple interactions and their importance in high energy hadron collisions. The following comments will summarize a few of them, without any claim of completeness. The first section lists a few recent studies of the magnitude of corrections due to multiple interactions. The second part summarizes results of a few recent studies devoted mainly to the hard scattering matrix elements inside the double parton cross section. In a third section a few comments will be made about the evolution of double parton densities. Finally, a few comments on open questions of the theory of multiple interactions, in particular related to rapidity gap final states,

2 Evidence for the presence of multiple interactions

For the analysis of experimental data it is important to address individual processes and investigate the size of corrections due to double parton scattering. A candidate for exhibiting the presence of double parton scattering is the production of same-sign W pairs [1, 2]. The paper [2] concludes that a small excess of events due to double parton scattering could be observed at the LHC. Particular attention is also given to the evolution of double parton densities: using evolution equations [3] which contain additional parton splitting processes and thus go beyond the simple 'double DGLAP' factorization ansatz (3), the authors observe novel and nontrivial kinematic correlations between the produced W bosons. Double Drell Yan production with two opposite side lepton pairs has been investigated in [4, 5].

A very promising class of processes is the double heavy meson production, in particular, double J/Ψ production [6],[7]. Ref. [6] makes a simple factorizing ansatz for the double parton cross section and shows, in a histogram of the mass distribution of the J/Ψ -pair, the need to include the double parton cross section. Ref. [7] estimates the integrated cross section and concludes that the double parton contribution is almost of the same order (2.0nb) as the single parton cross section (4.15nb). Both groups of authors argue that the observed LHCb cross section strongly supports the presence of double parton scattering.

Other processes for which double parton cross sections have been calculated include $b\bar{b}jet\ jet$ [8], and $Wb\bar{b}$ production [9, 10]. In particular, when plotting event rates as functions of variables which discriminate between single and double parton scattering, e.g.

$$S_{p_T} = \frac{1}{\sqrt{2}} \sqrt{\left(\frac{|p_T(b_1, b_2)|}{|p_T(b_1)| + |p_T(b_2)|}\right)^2 + \left(\frac{|p_T(l, \nu)|}{|p_T(l)| + |p_T(\nu)|}\right)^2} \quad (4)$$

one observes a fairly clear separation between single and double parton density contribution: double parton scattering prefers small values of this variable (pair-wise balancing). Also, 2-dimensional plots are useful for illustrating the separation of double and single parton scattering. The $Wb\bar{b}$ final states attracts interest, since it is a background for Higgs production in the HW^\pm mode.

With the experience obtained by these studies of individual processes it will be important to now perform dedicated studies of the final states relevant for new physics, e.g. the Higgs channels $\gamma\gamma$, WW , or ZZ .

3 Theory of multiple interactions

After the pioneering investigations of Treleani et al.[11, 12, 13, 14] recently several new efforts have been made to develop a QCD-based theory of multiple interactions [15, 16, 17] , [18, 19, 20, 21, 22].

An important point stressed by several of these papers is the structure of double parton interactions in transverse coordinates or transverse momenta (Fig.1). A particular aspect can be read off from Fig.1a: the double parton densities above and below the production vertices depend upon the additional momentum transfer $\vec{\Delta}$ (cf.eq.(1)): the neglect of this dependence, as it is done in the factorization approximation (3), loses this information. In transverse coordinates (Fig.1b) this means that part of the transverse dependence is washed out.

Apart from the momentum (coordinate) dependence, the general analysis of multiple interactions shows nontrivial structures in color and spin. For example, in Fig.1a the partons

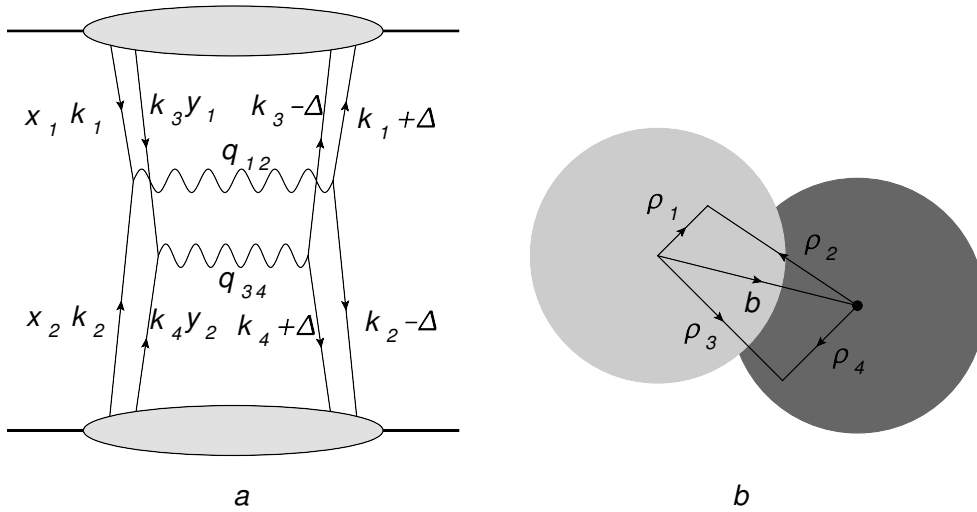


Figure 1: the transverse structure of double parton scattering: (a) transverse momenta (b) in the transverse coordinate plane

with momenta k_1 and $k_1 + \Delta$ do not have to be in a t -channel color singlet state (as it is assumed in the factorization ansatz). The detailed account of correlations in color and spin may lead to interesting observable effects. As an example, in double Drell Yan production, it has been pointed out that there are interesting transverse correlations in the azimuthal angular distributions of the final states.

An important issue is the momentum suppression of multiple interactions relative to single parton scattering. In Fig.1 the large momentum scales are given by the momenta $q_{12}^2 \sim q_{34}^2 \sim Q^2$. The overall scaling behavior of the differential double scattering cross section is $\sim 1/Q^4 \Lambda^2$, similar to the production in a single hard scattering. Therefore, in the fully differential cross section, multiple hard interactions are not power suppressed. The situation changes if one integrates over the transverse momenta \vec{q}_{12} and \vec{q}_{34} : in double scattering processes both produced momenta result from transverse parton momenta and are limited to size Λ , whereas in single hard scattering processes the individual transverse momenta can be large while their sum is of order Λ . Therefore, after integration over the transverse momenta one has the scaling results $\sim \Lambda^2/Q^4$ and $\sim 1/Q^2$ for double and single parton scattering, resp. , i.e. double parton scattering becomes higher twist. In more detail one finds that, in multijet final states, there exist special kinematic regions ('back to back kinematics') where multiple scattering has little or no suppression relative to single parton scattering.

A theoretical issue that has come up with the derivation of multiple parton cross sections is the role of the splitting of one parton into two partons (Fig.2). Whereas some authors have viewed this splitting as an additional contribution inside the double parton evolution (see below), it has also been argued that the contribution shown in Fig.2 should be viewed as a loop correction to the subprocess: 2 partons \rightarrow 2 gauge bosons in single parton scattering.

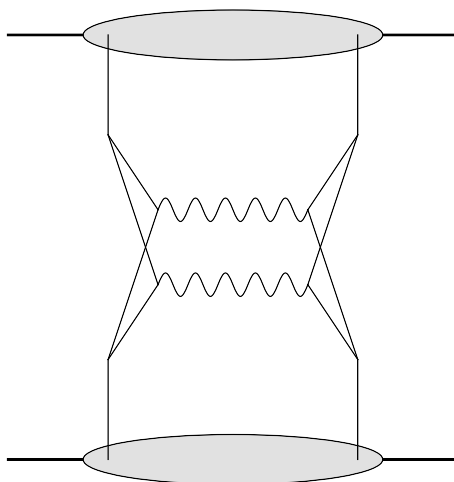


Figure 2: parton splittings

4 Theory of the evolution of multiparton correlators

As it has been said before, in phenomenological applications double parton densities are often assumed to factorize (cf.(3)), and consequently their evolution follows the 'double DGLAP' scheme. But as we already said, this approximation neglects correlations which may have also numerical significance. As to the general theory of multiparton evolution, we first remind that there exist two different approaches: one is based upon the evolution of quasipartonic higher twist operators in deep inelastic scattering [23] and can be viewed as an extension of the DGLAP leading twist framework. There exist no factorization theorems for multiparton correlators. The other one uses the BKP equations [24] and applies to small- x values; it is the extension of the BFKL equation to more than two t -channel gluons. This small- x framework allows the application of the AGK counting rules [25] which, among other predictions, also proves the absence of soft rescattering corrections in single or double inclusive cross section formulae. In the so-called double logarithmic approximation the two schemes overlap. Both schemes contain transitions from two to four partons (gluons) and, within four-partons t -channel states, the sum over pairwise interactions (Fig.3). The factorization ansatz corresponds to Fig.3b: it contains two noninteracting color singlet ladders with zero momentum transfer. In configuration space the production subprocesses from these two chains are completely uncorrelated.

In [3] a modified evolution scheme has been investigated in more detail: the evolution equations contain an additional term which accounts for the splitting of a single partons into two partons (Fig.2) (see also [26]). In more recent papers [28, 27] the splitting kernel illustrated in Fig.3e has been taken into account. The numerical study contained in [2] reports that this additional term in the evolution equations leads to observable correlation effects.

A slightly different step beyond the double DGLAP approximation is taken in [29]: in addition to the evolution of the two noninteracting ladders (14) and (23) in Fig.3b one can have a 'recombination' to two other ladders, e.g. the pairs (13) and (24) (Fig.3c). The numerical investigation in [30] which includes such 'switches' finds large correlation effects which again

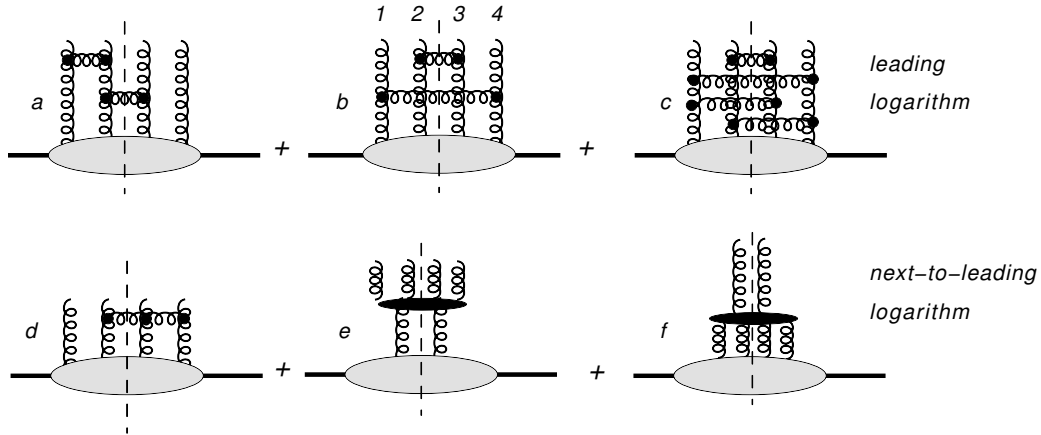


Figure 3: schematic view of evolution kernels in multiparton states

emphasizes the need to go beyond the factorizing approximation.

So far the discussion has been about small numbers of different parton chains. Large numbers of chains are expected to appear in the context of saturation, where the evolution of gluon densities is determined by number-changing kernels (Fig.3f). As an example, the recently observed ridge effect in pp collisions [31] has stimulated the idea [32, 33] that the observed characteristics (high multiplicity, long range rapidity correlation and azimuthal correlations, momentum scale in the region of the saturation scale) can be attributed to saturation. Interestingly, within the interpretation given in [32, 33] the two gluon correlators enter in a combination which resembles the 'recombination' mentioned before.

5 Diffraction

One of the aspects of multiple interactions which needs more attention is the account for final states with large rapidity gaps inside the underlying event. On the partonic level, large rapidity gaps occur if color singlet exchanges are included; radiation of partons from single parton chain tends to lead to small rapidity intervals. It is instructive to review the situation at HERA. Fig.4a illustrates the 'normal' event structure, where radiation from the single gluon or quark line produces final states without large rapidity separations. The momentum scale Q_0^2 separates the perturbative (hard) part from the nonperturbative (soft) part. Large rapidity gaps, however, may occur inside the proton remnants, mediated either by soft Pomeron exchange (Fig.4b) or by two gluon exchange (Fig.4c). The first case belongs to soft diffraction (characterized by momentum scales up to Q_0^2), the latter one to semihard diffraction (up to momenta of the order $Q_1^2 > Q_0^2$). It is clear that Fig.4b is part of Fig.4a (and must not be added separately), whereas Fig.4c has to be counted as an additional contribution (potentially of higher twist, e.g. diffractive vector meson production). For the evolution above the initial scale Q_0^2 (Fig.4b) or Q_1^2 (Fig.4c) one has the usual DGLAP evolution equations.

Turning to hadron hadron scattering the situation changes drastically. For single chains (Fig.5a) soft diffraction is contained inside the initial conditions (Figs.5b) whereas semihard

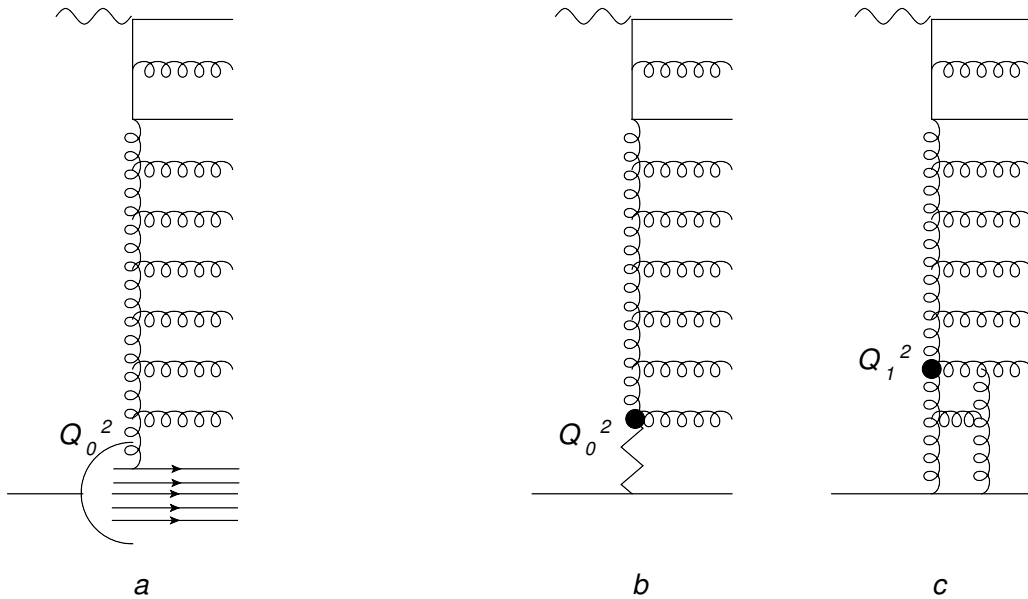


Figure 4: diffractive final states at HERA

diffractive needs to be included separately (Fig.5c). But it is known that these contributions are suppressed by radiation from additional chains (Fig.5d). As a result, in pp scattering the number of events with rapidity gaps is suppressed in comparison with deep inelastic scattering. This suppression is commonly encoded in the 'suppression factor' (Fig.5e). The consistent implementation of diffractive final states into event generators represents an important challenge for the near future.

Turning to diffractive cross sections, there is no consistent theory. But empirically cross section formulae can often, to a good approximation, be factorized into a hard and a soft part (Fig.5e); physically this corresponds to taking into account only low mass states between the rescattering and the hard process and thus neglecting so-called enhanced contributions. For the very interesting case of double diffractive Higgs production the question has been raised whether the factorization into a hard subprocess (gluon-gluon fusion into a Higgs particle) and a soft survival factor is a represents an adequate approximation, but no conclusive answer has been found.

6 Conclusions

This conference has shown that multiparton interactions represent a challenge, both for improving our theoretical understanding and for consistently implementing multiple interactions into event generators.

Acknowledgements: Helpful discussions with Markus Diehl are gratefully acknowledged.

MULTIPLE INTERACTIONS: SUMMARIZING REMARKS (THEORY)

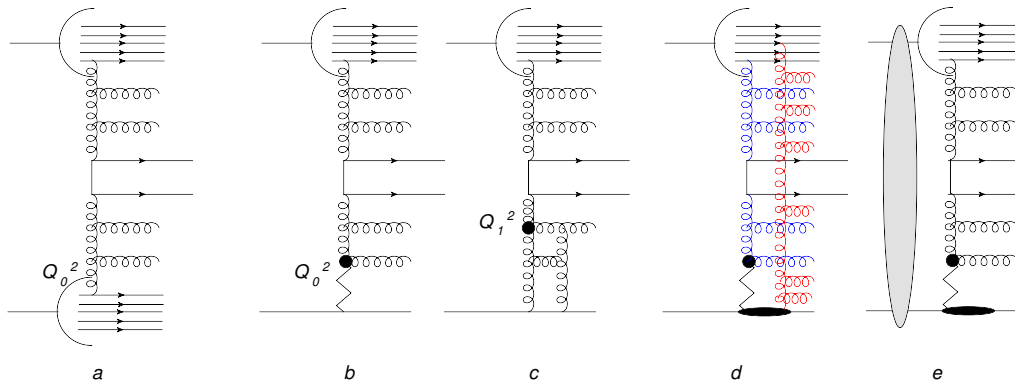


Figure 5: diffractive final states in pp collisions

References

- [1] A. Kulesza and W. J. Stirling, “Like sign W boson production at the LHC as a probe of double parton scattering,” *Phys. Lett. B* **475** (2000) 168 [hep-ph/9912232].
- [2] J. R. Gaunt, C. -H. Kom, A. Kulesza and W. J. Stirling, “Same-sign W pair production as a probe of double parton scattering at the LHC,” *Eur. Phys. J. C* **69** (2010) 53 [arXiv:1003.3953 [hep-ph]].
- [3] J. R. Gaunt and W. J. Stirling, “Double Parton Distributions Incorporating Perturbative QCD Evolution and Momentum and Quark Number Sum Rules,” *JHEP* **1003** (2010) 005 [arXiv:0910.4347 [hep-ph]].
- [4] J. R. Gaunt, C. H. Kom, A. Kulesza and W. J. Stirling, “Probing double parton scattering with leptonic final states at the LHC,” arXiv:1110.1174 [hep-ph].
- [5] C. H. Kom, A. Kulesza and W. J. Stirling, “Prospects for observation of double parton scattering with four-muon final states at LHCb,” *Eur. Phys. J. C* **71** (2011) 1802 [arXiv:1109.0309 [hep-ph]].
- [6] C. H. Kom, A. Kulesza and W. J. Stirling, “Pair production of J/ψ as a probe of double parton scattering at LHCb,” *Phys. Rev. Lett.* **107** (2011) 082002 [arXiv:1105.4186 [hep-ph]].
- [7] S. P. Baranov, A. M. Snigirev and N. P. Zotov, “Double heavy meson production through double parton scattering in hadronic collisions,” *Phys. Lett. B* **705** (2011) 116 [arXiv:1105.6276 [hep-ph]].
- [8] E. L. Berger, C. B. Jackson and G. Shaughnessy, “Characteristics and Estimates of Double Parton Scattering at the Large Hadron Collider,” *Phys. Rev. D* **81** (2010) 014014 [arXiv:0911.5348 [hep-ph]].
- [9] E. L. Berger, C. B. Jackson, S. Quackenbush and G. Shaughnessy, “Calculation of $W b \bar{b}$ Production via Double Parton Scattering at the LHC,” *Phys. Rev. D* **84** (2011) 074021 [arXiv:1107.3150 [hep-ph]].
- [10] S. Quackenbush, E. L. Berger, C. B. Jackson and G. Shaughnessy, “LHC Sensitivity to $W b \bar{b}$ Production via Double Parton Scattering,” arXiv:1109.6271 [hep-ph].
- [11] L. Ametller, N. Paver and D. Treleani, “Possible Signature Of Multiple Parton Interactions In Collider Four Jet Events,” *Phys. Lett. B* **169** (1986) 289.
- [12] N. Paver and D. Treleani, “Multiple Parton Processes In The Tev Region,” *Z. Phys. C* **28** (1985) 187.
- [13] N. Paver and D. Treleani, “Multiple Parton Interactions And Multi - Jet Events At Collider And Tevatron Energies,” *Phys. Lett. B* **146** (1984) 252.
- [14] G. Calucci and D. Treleani, “Disentangling correlations in Multiple Parton Interactions,” *Phys. Rev. D* **83** (2011) 016012 [arXiv:1009.5881 [hep-ph]].
- [15] M. Diehl, D. Ostermeier and A. Schafer, “Elements of a theory for multiparton interactions in QCD,” *JHEP* **1203** (2012) 089 [arXiv:1111.0910 [hep-ph]].
- [16] M. Diehl, “Multiparton interactions and multiparton distributions in QCD,” *Few Body Syst.* **52** (2012) 249 [arXiv:1111.0272 [hep-ph]].

- [17] M. Diehl and A. Schafer, “Theoretical considerations on multiparton interactions in QCD,” *Phys. Lett. B* **698** (2011) 389 [arXiv:1102.3081 [hep-ph]].
- [18] Y. .L. Dokshitzer, “A new look at Multiple Parton Collisions,” arXiv:1203.0716 [hep-ph].
- [19] B. Blok, Y. .Dokshitzer, L. Frankfurt and M. Strikman, “The Four jet production at LHC and Tevatron in QCD,” *Phys. Rev. D* **83** (2011) 071501 [arXiv:1009.2714 [hep-ph]].
- [20] B. Blok, Y. .Dokshitzer, L. Frankfurt and M. Strikman, “pQCD physics of multiparton interactions,” *Eur. Phys. J. C* **72** (2012) 1963 [arXiv:1106.5533 [hep-ph]].
- [21] M. Strikman and W. Vogelsang, “Multiple parton interactions and forward double pion production in pp and dA scattering,” *Phys. Rev. D* **83** (2011) 034029 [arXiv:1009.6123 [hep-ph]].
- [22] Tomas Kasemets, these proceedings
- [23] A. P. Bukhvostov, G. V. Frolov, L. N. Lipatov and E. A. Kuraev, “Evolution Equations For Quasi-Partonic Operators,” *Nucl. Phys. B* **258** (1985) 601.
- [24] J. Bartels, “High-Energy Behavior in a Nonabelian Gauge Theory. 2. First Corrections to $T(n\rightarrow m)$ Beyond the Leading LNS Approximation,” *Nucl. Phys.* **B175** (1980) 365. J. Kwiecinski, M. Praszalowicz, “Three Gluon Integral Equation and Odd c Singlet Regge Singularities in QCD,” *Phys. Lett.* **B94** (1980) 413.
- [25] V. A. Abramovsky, V. N. Gribov and O. V. Kancheli, “Character Of Inclusive Spectra And Fluctuations Produced In Inelastic Processes By Multi - Pomeron Exchange,” *Yad. Fiz.* **18** (1973) 595 [Sov. J. Nucl. Phys. **18**];
M. Salvadore, J. Bartels and G. P. Vacca, “Multiple interactions and AGK rules in pQCD,” arXiv:0709.3062 [hep-ph].
- [26] F. A. Ceccopieri, *Phys. Lett. B* **697** (2011) 482 [arXiv:1011.6586 [hep-ph]].
- [27] M. G. Ryskin and A. M. Snigirev, “Double parton scattering in double logarithm approximation of perturbative QCD,” arXiv:1203.2330 [hep-ph].
- [28] M. G. Ryskin and A. M. Snigirev, “A Fresh look at double parton scattering,” *Phys. Rev. D* **83** (2011) 114047 [arXiv:1103.3495 [hep-ph]].
- [29] J. Bartels and M. G. Ryskin, “Recombination within multi-chain contributions in pp scattering,” arXiv:1105.1638 [hep-ph].
- [30] C. Flensburg, G. Gustafson, L. Lonnblad and A. Ster, “Correlations in double parton distributions at small x,” arXiv:1103.4320 [hep-ph].
- [31] V. Khachatryan *et al.* [CMS Collaboration], “Observation of Long-Range Near-Side Angular Correlations in Proton-Proton Collisions at the LHC,” *JHEP* **1009** (2010) 091. [arXiv:1009.4122 [hep-ex]].
- [32] A. Dumitru, K. Dusling, F. Gelis, J. Jalilian-Marian, T. Lappi, R. Venugopalan, “The Ridge in proton-proton collisions at the LHC,” *Phys. Lett.* **B697** (2011) 21-25. [arXiv:1009.5295 [hep-ph]].
- [33] K. Dusling and R. Venugopalan, “Azimuthal collimation of long range rapidity correlations by strong color fields in high multiplicity hadron-hadron collisions,” arXiv:1201.2658 [hep-ph].

MPI and Monte Carlo event generators

Hannes Jung and Simon Plätzer

DOI: <http://dx.doi.org/10.3204/DESY-PROC-2012-03/89>

This contribution summarizes recent developments in modeling multiple parton interactions within Monte Carlo event generators. We will review few selected topics driving current research in the field and address open questions.

1 Introduction

Monte Carlo event generators are indispensable tools for describing fully exclusive final states at collider experiments. In hadron collisions, multiple parton interactions not only play a crucial role in driving phenomena such as the underlying event, but are the key ingredient to modeling the ‘average’ (inelastic) hadron collision, commonly referred to as minimum bias physics.

Besides being of interest on its own, the underlying event impacts on all final states observed at the LHC and thus requires a sound understanding to identify the hard physics of interest; an accurate modeling of minimum bias physics is needed to simulate pile-up, multiple collisions during one bunch crossing.

Starting from simple parameterizations of the underlying event activity as measured by the UA5 experiment, more sophisticated models based on eikonalized cross sections have been developed. These models have received tremendous improvements over recent years, particularly towards the inclusion of soft underlying event activity, taking into account correlations between longitudinal and transverse structure inside the colliding hadrons, as well as an equivalent reformulation in terms of secondary scatters competing with initial state radiation.

Diffraction contributions to inelastic scattering have so far been treated mostly independent, but efforts are now underway to setup a unified framework including cut and uncut chain contributions on equal footing.

Besides these traditional models, independent approaches have set out to describe underlying event and minimum bias physics motivated by BFKL evolution. Most prominently, event generators are available incorporating CCFM evolution of initial state partons, as well as the dipole formulation of BFKL.

In this summary, we will first focus on developments within the class of eikonal models, as presented at this workshop and then briefly address BFKL motivated approaches. We will close with a selection of open questions before drawing general conclusions.

2 Eikonal approaches

Most of the established models for the description of inimum bias and underlying event physics are based on the eikonal ansatz of unitarized total cross sections. These approaches have

been implemented in a variety of different model assumptions in all of the multi-purpose event generators used at LHC and previous hadron collider experiments.

Within the eikonal approaches of multiple partonic interactions, the connection to hadronization models seems to be crucial. Particularly, the color structure assigned to a sequence of several scatterings including subsequent radiation by parton showering does typically not seem to generate final states minimizing the energy of hadron progenitors, *i.e.* string pieces or clusters. The effect of these configurations can readily be recognized in predicting too much and mostly too forward hadronic activity. Most eikonal models are thus supplemented by a model of color reconnection, describing nonperturbative exchange of color charge such as to minimize the overall string length or sum of cluster masses. Driven by few parameters which need to be tuned to data, very reasonable descriptions of underlying event and minimum bias data can be achieved by including these models. Recent developments in this area, particularly statistical models for colour reconnection, have been discussed by Stefan Gieseke and Peter Skands. Tuning efforts which are required to fix the parameters of these models from data, showing the huge impact of colour reconnection on a sensible description of minimum bias and underlying event data have been presented by Deepak Kar and Andrzej Siodmok.

A crucial ingredient to all eikonal models of multiple parton interactions is the assumption on the quark and gluon distribution in the proton as a function of transverse degrees of freedom (impact parameter) and the longitudinal momentum fraction carried by each parton. The basic assumption is that the distribution factorizes into a transverse and a longitudinal contribution. This simple assumption does indeed seem to work very well, though there is no first-principle mechanism which would ensure its validity. Indeed, on very general grounds, it is expected that the width of the transverse distribution of partons will grow logarithmically with smaller momentum fractions. A model along these lines and its implementation in *Pythia* has been outlined by Peter Skands.

Closely connected to the modelling of the matter overlap of two colliding hadrons are potential explanations of the so-called ridge effect. CMS has reported the measurement of two-particle correlations as a function of the event multiplicity and track transverse momenta. Besides the known behavior of the measured correlation function, a new feature of long-range (in rapidity), near-side (in azimuth) correlations has been observed in events with high multiplicity and moderate $p_{\perp} \sim 2\text{GeV}$. A similar behavior has been observed in heavy ion collisions at RHIC, but not so far in pp collisions. The effect is not reproduced by any Monte Carlo simulation available so far. Sara Alderweireldt has presented a possible solution to explain this effect within the framework of multiple interactions. In a modified version of *Pythia*, additional azimuthal correlations have been introduced as a function of impact parameter, where a preferred plane is emerging in more peripheral collisions. A new tune has been required to still give an acceptable description of minimum bias and underlying event data, and the model indeed reproduces the ‘ridge effect’ at least qualitatively.

The description of diffractive contributions has so far been treated mostly independent of the eikonal models for multiple partonic interactions. Diffractive event generation is up to now rooted in the Ingelmann-Schlein model, assigning a partonic substructure to a pomeron along with appropriate parton distribution functions, which have been obtained from *e.g.* diffractive events measured at HERA. Additional gap survival factors need to be included to arrive at a reasonable description of diffractive events. Physically, the different diffractive, non-diffractive and elastic contributions can and should be treated on equal footing, though: they correspond to different cuts of diagrams contributing to the total cross section. Frank Krauss presented first steps towards a minimum bias simulation based on this motivation, more precisely on the

model of Khoze, Martin and Ryskin. While there are many open issues until this simulation can be regarded a full-fledged model including the underlying event physics, first comparisons to minimum bias data look promising.

Event generators which are based on a Regge-physics picture right from the start are mainly used in the description of cosmic ray physics, but now receive increasing attention for hadron colliders, as well. Within this context, recent improvements to the DPMJET generator have been discussed by Fritz Bopp.

3 BFKL motivated approaches

At high energies, where the parton densities become large and where multiparton interactions can be expected, the longitudinal momentum fractions x at which the hard processes occur, can reach very small values, and deviations from the collinear DGLAP type evolution can be expected. The amount of multiparton interaction, which is needed to describe experimental measurements depends on the amount of activity from a single interaction and on the size of the parton distribution function. Thus one can expect, that a small x improved parton shower would imply a different contribution from multiparton interactions. This has been discussed in the contribution of F. Hautmann. The inclusive jet production at Tevatron and LHC energies is reasonably well described using unintegrated gluon distributions together with the $g^*g^* \rightarrow g$ process as discussed by V. Saleev. A reasonable description of also low p_t particle production at LHC energies is obtained by a gluon density which includes saturation effects (G. Lykasov). The small x behavior of the parton distribution is studied in a analytical way by A. Kotikov.

Not only a different parton evolution might play a role at highest energies, also parton recombination and saturation effects as well as diffractive interactions must appear, as predicted and described by the AGK rules (see the contribution by J. Bartels). The small x BFKL evolution can be described by the dipole picture of A. Mueller, which allows an extension to include also recombination effects (swing) as well as color singlet exchanges (diffraction), as described by the Lund Dipole Model and its Monte Carlo implementation DIPSI. This approach is successful describing diffractive processes from HERA as well as minimum bias and multiparton interaction processes at LHC, as discussed in the contribution by L. Lönnblad.

4 Open questions

The implementation of multiparton interactions in Monte Carlo event generators does not yet include small x improved parton showering, nor does it include saturation and recombination effect. However, using the DGLAP based collinear parton shower with the concept of multiparton interactions gives a surprisingly good description of experimental measurements.

- Can effects expected from small x evolution, like the energy and rapidity dependence of forward-backward jets (Mueller Navelet jets) be mimicked by multiparton interactions ? Is there a way to tell the difference ?
- Where is the signal from (soft as well as hard) diffractive processes, which must be present in multiparton interactions, seen ? Is the so-called "gap-survival" probability just a consequence of multiparton interactions ? Where do diffractive parton densities, as measured at HERA, play a role ?

- Is there a difference in the hadronic final state from a scenario with a BFKL like parton density, which needs saturation, compared to a parton density which has a less steep energy dependence ?
- Where is a signal from interfering multiparton ladders, apart from a schematic description of the Ridge effect in pp ?
- Where is the tension between a description of min-bias data and a description of the underlying event data coming from ? Does this indicate limitations of the present models of multiparton interactions ?
- How is the color distributed between different multiparton ladders ? Is color reconnection a effective parameterization of diffraction ?
- etc.

5 Conclusions

Many new and interesting measurements from LHC, HERA and Tevatron have been presented, which are in general reasonably well described by adjusting free parameters in the models of multiparton interactions. However, several questions on the consistency of the multiparton interaction approach have been raised. The measurements at LHC have reached a level of precision, that more fundamental questions can be addressed. The measurements and the model description has already after 2 years of LHC running reached a level comparable to what was achieved at the Tevatron. The much larger energy and the much larger fiducial coverage of the LHC detectors allow further measurements which can constrain the models much better and eventually lead to a understanding of the high energy behavior of hadronic interactions. The high energy behavior of hadronic cross sections is of fundamental importance: without multiparton interaction, saturation and diffraction, the hadronic cross section would increase too fast, leading to unitarization problems, similar to what happens with the longitudinal part of WW scattering without a Higgs. However, the unitarization problem of hadronic interactions is of much higher relevance, as the hadronic cross section dominates the interaction with matter.

List of Authors

Alderweireldt, Sara, 33

Bansal, Sunil, 3

Baranov, Sergey P., 107

Bartels, Jochen, 151, 265

Berger, Edmond L., 81

Bopp, Fritz W., 41

Capua, Marcella, 137

Choudhury, Dilip K., 145

Diehl, Markus, 235

Dobson, Eleanor, 117

Dokshitzer, Yuri L., 187

Gaunt, Jonathan R., 197

Gieseke, Stefan, 51, 67

Golovanov, Georgy, 127

Grinyuk, Andrei, 169

Hautmann, Francesco, 221

Illarionov, Alexey Yu., 161

Jahan, Akbari, 145

Jung, Hannes, 169, 273

Kar, Deepak, 57

Kasemets, Tomas, 89

Kniehl, Bernd, 177

Kotikov, Anatoly V., 161

Lappi, Tuomas, 205

Leyton, Michael, 11

Lipatov, Artem, 169

Lykasov, Gennady, 169

Mechelen, Pierre Van, 33

Moraes, Arthur, 257

Noda, Koji, 247

Ostermeier, Daniel, 235

Plätzer, Simon, 273

Porteboeuf-Houssais, Sarah, 21

Röhr, Christian A., 51, 67

Ranft, Johannes, 41

Rogers, Ted C., 215

Ryskin, Mikhail G., 227

Saleev, Vladimir, 177

Schäfer, Andreas, 235

Shipilova, Alexandra, 177

Siódmok, Andrzej, 51, 67

Snigirev, Alexander M., 107, 227

Stirling, W. James, 197

Strikman, Mark, 97, 215

Wahrmund, Sebastian, 75

Zotov, Nikolai P., 107, 169